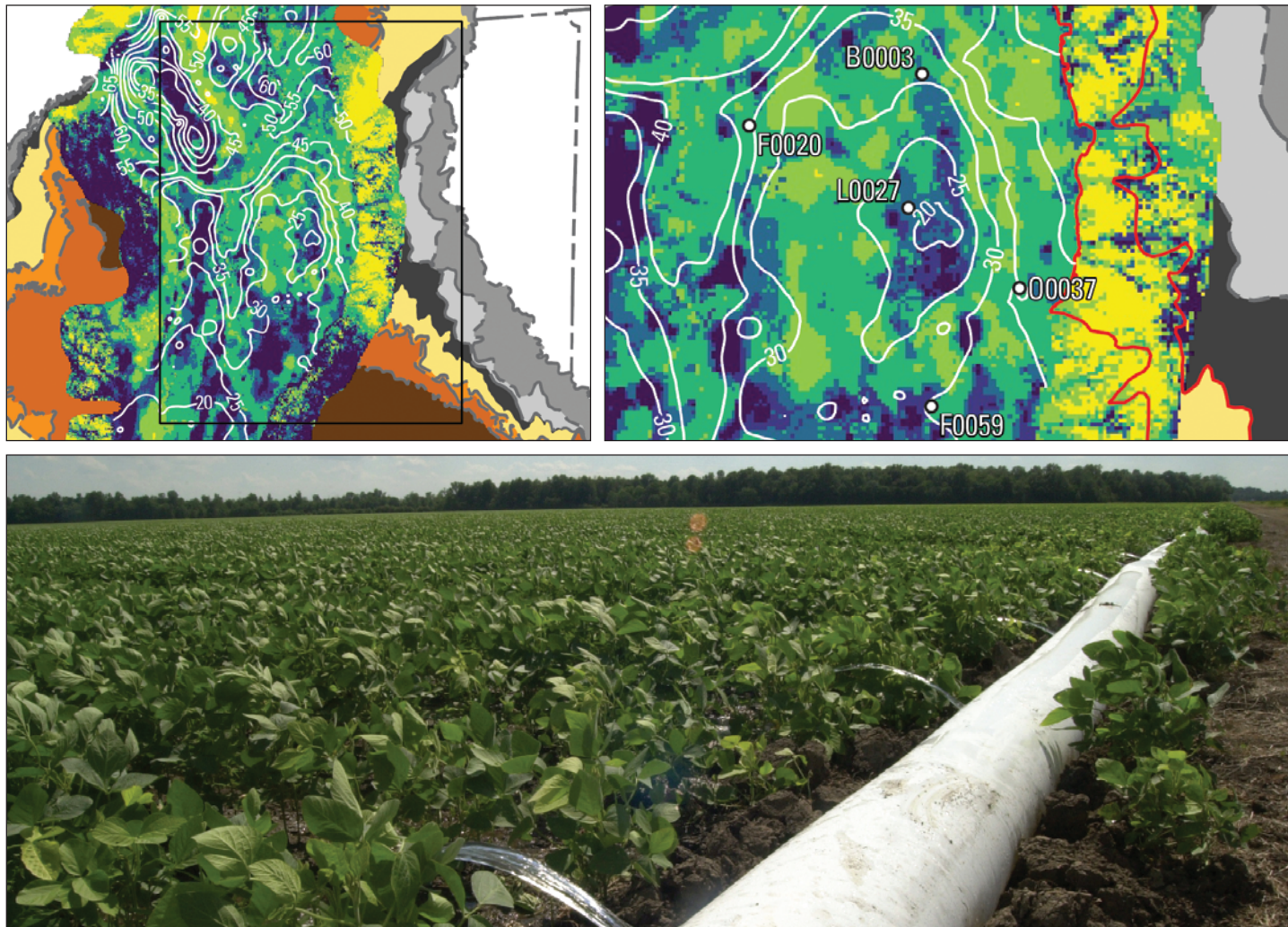


Water Availability and Use Science Program

## Simulating Groundwater Flow in the Mississippi Alluvial Plain with a Focus on the Mississippi Delta



Scientific Investigations Report 2023-5100

Surficial connectivity classifications developed by Minsley and others (2021), with mapped groundwater levels (McGuire and others, 2021a), at the scale of the Mississippi Embayment Regional Aquifer Study area.

Surficial connectivity classifications developed by Minsley and others (2021), with mapped groundwater levels (McGuire and others, 2021a), inset of the Mississippi Delta region.

Furrow irrigation. Photograph credit: Mississippi State University Extension, Office of Agricultural Communications.

# **Simulating Groundwater Flow in the Mississippi Alluvial Plain with a Focus on the Mississippi Delta**

By Andrew T. Leaf, Leslie L. Duncan, Connor J. Haugh, Randall J. Hunt, and  
James R. Rigby

Water Availability and Use Science Program

Scientific Investigations Report 2023–5100

**U.S. Department of the Interior  
U.S. Geological Survey**

## U.S. Geological Survey, Reston, Virginia: 2023

For more information on the USGS—the Federal source for science about the Earth, its natural and living resources, natural hazards, and the environment—visit <https://www.usgs.gov> or call 1-888-ASK-USGS.

For an overview of USGS information products, including maps, imagery, and publications, visit <https://store.usgs.gov/>.

Any use of trade, firm, or product names is for descriptive purposes only and does not imply endorsement by the U.S. Government.

Although this information product, for the most part, is in the public domain, it also may contain copyrighted materials as noted in the text. Permission to reproduce copyrighted items must be secured from the copyright owner.

Suggested citation:

Leaf, A.T., Duncan, L.L., Haugh, C.J., Hunt, R.J., and Rigby, J.R., 2023, Simulating groundwater flow in the Mississippi Alluvial Plain with a focus on the Mississippi Delta: U.S. Geological Survey Scientific Investigations Report 2023-5100, 143 p., <https://doi.org/10.3133/sir20235100>.

Associated data for this publication:

Leaf, A.T., Duncan, L.L., and Haugh, C.J., 2023, MODFLOW 6 models for simulating groundwater flow in the Mississippi Embayment with a focus on the Mississippi Delta: U.S. Geological Survey data release, <https://doi.org/10.5066/P971LPOB>.

Torak, L.J., 2023, Digital surfaces and site data of well-screen top and bottom altitudes defining the irrigation production zone of the Mississippi River Valley alluvial aquifer within the Mississippi Alluvial Plain project region: U.S. Geological Survey data release, <https://doi.org/10.5066/P9TSDEAC>.

Villers, J.J., and Ladd, D.E., 2023, Soil-Water-Balance forecasted climate model output for simulations of water budget components in the Mississippi Embayment Regional Aquifer System, 2020 to 2055: U.S. Geological Survey data release, <https://doi.org/10.5066/P9BC6UB8>.

Westenbroek, S.M., Nielsen, M.G., and Trost, J.J., 2023, Model archive and output files for net infiltration, runoff, and irrigation water use for the Mississippi Embayment Regional Aquifer System, 2000 to 2020, simulated with the Soil-Water-Balance model: U.S. Geological Survey data release, <https://doi.org/10.5066/P97KK17G>.

## Acknowledgments

We acknowledge the World Climate Research Programme's Working Group on Coupled Modelling, which is responsible for the Coupled Model Intercomparison Project (CMIP), and we thank the climate modeling groups (listed in table 4.1 of this report) for producing and making available their model output. For CMIP, the U.S. Department of Energy's Program for Climate Model Diagnosis and Intercomparison provided coordinating support and led development of software infrastructure in partnership with the Global Organization for Earth System Science Portals.

The authors would also like to acknowledge Jonathan (JP) Traylor, Moussa Guira and Wade Kress (of the U.S. Geological Survey [USGS]) for technical discussions that shaped the model development. Martha Nielsen (USGS) and Daniel Abrams (Illinois State Water Survey) provided thoughtful review comments that greatly improved the quality of the report. Sam Rendon (USGS) worked on a Hydrologic Engineering Center River Analysis System (HEC–RAS) simulation of interior streams in the Mississippi Delta as a potential alternative method for simulating stream stage. Aaron Heldmyer (USGS) selected and compiled the downscaled General Circulation Model outputs for the future climate scenarios. Steve Westenbroek (USGS) ran a version of the Soil-Water-Balance code model with each set of downscaled climate output and provided us with the results.



# Contents

Acknowledgments.....	iii
Abstract.....	1
Introduction.....	1
Previous Work.....	3
Limitations of Previous Models and Recent Advances.....	4
Modeling Goals and Approach.....	5
Purpose and Scope .....	5
Study Area Description and Hydrogeologic Setting.....	5
Climate .....	6
Hydrostratigraphy.....	6
Conceptual Model.....	7
Terrestrial Water Balance .....	7
Groundwater Balance and Water Use.....	7
Effects of Surficial Geology on Groundwater .....	7
Regional Groundwater Flow System .....	9
Groundwater Flow in the Mississippi Delta .....	10
Aquifer Thickness and Hydraulic Properties .....	10
Modeling Approach.....	10
Model Domains and Discretization.....	10
Boundary Conditions.....	12
Subsurface Properties.....	12
Parameter Estimation and Uncertainty Analysis.....	14
Results and Discussion.....	14
History Matching Results .....	15
Historical Mississippi Delta Model Results.....	19
Future Climate Scenarios and Forecast Hydrologic Effects.....	23
Future Model Forcings .....	23
Potential Changes in Groundwater Levels, Streamflow, and Saturated Thickness.....	25
Assumptions, Limitations, and Suggestions for Future Work.....	30
MERAS 3 Regional Model .....	30
Mississippi Delta Model .....	30
Limitations of the Estimated Water Balances.....	31
Limitations of the Future Climate Scenarios .....	31
Summary and Conclusions.....	32
References Cited.....	33
Appendix 1. Groundwater Flow Model Constructions .....	39
Appendix 2. Parameter Estimation and Uncertainty Analysis .....	59
Appendix 3. Additional Model Results.....	138
Appendix 4. General Circulation Models Used in the Future Climate Scenarios .....	142

## Figures

1. Maps showing extents of the Mississippi Embayment Regional Aquifer Study and Mississippi Delta groundwater models.....	2
2. Maps showing generalized regions of the Mississippi Alluvial Plain .....	3
3. Maps showing surficial connectivity classifications developed by Minsley and others (2021), with mapped groundwater levels .....	8
4. Cross sections showing the regional model aquifer property zones .....	11
5. Cross sections showing Mississippi Delta model aquifer property zones .....	13
6. Graphs showing times series of measured heads and simulated equivalents at selected wells of focus.....	16
7. Graphs showing times series of monthly averages of measured streamflows and simulated equivalents at selected streamgages.....	18
8. Graphs showing times series of monthly averages of measured changes in streamflow between streamgages, and simulated equivalents.....	19
9. Maps showing water table elevations and stream leakage in the Mississippi Delta as simulated by the Mississippi Delta model under dry and wet conditions.....	21
10. Graphs showing groundwater budget results for the Mississippi Delta .....	23
11. Graphs showing streamflow routing package budget results for the Mississippi Delta model area.....	24
12. Graphs showing future annual mean temperature and precipitation forecasts for Sunflower County, Mississippi .....	25
13. Graph showing future simulated average net annual groundwater budgets for the Mississippi Delta, 2045–56.....	26
14. Graphs showing time series of forecasted groundwater levels out to 2056 at selected “priority” wells of focus .....	27
15. Graph showing time series of observed and forecasted annual minimum monthly stream flows in the Sunflower River at Sunflower, Mississippi .....	28
16. Maps showing forecasted changes out to 2056 of saturated thickness in the Mississippi River Valley alluvial aquifer.....	29

## Tables

1. Comparison of average model input terms for the Mississippi Embayment Regional Aquifer Study and Mississippi Delta models with previous modeling studies .....	20
---	----

## Conversion Factors

U.S. customary units to International System of Units

Multiply	By	To obtain
Length		
inch (in.)	2.54	centimeter (cm)
foot (ft)	0.3048	meter (m)
mile (mi)	1.609	kilometer (km)
Area		
square mile (mi <sup>2</sup> )	2.590	square kilometer (km <sup>2</sup> )
Volume		
gallon (gal)	0.003785	cubic meter (m <sup>3</sup> )
million gallons (Mgal)	3,785	cubic meter (m <sup>3</sup> )
cubic foot (ft <sup>3</sup> )	0.02832	cubic meter (m <sup>3</sup> )
Flow rate		
cubic foot per second (ft <sup>3</sup> /s)	0.02832	cubic meter per second (m <sup>3</sup> /s)
cubic foot per day (ft <sup>3</sup> /d)	0.02832	cubic meter per day (m <sup>3</sup> /d)
Hydraulic conductivity		
foot per day (ft/d)	0.3048	meter per day (m/d)
Hydraulic gradient		
foot per mile (ft/mi)	0.1894	meter per kilometer (m/km)
Transmissivity		
foot squared per day (ft <sup>2</sup> /d)	0.09290	meter squared per day (m <sup>2</sup> /d)

International System of Units to U.S. customary units

Multiply	By	To obtain
Length		
centimeter (cm)	0.3937	inch (in.)
meter (m)	3.281	foot (ft)
kilometer (km)	0.6214	mile (mi)
Area		
square kilometer (km <sup>2</sup> )	0.3861	square mile (mi <sup>2</sup> )
Volume		
cubic meter (m <sup>3</sup> )	264.2	gallon (gal)
cubic meter (m <sup>3</sup> )	0.0002642	million gallons (Mgal)
cubic meter (m <sup>3</sup> )	35.31	cubic foot (ft <sup>3</sup> )
Flow rate		
cubic meter per second (m <sup>3</sup> /s)	35.31	cubic foot per second (ft <sup>3</sup> /s)
cubic meter per day (m <sup>3</sup> /d)	35.31	cubic foot per day (ft <sup>3</sup> /d)
cubic meter per day (m <sup>3</sup> /d)	264.2	gallon per day (gal/d)
Hydraulic conductivity		
meter per day (m/d)	3.281	foot per day (ft/d)
Transmissivity		
meter squared per day (m <sup>2</sup> /d)	10.76	foot squared per day (ft <sup>2</sup> /d)

Temperature in degrees Celsius (°C) may be converted to degrees Fahrenheit (°F) as follows:

$$^{\circ}\text{F} = (1.8 \times ^{\circ}\text{C}) + 32.$$

## Datum

Vertical coordinate information is referenced to the North American Vertical Datum of 1988 (NAVD 88).

Horizontal coordinate information is referenced to the North American Datum of 1983 (NAD 83).

## Abbreviations

AEM	airborne electromagnetic
AIWUM	Aquaculture and Irrigation Water-Use Model
CMIP	Coupled Model Intercomparison Project
EPA	U.S. Environmental Protection Agency
iES	iterative ensemble smoother
MERAS	Mississippi Embayment Regional Aquifer Study
NWIS	National Water Information System
RCP	representative concentration pathway
RMSE	root mean squared error
SFR	Streamflow-Routing
SWB	Soil-Water-Balance
USGS	U.S. Geological Survey

# Simulating Groundwater Flow in the Mississippi Alluvial Plain with a Focus on the Mississippi Delta

By Andrew T. Leaf, Leslie L. Duncan, Connor J. Haugh, Randall J. Hunt, and James R. Rigby

## Abstract

The Mississippi Alluvial Plain has become one of the most important agricultural regions in the United States but relies heavily on groundwater for irrigation. On average, more than 12 billion gallons are withdrawn daily from the Mississippi River Valley alluvial aquifer. Declining groundwater levels, especially in the Delta region of northwest Mississippi and the Cache and Grand Prairie regions of eastern Arkansas, have led to concerns about future sustainability. The U.S. Geological Survey Mississippi Alluvial Plain Project is focused on quantifying the groundwater system in the alluvial plain and the response of groundwater resources to future development. A key objective of the project is to provide updated groundwater flow models supported by extensive data collection and analyses. MODFLOW 6, PEST++, and several open-source python packages were used to develop a simplified, faster running version of the Mississippi Embayment Regional Aquifer Study model that can provide boundary conditions for local inset models, including the Mississippi Delta model described in this report. An automated workflow was used for model construction, history matching, and development of baseline future climate scenarios. The models incorporate information from a Soil-Water-Balance code simulation of the terrestrial water balance, metering-based estimates of water use from thousands of wells, measured and estimated streamflow and stages, and the largest airborne electromagnetic survey flown to date in the United States. Baseline scenarios for the Mississippi Delta under potential future climates were constructed using recharge, surface runoff and irrigation pumping forcings from a future version of the Soil-Water-Balance model, driven by downscaled temperature and precipitation output from 10 general circulation model simulations, including high and moderate carbon emissions pathways.

Results indicate a complex water balance that varies in time and space in terms of the terrestrial recharge, stream leakage, and regional groundwater flow components, which are affected by seasonal forcings, human activity, and alluvial geomorphology. The general circulation model outputs indicate a continued rise in average temperatures but no clear precipitation trend. Increased crop water demand is anticipated

from the higher temperatures, resulting in increased irrigation withdrawals to sustain current levels of irrigated agriculture. Simulated drawdowns in groundwater levels at the mid-21st century vary greatly. Under moderate or wet climate scenarios, and in parts of the aquifer that are well connected to surface water, little to no additional drawdown is anticipated. Under dry or warm scenarios, drawdowns of as much as 10 meters or more are possible in parts of the aquifer that are relatively disconnected from surface water. Under dry or warm scenarios, the portion of the Delta with greater than 60 feet of saturated thickness could be reduced from near 100 percent currently (2018) to 80–90 percent by mid-century. Future simulations with the model could include alternative management scenarios to identify options for improving groundwater sustainability. The automated model construction workflows are designed to facilitate regular updating, making this a “living” framework that the Mississippi Department of Environmental Quality and other stakeholders can use for adaptive management going forward.

## Introduction

The Mississippi Embayment region is a historical bay of the Gulf of Mexico that extends southward from the confluence of the Ohio and Mississippi Rivers (fig. 1) to the gulf shoreline. The embayment was formed by crustal down-warping during the Cretaceous period (for example, Saucier, 1994; Van Arsdale and Cox, 2007). Subsequent sedimentation during the Tertiary period created the deposits that now constitute part of the Mississippi Embayment aquifer system. The Mississippi Alluvial Plain (abbreviated “MAP” in associated products; for example, Alhassan and others, 2019) is a broad, nearly flat region within the Mississippi Embayment that encompasses the historical floodplain of the Mississippi and Ohio Rivers, extending from their modern confluence to the Gulf of Mexico (Woods and others, 2004; fig. 1). The Mississippi River Valley alluvial aquifer consists of the Quaternary alluvial sediments within the alluvial plain that overly the older Tertiary deposits of the embayment. The Mississippi Delta (also referred to as “the Delta”) can be defined as the part of the alluvial plain that runs through Mississippi (fig. 2).

## 2 Simulating Groundwater Flow in the Mississippi Alluvial Plain with a Focus on the Mississippi Delta

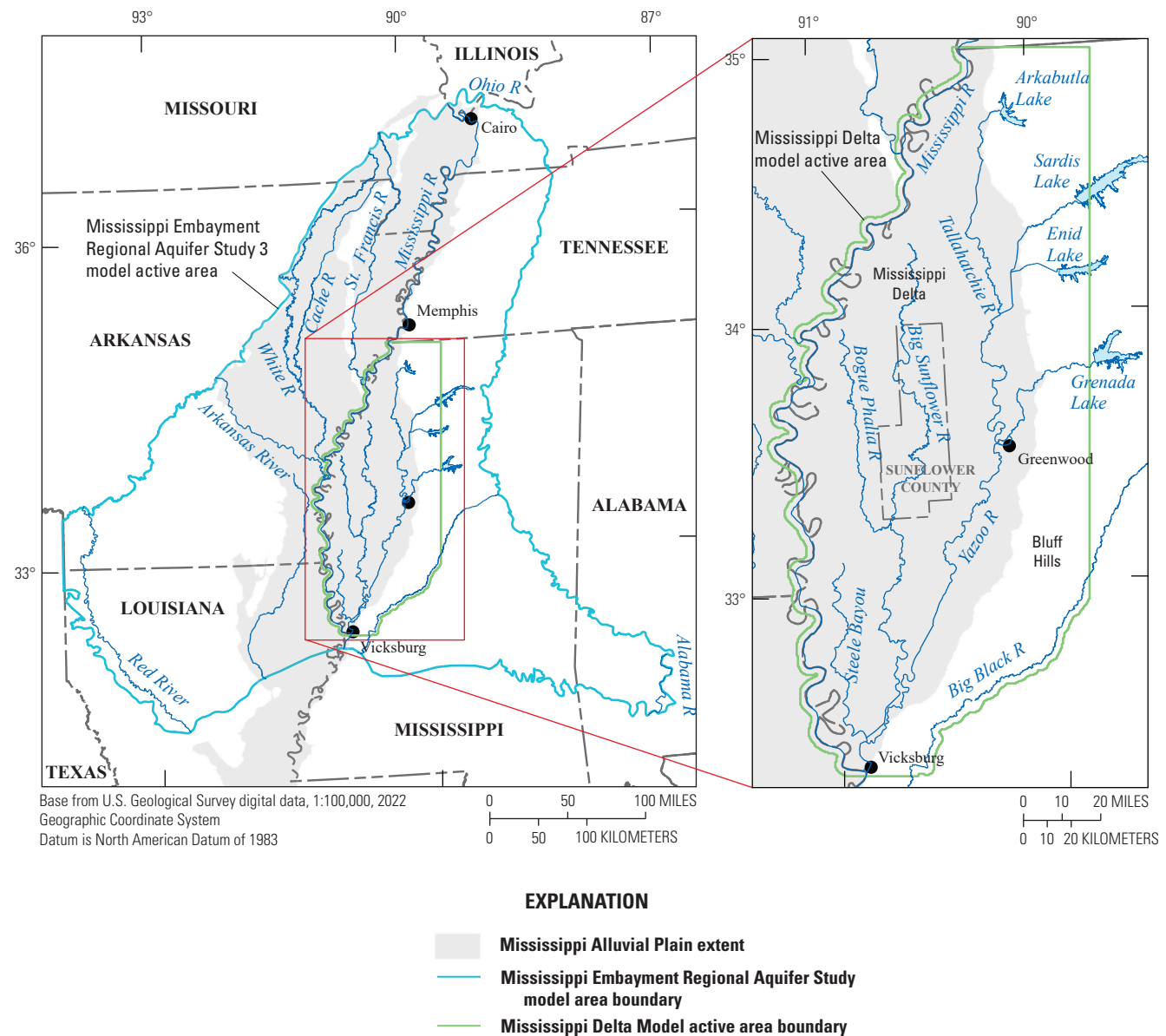


**Figure 1.** Extents of the Mississippi Embayment Regional Aquifer Study (MERAS 3) and Mississippi Delta groundwater models.

The Mississippi Alluvial Plain has become one of the most important agricultural regions in the United States, and it relies heavily on a groundwater system that is poorly understood and shows signs of substantial change. The heavy use of the available groundwater resources has resulted in significant declines in groundwater-levels and base-flows in streams within the alluvial plain (Arthur, 2001; Barlow and Clark, 2011; Clark and others, 2013; Haugh and others, 2020b). These effects are limiting well production and threatening future water availability for the region (Czarnecki and others, 2003; Barlow and Clark, 2011). More than 12 billion gallons per day of groundwater are withdrawn on average for irrigation to support agricultural production across the alluvial plain (Lovelace and others, 2020).

Groundwater-level declines are most notable in the Cache and Grand Prairie regions of Arkansas and in the Mississippi Delta (fig. 2; Clark and others, 2013; Haugh and others, 2020b).

The largest agricultural region within Mississippi is the northwestern Mississippi River alluvial plain, locally referred to as the “Delta” (Economic Research Service, 2010). About 1,710 million gallons per day (Mgal/d) of water are withdrawn from the Mississippi River Valley alluvial aquifer in Mississippi, which makes it the most heavily used aquifer in the State (Lovelace and others, 2020). Although the alluvial aquifer has a large reserve, it is finite, and evidence indicates declining water levels especially in the central Delta region (fig. 2; Arthur, 2001; Barlow and Clark, 2011; Haugh and others, 2020a; McGuire and others, 2021a). Water-level declines have also decreased baseflow in many Delta streams, most notably

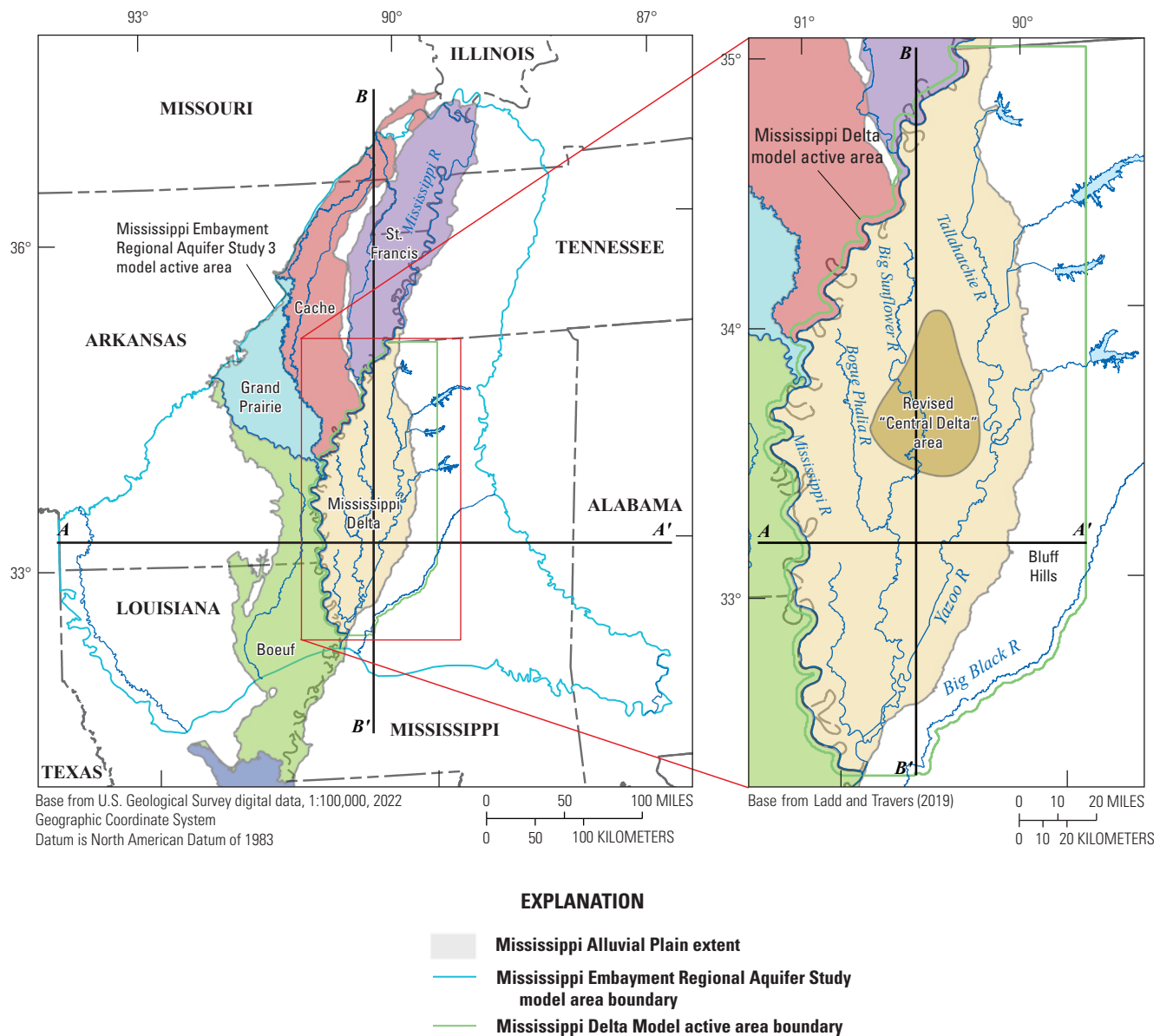


**Figure 2.** Generalized regions of the Mississippi Alluvial Plain. Modified from Ladd and Travers (2019).

in the Big Sunflower River (Barlow and Clark, 2011, p. 6), to the extent that in the absence of rainfall or irrigation return flow, some stream reaches can now run dry during the summer months (Barlow and Clark, 2011, p. 6).

The U.S. Geological Survey (USGS) Water Availability and Use Science Program (WAUSP) is supporting a regional groundwater availability study of the Mississippi Alluvial Plain to provide stakeholders and managers with information and tools to better understand and manage groundwater resources. The study focus is on quantifying the status of the groundwater system in the alluvial plain and determining how groundwater resources respond to development.

## Previous Work

Previous investigations of groundwater flow in the Mississippi Embayment as part of the USGS Gulf Coast Regional Aquifer System Analysis studies include Arthur and Taylor (1990, 1998), which focused on describing the hydrogeologic framework and groundwater flow in the Tertiary System, and Ackerman (1989, 1996), which described groundwater flow in the Mississippi River Valley alluvial aquifer. These models simulated groundwater flow in the Tertiary System from 1886 to 1987 and in the alluvial aquifer from 1906 to 1987 using a uniform grid with cells of 5 miles on each side. Arthur (2001) modeled transient groundwater flow in the alluvial aquifer in the Mississippi Delta area from

## 4 Simulating Groundwater Flow in the Mississippi Alluvial Plain with a Focus on the Mississippi Delta

January 1988 to December 1996, with a uniform grid with cells of 1 mile on each side, to help determine the capacity of the aquifer for continuing agricultural growth.

As part of the Mississippi Embayment Regional Aquifer Study (MERAS), Hart and others (2008) improved the hydrogeologic framework of the area. Clark and Hart (2009) and Clark and others (2011) modeled the Mississippi River Valley alluvial aquifer and the Tertiary System in a single groundwater flow model (referred to here as the “MERAS 1 model”) to quantify groundwater availability throughout the Mississippi Embayment. The MERAS 1 model simulated groundwater flow from 1870 to 2007 in 13 layers using a uniform grid with cells of 1 mile on each side. Clark and others (2013) improved MERAS 1 (MERAS 2.0 model) and used it to evaluate potential future water-level conditions. Additionally, Barlow and Clark (2011), Clark and others (2011), and Haugh (2012, 2016) all used the MERAS model to evaluate future water withdrawal scenarios. Haugh and others (2020a) extended the MERAS 2 model simulation through 2014 (MERAS 2.1) to evaluate water management scenarios in the Mississippi Delta; furthermore, Hunt and others (2021) updated the MERAS 2 model with the Newton-Raphson solver in MODFLOW–NWT (Niswonger and others, 2011) and an increased density of simulated streams for a study focused on the alluvial aquifer in the Delta (MERAS–NWT).

Each of these modeling efforts showed significant changes in the water budget and flow system because of increased groundwater pumping over time. In all studies, the sources of water to meet pumping demand included recharge, streamflow leakage, and storage, but the relative contribution of water from each of these sources varied considerably in the previous models. In a study comparing satellite-derived estimates of storage changes in major U.S. aquifers with monitoring and modeling results (Rateb and others, 2020), the MERAS model had the largest discrepancy in simulated storage change compared to the satellite-derived estimates, which may indicate oversimulation of the contribution of water from storage to meet pumping demand. Water budgets from Hunt and others (2021; MERAS–NWT) indicated larger contributions of water from stream leakage than previous MERAS models, likely because of the increased density of simulated streams. Accurate characterization of the water balance in the Mississippi Alluvial Plain—especially the inflows to the groundwater system and the distribution of terrestrial recharge compared to leakage from streams—remains a key topic of interest.

## Limitations of Previous Models and Recent Advances

Use of the MERAS model for decision support in the Mississippi Delta is limited by a large number of computational cells, most of which are outside of the Delta. Additionally, most of the hydrostratigraphic units represented in the 13 layers of the MERAS model are not present

everywhere in the model domain. The MODFLOW–2005 framework (Harbaugh, 2005) used for the MERAS model requires layer continuity. Discretization approaches that use layers to represent individual units are thus required to include thin “pinch out” cells where the units are absent, which can contribute to solution instability and greatly increase the number of active cells. In previous versions of the MERAS models, these issues resulted in long runtimes of as much as 16 hours or more for the model spin up and history matching periods.

The MERAS and Arthur (2001) models were also limited by their representation of surface water and recharge. The MERAS 2 models represented recharge in piecewise-constant zones based on soil type and surficial geology, with temporal rates based on fractions of precipitation. Arthur (2001) used a single recharge zone for the entire Mississippi Delta, with rates also based on fractions of precipitation. Both the Arthur (2001) and the MERAS 2 model included only the largest streams as boundary conditions. Arthur (2001) represented streams using the River (RIV) Package, with monthly stages specified from measurements collected by the U.S. Army Corps of Engineers. Although the MERAS 2 models used the Streamflow-Routing (SFR) Package, seasonal variability in streamflow and stages was simplified to a temporal discretization of biannual stress periods. Surface water runoff was based on assumed fractions of precipitation and was not parameterized in the history matching process. Simulated stream stages, a key driver of groundwater/surface water interactions, were also not considered (Clark and Hart, 2009). Since the construction of the MERAS model, there has also been increasing recognition of the importance of groundwater/surface water interactions and the larger integrated water cycle in groundwater flow simulations. Although the importance of surface water to the groundwater flow system in the Mississippi Delta has long been recognized (for example, Arthur, 2001), its inclusion in these models was historically limited by available software and computing resources and accompanying standards of practice.

Recent software advances have facilitated the incorporation of more realistic processes in groundwater models in a way that is tractable for decision support. An enhanced solver for MODFLOW (MODFLOW–NWT; Niswonger and others, 2011) provides superior handling of dry model cells (Hunt and Feinstein, 2012), which facilitates better representations of aquifer storage. The Soil-Water-Balance (SWB; Westenbroek and others, 2018) code provides a more representative simulation of groundwater recharge using an easy-to-use, physics-based approach that estimates net infiltration past the root zone, surface water runoff, and crop water demand on a cell-by-cell basis. SFRmaker (Leaf and others, 2021) automates the construction of realistic surface water input to the MODFLOW SFR Package from existing hydrography data such as NHDPlus (McKay and others, 2012). Machine learning techniques have allowed for monthly surface water inflows from other basins to be reliably estimated from climate and drainage basin characteristics (Dietsch and others, 2022).

Finally, since the creation of the original MERAS model structure (Clark and Hart, 2009), there has been extensive new data collected in the Mississippi Embayment, including the largest airborne electromagnetic (AEM) survey flown in the United States to date (Minsley and others, 2021), waterborne electrical resistivity profiling of streambed sediments in major streams (Miller and others, 2016), improvements in water use metering and estimation (for example, Wilson, 2021), and detailed simulation of the terrestrial water balance (Nielsen and Westenbroek, 2023).

Although some of these updates were incorporated into the existing MERAS framework by Hunt and others (2021), the MERAS–NWT model had long runtimes (greater than 6 hours) because of simulating the entire embayment and an abundance of thin cells. The MODFLOW 6 groundwater modeling framework (Langevin and others, 2017) allows for discontinuous layering in the context of a regular grid via “vertical pass-through cells.” This capability, along with more efficient solution techniques, can produce faster model runtimes that are critical for effective decision support (for example, Doherty and Moore, 2020).

## Modeling Goals and Approach

This study sought to produce updated groundwater models for quantifying current groundwater resources in the Mississippi Alluvial Plain and potential responses to future conditions, including expansion of agriculture, water conservation, climate change, and water supply mitigation. The work here focuses on the Mississippi Delta region. A key objective of the updated models was to leverage the previously mentioned advances in modeling techniques and software and synthesize the many new data and analyses produced by the larger USGS Mississippi Alluvial Plain Project. A secondary goal was to achieve faster runtimes to maximize model usefulness for decision support. Finally, automation was used in the model construction workflows to facilitate rapid refinement of local areas within the model domain and rapid model updating for new forecasts in response to new data or new questions or areas of interest.

Unlike previous studies that focused on a single model covering the entire Mississippi Embayment, the work here uses a simplified, faster-running model of the MERAS footprint (fig. 1) that can be used to produce specified flux boundary conditions for more detailed inset models of local areas. This updated MERAS model (MERAS 3.0 or MERAS 3; also referred to in this report as the “regional model”) uses a horizontal discretization of 1 kilometer (km; Clark and others, 2018a) and a vertical discretization of three layers. A more detailed inset model of the Mississippi Delta region (Mississippi Delta model or “Delta model”) with 500-m horizontal discretization and 21 layers was inset within the regional model solution using specified flux boundaries. Both models

were created using MODFLOW 6 (version 6.3.0; Langevin and others, 2022). Detailed information on the discretization and construction of these models is included in [appendix 1](#).

Python packages were developed (Leaf and Fienien, 2022; Leaf and others, 2021) to robustly automate the construction of the regional model and any inset model within the MERAS footprint. A stepwise approach (Haitjema, 1995) was taken starting with an easily achievable model configuration and adding features such as surface water runoff or denser parametrization as needed to better fit observed time series of groundwater levels, stream flows, and stream stages. Parametrization of model inputs was done using the `PstFrom` automated framework in `pyEMU` (White and others, 2021), which allows parametrization schemes at different scales (for example, adjusting hydraulic conductivity via pilot points or by zone) to be rapidly implemented and tested. History matching for parameter estimation was done using the iterative ensemble smoother (iES) algorithm implemented `PEST++` version 5 (White and others, 2020). The iES method generates a stochastic ensemble of model input parameter configurations (conditioned on observations) that calculates probabilistic model uncertainty.

## Purpose and Scope

This report documents the construction of the conceptual model and the construction and history matching of the MERAS 3 and Mississippi Delta models; formulation of the numerical models from preexisting data and data produced by other components of the USGS MAP project; history matching methods and results; simulated water budgets, groundwater levels and groundwater/surface water interactions; and the development and results of baseline forecast scenarios under varying potential future climates.

## Study Area Description and Hydrogeologic Setting

The MERAS 3 model of the Mississippi Embayment covers the same footprint as previous MERAS model versions, about 200,000 square kilometers (km<sup>2</sup>) in parts of eight States: Alabama, Arkansas, Illinois, Kentucky, Louisiana, Mississippi, Missouri, and Tennessee (fig. 1). From its apex at the confluence of the Mississippi and Ohio Rivers in southern Illinois, the embayment broadens southward to about the 32nd parallel and from the Red River near the Louisiana–Texas state line eastward to the Alabama River in southwestern Alabama. The embayment is approximately bisected by the Mississippi River. The inset model area includes almost 20,000 km<sup>2</sup> in an area in northwestern Mississippi locally referred to as “the Delta.” The Delta extends roughly 300 km from the Mississippi–Tennessee border at Memphis, Tennessee, to Vicksburg, Mississippi, and is about 100 km wide at the

## 6 Simulating Groundwater Flow in the Mississippi Alluvial Plain with a Focus on the Mississippi Delta

latitude of Greenwood, Miss. The present meander belt of the Mississippi River forms the western boundary of the Delta. The inset model area extends about 5 km from the west bank of the river to include the Mississippi River meander belt ridge. The loess-capped Bluff Hills form the eastern boundary of the Delta. The inset model area extends beyond the eastern extent of the Delta nearly to Grenada Lake to the east and the Big Black River to the southeast (fig. 1).

Several large streams drain the embayment, with most of the streams in the Mississippi River system including the St. Francis River in Arkansas and Missouri, the White and Arkansas Rivers in Arkansas, and the Yazoo and Big Black Rivers in Mississippi. Tributaries of streams that flow separately into the Gulf of Mexico drain an area in the southeastern corner of the embayment. The Yazoo-Yalobusha-Tallahatchie-Yocona-Coldwater River system drains the eastern part of the Delta and a large upland area to the east of the alluvial plain. The Sunflower-Bogue Phalia River system drains most of the central and western part of the alluvial plain outside of the Mississippi River levee system. All the water drained by the Sunflower-Bogue Phalia River system originates within the Delta and flows into the Yazoo River to the north of Vicksburg, Miss.

### Climate

The region has a humid subtropical climate, with mean annual temperature ranging from about 15.5 degrees Celsius (°C) at Cairo, Illinois, in the north to 19.4 °C at Vicksburg, Miss., in the south (Alder and Hostetler, 2013) and mean annual precipitation ranging from about 122 centimeters per year (cm/yr) in the north to about 142 cm/yr or more in the south (for example, Clark and others, 2011; Reitz and Kress, 2019). Precipitation is generally highest in the winter and spring and lowest in later summer or early fall (Alder and Hostetler, 2013). Droughts are not uncommon during the summer and fall (Cushing and others, 1964).

### Hydrostratigraphy

The Mississippi Embayment is a southward-plunging syncline with an axis primarily paralleling the present-day Mississippi River except where the axis curves around structural uplifts in southeastern Arkansas-northwestern Louisiana and southwestern Mississippi (Hart and others, 2008). Sedimentary deposits within the embayment generally dip and thicken towards the syncline axis and southward. Initial folding associated with the Ouachita orogeny during the Paleozoic Era was later deepened with additional downwarping and downfaulting associated with sedimentation during the Cretaceous period, creating the Mississippi Embayment (Hosman, 1996; Saucier, 1994). Subsequent cyclic advances and retreats of Cretaceous seas deposited mostly marine sediments throughout the embayment, creating the base for ensuing Tertiary and Quaternary deposits (Arthur and Taylor, 1998,

Hosman, 1996; Saucier, 1994). Pleistocene glaciation resulted in incision of the Mississippi River Valley by glacial melt-water flowing towards the Gulf of Mexico. As sea level rose, sediments filled the entrenched valley, forming the Mississippi River Valley alluvial aquifer.

The primary hydrogeologic units in the MERAS area include the 10 units described by Hart and others (2008). Table 1 in Clark and Hart (2009) shows a comprehensive depiction of the major units and their relation to local hydrostratigraphy and MERAS model layers. Together, the following units constitute the Mississippi Embayment aquifer system: the Quaternary Mississippi River Valley alluvial aquifer (alluvial aquifer), and underlying Tertiary-aged units: (the Vicksburg-Jackson confining unit, the upper Claiborne aquifer, the middle Claiborne confining unit, the middle Claiborne aquifer [also referred to as the Sparta aquifer in many places; for example Fitzpatrick and others (1990)], the lower Claiborne confining unit, the lower Claiborne aquifer, the middle Wilcox aquifer, the lower Wilcox aquifer, and the Midway confining unit). In this report, the term “Tertiary aquifer system” is used to differentiate the Tertiary units below the alluvial aquifer from the “Mississippi Embayment aquifer system,” which may include the alluvial aquifer. The alluvial aquifer consists primarily of gravel and sand deposits, and the middle Claiborne aquifer consists primarily of sand, silt, and clay deposits (Clark and others, 2011). The upper and middle Claiborne aquifers are bounded above and below by confining units in most places. The lower Claiborne-upper Wilcox aquifer and the middle and the lower Wilcox aquifers are not separated by confining units. The lower Claiborne confining unit and the lower Claiborne aquifer undergo a facies change and merge into the middle Claiborne aquifer in the northern part of the embayment model area (Hart and others, 2008).

Throughout much of Mississippi because of a facies change, the lower part of the lower Claiborne confining unit is the Winona-Tallahatta aquifer, which includes the greenish-gray, siliceous, sandy claystone of the Tallahatta Formation of Claiborne Group and the glauconitic, fossiliferous, medium- to coarse-grained sandstone of the Winona Sand of Claiborne Group (Spiers, 1977; Mancini and Tew, 1994; Clark and Hart, 2009). The sandy deposits of the three Wilcox aquifers are more heterogeneous than the other Tertiary units and consist of a highly variable arrangement of massive to thinly bedded sand and thin clay beds (Renken, 1998). The middle Wilcox aquifer differs substantially from the upper and lower Wilcox aquifers because its thin beds of sand and clay result in lower hydraulic conductivity than that of the massive, more permeable units above and below it (Renken, 1998). The middle and lower Wilcox aquifers, however, are undifferentiated throughout most of Arkansas and Louisiana (Clark and Hart, 2009). In parts of Tennessee and Mississippi, the lower Wilcox aquifer may be separated into two units, the lower Wilcox aquifer and the Old Breastworks confining unit (Clark and Hart, 2009), with the Old Breastworks Formation of Wilcox Group

consisting of clay, silt, and lignite (Warwick and others, 1997). The lower Wilcox aquifer is the bottommost Tertiary aquifer within the embayment (Lloyd and Lyke, 1995).

Both the Vicksburg-Jackson and the Midway confining units consist of massive clay beds. In the southern part of the embayment, the Vicksburg-Jackson confining unit separates the embayment aquifer system from the overlying coastal lowlands aquifer system (Weiss, 1992). The top of the Midway confining unit forms the base of the embayment aquifer system, separating the aquifers in sediments of Tertiary age from underlying aquifers of Cretaceous age.

## Conceptual Model

The groundwater flow system, including the Mississippi River Valley alluvial aquifer and underlying Tertiary units down to the Midway confining unit top, was analyzed at two scales. The regional scale encompasses the MERAS footprint (fig. 1) and is intended to provide boundary conditions for inset groundwater flow models that focus on individual subregions or locations. The inset model described here focuses on groundwater flow in the Mississippi Delta.

## Terrestrial Water Balance

The terrestrial water balance describes the partitioning of precipitation input into evapotranspiration, near-surface runoff to streams, and net infiltration past the root zone that ultimately becomes groundwater recharge. Average annual precipitation ranges from about 122 cm/yr in the north to about 142 cm/yr or more in the south (for example, Clark and others, 2011; Reitz and Kress, 2019). Evapotranspiration (ET) accounts for about 65 percent of the terrestrial water balance (Reitz and Kress, 2019). Previous estimates of average annual groundwater recharge have ranged from near 0 to 14.5 cm/yr, with values of around 5 cm/yr or less being common (for example, Broom and Lyford, 1981; Arthur and Taylor, 1990; Arthur, 2001; Reed, 2003; Clark and Hart, 2009). More recent studies by Reitz and Kress (2019), Hunt and others (2021), and Westenbroek and others (2021) have estimated higher values of around 10–13 cm/yr (about 8 percent of the water balance). It should be noted that the estimate of Westenbroek and others (2021), produced by SWB, denotes net infiltration past the root zone and not actual recharge to the water table (see also Nielsen and Westenbroek, 2023). Some net infiltration may discharge laterally to streams through perched aquifer systems or as interflow, resulting in a lower amount of recharge to the regional aquifer.

The remainder of precipitation—27 percent by Reitz and Kress's (2019) estimate—runs off to streams. A key question for groundwater sustainability in the Mississippi Embayment and especially the Mississippi Delta is the amount of water that ultimately reaches the water table as recharge. Given the small size of the recharge component relative to

evapotranspiration and surface water runoff and that recharge is estimated via water balance closure, small errors in evapotranspiration or surface water runoff could result in large errors in estimated recharge (for example, Reitz and Kress, 2019).

## Groundwater Balance and Water Use

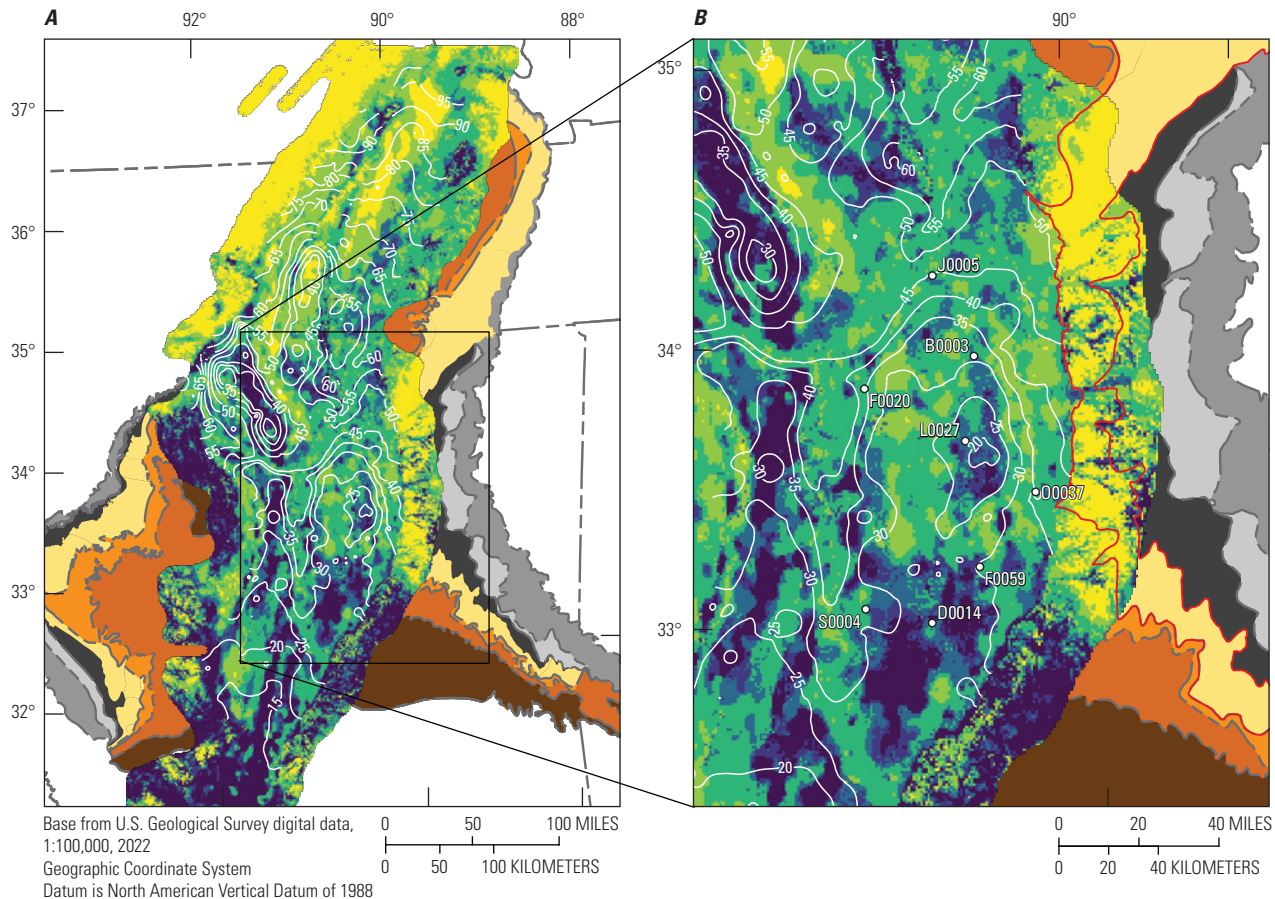
The groundwater system is fed primarily by terrestrial recharge. Stream leakage during periods of high stage and along major rivers that originate outside of the Mississippi Embayment constitutes an important secondary source of water, especially in localized areas. Groundwater within the Mississippi Alluvial Plain discharges primarily to pumping wells. Along the margins of the Mississippi Embayment, a greater part of groundwater discharges to streams.

Agricultural water use in the Mississippi Embayment varies widely depending on the year, location and crop, but is heavily concentrated in the alluvial plain (for example, Wilson, 2021). Irrigation accounts for most groundwater use: 87 percent or more in the alluvial plain (Clark and others 2011) and 97 percent of water use in the Mississippi River Valley alluvial aquifer (Lovelace and others, 2020). Estimates of average annual irrigation in the alluvial plain range up to 100 cm, with areal average values (including nonirrigated lands) of around 23–25 cm (Bristow and Wilson, 2023; Westenbroek and others, 2021). On irrigated lands, average annual irrigation estimates range from about 28 to 43 cm (Westenbroek and others, 2021). Annual irrigation for a single year can vary from the mean by as much as 50 percent depending on precipitation (Wilson, 2021).

The large amount of pumping relative to recharge has resulted in a loss of groundwater from storage and a chronic decline in water levels in many parts of the alluvial plain since at least the 1940s (see, for example, Barlow and Clark, 2011; or the water level record at National Water Information System [NWIS] site 333959090435001 near Cleveland, Miss.).

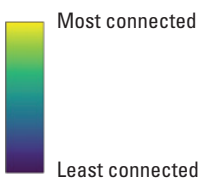
## Effects of Surficial Geology on Groundwater

Previous mapping efforts (for example, McGuire and others, 2021a) indicate a correspondence between drawdown of groundwater levels within the alluvial plain and the presence of fine-grained, low-permeability deposits near the land surface. The surficial geology of the alluvial plain is complex and highly variable, ranging from coarse sands and gravels deposited by stream channels to fine-grained materials deposited in backwater areas. Stream channel meandering through time has produced variability with depth in addition to the spatial variability apparent in the recent AEM survey (Minsley and others 2021; fig. 3). Saucier (1994) provides a more detailed description of the depositional history and plates of mapped surficial geology. McGuire and others (2021a) provide detailed maps of current groundwater levels throughout the alluvial plain and its subregions.

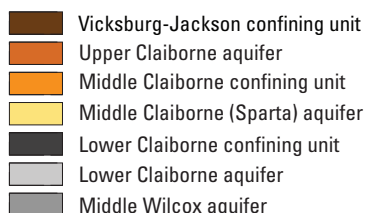


## EXPLANATION

## Airborne electromagnetic-derived surficial connectivity



## Mississippi Embayment Regional Aquifer Study hydrostratigraphic unit



— 26 — **Potentiometric contour**—Shows altitude at which water level would have stood in tightly cased wells, 2022. Contour interval is 5 meters. Datum is North American Vertical Datum of 1988

— Sparta subcrop

D0014      Mississippi Delta "priority" wells of interest and identifier

**Figure 3.** Surficial connectivity classifications developed by Minsley and others (2021), with mapped groundwater levels (McGuire and others, 2021a). *A*, at the scale of the Mississippi Embayment Regional Aquifer Study area. *B*, inset of the Mississippi Delta region.

Figure 3 shows surficial connectivity classifications developed by Minsley and others (2021) based on the thickness of low electrical resistivity layers detected in the AEM survey within the upper 15 meters (m) of sediment. Yellow colors indicate high electrical resistivities near the surface, which are interpreted to indicate a lack of fine-grained, low-permeability materials and therefore a strong connection between the surface and regional water table that can more readily transmit recharge or stream leakage. Purple colors indicate a high thickness of low electrical resistivity (and presumably low permeability materials) and therefore a poor

connection between the surface and regional water table. The patchy, linear patterns in the classification zones that parallel the course of the Mississippi River reflect shifting depositional environments through time in response to stream channel meandering.

In contrast, the underlying Tertiary sediments that subcrop along the margins of the embayment (orange and gray colors) are relatively continuous because of their marine origin. Higher permeability units such as the Sparta Sand (part of the Middle Claiborne aquifer) that subcrop at the land surface can provide important sources of recharge to the regional

aquifer (for example, Arthur, 2001); for example, in [figure 3B](#) the parts of the Bluff Hills underlain by the Sparta Sand (outlined in red) are apparent in the AEM results as having high surficial connectivity.

Where present, fine-grained deposits at the land surface serve to limit terrestrial recharge and interactions between surface water and the regional groundwater system. Conversely, coarse-grained materials at the surface may allow for focused groundwater recharge and especially leakage from perennial streams. Inspection of the potentiometric surface ([fig. 3B](#)) indicates a correspondence between low groundwater levels and low surficial connectivity. Fine-grained deposits at intermediate depths between the rooting zone and water table may allow for perched aquifer or variably saturated interflow systems that intercept net infiltration past the root zone and convey it to nearby streams, effectively bypassing the regional groundwater system. In times of high stream stages, such systems may also accept bank storage (leakage) from streams and later return the water to the streams in times of low stage. Such perched systems are difficult to simulate numerically in a regional groundwater model and therefore present a key challenge to effective simulation of the flow system as they create conditions of apparently high recharge and base flow that are inconsistent with regional groundwater levels. Examples of such systems in the Mississippi Embayment may include the L'Anguille River in Arkansas, which flows perennially yet originates in an area where the regional water table is too deep for the alluvial aquifer to provide any discharge, and the central part of the Big Sunflower River in Mississippi, which supports local groundwater levels that are often 6 m above the regional water table, as indicated at NWIS site 333251090323801 (USGS, 2021).

Finally, thick low-permeability deposits near the surface may create locally confined conditions and therefore locally higher drawdown because of the smaller amounts of water released by confined storage (aquifer compression) compared to unconfined storage (aquifer drainage). As indicated by [figure 3B](#), the presence or absence of low permeability deposits near the surface may have a controlling influence on the groundwater flow system.

## Regional Groundwater Flow System

Although the MERAS area receives streamflow input from many regional watersheds outside of the model domain, groundwater flow across its perimeter is assumed to be negligible because of the presence of the Midway confining unit near the surface (Clark and Hart, 2009) or assumed to be limited to local areas such as the interface with the Ozark System (Clark and others, 2018b). Within the MERAS area, groundwater generally flows from topographically high (and relatively low water use) areas along the margins towards the lower-lying streams and pumping centers within the interior of the embayment including the alluvial plain and the Mississippi Delta. Regional groundwater flow from the Tertiary system

may enter the alluvial aquifer laterally through shallow flow paths or vertically through deeper flow paths where the bottom of the alluvial aquifer overlies aquifer units such as the Sparta Sand and Cockfield Formation of Claiborne Group (part of the Middle Claiborne and Upper Claiborne aquifers, respectively; for example, Minsley and others, 2021; Arthur, 2001).

Water-level declines have altered the flow system by reducing groundwater discharge to streams and in many cases reversing the hydraulic gradient such that streams that previously drained the alluvial aquifer now provide recharge on average through stream leakage (for example, the Big Sunflower system in Mississippi; Clark and others, 2011; Arthur, 2001). Flow directions have also been altered. In large parts of the Mississippi Delta and alluvial plain regions of Arkansas, groundwater that previously flowed towards streams now flows inward towards regional cones of depression (McGuire and others, 2021a; Clark and others, 2011; Arthur, 2001). In theory, declining groundwater levels in these areas reduce the aquifer thickness available to transmit water, which can in turn increase the loss of water from storage in a nonlinear feedback loop. Observed water level declines thus far have been mostly linear, with the exception of recent wet years in the mid to late 2010s that have slowed declines or produced rebounds in some areas (for example, NWIS site 333742090303801 [L0027] in Sunflower County, Miss.; [fig. 3](#)), indicating that groundwater sustainability in the alluvial plain may depend at least in part on future precipitation patterns.

In addition to multi-decadal trends, groundwater flow and groundwater/surface water interactions in the Mississippi Embayment and especially the alluvial plain are highly transient on a seasonal basis (see for example, Arthur, 2001). Stream hydrographs are generally flashy because of the high ratio of surface runoff to recharge. As a result, even moderately sized streams such as the Big Sunflower River near Merigold, Miss. (NWIS site 07288280), can experience swings in stage of as much as 10 m or more over periods of days to months. At any given point in time, groundwater/surface water exchanges are controlled by the stream stage relative to groundwater levels in the underlying aquifer. Precipitation events can cause stream leakage as stage rises more rapidly than surrounding groundwater levels. Subsequently, groundwater discharge to streams can occur if groundwater levels are high and stage subsides more rapidly. Conversely, dry conditions that would otherwise be base-flow dominated in unaltered areas can produce stream leakage to groundwater where groundwater levels are chronically below the stream stage and ultimately cause streams to run dry at times (for example, Barlow and Clark, 2011). In other instances, streams perched above the water table may be supported during dry periods by agricultural return flows, bank storage and local perched aquifer systems, or groundwater-derived base flows from headwater areas.

## Groundwater Flow in the Mississippi Delta

Similar to other parts of the alluvial plain, the groundwater system in the Mississippi Delta receives water from terrestrial recharge through surficial sediments, stream leakage, and regional groundwater flow. The Mississippi River forms a hydraulic boundary along the western side that fully penetrates the alluvial aquifer although some localized underflow through the Tertiary units may be possible. The Tallahatchie/Yazoo system forms a major hydraulic boundary near the eastern edge. All other streams within the Delta originate within its boundaries. The Tallahatchie/Yazoo system is fed by four flood control reservoirs (Arkabutla, Sardis, Enid, and Grenada Lakes; [fig. 1](#)) in the Bluff Hills, which are managed to store water from large events (thereby dampening discharge peaks downstream) and release water during lower flow periods. Together, outflows from the flood control reservoirs account for approximately one third of the flow in the Yazoo River at the Redwood, Miss., streamgage (NWIS site 07288800). Regional groundwater flow into the Delta mostly comes from the Bluff Hills and areas to the east. Although the Tallahatchie/Yazoo river system intercepts at least some of this flow, it also likely acts as a source of recharge in many areas, especially in the central part of the Delta where the rivers run over coarse surficial deposits (for example, Minsley and others, 2021).

The area of drawdown in the central part of the Mississippi Delta receives groundwater flow from all directions. In predevelopment times, this flow would have drained to the Big Sunflower and Bogue Phalia Rivers (Arthur, 2001). Current water levels, however, are mostly below the beds of these streams; most groundwater flow in this area therefore discharges to irrigation wells.

Previous work has suggested that the overall net flow of water between the alluvial aquifer and Mississippi River is small, with large inflows from the Mississippi River during periods of high stage approximately balanced by large outflows to the river during periods of low stage (Arthur, 2001).

## Aquifer Thickness and Hydraulic Properties

Within the MERAS footprint, the Mississippi River alluvial sediments mostly range from 25 to 50 m thick, with an average thickness of about 39 meters (see Minsley and others, 2021 for a map of thickness). In the Mississippi Delta, the saturated thickness of the alluvial aquifer averages about 34 m. Literature values for hydraulic conductivity in the alluvial aquifer generally range from tens of meters per day up to about 200–300 meters per day, reflecting bulk averages at the scale of groundwater models (for example, 1 square mile [ $\text{mi}^2$ ] cells; Arthur, 2001; Reed, 2003; Clark and Hart, 2009; Clark and others, 2013) or testing in wells completed in the productive intervals of the alluvial sediments (for example, Pugh, 2022; James Hoffman, Mississippi Department of Environmental Quality, written commun., 2020). As noted previously, the Mississippi River alluvial sediments are highly

heterogeneous, ranging from coarse gravel channel deposits to very fine backwater deposits. Local values of hydraulic conductivity could therefore be substantially higher or lower than the literature estimates. In general, hydraulic conductivities of the fine-grained backwater deposits are not well characterized.

The Tertiary deposits below and adjacent to the alluvial aquifer vary greatly in thickness throughout the MERAS footprint, from thin to absent along the margins to more than 1,000 meters thick in the central and southern areas of the domain. As noted previously, the Tertiary deposits are thought to be less heterogeneous within mapped units, but widely varying in permeability between units. Literature values of hydraulic conductivity from previous modeling studies range from less than 1 meter per day in the confining units to about 40 meters per day in parts of the Middle Claiborne aquifer (Clark and Hart, 2009; Clark and others, 2013).

## Modeling Approach

Groundwater flow models were developed for the MERAS and Mississippi Delta areas. The MODFLOW 6 groundwater flow code (version 6.3.0; Langevin and others, 2022) was used with a Newton-Raphson formulation that handles drying and wetting of nodes, thus allowing for simulation of both confined and unconfined aquifer storage. The new MERAS version 3.0 model (MERAS 3) is a simplified, faster-running representation of the Mississippi Embayment aquifer system that is primarily aimed at providing boundary fluxes for more detailed inset models within the MERAS area, such as the Mississippi Delta model described in this study. The Mississippi Delta model (Delta model) is intended to focus on future groundwater sustainability in the Mississippi Delta region at a higher level of detail than what is feasible at the scale of the MERAS. Historical versions of each model simulate a “spin-up” period of 1900 through 2009 to represent historical pumping and drawdown of groundwater levels followed by a history matching period from 2010 through 2018 in which model parameters were adjusted to match model outputs to field measurements. Model parameters estimated from history matching were then applied to future scenario versions of the Mississippi Delta model, which are described in the “Future Climate Scenarios” section. Model files and reproducible model construction workflows are provided in an associated data release (Leaf and others, 2023).

## Model Domains and Discretization

An extensive description of the model construction is given in [appendix 1](#); a simplified version is presented here. The spatial extents for the MERAS 3 and Mississippi Delta models are shown in [figure 1](#). The MERAS 3 model covers the same extent as previous MERAS models (Clark and Hart, 2009; Haugh and others, 2020a; Hunt and others, 2021; [fig. 1](#)) at a 1-km uniform grid resolution that aligns with

the USGS National Hydrogeologic Grid (Clark and others, 2018b). Vertically, the MERAS 3 model consists of three layers that distill the regional aquifer system into three parts: the Mississippi River Valley alluvial aquifer (layer 1); a lumped confining unit consisting of the Vicksburg-Jackson confining

unit, the Upper Claiborne aquifer, and the Middle Claiborne confining unit (layer 2); and a lumped lower aquifer (layer 3) that includes the Middle Claiborne aquifer and all underlying units in the Tertiary sequence down to the top of the Midway confining unit (fig. 4).

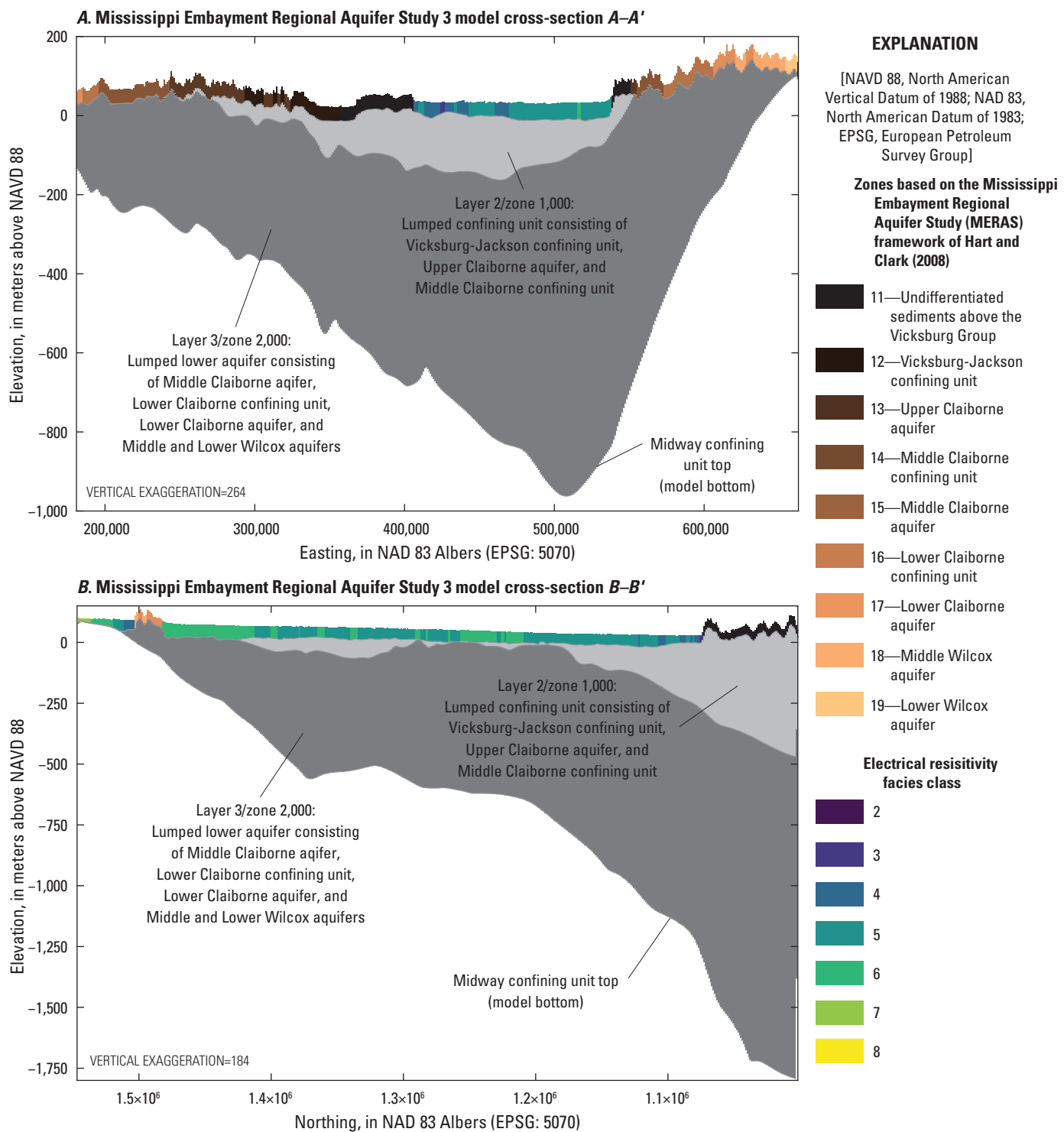


Figure 4. Regional model aquifer property zones. A, west to east. B, south to north. Cross section locations are shown in figure 2.

The Mississippi Delta model includes the geographic extent of the Mississippi Delta (fig. 1) and the outlets of the flood control reservoirs in the Tallahatchie/Yazoo River system at a uniform horizontal resolution of 500 meters that also is aligned with the National Hydrogeologic Grid (Clark and others, 2018b). Layering in the Delta model consists of uniform 5-m-thick layers down to the base of the alluvial aquifer (bottom of layer 8); uniform layering of expanding thickness below the alluvial aquifer bottom to the deepest extent of AEM data; and layer surfaces based on the hydrostratigraphic surfaces of Hart and others (2008) between the deepest AEM data and the top of the Midway confining unit (see [app. 1](#); [fig. 5](#)).

Time discretization for both models begins in 1900, with an initial predevelopment steady-state period (without pumping) followed by 6 multiyear stress periods extending to April 2007. The multiyear stress periods are structured to approximately align with step changes in the pumping history in previous MERAS models (Clark and Hart, 2009, fig. 10). Starting April 1, 2007, and extending to the history matching end time of January 1, 2019, the models have monthly stress periods of one timestep each (see [app. 1](#), [table 1.1](#)).

## Boundary Conditions

Boundary conditions in the MERAS 3 and Mississippi Delta models include terrestrial recharge originating from precipitation, groundwater/surface water interactions, and pumping fluxes representing water use. Similar to past MERAS models, MERAS 3 assumes a no-flow boundary around its perimeter. The Mississippi Delta model perimeter consists of transient fluxes extracted from the independent MERAS 3 model solution. Interior boundary conditions are summarized as follows (with more detail given in [app. 1](#)):

- Recharge to the groundwater system was simulated using the Recharge Package in MODFLOW 6; input to both models was based on net infiltration results from the SWB simulation by Nielsen and Westenbroek (2023).
- Rivers and streams were simulated using the SFR Package, except for the Mississippi and Big Black Rivers in the Mississippi Delta model, which were simulated using the River Package.
- Inflows to the stream network along the perimeter of the MERAS 3 model were derived from the random forest regression model by Dietsch and others 2022; in the Delta model, inflows from the four major flood control reservoirs (Arkabutla, Enid, Sardis, and Grenada Lakes) were developed from measured outflow data (Tim Rodgers, U.S. Army Corps of Engineers, written commun., March 19, 2020; Leaf and others, 2023).

- Average surface water runoff (as overland flow) to the stream network was estimated from the SWB simulation by Nielsen and Westenbroek (2023).
- Water use was simulated using the Well Package. Rates before April 2007 were developed from the MERAS 2.2 model (Haugh and others, 2020b). Agricultural water use for the monthly history matching stress periods (April 1, 2007, through 2018) was estimated using the Aquaculture and Irrigation Water-Use Model version 1.1. (AIWUM; Bristow and Wilson, 2023; Wilson, 2021). Nonagricultural rates for that period were developed from the USGS Site-Specific Water Use Data System and national estimates for water use associated with thermoelectric power generation in 2010 and 2015 (Diehl and Harris, 2014; Harris and Diehl, 2019a, b). Irrigation pumping estimates for 2019 and future years out to 2056 were based on crop water demand from the SWB simulation by Nielsen and Westenbroek (2023), and a future version of that simulation driven by downscaled general circulation (climate) model outputs (see the “Future Climate Scenarios” section).

## Subsurface Properties

Aquifer hydraulic conductivity and storage properties were represented structurally in the MERAS 3 and Mississippi Delta models at multiple scales using a blend of the conceptual models produced by the AEM survey by Minsley and others (2021) and the original MERAS framework by Hart and others (2008). In both models, aquifer properties were represented at the coarsest level using piecewise-constant zones based on the logarithmically binned electrical resistivity facies classes by Minsley and others (2021). In the MERAS 3 model, electrical resistivities were vertically averaged to develop zones for the single layer representing the alluvial aquifer. In both models, areas lacking AEM data were zoned based on the relation of their cell centers to the hydrostratigraphic surfaces of Hart and others (2008). Finer-scale variability in horizontal and vertical hydraulic conductivity and specific yield (in the AEM based zones only) was incorporated within zones using pilot points spaced every 5 km as described in [appendix 2](#). Initial streambed leakance input to the SFR Package was estimated on a cell-by-cell basis using results from waterborne surveys of subsurface electrical resistivity (Leaf, 2023; Adams and others, 2019; Killian, 2018). Additional details describing the generation of the subsurface properties and how they were parameterized for both models can be found in [appendix 2](#). Maps of the final aquifer properties for the models are also shown in [appendix 2](#).

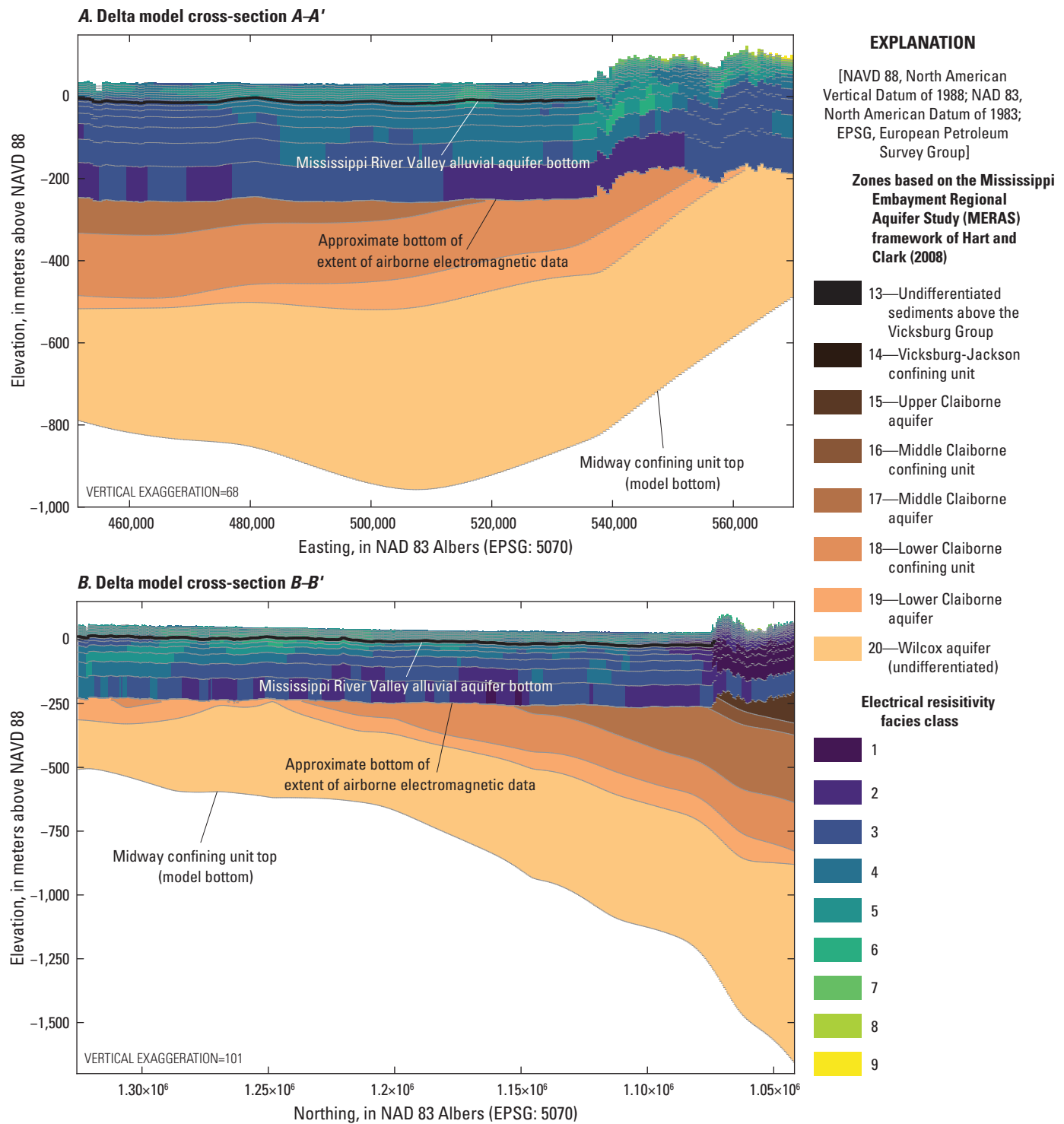


Figure 5. Mississippi Delta model aquifer property zones. A, west to east. B, south to north. Cross section locations are shown in figure 2.

## Parameter Estimation and Uncertainty Analysis

After constructing the models, parameter estimation was performed via history matching (for example, Anderson and others, 2015, chap. 9). The models were parameterized to allow for systematic adjustments to their inputs in response to model fit to field observations (history matching). A more detailed description of the parameter estimation methods and results is given in [appendix 2](#). The overall approach to history matching is similar to that of Corson-Dosch and others (2022).

Parametrization of the models followed a multiscale approach as described in White and others (2021) and references therein. At the coarsest scale, piecewise-constant parameter values were estimated for zones covering large areas of the model. At successively finer scales, one or more multiplier parameters were then applied cumulatively on top of the coarse scale parameters. This approach apportions model input uncertainty at different scales, which can improve history matching, reduce overfitting and improve detection of model error phenomena such as parameter compensation (White and others, 2021). For example, the coarse scale parameters address large-scale biases in the model input, while the finer multipliers can address the effects of local-scale heterogeneity. Setup of the multiscale parametrization was enabled by the `PstFrom` routines in the `pyEMU` Python package (White and others, 2016; White and others, 2021).

Horizontal hydraulic conductivity, hydraulic conductivity vertical anisotropy, specific storage, specific yield, aquifer recharge, surface runoff and specified inflows to the SFR Package, streambed leakance, and water use (pumping) were all parametrized. Coarse-scale parameters included piecewise-constant zones representing spatial scales ranging up to the extents of the models. Intermediate scale parameters included multipliers on the parts of individual zones within a layer or within a geographic area. Fine-scale parameters included pilot points and stream-reach multipliers at approximately the kilometer scale, and temporal multipliers that applied to certain boundary conditions within a stress period. [Table 2.2](#) provides a summary of the model parametrizations.

Field observations of aquifer heads and stream flows were processed into multiyear or monthly averages corresponding to model stress periods. An objective function consisting of the sum of squared weighted residuals between observed values and their simulated equivalents (phi) was assembled. Observations were initially weighted based on measurement uncertainty, and grouped by observation type (heads, flows, etc.), geographic area and other criteria ([table 2.1](#)). Subsequently, observation weights in each group were multiplied together to achieve a desired balance in the objective function that resulted in an acceptable model fit to the primary observations of interest.

Initial trial-and-error model runs focused on manual adjustment of coarse-scale parameters to improve history matching and gain insight about the key aspects of the groundwater flow system. The iES algorithm implemented in PEST++ (White, 2018; White and others, 2020) was then used

to formally estimate both coarse- and fine-scale parameters. In the iES, an ensemble of parameter sets (realizations) is carried through the analysis. At each step, empirical correlations between the parameter ensemble and changes in observation values are used to iteratively improve model fit to observations while constraining the parameter values (reducing uncertainty). The iES results therefore provide estimates of parameter uncertainty in addition to a minimum error variance set of “base” parameter values that can be used as a “best” parameter set.

Successful history matching required numerous iterations following a stepwise approach in which the iES was run, the results were evaluated, and the model structure, parametrization, observations, or observation weighting were adjusted in response to the results. In particular, the history matching focused on a set of “priority wells” that were distributed around the Mississippi Delta and familiar to cooperators, as well as the overall fit to all head observations, especially in the central Delta region of greatest drawdown ([fig. 2](#)). History matching was considered complete when a satisfactory fit was achieved to head observations with a coherent mass balance, reasonable stream stages, and reasonable model input values that were consistent with the conceptual model(s) for the Mississippi Delta and larger Mississippi Embayment region.

## Results and Discussion

Over successive iterations of history matching, several key aspects of the model and parameter estimation formulation were identified. Given the project goal of reducing model runtimes, early versions of the models experimented with abbreviated “spin-up” periods, where the simulations were started in the 1980s or 1990s, with greater amounts of pumping applied before 2007 to reproduce the observed drawdowns. Ultimately, truncations to antecedent conditions imparted undesirable artifacts on the history matching, and the best results were achieved by starting the simulations in a “predevelopment” steady-state condition (without pumping) in the year 1900.

Accurate representation of surface water boundary conditions was also found to be important. Early versions of the models focused on base flows in streams—a common groundwater modeling strategy in areas where base flows are primarily derived from groundwater. In much of the Mississippi Embayment and especially the Mississippi Alluvial Plain, however, streamflow is dominated by streamflow generation upstream from the model domain, surface water runoff, and intermediate or interflow processes that potentially include local perched groundwater and bank storage. During low-flow periods, streamflow in many areas may also be sustained in part by irrigation return flows. In recognition of this, total stream flows were incorporated using the random forest regression model by Dietsch and others (2022) for external inflows and the runoff estimates by Nielsen and Westenbroek

(2023). Although this improved results, a low bias remains in the stream flows simulated by the model, because the SWB runoff estimates do not account for the aforementioned intermediate flow processes or agricultural return flows. Informal incorporation of stage observations in the history matching process, along with the SFR Package stream depth corrections described by Leaf (2023), helped ensure accurate representation of transient gradients (and therefore flows) between groundwater and surface water.

The best fits and most realistic parameter fields were achieved with multiscale parametrization that allowed for both coarse- and fine-scale adjustments to the model inputs. Assuming a suitable model structure, coarse-scale parameters (for example, piecewise-constant zones or dataset-wide multipliers) that affect many model inputs can help the iES reduce large-scale biases in the model inputs while fine-scale parameters controlling individual pilot points or stream reaches can reduce localized errors and limit the spread of parameter compensation (for example, White and others, 2021).

Specifically, incorporating pilot points (Doherty, 2003) for aquifer properties (especially hydraulic conductivity) and recharge helped improve simulation of observed drawdowns in the central Delta area by allowing for variability within the lithology-based zones that often covered much of the model area. The pilot points were most effective when interpolation between them was allowed across zone boundaries instead of being compartmentalized to within zones. At a larger scale, incorporation of the surficial connectivity zones of Minsley and others (2021; [fig. 3](#)) and subdividing these zones by region ([fig. 2.3](#)) also appeared to greatly help the iES achieve a satisfactory fit to heads in the central Delta area, presumably through the larger phi changes produced by simultaneous adjustment of multiple stream reaches or larger flow quantities compared to independent adjustment of individual stream reaches or pilot points.

Finally, like any model, the MERAS 3 and Mississippi Delta models imperfectly represent complex and ultimately unknowable natural systems. As a result, parameter estimation involved tradeoffs where improving fit in one area of the model came at the expense of fit (or at least phi) in other areas. Observation weighting can be key to prioritizing the most salient aspects of the hydrologic system (Doherty and Hunt, 2010) that best capture the processes relevant to the predictions of interest (in this case future declines in groundwater levels, especially in the Mississippi River Valley alluvial aquifer). During history matching, it became apparent that the MERAS 3 model could not match heads well in the Sparta/Middle Claiborne aquifer ([fig. 2.6](#)). This could be because of important local hydrogeologic features such as confining units and faults (for example, Clark and Hart, 2009; McKee and Clark, 2003) that are not well represented in the current three-layer structure of the MERAS 3 model or misallocation of irrigation pumping between the alluvial aquifer and Sparta systems, which is not well characterized in Arkansas (McKee and Clark, 2003). Incomplete representation of municipal and industrial pumping around Memphis and southern Arkansas

could also explain some of the model bias in these areas. Given the focus of this study on the Mississippi Delta and the alluvial aquifer, head observations in the Tertiary units were excluded from the MERAS 3 history matching to avoid unrealistic parameter compensation that could bias the flux outputs extracted for inset models (see for example the discussion of prior data conflict in White and others, 2021). Future work may seek to improve the representation of the Tertiary system in MERAS 3. For weighted head observations in the alluvial aquifer, a root mean squared error (RMSE) of 3.40 m was achieved with the selected base ensemble member from the second iteration of the iES run. This compares favorably to a previous RMSE of 4.31 meters reported by Clark and others (2013) for alluvial aquifer observations in the MERAS 2.0 model.

The best history matching results for the Mississippi Delta model were achieved by giving higher importance to absolute heads, especially in the central Delta area and “priority wells” group, as well as “head trend” observations that captured the average rate of head change. For weighted head observations, an RMSE of 2.07 m was achieved with the selected base ensemble member from the second iteration of the iES run. This represents a 67-percent reduction in RMSE compared to the value of 6.31 m reported by Haugh and others (2020a) for the MERAS 2.1 model in the Mississippi Delta region.

## History Matching Results

History matching results are described in detail in [appendix 2](#); for brevity, only time series of observed and simulated heads and streamflows of interest in the Mississippi Delta (simulated by the Delta model) are shown here.

In general, heads at the priority wells of interest are well matched in terms of absolute water levels and the seasonal fluctuation between high water levels in April and low October water levels at the end of the growing season ([fig. 6](#)). The “base” member of the ensemble shows the results from the best-fit parameter set, and the remaining ensemble members show the possible spread (or uncertainty) in the simulation results. Differing degrees of influence from surface water can be seen in these hydrographs from sites scattered around the Delta geographically ([fig. 2.1](#)). The two Sunflower County wells (L0027 and B0003; [figs. 6B, 6C](#)) are respectively near the center and edge of the central Delta area of greatest drawdown ([figs. 2 and 3](#)) and are relatively distant from surface water influence. A lack of surface water connection because of a surficial confining unit ([fig. 3](#)) is thought to be a key driver of drawdown in this area. Water levels at these sites exhibit less seasonal variability than other wells such as O0037 ([fig. 6G](#)), and the spread of water levels simulated by the ensemble is wide, indicating differing degrees of surface water connection allowed by the different parameter sets. Identifying a suitable parametrization structure and parameter values to match observed drawdowns in this area posed a key challenge

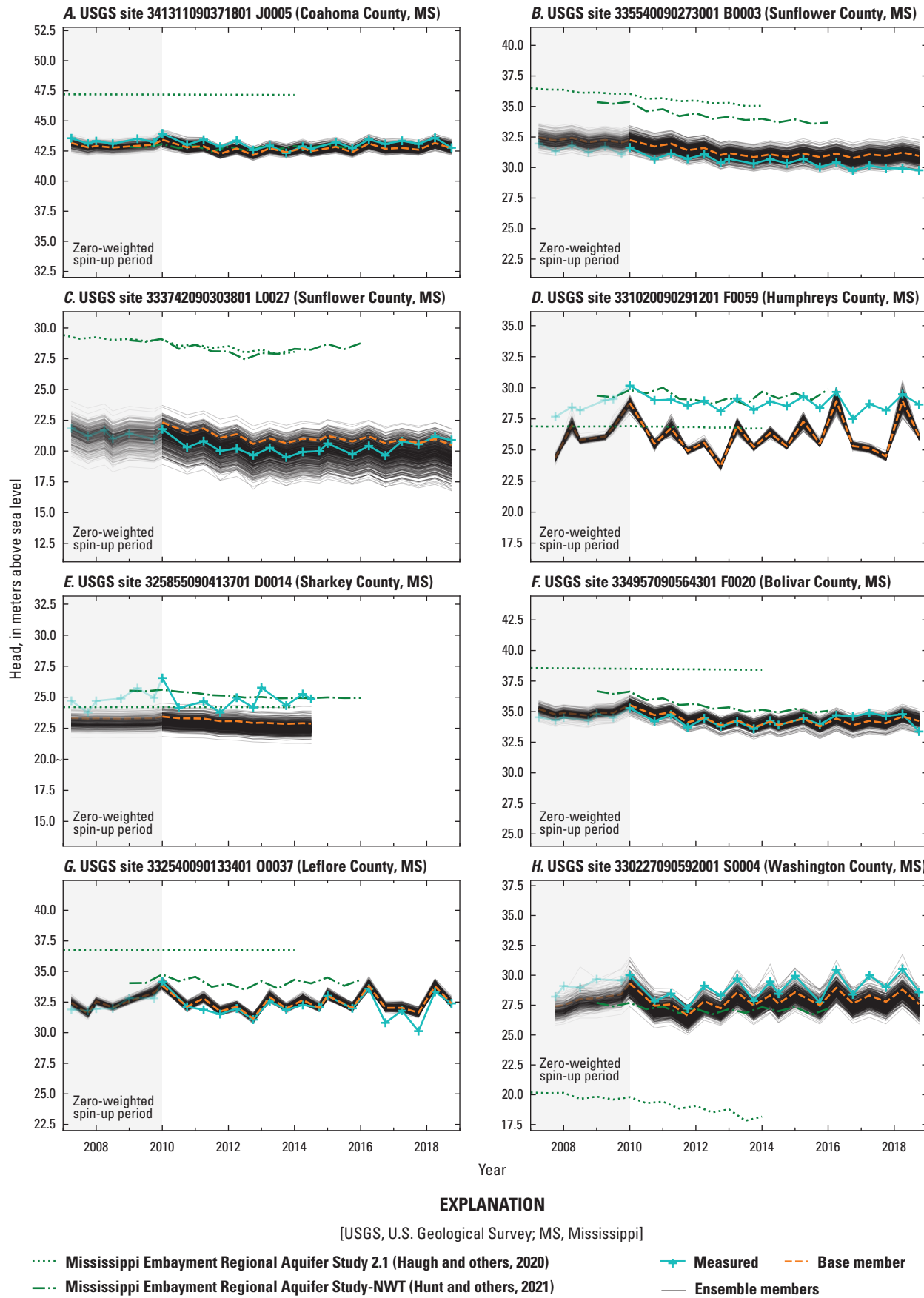


**Figure 6.** Times series of measured heads and simulated equivalents at selected wells of focus (“priority\_wells” group; see figure 2.1 for locations).

in past studies too as indicated in [figure 6B](#) and [6C](#) where there is a larger difference between the green lines (from the MERAS 2.1 and MERAS–NWT models by Haugh and others [2020a] and Hunt and others [2021]) and the measured values.

In contrast, the Leflore County (O0037; [fig. 6G](#)) and Humphreys County (F0059; [fig. 6D](#)) sites illustrate strong connections with surface water. Drawdown at these two locations is minimal, with heads close to the average levels of nearby surface water. Experimental model runs indicated that the fit for the Leflore site was mostly controlled by the streambed leakance in nearby reaches of the Yazoo River, which is approximately 500 m away (and 100 m above the open interval for O0037). As a result, the hydrograph for this well exhibits more seasonal influence from the river but also is well fit by the model. Variability in the ensemble results is low at this site because simulated stages are similar across all members. The Humphreys site is similar; it is only 250 m away from the Yazoo River (with a shallow screen), but there is a greater mismatch between the simulated and observed time series, indicating a structural defect in the model at this location. In other words, an essential process driving the hydrograph at this site is apparently not captured in the model.

The Bolivar County site (F0020; [fig. 2.1F](#)), which is about 9 km from the Mississippi River and about 4 km from the Bogue Phalia River, represents an in-between condition that is relatively well matched by the model. A somewhat wider set of ensemble results here indicates variability in hydraulic conductivity and recharge parametrization across the ensemble members.

[Figure 7](#) shows time series of monthly mean observed stream flows and their simulated equivalents for 2007 through 2018 for six priority streamflow gages in the Delta area. The “base” member of the ensemble shows the results from the best-fit parameter set, and the remaining ensemble members show the possible spread (or uncertainty) in the simulation results. Streamflow observations were not weighted highly in the history matching ([table 2.1](#)) because of incomplete representation of key streamflow generating processes in the model including the approximate nature of the runoff estimates from SWB, missing intermediate processes including perched groundwater, interflow and bank storage, and lack of information on agricultural return flows and their contributions to base flow during low-flow periods. Logarithmic y-axes are provided here to better illustrate match across the full range of stream flows.

The general agreement between simulated and observed values seen in all the plots indicates a realistic stream water balance in the model; however, the missing streamflow generating processes are evident in the bias towards undersimulation, especially in the low-flow periods within the three Sunflower River sites’ time series ([figs. 7A, 7B, 7C](#)). The Tallahatchie and Yazoo River time series ([figs. 7E, 7F](#)) have less undersimulation bias, because a substantial part of their flow (about 50 and 30 percent, respectively) comes from the Arkabutla, Enid, Sardis, and Grenada flood control reservoirs.

Outflows from the flood control reservoirs are measured daily by the U.S. Army Corps of Engineers and were specified in the model.

[Figure 8](#) shows time series of streamflow gain between three pairs of upstream and downstream locations and their simulated equivalents. In many streams, gains or losses of streamflow between sites can provide valuable integrated measurements of groundwater discharge to surface water and, ultimately, recharge into the groundwater system. In the Mississippi Delta, however, interpretation of streamflow gains or losses is less straightforward because of the confounding effects of poorly characterized intermediate runoff processes and an often small groundwater discharge component. In the case of the Sunflower River between sites 07288280 and 07288500 ([fig. 8A](#)), the river stage is mostly above the water table (indicating stream leakage to groundwater), but the difference in the monthly mean flows measured at the two sites generally indicates an increase in streamflow. Much of the increase is probably because of runoff from storm events that is included in the monthly means, but previously mentioned intermediate flow processes (perched groundwater and bank storage) and agricultural return flows may also be contributing to the gains. The measured record does show a few instances (for example, in early 2010 and 2011) of a net loss in flow between the two sites, but there are many more of these events simulated by the model, which is an artifact of the missing processes in the model. More frequent months of streamflow loss and the very low flows or drying simulated at 07288500 ([fig. 7C](#)) mean that any future flow conditions in the Sunflower River simulated by the model are probably conservative (less than what might be expected in reality for a given scenario).

The gain in flow across the Tallahatchie/Yazoo system downstream from the flood control reservoirs ([fig. 8B](#)) and the total outflow from Steele Bayou ([fig. 8C](#); which includes the Sunflower and Bogue Phalia Rivers) show that overall, the stream water balance is well represented in the model. Periodic sharp reversals in the measured flow record are associated with backwater periods, when high water levels in the Mississippi River cause water to flow upstream.

Average parameter estimates for the two models are generally consistent with previous work ([table 1](#)). A 24-percent higher simulated mean annual recharge for the Mississippi Delta model compared to Arthur (2001) may reflect relatively wet conditions during the history matching period, especially after 2012. Substantially lower recharge simulated in the MERAS 2.2 model (Haugh and others, 2020a,b) may reflect parameter compensation to limit excessive rise of the water table between sparsely represented streams (Leaf, 2023). Different storage values estimated for the MERAS 3 model compared to the Mississippi Delta model and other models may reflect local heterogeneity in the various storage mechanisms (pore drainage, confining unit leakage, and aquifer compression) that is not well resolved in the three-layer representation of the system. Vertical hydraulic conductivity is difficult to assess because it is not easily measured in the field and, more importantly, is scale dependent.

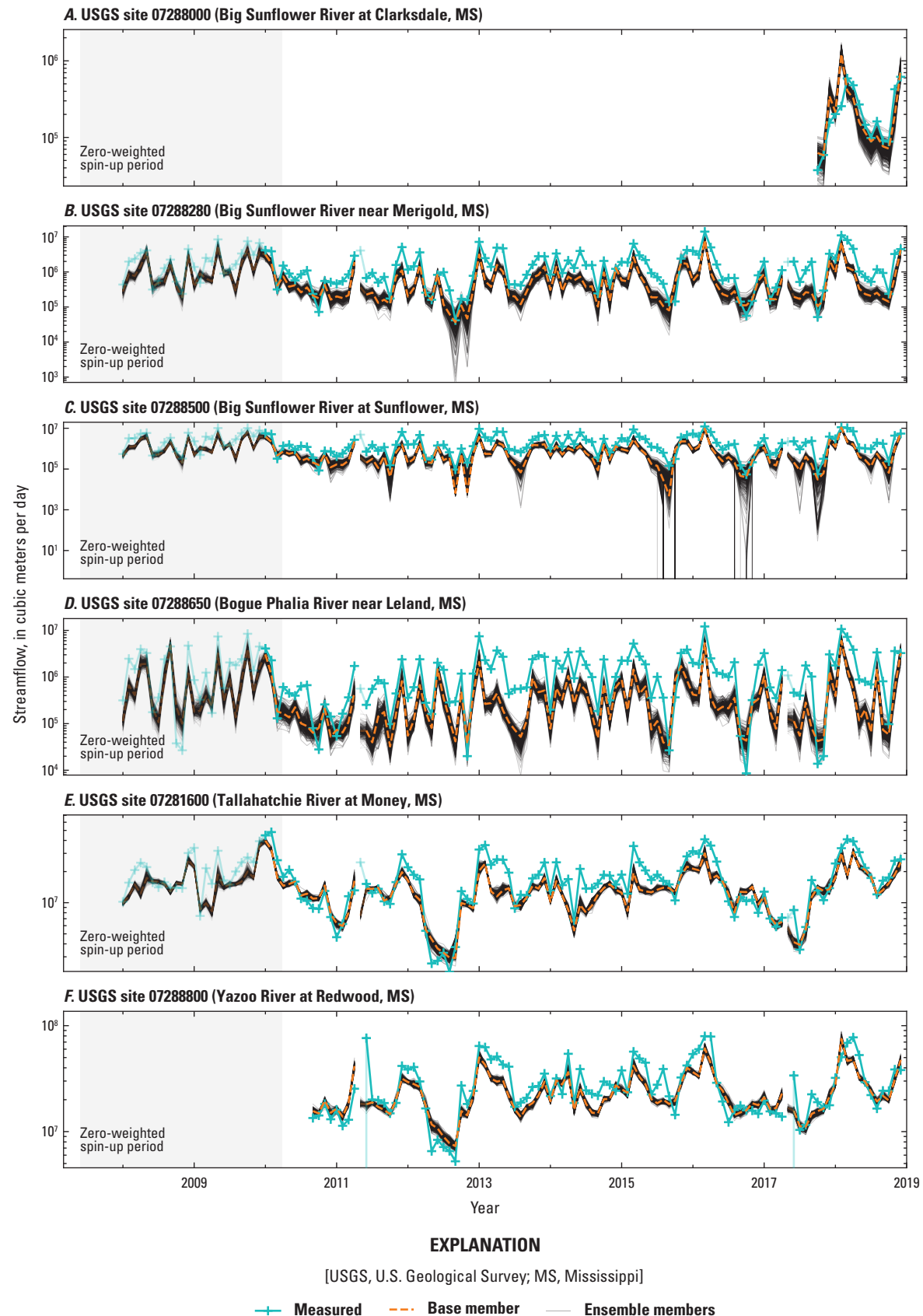


**Figure 7.** Times series of monthly averages of measured stream flows and simulated equivalents at selected stream gages.

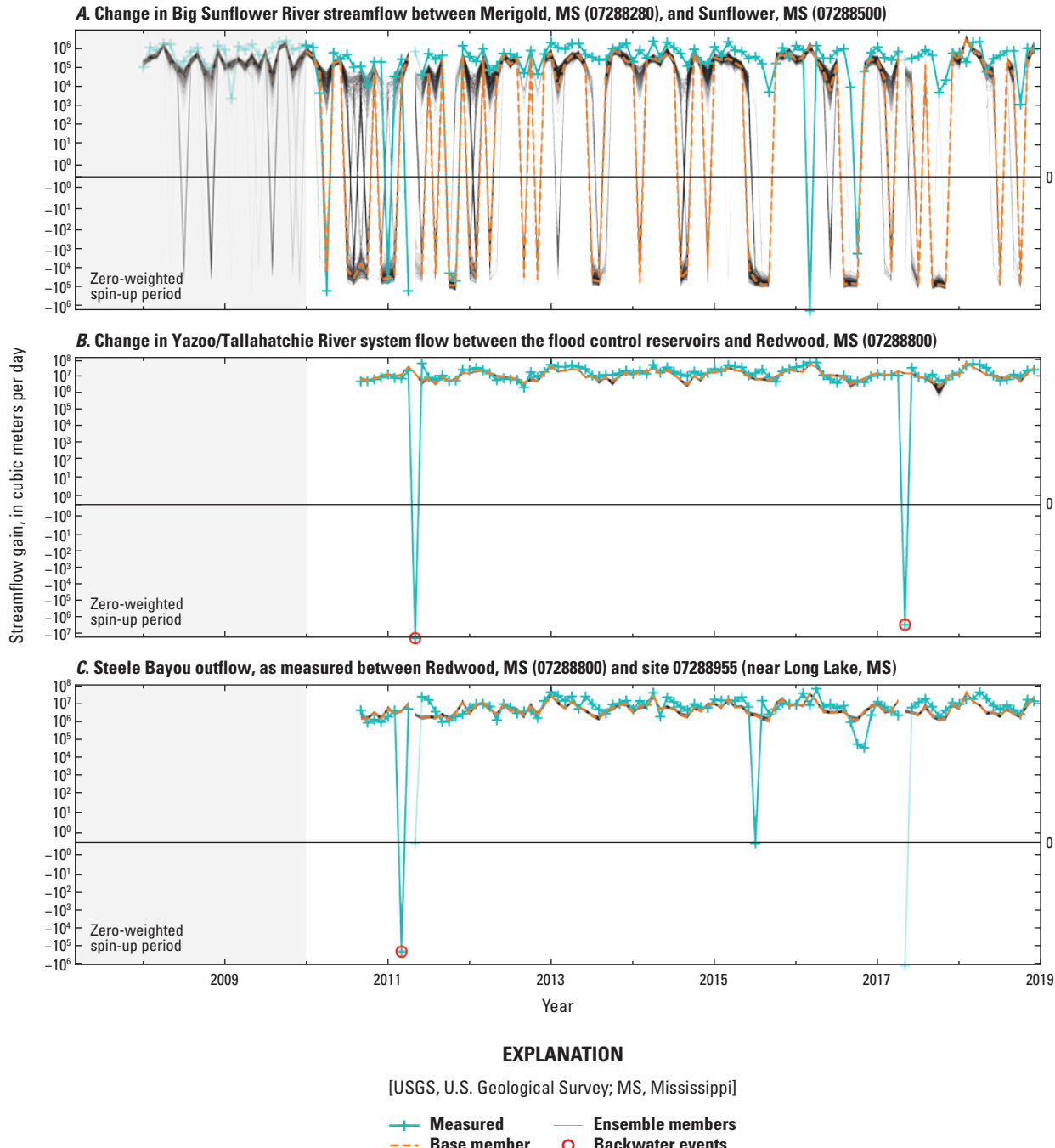


**Figure 8.** Times series of monthly averages of measured changes in streamflow between streamgages, and simulated equivalents.

## Historical Mississippi Delta Model Results

Results for the historical version of the Mississippi Delta model (before 2019) are presented here; selected results for the MERAS 3 model are presented in [appendix 3](#). [Figure 9](#) shows simulated water table elevations and groundwater/surface water interactions in the Mississippi Delta. Under relatively dry conditions such as those at the end of September 2016 ([figs. 9A, 9B](#)), when stream stages are low, many streams,

including the Mississippi River, receive groundwater discharge. Other streams are dry or leaking because the regional water table is below the streambed or stream stage. In the central Delta, streams generally always lose water to the alluvial aquifer, though they may intermittently receive groundwater discharge from perched water, including bank storage (which is not simulated in the model). Lighter shades of red or gray in this area indicate lower rates of stream leakage because of the intervening presence of the shallow confining unit. Under wet

**Table 1.** Comparison of average model input terms for the Mississippi Embayment Regional Aquifer Study (MERAS 3) and Mississippi Delta models with previous modeling studies.

[MERAS, Mississippi Embayment Regional Aquifer Study; --, not applicable]

Model input	MERAS 3 (this study) <sup>1</sup>	Mississippi Delta model (this study) <sup>1</sup>	MERAS 2.2 (Haugh and others, 2020a)	Arthur (2001)
Average horizontal hydraulic conductivity in the Mississippi River Valley alluvial aquifer, in meters per day <sup>2</sup>	108	127	66.2	130
Average specific yield in the Mississippi River Valley alluvial aquifer, unitless	0.19	0.29	0.30	0.32
Average horizontal hydraulic conductivity in the Tertiary system, in meters per day	14.7	23.5	13.2	--
Specific storage in the Tertiary system, geometric mean, per meter	$3.8 \times 10^{-5}$	$2.5 \times 10^{-6}$	$2.4 \times 10^{-6}$	--
Average annual recharge, in centimeters per year <sup>3</sup>	6.30	8.18	1.90	6.60

<sup>1</sup>Data are summarized from Leaf and others (2023).

<sup>2</sup>Average values are for model cells within the Mississippi Delta area.

<sup>3</sup>MERAS 3 and Mississippi Delta model recharge values are for 2007–18; MERAS 2.2 recharge is for 2007–14; Arthur (2001) recharge is for 1988–96.

conditions such as those at the end of February 2018 (figs. 9C, 9D), when stream stages are high, most streams leak water to the groundwater system, except for some streams in the Bluff Hills. Figure 3.1 shows similar results for the larger alluvial plain simulated by the MERAS 3 model.

Figure 10 shows average annual net groundwater budgets for the Mississippi Delta. The years before 2007 in figure 10A represent averages for the multiyear spin-up stress periods (table 1.1). Historically, streams in the Mississippi Delta were mostly gaining from groundwater flow (see fig. 10, 1900 and 1950 budgets), but pumping since the mid-twentieth century has shifted the balance to be more variable on an annual basis between net leakage and net discharge (see also fig. 11). In dry years, such as 2007, 2012, and 2010, the loss of aquifer storage can constitute a significant source of water to meet increased pumping demand and groundwater discharge to streams at low stages. Conversely, in wet years such as 2009 and 2018, some aquifer storage is replenished by increased recharge, stream leakage to groundwater, and reduced pumping demand. Over the long term, however, aquifer storage has declined, resulting in the observed drawdowns in groundwater levels. In recent years (since about 2012), declines in water levels have leveled off or even rebounded at some sites (for example, L0027 in Sunflower County and F0020 in Bolivar County; figs. 6C, 6F), presumably because of wetter-than-normal conditions leading to increased recharge and stream leakage and less irrigation pumping. The hydrographs in figure 6 show the model generally capturing this trend.

During the history matching period of 2010 through 2018, terrestrial recharge constituted the largest inflow component at 56.8 percent (fig. 10B) of the overall groundwater budget or 3.2 annual inches (fig. 2.20; see app. 2 for additional discussion of estimated recharge). Groundwater flow from the Bluff Hills was second at 34.9 percent and seems to be relatively steady in absolute terms across years. A 7.6-percent net inflow from aquifer storage indicates a net loss of aquifer storage through the history matching period. Groundwater/surface water interactions with interior streams (excluding the Mississippi River) were nearly balanced between groundwater discharge to streams and stream leakage to groundwater. Similar to previous studies (for example, Arthur, 2001), the net groundwater flow to the Mississippi River is close to zero. Note that the Mississippi River component here also includes potential underflow to or from Arkansas, which cannot be distinguished from flows to or from the Mississippi in the current modeling framework, but regardless, net groundwater flow to the Mississippi is most likely small on an average net basis.

Budget results from the SFR Package (fig. 11) of the Mississippi Delta model illustrate the sources of streamflow in the Mississippi Delta model. Outflows from the four flood control reservoirs to the Tallahatchie and Yazoo Rivers (external inflows term in fig. 11) constitute approximately one-third of all streamflow. Groundwater discharge makes up approximately 20.9 percent of the remaining streamflow generated within the model area, with the remaining 79.1 percent coming from various other runoff processes. Inspection of the SFR

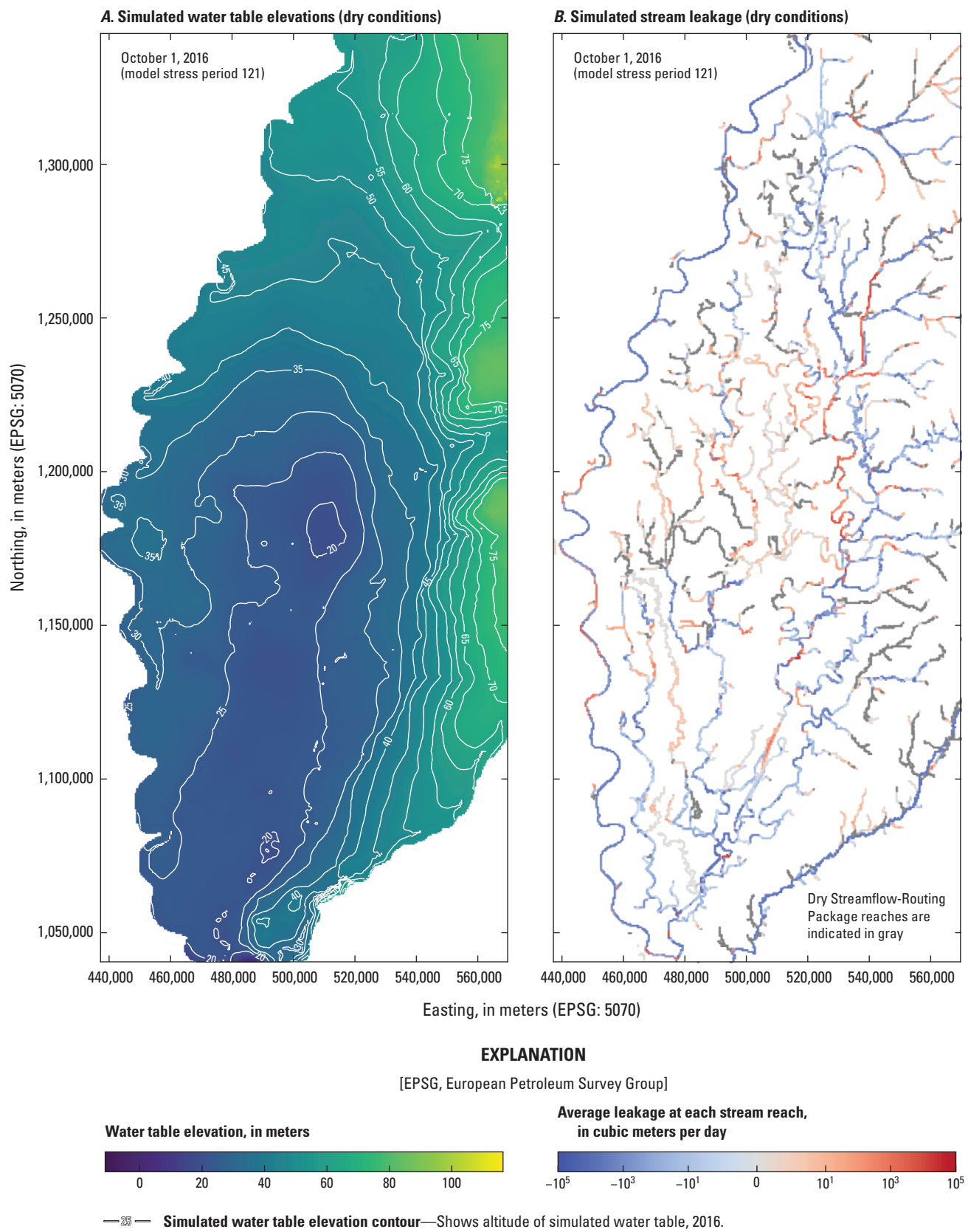


**Figure 9.** Water table elevations and stream leakage in the Mississippi Delta as simulated by the Mississippi Delta model under dry (A, B) and wet (C, D) conditions.

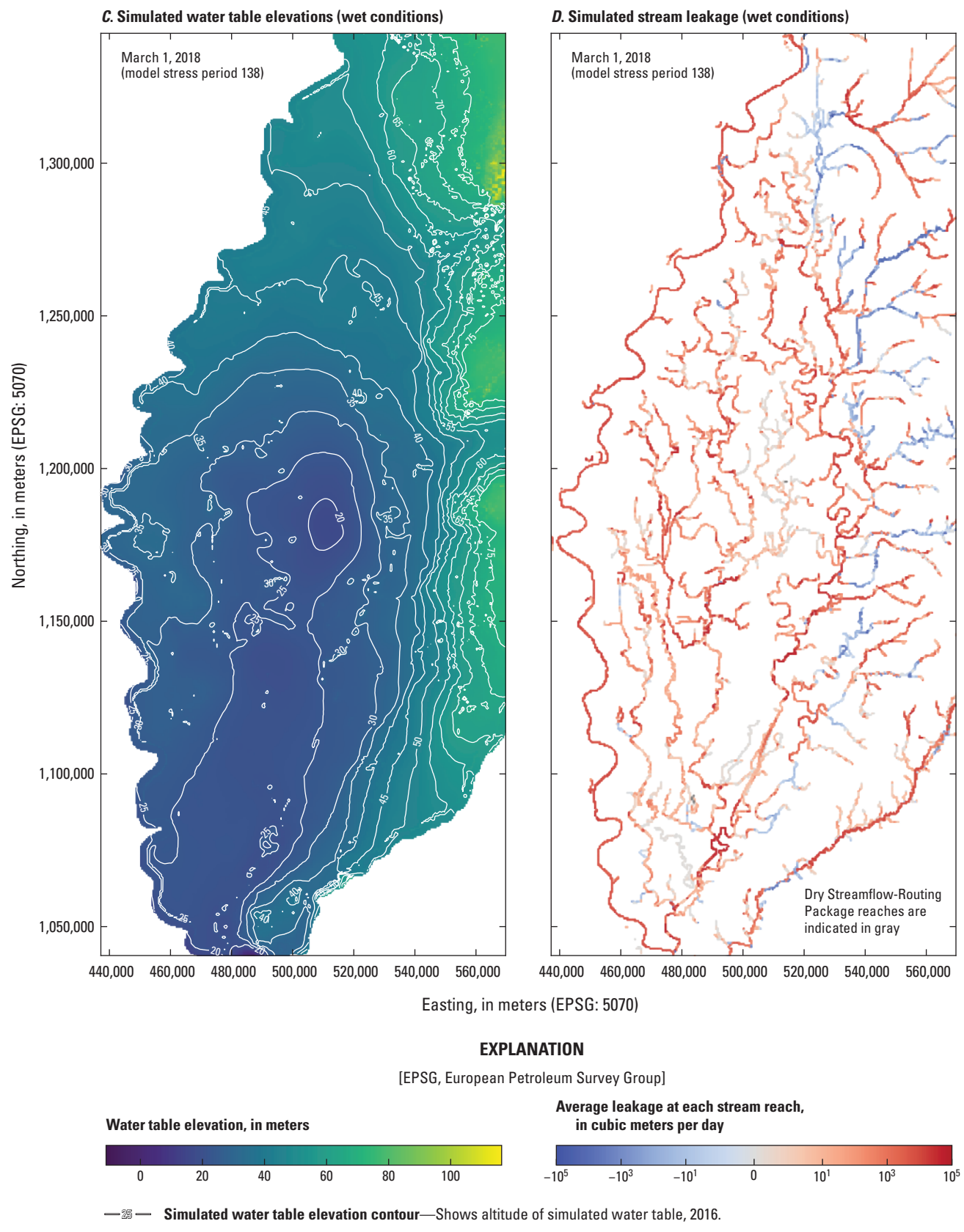
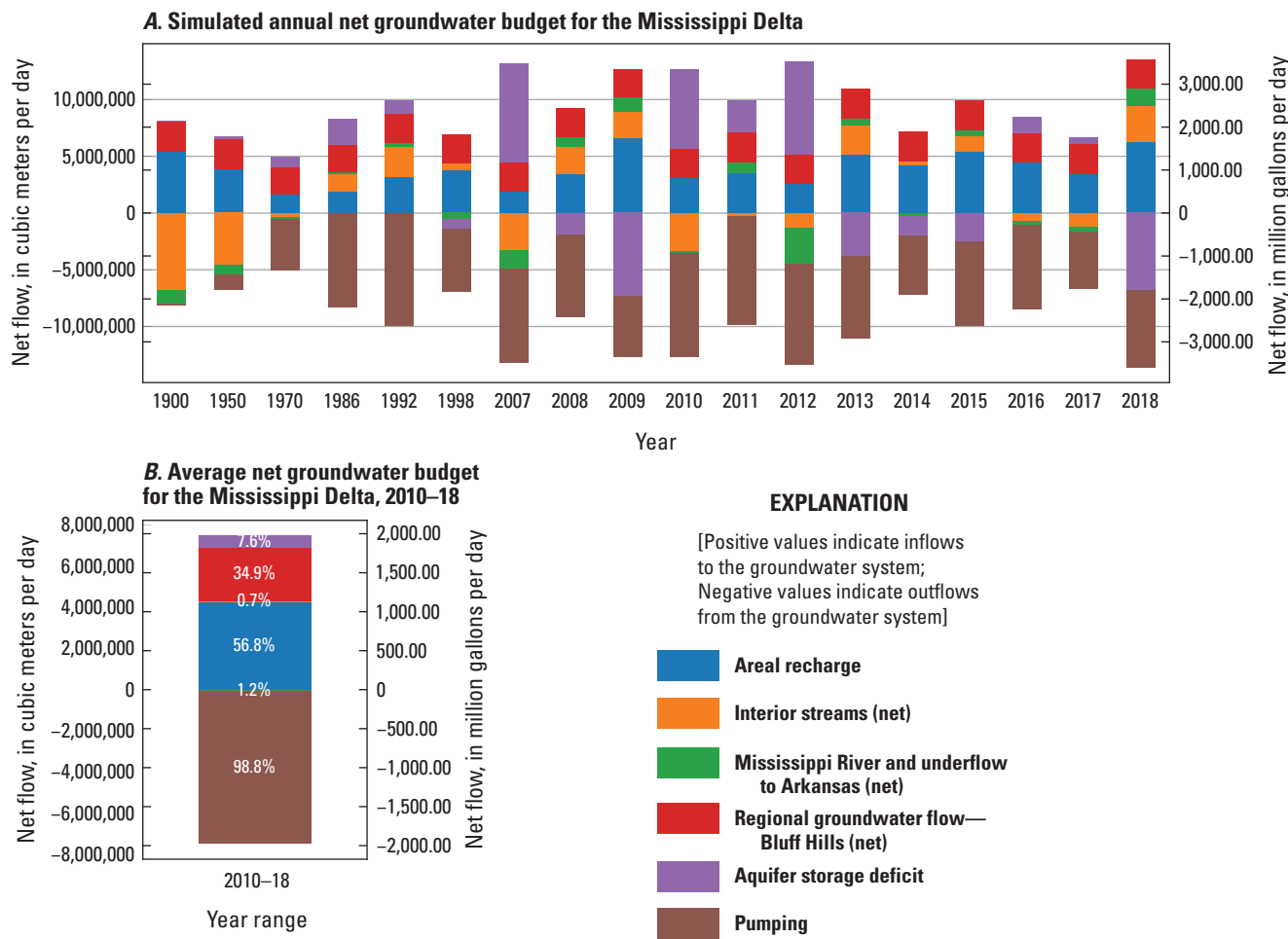


Figure 9.—Continued



**Figure 10.** Groundwater budget results for the Mississippi Delta. *A*, on a net annual basis, with the years before 2007 representing multiyear averages over the model spin-up stress periods (table 1.1). *B*, Net averages for the history matching period of 2010 through 2018. Note that the Mississippi River component here also includes potential underflow to or from Arkansas, which cannot be distinguished from flows to or from the Mississippi under the current modeling framework but is most likely small on an average net basis.

Package budget for the Mississippi Delta footprint, which excludes the eastern tributaries to the Tallahatchie/Yazoo system, yields a similar proportion of groundwater-derived streamflow (24.9 percent; not shown).

## Future Climate Scenarios and Forecast Hydrologic Effects

A key motivation for developing the Mississippi Delta model was to provide a tool to quantify groundwater responses to a range of potential future conditions. To demonstrate the model's utility for this objective, a baseline scenario was developed to forecast groundwater levels out to 2056 under a range of potential future climate forcings. The baseline scenario assumes that current agricultural practices including the amount of irrigated acreage, crop types, and current levels of irrigation efficiency will continue but that the amount

of irrigation pumping may change in response to changes in future climate. As such, the baseline scenario can be used to evaluate the potential effects of climate change on groundwater levels and as a basis for evaluating potential management scenarios such as changes in irrigated acreage, improvements in irrigation efficiency, changes in crop types, or water transfers. Input files and a reproducible workflow for setting up the baseline future climate scenario are provided in an associated data release (Leaf and others, 2023).

## Future Model Forcings

Ten potential future climate forcings were applied to the Mississippi Delta model via the SWB model by Nielsen and Westenbroek (2023). Downscaled daily precipitation and temperature output (Localized Constructed Analogs method; Pierce and others, 2014; 2015) were obtained from the downscaled Coupled Model Intercomparison Project Phase 3

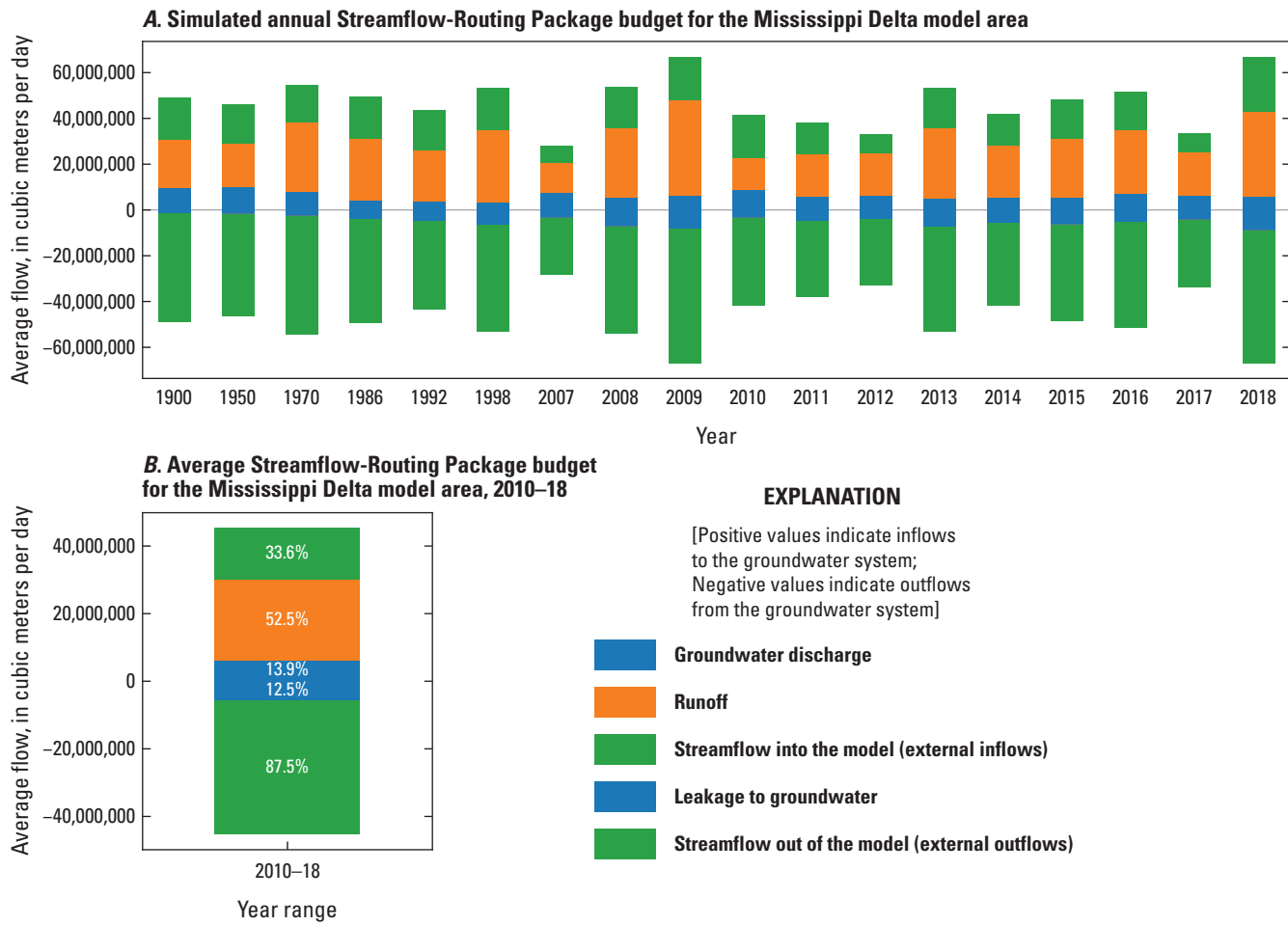


**Figure 11.** Streamflow-Routing Package budget results for the Mississippi Delta model area (including the Bluff Hills but not the Mississippi or Big Black Rivers). *A*, on a net annual basis, with the years before 2007 representing multiyear averages over the model spin-up stress periods (table 1.1). *B*, net averages for the history matching period of 2010 through 2018.

(CMIP3) and 5 (CMIP5) climate and hydrology projections (Bureau of Reclamation, 2022). Five General Circulation Models (GCMs) were selected for each of two future climate scenarios representing “middle” (representative concentration pathway [RCP] 4.5) and “high” (RCP 8.5) greenhouse gas emissions pathways (for example, Moss and others, 2010). The models were selected from the larger group of CMIP5 models included in the National Climate Change Viewer (Alder and Hostetler, 2013) based on the relative changes in mean precipitation and temperature simulated for the period of 2025–49 compared to 1981–2000. “Cool” (least temperature increase), “warm,” “wet,” and “dry” endmembers were selected from the RCP 4.5 and 8.5 scenarios, as well as the model that most closely matched the mean simulated temperature and precipitation changes for the state of Mississippi. Table 4.1 in appendix 4 summarizes the combinations of GCMs and scenarios included in the future climate ensemble used in this study.

Future climate forcings for Sunflower County, Miss., projected by all the CMIP5 models included in the National Climate Change Viewer (Alder and Hostetler, 2013) are summarized in figure 12. Although the magnitude varies, there is a clear consensus among the models that temperature increases observed since the late 20th century will continue, with the rate of increase diverging between the RCP 4.5 and 8.5 scenarios after 2050. Precipitation is more ambiguous, with substantial uncertainty and a flat central tendency out to 2100.

Gridded daily precipitation and minimum and maximum temperature output from the future climate ensemble of GCM/scenario combinations were used to drive 10 SWB simulations from 2020 to 2056 (Villers and Ladd, 2023). Results from the 10 future SWB runs were applied to the base ensemble member from the second iteration of the iES history matching run (containing the “best” parameter set). Only the base ensemble member was included in the future scenarios, as the effect of future climate forcings on model forecast

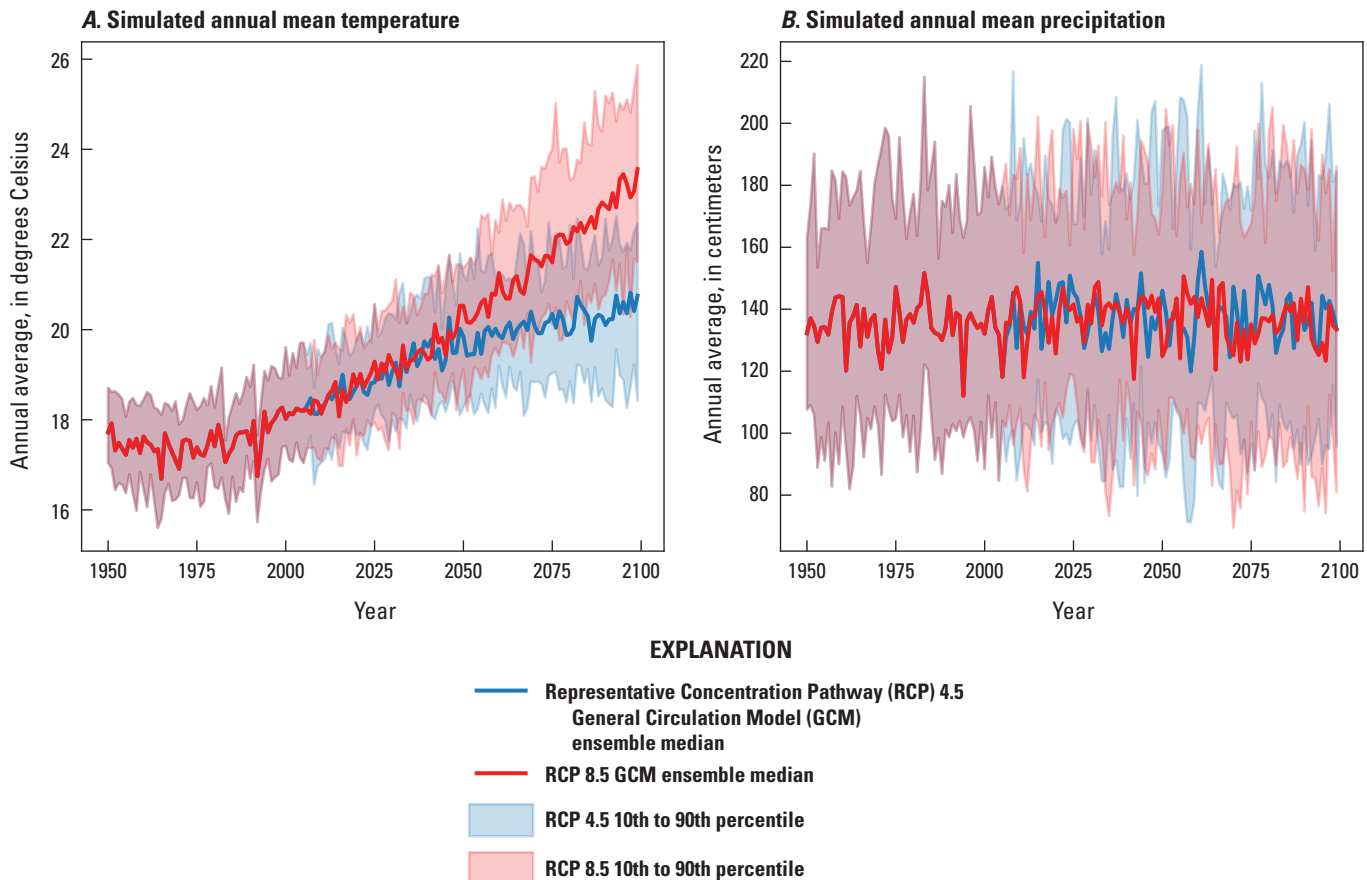


**Figure 12.** Future annual mean temperature and precipitation forecasts for Sunflower County, Mississippi.

uncertainty is typically much greater than the effect of model parameter uncertainty (for example, Hunt and others, 2013). This resulted in a future climate ensemble of 10 members (table 4.1). Model forcings not obtained from SWB (including perimeter groundwater fluxes, specified inflows to the SFR Package, and River Package stages) were developed from historical values, by repeating monthly averages for the period of 2010–15, which includes wet and dry years.

Daily net infiltration and surface runoff were averaged to the monthly stress periods and mapped to the nearest model grid cells (each 1-km SWB cell corresponds to exactly four 500-m groundwater model cells). All applicable time-invariant multiplier parameters (for example, those representing surficial connectivity zones or pilot points) were then applied to the mapped SWB output, using the same workflow as the historical model. Future pumping rates from SWB based on crop water demand were applied to the groundwater model in the same way, with layers for the pumping wells selected based on estimated production intervals (Torak, 2023; Knierim and others, 2019). To account for an apparent bias in historical SWB irrigation estimates relative to the AIWUM, a multiplier of 1.2 was applied to the SWB irrigation estimates used after 2019.

## Potential Changes in Groundwater Levels, Streamflow, and Saturated Thickness

Figure 13 compares mean annual net water budgets simulated by the future climate ensemble (see table 4.1 in app. 4 for descriptions of each of the ensemble members) with the net water budget for the historical base period 2010–19. The ensemble members simulate varying amounts of potential future precipitation and temperature increase and, therefore (via SWB), differing amounts of net infiltration, runoff, and irrigation pumping. In general, the warm and dry climate scenarios (table 4.1) simulate greater amounts of pumping, lower amounts of recharge, and greater amounts of stream leakage and aquifer storage loss.

Figure 14 shows future groundwater levels simulated at the priority wells of focus (locations shown in fig. 2.1). The results vary depending on proximity to surface water. Wells that are well connected to surface water such as the Leflore County (O0037) and Humphreys County (F0059) sites (figs. 14C, 14D) show little drawdown into the future and little variability among the climate ensemble members. In contrast, the Sunflower County wells (L0027 and B0003; figs. 14E, 14G)

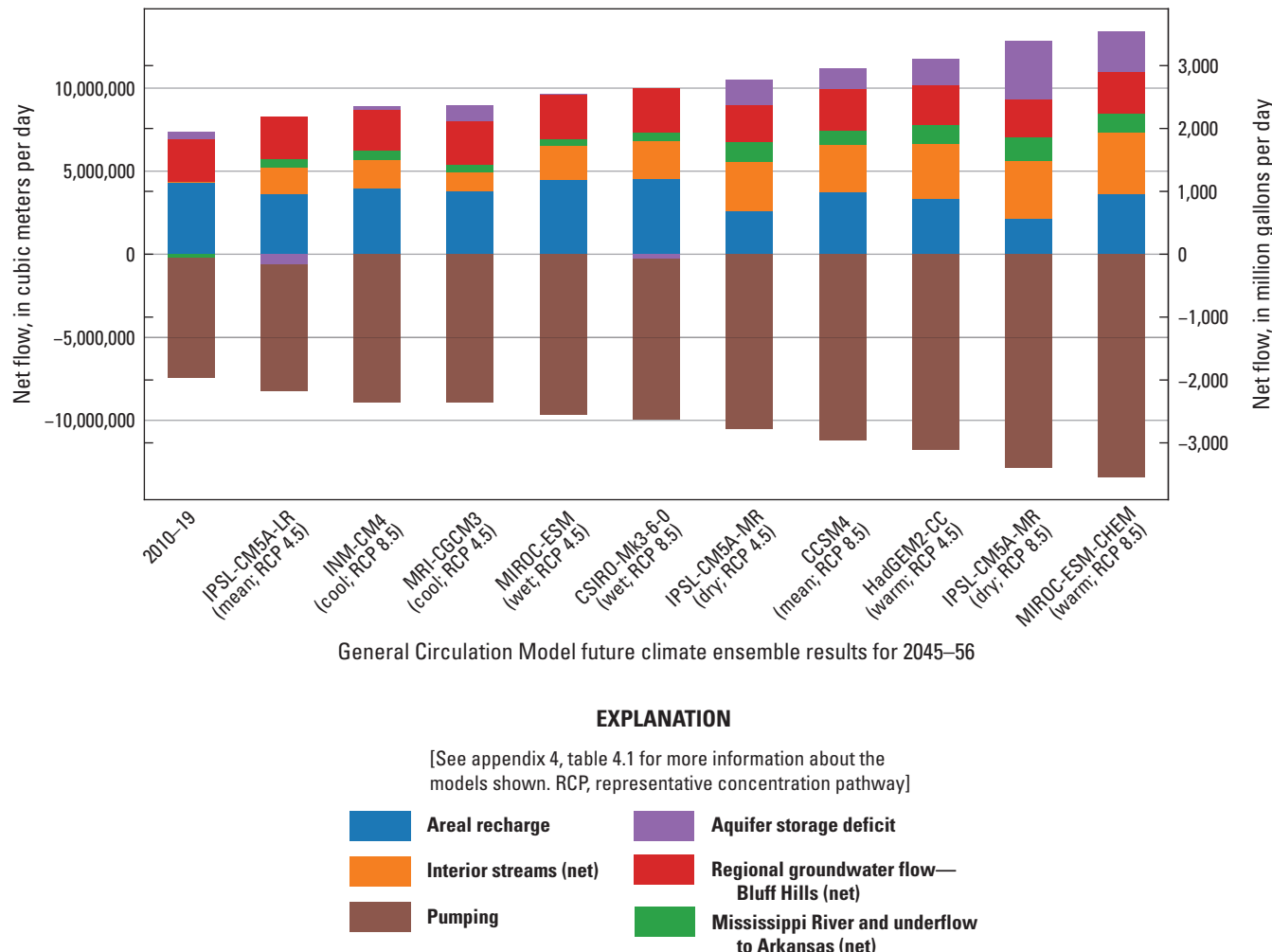


**Figure 13.** Future simulated average net annual groundwater budgets for the Mississippi Delta, 2045–56.

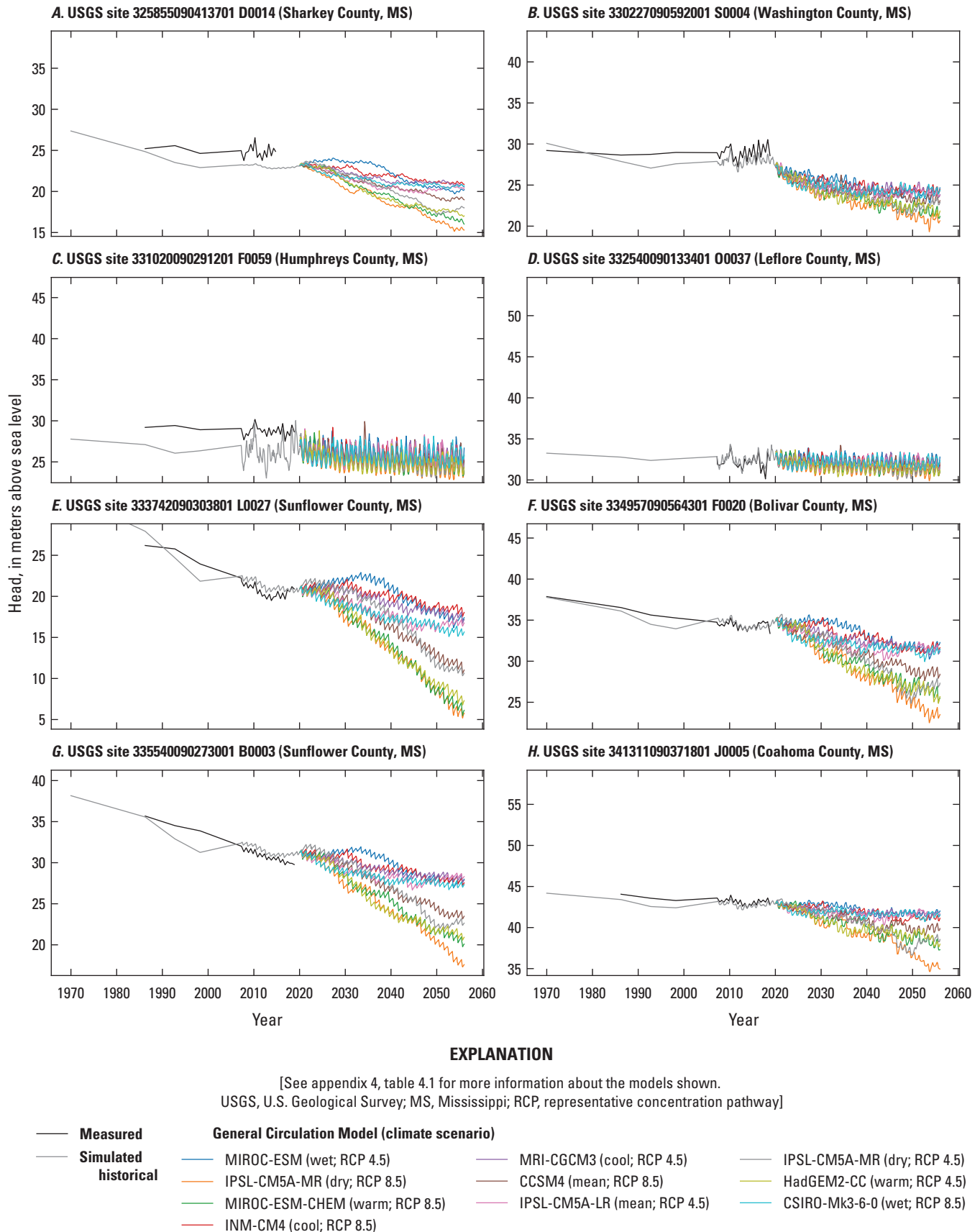
that are less connected to surface water show a wide range of potential future drawdowns. This illustrates a relatively large uncertainty range (in drawdown) from future climate at many sites (about 10–15 m at B0003 and L0027) compared to the uncertainty range from model parameters (about 2–4 m at B0003 and L0027; illustrated by the ensemble results in fig. 6).

Figure 15 shows annual minimum monthly stream flows (the lowest monthly mean in each year) in the Sunflower River at USGS site 07288500, near Sunflower, Miss. (see fig. 2.2 for the location). The historical record (in black) shows substantial year-to-year variability but an overall declining trend consistent with the decline in groundwater levels. In recent years, the decline has resulted in periodic drying of some Sunflower River stream reaches during the summer months (Barlow and Clark, 2011). Future annual minimum monthly stream flows forecast by the climate ensemble show a continuation of the declining trend, with at least one month of contiguous dry conditions a year predicted in all the scenarios by mid-century. Although the stream flows simulated by the groundwater model may be biased low because of a lack of representation

of some surface water processes (interflow, storage, and irrigation returns), they nevertheless indicate an increase in the frequency and duration of drying events.

Maintaining sufficient saturated thickness in the alluvial aquifer to allow for the production of irrigation water is a key concern of stakeholders. Figure 16 shows forecast changes in saturated thickness, determined as the difference between the simulated water table and the alluvial aquifer bottom surface (James and Minsley, 2021), between the end of the history matching period in 2019 and 2056. Sixty feet (ft) is often applied as a saturated thickness that provides sufficient capacity for typical alluvial plain irrigation pumping. Overall, across the 10 climate scenarios considered, the area fraction of the Mississippi Delta with at least 60 ft of saturated thickness could decline from near 100 percent currently to 80–90 percent by mid-century.

The largest declines in saturated thickness occur in the western part of the Delta between the Bogue Phalia and Mississippi Rivers. In this area, the alluvial aquifer is underlain by the Yazoo Clay of the Jackson Group and may also include lower permeability deposits or have a higher bottom



**Figure 14.** Time series of forecasted groundwater levels out to 2056 at selected “priority” wells of focus.

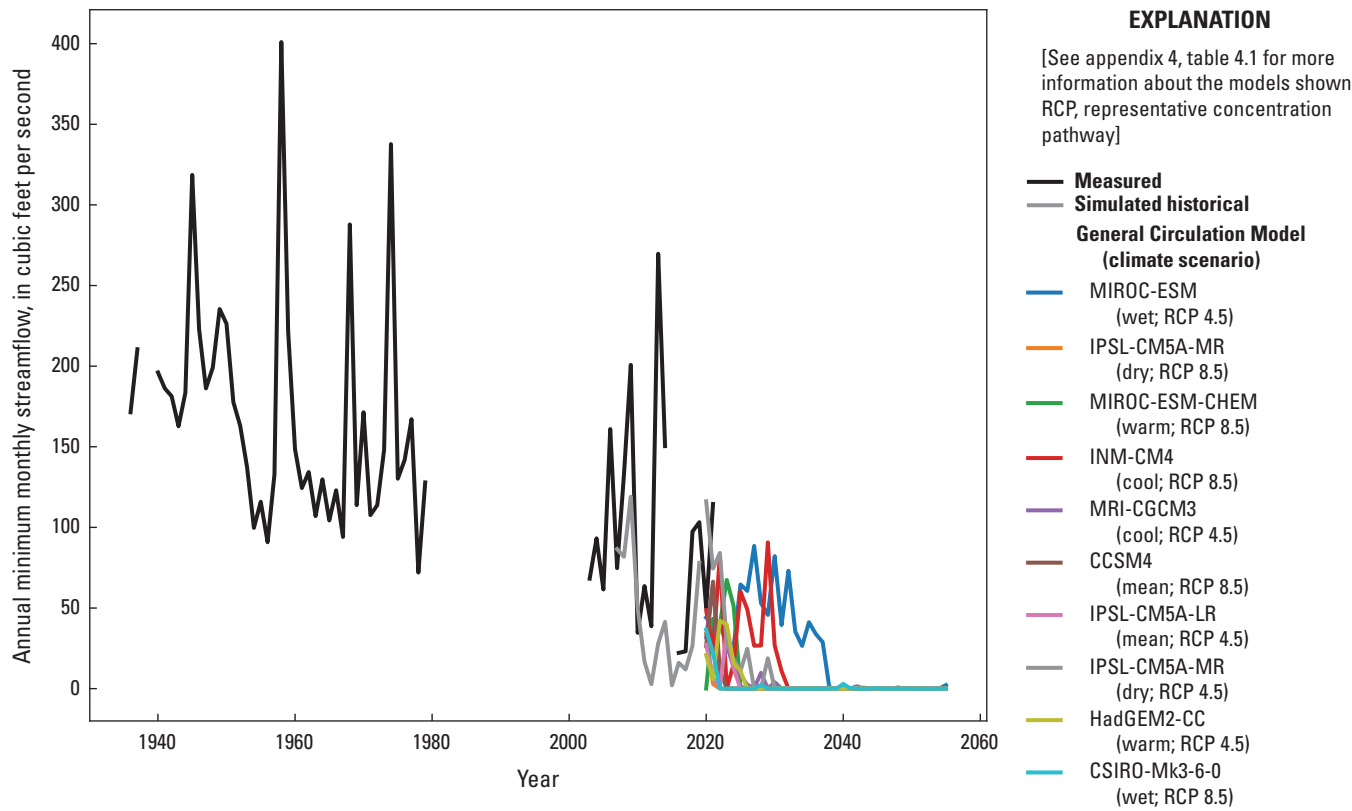


**Figure 15.** Time series of observed and forecasted annual minimum monthly stream flows (the lowest monthly mean in each year) in the Sunflower River at Sunflower, Mississippi (U.S. Geological Survey site 07288500). Only model results since 2007 (the start of monthly stress periods, when the annual monthly minimum can be calculated) are shown.

elevation than reported by James and Minsley (2021); for example, the cross section in [figure 5A](#) indicates the presence of electrical resistivity facies class 3 (interpreted to represent lower hydraulic conductivities) at shallow depths approaching sea level near the Mississippi River (left side of the cross section). In plan view, [figure 2.16](#) shows lower electrical resistivity facies classes and lower hydraulic conductivity estimates in this area (near the west side of the model domain) between approximate model rows 300 and 400. In addition

to the increased drawdown that would be expected at lower permeabilities, a thin aquifer could promote accelerating drawdown rates with time, as a lowering of the water table results in a declining saturated thickness (transmissivity), which feeds back into larger decreases in the water table. Continued decline also occurs in the central Delta, and areas to the west between the Big Sunflower and Bogue Phalia Rivers. By mid-century, parts of this area may be at or below the saturated thickness threshold for sustaining irrigation pumping.

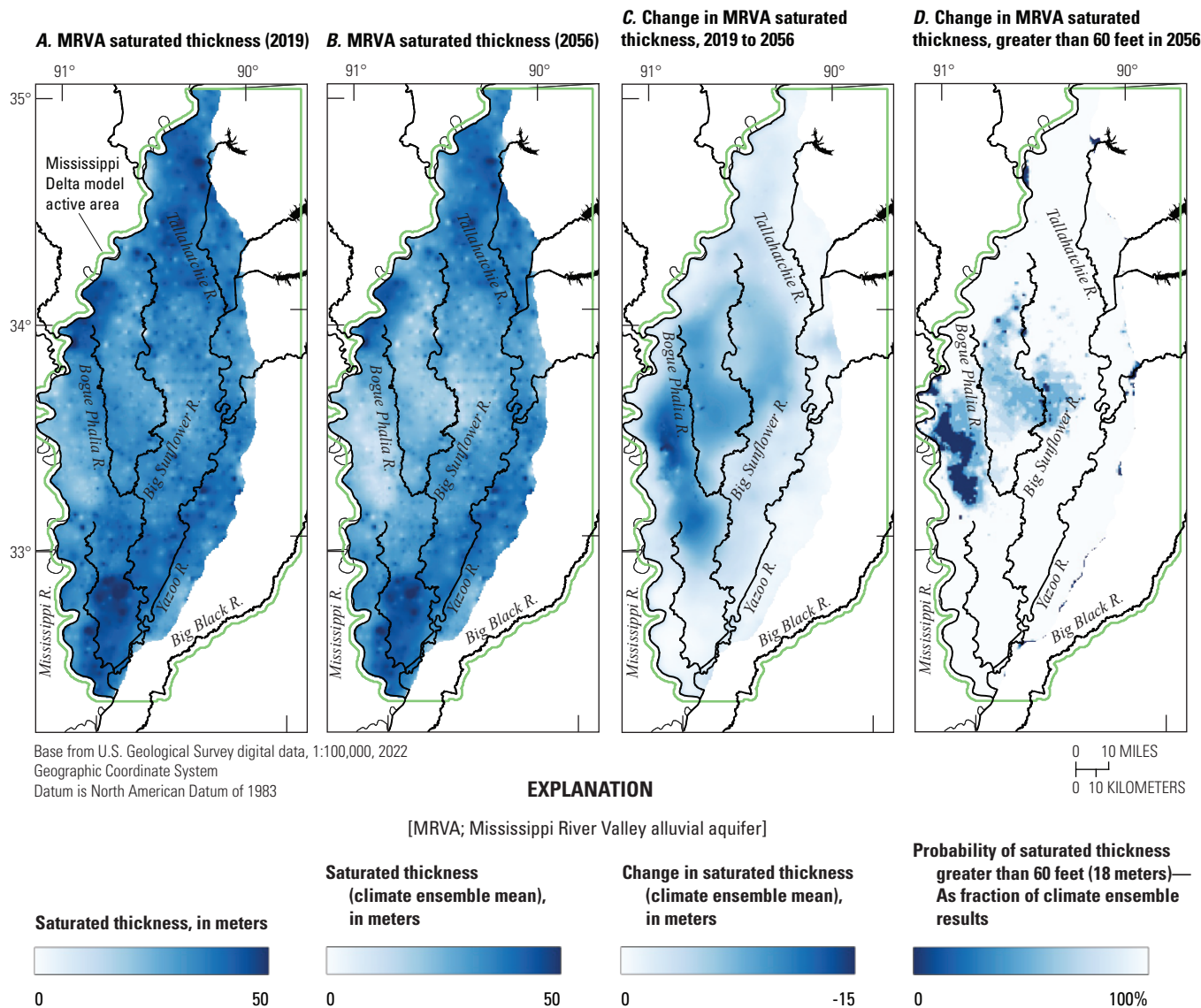


**Figure 16.** Forecasted changes out to 2056 of saturated thickness in the Mississippi River Valley alluvial aquifer.

## Assumptions, Limitations, and Suggestions for Future Work

Like all models, the MERAS 3 and Mississippi Delta models described here are simplified representations of an unknowably complex natural system. As a result, the models are limited in their ability to accurately simulate this system and to forecast future system states. Here the important assumptions and limitations are described and potential future work that could improve simulation capabilities is discussed.

### MERAS 3 Regional Model

In its current version (3.0), the MERAS 3 model was primarily designed to provide perimeter flux boundary conditions to smaller-scaled local inset models; thus, MERAS 3.0 greatly simplifies the heterogeneous Tertiary aquifer system into two layers, with the goal of maintaining fast model runtimes while retaining the Mississippi Embayment-wide footprint of previous MERAS models. This simplification of the Tertiary aquifer system may contribute in part to the poor match of model output to many observed water levels in the Tertiary. Future work may seek to improve the MERAS 3 model by doing the following:

- Incorporating salient hydrostratigraphy; for example, by using layer 2 to better represent local confining units in Arkansas or adding additional layers to specific regions (that are pinched out elsewhere) as needed.
- Explicitly representing the surficial confining unit above the Mississippi River Valley alluvial aquifer (where present) in its own layer. This would allow for MODFLOW to use a realistic (small) specific storage term for early-time declines under confined conditions, and a larger specific yield storage term for late-time declines when the water table has dropped below the base of the confining unit. Currently, the model lumps the alluvial aquifer and surficial confining unit into a single layer.
- Redistributing some irrigation pumping in Arkansas to the Tertiary system. As noted previously, the distribution of irrigation pumping between the alluvial aquifer and Sparta aquifer is not well understood in parts of Arkansas, including the Grand Prairie region. Parametrizing the distribution of pumping between the two connected systems and then estimating the fraction of pumping in each aquifer based on observed water levels could potentially improve history matching and the ability of the MERAS 3 model to simulate heads in the Tertiary system. Currently, the model assumes that all irrigation pumping occurs in the alluvial aquifer.

Although a good match to observed water levels comparable to previous work was achieved for alluvial aquifer wells, future inset models can minimize deficiencies in the

MERAS 3 solution by using specified flux perimeter boundaries (which enhance model sensitivity as compared to perimeter specified head boundary conditions; for example, Anderson and others, 2015, p. 136). The locations of inset model perimeter boundaries can also be selected to minimize the sensitivity of forecasts of interest; for example, by locating inset perimeters away from the area of interest, using large rivers for natural boundaries, or by aligning the model edges with the primary directions of groundwater flow. Cursory evaluation of the Mississippi Delta model with perimeter boundaries from different versions of the MERAS 3 model indicated that the priority well groundwater level forecasts were relatively insensitive to tested changes in the perimeter boundary. Future inset modeling would likely benefit from similar testing.

### Mississippi Delta Model

The primary purpose of the Mississippi Delta model is simulation of groundwater levels in the alluvial aquifer, especially long-term trends associated with irrigation pumping and climate change. As described in this report, the Mississippi Delta model incorporates numerous advances compared to previous models including a more detailed subsurface structure (of zones) based on an AEM survey, improved representation of surface water including monthly total flows in streams based on a surface water balance from SWB, and measured outflows at the flood control reservoirs. Despite the more realistic representation, several limitations remain:

- The model cannot accurately resolve water levels at scales smaller than 500–1,000 meters because of its discretization. This can affect small-scale forecasts; for example, when wells are in the same cell as a stream reach.
- Similarly, hydrologic events occurring on submonthly scales also cannot be resolved; for example, streams that are dry for periods of less than a full calendar month would not be represented with zero flows in the model. Although a daily timestep could be used to simulate such events, information on irrigation pumping is currently only available monthly, and many of the surface water processes that contribute to streamflow are not resolved enough to be simulated daily.
- Although the electrical resistivities mapped by the AEM survey provide information on the relative distribution of hydraulic conductivity, field measurements of hydraulic conductivity (for example, Pugh, 2022; James Hoffman, Mississippi Department of Environmental Quality, written commun., 2020) are relatively sparse and biased towards the productive parts of the Mississippi River Alluvium. As noted previously, the alluvium is highly heterogeneous, ranging from coarse gravel channel deposits to very fine backwater deposits. Hydraulic conductivities of the fine-grained backwater deposits are generally not

well characterized; therefore, the representative range in hydraulic conductivity selected for the Delta model (called the “prior”) is uncertain and may be biased high in areas. Where field head and flow data are sparse, history matching may not be able to reduce error in the prior estimates. Multiscale parametrization (for example, White and others, 2021) as was used here can help reduce biases affecting large areas and facilitate the transfer of information from the observations for more localized areas of the model domain.

- Vertical hydraulic conductivity is inherently uncertain as it is difficult to measure in the field and is scale dependent. The imprecise vertical location of field observations, differences in scale between field observations and model cells, and sparsity of suitable collocated well pairs spanning meaningful vertical intervals can also complicate estimation of vertical hydraulic conductivity from hydraulic head and streamflow data. Estimation of vertical hydraulic conductivity in the Mississippi Delta model may also be complicated by the imprecise vertical location of irrigation wells (statistically estimated production zone surfaces from Torak [2023] were used because of a lack of open interval data). The implications of uncertainty in vertical hydraulic conductivity are at least partially visible in the spread of ensemble results in the simulated heads and fluxes (for example, [figs. 6, 7, 8](#)).
- Historical monthly instream flows simulated by the SFR Package are biased low, reflecting the temporal smearing of monthly stress periods and incomplete representation of surface water processes in the model including interflow, local storage (for example, in perched aquifers or riverbanks), and irrigation returns; therefore, forecasts of future monthly instream flows should also be viewed as biased low, which could affect potential future model uses such as a constraint in optimization modeling. For some forecasts, the model’s representation of surface water in space and time may require improvement to adequately simulate the surface water balance.
- The models described here omit unsaturated zone processes that lag and combine infiltration as it travels from the root zone to the water table (Hunt and others, 2008); therefore, net infiltration calculated by the SWB model is assumed to reach the water table in the same month it leaves the root zone. This assumption is reasonable for areas of the model domain with thin unsaturated zones (for example, less than 3–5 m) but likely underestimates the time needed to reach the water table when the unsaturated zone is thicker, such as occurs in areas with appreciable pumping. Future simulations having higher temporal density (for example, biweekly, weekly, or daily) would benefit from explicit inclusion of unsaturated zone processes.

## Limitations of the Estimated Water Balances

The water balance estimates in both models rely on fluxes estimated by the SWB model (groundwater recharge, runoff, and future irrigation pumping; Nielsen and Westenbroek, 2023) and AIWUM model (historical irrigation; Bristow and Wilson, 2023; Wilson, 2021). Net infiltration estimates from the SWB model, which provide the basis for recharge (the primary source of water to the groundwater system), are particularly uncertain in that they represent a small part of the surface water balance (about 8 percent) compared to evapotranspiration and runoff. As a result, relatively small errors in evapotranspiration or runoff can correspond to larger errors in net infiltration. Net infiltration (and aquifer recharge in the groundwater model) is difficult to constrain with field data because of issues with upscaling point measurements, the prevalence of stream leakage, and the relatively small part of groundwater-derived streamflow. Estimates of irrigation pumping, the primary sink for the groundwater system, are also uncertain, with comparisons among various sources yielding differences in excess of 20 percent (for example, Wilson, 2021 and this study). During history matching, recharge and pumping rates were adjusted in space and time (within the constraints listed in [table 2.2](#)) to optimize the model fit to observed groundwater levels and stream flows. Although this provides a test of the overall reasonableness of these important model inputs and associated simulated water balance, the specific quantities should be viewed as having appreciable uncertainty; for example, the difference in average annual recharge for the Mississippi Delta simulated by the MERAS 3 model (2.48 inches per year) vs the Delta model (3.22 inches per year) may not be meaningful given the assumptions used and datasets available for history matching. Future pumping rates based on irrigation estimates from SWB and history matching adjustments to AIWUM pumping rates should also be viewed as uncertain.

## Limitations of the Future Climate Scenarios

The limitations of any future projection such as those provided by the GCM-derived climate forecasts are well understood (for example, Pörtner and others, 2022), with projected temperatures and precipitation varying by model and by scenario. The range of results across the ensemble of climate models ([fig. 12](#)) reflects uncertainty in both the nonlinear dynamics of the atmosphere and in future human behavior. GCMs were selected to represent endmember and mean conditions across two climate scenarios (RCP 4.5 and 8.5). Because of the nonlinearity of GCMs, however, the selected subset of models may not capture the full variability of the larger CMIP5 ensemble. With recent developments in the energy sector, the plausibility of higher emissions scenarios such as RCP 8.5 has been debated (for example, Pielke and others, 2022). In addition, forecasts of more distant time periods are inherently more uncertain; therefore, although [figure 12](#) indicates an overall similarity between RCP 8.5 and RCP 4.5 for the

Mississippi Delta out to mid-century, differences in simulation results beyond 2050 are likely better considered a heuristic exploration of potential futures. Future work may leverage the automated workflow for the scenarios to incorporate additional GCMs or emissions scenarios.

Many model stresses in the future climate scenarios, including Mississippi River stages, outflows from the flood control reservoirs, and groundwater fluxes along the model perimeter, are assumed to remain constant at their 2010–15 monthly averages. This assumption is likely inconsistent with some future climate projections that are used to calculate future recharge, runoff, and pumping; for example, in October 2022, the Mississippi River at Memphis reached record low stages (U.S. Army Corps of Engineers, 2022). Prolonged periods of higher or lower stages could mitigate or exacerbate the effects of the future climate scenarios considered here.

The baseline future scenarios presented here assume that current agricultural practices, including the amount of irrigated acreage, crop types, and current levels of irrigation efficiency, will continue in the future, but any of these practices may change or water transfers may be implemented in response to climate, economic, or regulatory conditions. Future work can use the baseline scenarios here to evaluate the relative effectiveness of different management and mitigation scenarios.

## Summary and Conclusions

The Mississippi Alluvial Plain (abbreviated “MAP” in associated products) is an important agricultural region that relies heavily on groundwater for irrigation. Consumption of groundwater resources, especially in the Mississippi River Valley alluvial aquifer, has led to declines in groundwater levels since the mid-20th century and concerns about future sustainability. The Mississippi Delta, which encompasses the extent of the alluvial plain within the State of Mississippi, is the largest agricultural region in Mississippi and an area of concern for groundwater level declines.

As part of the Mississippi Alluvial Plain Project, the U.S. Geological Survey created an updated groundwater flow model of the Mississippi Delta that is inset within an initial draft of a third-generation Mississippi Embayment Regional Aquifer Study model (MERAS 3.0). The two models incorporate many recent advances in modeling techniques and software and extensive data and analyses produced by the Mississippi Alluvial Plain Project including the largest airborne electromagnetic (AEM) survey flown in the United States to date. The models were constructed using the MODFLOW 6 code. Development of the basic model structures, history matching parametrization, and future scenario forcings was fully automated with Python scripts that are included with the model files in an associated data release (<https://doi.org/10.5066/P971LPOB>).

The MERAS 3.0 model is uniformly discretized horizontally at a 1-kilometer resolution and vertically into three layers. The Mississippi Delta model has a uniform 500-meter horizontal discretization, 21 layers representing mapped electrical resistivity “facies” from the AEM survey, and hydrostratigraphic surfaces from the existing MERAS framework. Both models simulate transient groundwater flow and total streamflow from 1900, using multiyear stress periods before April 2007 followed by monthly stress periods through 2018. The Mississippi Delta model receives boundary fluxes from the MERAS 3 groundwater flow solution, and both models include recharge and surface water runoff forcings from a separate Soil-Water-Balance code model (<https://doi.org/10.5066/P97KK17G>).

Initial estimates of model input parameter values were refined via history matching for the period of 2010 through 2018, using the PEST++ iterative ensemble smoother. History matching focused primarily on fitting head observations especially in the central part of the Mississippi Delta and within a group of priority wells of focus identified by stakeholders. Total streamflow observations were assigned lesser weight because of their dependence on complex surface or near surface processes not considered in the model, which may include interflow, bank storage, perched groundwater, and irrigation return flows. Regardless, total stream flows (along with heads) were mostly well matched by the models. Through successive history matching runs in which the model structure and parametrization were varied, multiscale parametrization that incorporated subsurface structure(s) identified in the AEM survey and accurate representation of transient surface water stages were important for matching observed heads, especially in the central Mississippi Delta area of greatest drawdown. Ultimately, with the Mississippi Delta model a 67-percent reduction in root mean square error in head observations was achieved, compared to previous work.

Potential future baseline climate scenarios that assume a continuation of current agricultural practices were constructed by applying recharge, surface runoff, and irrigation pumping forcings from a future version of the Soil-Water-Balance model that was driven by temperature and precipitation output from 10 general circulation model simulations considering high and moderate carbon emissions pathways. The results indicate a continued rise in average temperatures but no clear precipitation trend. Increased crop water demand is anticipated from the higher temperatures, resulting in increased irrigation withdrawals to sustain current levels of irrigated agriculture. Simulated drawdowns in groundwater levels at mid-century vary greatly. Under moderate or wet climate scenarios and especially in parts of the aquifer that are well connected to major streams, drawdown may be limited to a few meters or less. Under dry or warm climate scenarios, and at wells less connected to surface water, future drawdown could exceed 10 meters in many areas by mid-century, potentially reducing the fraction of the Mississippi Delta with greater than 60 feet of saturated thickness from near 100 percent currently to 80–90 percent. Future simulations with the model may include alternative management scenarios to identify options for improving groundwater sustainability.

## References Cited

Ackerman, D.J., 1989, Hydrology of the Mississippi River Valley alluvial aquifer, south-central United States—A preliminary assessment of the regional flow system: U.S. Geological Survey Water-Resources Investigations Report 88-4028, 74 p. [Also available at <https://doi.org/10.3133/wri884028>.]

Ackerman, D.J., 1996, Hydrology of the Mississippi River Valley alluvial aquifer, south-central United States: U.S. Geological Survey Professional Paper 1416-D, 56 p. [Also available at <https://doi.org/10.3133/pp1416D>.]

Adams, R.F., Miller, B.V., and Kress, W.H., 2019, Waterborne resistivity inverted models, Mississippi Alluvial Plain, 2016–2018: U.S. Geological Survey data release, accessed July 18, 2023, at <https://doi.org/10.5066/P9WQPRFB>.

Alder, J.R., and Hostetler, S.W., 2013, USGS National Climate Change Viewer (ver. 2.0.2): U.S. Geological Survey digital data, accessed July 18, 2023 at <https://doi.org/10.5066/F7W9575T>.

Alhassan, M., Lawrence, C., Richardson, S., and Pindilli, E.J., 2019, The Mississippi Alluvial Plain aquifers—An engine for economic activity: U.S. Geological Survey Fact Sheet 2019-3003, 4 p., accessed April 1, 2023, at <https://doi.org/10.3133/fs20193003>.

Anderson, M.P., Woessner, W.W., and Hunt, R.J., 2015, Applied groundwater modeling—Simulation of flow and advective transport (2d ed.): Academic Press, 564 p.

Arthur, J.K., 2001, Hydrogeology, model description, and flow analysis of the Mississippi River alluvial aquifer in northwestern Mississippi: U.S. Geological Survey Water-Resources Investigations Report 2001-4035, 47 p. [Also available at <https://doi.org/10.3133/wri014035>.]

Arthur, J.K., and Taylor, R.E., 1990, Definition of the hydrogeologic framework and preliminary simulation of groundwater flow in the Mississippi embayment aquifer system, Gulf Coastal Plain, United States: U.S. Geological Survey Water-Resources Investigations Report 86-4364, 97 p. [Also available at <https://doi.org/10.3133/wri864364>.]

Arthur, J.K., and Taylor, R.E., 1998, Ground-water flow analysis of the Mississippi embayment aquifer system, south-central United States: U.S. Geological Survey Professional Paper 1416-I, 148 p. [Also available at <https://doi.org/10.3133/pp1416I>.]

Barlow, J.R.B., and Clark, B.R., 2011, Simulation of water-use conservation scenarios for the Mississippi Delta using an existing regional groundwater flow model: U.S. Geological Survey Scientific Investigations Report 2011-5019, 14 p. [Also available at <https://doi.org/10.3133/sir20115019>.]

Bristow, E., and Wilson, J.L., 2023, Aquaculture and irrigation water-use model (AIWUM) version 1.1 estimates and related datasets for the Mississippi Alluvial Plain: U.S. Geological Survey data release, <https://doi.org/10.5066/P9RGZOBZ>.

Broom, M.E., and Lyford, F.P., 1981, Alluvial aquifer of the Cache and St. Francis River Basins, northeastern Arkansas: U.S. Geological Survey Open-File Report 81-476, 48 p., accessed November 30, 2021, at <https://doi.org/10.3133/ofr81476>.

Bureau of Reclamation, 2022, Dowscaled CMIP3 and CMIP5 climate and hydrology projections: U.S. Department of Energy web page, accessed January 28, 2022, at [https://gdo-dcp.ucrlnl.org/downscaled\\_cmip\\_projections](https://gdo-dcp.ucrlnl.org/downscaled_cmip_projections).

Clark, B.R., Barlow, P.M., Peterson, S.M., Hughes, J.D., Reeves, H.W., and Viger, R.J., 2018a, National-scale grid to support regional groundwater availability studies and a national hydrogeologic database: U.S. Geological Survey data release, accessed July 18, 2023, at <https://doi.org/10.5066/F7P84B24>.

Clark, B.R., and Hart, R.M., 2009, The Mississippi Embayment Regional Aquifer Study (MERAS)—Documentation of a groundwater-flow model constructed to assess water availability in the Mississippi embayment: U.S. Geological Survey Scientific Investigations Report 2009-5172, 61 p., accessed July 18, 2023 at <https://doi.org/10.3133/sir20095172>.

Clark, B.R., Hart, R.M., and Gurdak, J.J., 2011, Groundwater availability of the Mississippi embayment: U.S. Geological Survey Professional Paper 1785, 62 p. [Also available at <https://doi.org/10.3133/pp1785>.]

Clark, B.R., Richards, J.M., and Knierim, K.J., 2018b, The Ozark Plateaus Regional Aquifer Study—Documentation of a groundwater-flow model constructed to assess water availability in the Ozark Plateaus: U.S. Geological Survey Scientific Investigations Report 2018-5035, 33 p., accessed July 18, 2023, at <https://doi.org/10.3133/sir20185035>.

Clark, B.R., Westerman, D.A., and Fugitt, D.T., 2013, Enhancements to the Mississippi Embayment Regional Aquifer Study (MERAS) groundwater-flow model and simulations of sustainable water-level scenarios: U.S. Geological Survey Scientific Investigations Report 2013-5161, 29 p., accessed May 26, 2017, at <https://doi.org/10.3133/sir20135161>.

Corson-Dosch, N.T., Fienen, M.N., Finkelstein, J.S., Leaf, A.T., White, J.T., Woda, J., and Williams, J.H., 2022, Areas contributing recharge to priority wells in valley-fill aquifers in the Neversink River and Rondout Creek drainage basins, New York: U.S. Geological Survey Scientific Investigations Report 2021-5112, 50 p., accessed July 18, 2023 at <https://doi.org/10.3133/sir20215112>.

Cushing, E.M., Boswell, E.H., and Hosman, R.L., 1964, General geology of the Mississippi embayment: U.S. Geological Survey Professional Paper 448-B, 28 p. [Also available at <https://doi.org/10.3133/pp448B>.]

Czarnecki, J.B., Clark, B.R., and Reed, T.B., 2003, Conjunctive-use optimization model of the Mississippi River Valley alluvial aquifer of northeastern Arkansas: U.S. Geological Survey Water-Resources Investigations Report 2003-4230, 29 p. [Also available at <https://doi.org/10.3133/wri034230>.]

Diehl, T.H., and Harris, M.A., 2014, Withdrawal and consumption of water by thermoelectric power plants in the United States, 2010: U.S. Geological Survey Scientific Investigations Report 2014-5184, 28 p. [Also available at <https://doi.org/10.3133/sir20145184>.]

Dietsch, B., Asquith, W.H., Breaker, B.K., Westenbroek, S.M., and Kress, W.H., 2022, Simulation of monthly mean and monthly base flow of streamflow using random forests for the Mississippi River Alluvial Plain, 1901 to 2018: U.S. Geological Survey Scientific Investigations Report 2022-5079, 17 p., accessed July 18, 2023, at <https://doi.org/10.3133/sir20225079>.

Doherty, J., 2003, Ground water model calibration using pilot points and regularization: *Groundwater*, v. 41, no. 2, p. 170–177. [Also available at <https://doi.org/10.1111/j.1745-6584.2003.tb02580.x>.]

Doherty, J.E., and Hunt, R.J., 2010, Approaches to highly parameterized inversion—A guide to using PEST for groundwater-model calibration: U.S. Geological Survey Scientific Investigations Report 2010-5169, 59 p. [Also available at <https://doi.org/10.3133/sir20105169>.]

Doherty, J.[E.], and Moore, C., 2020, Decision support modeling—Data assimilation, uncertainty quantification, and strategic abstraction: *Groundwater*, v. 58, no. 3, p. 327–337. [Also available at <https://doi.org/10.1111/gwat.12969>.]

Economic Research Service, 2010, The economics of food, farming, natural resources, and rural America—State fact sheets—Mississippi: U.S. Department of Agriculture, Economic Research Service, accessed January 20, 2011, at <http://www.ers.usda.gov/StateFacts/MS.htm>.

Fitzpatrick, D.J., Kilpatrick, J.M., and McWreath, H., 1990, Geohydrologic characteristics and simulated response to pumping stresses in the Sparta aquifer in east-central Arkansas: U.S. Geological Survey Water-Resources Investigations Report 88-4201, 50 p., accessed September 1, 2023, at <https://doi.org/10.3133/wri884201>.

Haitjema, H.M., 1995, Analytic element modeling of groundwater flow: San Diego, Calif., Academic Press, 394 p.

Harbaugh, A.W., 2005, MODFLOW-2005, the U.S. Geological Survey modular ground-water model—The ground-water flow process: U.S. Geological Survey Techniques and Methods, book 6, chap. A16, [variously paged]. [Also available at <https://doi.org/10.3133/tm6A16>.]

Harris, M.A., and Diehl, T.H., 2019a, Water withdrawal and consumption estimates for thermoelectric power plants in the United States, 2015 (ver. 1.1, February 2021): U.S. Geological Survey data release, accessed July 18, 2023, at <https://doi.org/10.5066/P9V0T04B>.

Harris, M.A., and Diehl, T.H., 2019b, Withdrawal and consumption of water by thermoelectric power plants in the United States, 2015: U.S. Geological Survey Scientific Investigations Report 2019-5103, 15 p. [Also available at <https://doi.org/10.3133/sir20195103>.]

Hart, R.M., Clark, B.R., and Bolyard, S.E., 2008, Digital surfaces and thicknesses of selected hydrogeologic units within the Mississippi Embayment Regional Aquifer Study (MERAS): U.S. Geological Survey Scientific Investigations Report 2008-5098, 33 p., accessed July 18, 2023, at <https://doi.org/10.3133/sir20085098>.

Haugh, C.J., 2012, Effects of groundwater withdrawals associated with combined-cycle combustion turbine plants in West Tennessee and northern Mississippi: U.S. Geological Survey Scientific Investigations Report 2012-5072, 22 p., accessed July 18, 2023, at <https://doi.org/10.3133/sir20125072>.

Haugh, C.J., 2016, Evaluation of effects of groundwater withdrawals at the proposed Allen combined-cycle combustion turbine plant, Shelby County, Tennessee: U.S. Geological Survey Scientific Investigations Report 2016-5072, 8 p., accessed July 18, 2023, at <https://doi.org/10.3133/sir20165072>.

Haugh, C.J., Killian, C.D., and Barlow, J.R.B., 2020a, MODFLOW-2005 model used to evaluate water-management scenarios for the Mississippi Delta: U.S. Geological Survey data release, accessed July 18, 2023, at <https://doi.org/10.5066/P9906VM5>.

Haugh, C.J., Killian, C.D., and Barlow, J.R.B., 2020b, Simulation of water-management scenarios for the Mississippi Delta: U.S. Geological Survey Scientific Investigations Report 2019-5116, 15 p. [Also available at <https://doi.org/10.3133/sir20195116>.]

Hosman, R.L., 1996, Regional stratigraphy and subsurface geology of Cenozoic deposits, Gulf Coastal Plain, south-central United States: U.S. Geological Survey Professional Paper 1416-G, 35 p.

Hunt, R.J., Pradic, D.E., Walker, J.F., and Anderson, M.P., 2008, Importance of unsaturated zone flow for simulating recharge in a humid climate: *Journal of Ground Water*, v. 46, no. 4, p. 551–560. [Also available at <https://doi.org/10.1111/j.1745-6854.2007.00427.x>.]

Hunt, R.J., and Feinstein, D.T., 2012, MODFLOW–NWT—Robust Handling of Dry Cells Using a Newton Formulation of MODFLOW–2005: *Ground Water*, v. 50, p. 659–663. [Also available at <https://doi.org/10.1111/j.1745-6584.2012.00976.x>.]

Hunt, R.J., Walker, J.F., Selbig, W.R., Westenbroek, S.M., and Regan, R.S., 2013, Simulation of climate-change effects on streamflow, lake water budgets, and stream temperature using GSFLOW and SNTEMP, Trout Lake Watershed, Wisconsin: U.S. Geological Survey Scientific Investigations Report 2013–5159, 118 p. [Also available at <https://doi.org/10.3133/sir20135159>.]

Hunt, R.J., White, J.T., Duncan, L.L., Haugh, C.J., and Doherty, J., 2021, Evaluating lower computational burden approaches for calibration of large environmental models: *Groundwater*, v. 59, no. 6, p. 788–798. [Also available at <https://doi.org/10.1111/gwat.13106>.]

James, S.R., and Minsley, B.J., 2021, Combined results and derivative products of hydrogeologic structure and properties from airborne electromagnetic surveys in the Mississippi Alluvial Plain: U.S. Geological Survey data release, accessed July 18, 2023, at <https://doi.org/10.5066/P9382RCI>.

Killian, C., 2018, Characterizing spatial and temporal changes and driving factors of groundwater and surface-water interactions within the Mississippi portion of the Mississippi Alluvial Plain: Starkville, Miss., Mississippi State University, Ph.D. dissertation, 89 p., accessed April 8, 2019, at <https://scholarsjunction.msstate.edu/cgi/viewcontent.cgi?article=2043&context=td>.

Knierim, K.J., Kingsbury, J.A., and Haugh, C.J., 2019, Groundwater withdrawal zones for drinking water from the Mississippi River Valley alluvial aquifer and Mississippi embayment aquifers: U.S. Geological Survey data release, accessed July 18, 2023, at <https://doi.org/10.5066/P9FZV4ED>.

Ladd, D.E., and Travers, L.R., 2019, Generalized regions of the Mississippi Alluvial Plain: U.S. Geological Survey data release, accessed July 18, 2023, at <https://doi.org/10.5066/P915ZZQM>.

Langevin, C.D., Hughes, J.D., Provost, A.M., Russcher, M.J., Niswonger, R.G., Panday, S., Merrick, D., and Banta, E.R., 2022, MODFLOW 6 Modular Hydrologic Model (ver. 6.3.0): U.S. Geological Survey software release, accessed July 18, 2023, at <https://doi.org/10.5066/P97FFF9M>.

Leaf, A.T., 2023, Automated construction of Streamflow-Routing networks for MODFLOW—Application in the Mississippi Embayment region: U.S. Geological Survey Scientific Investigations Report 2023–5051, 27 p., <https://doi.org/10.3133/sir20235051>.

Leaf, A.T., Duncan, L.L., and Haugh, C.J., 2023, MODFLOW 6 models for simulating groundwater flow in the Mississippi Embayment with a focus on the Mississippi Delta: U.S. Geological Survey data release, <https://doi.org/10.5066/P971LPOB>.

Leaf, A.T., and Fienen, M.N., 2022, Modflow-setup—Robust automation of groundwater model construction: *Frontiers in Earth Science*, v. 10, art. 903965, 11 p. [Also available at <https://doi.org/10.3389/feart.2022.903965>.]

Leaf, A.T., Fienen, M.N., and Reeves, H.W., 2021, SFRmaker and Linesink-maker—Rapid construction of streamflow routing networks from hydrography data: *Groundwater*, v. 59, no. 5, p. 761–771. [Also available at <https://doi.org/10.1111/gwat.13095>.]

Lloyd, O.B., Jr., and Lyke, W.L., 1995, Segment 10—Illinois, Indiana, Kentucky, Ohio, Tennessee, chap. K of U.S. Geological Survey, *Groundwater Atlas of the United States: U.S. Geological Survey Hydrologic Investigations Atlas 730–K*, 30 p. [Also available at <https://doi.org/10.3133/ha730K>.]

Lovelace, J.K., Nielsen, M.G., Read, A.L., Murphy, C.J., and Maupin, M.A., 2020, Estimated groundwater withdrawals from principal aquifers in the United States, 2015 (ver. 1.2, October 2020): U.S. Geological Survey Circular 1464, 70 p. [Also available at <https://doi.org/10.3133/cir1464>.]

Mancini, E.A., and Tew, B.H., 1994, Claiborne-Jackson Group contact (Eocene) in Alabama and Mississippi: *Gulf Coast Association of Geological Societies Transactions*, v. 44, p. 431–439.

McGuire, V.L., Seanor, R.C., Asquith, W.H., Strauch, K.R., Nottmeier, A.M., Thomas, J.C., Tollett, R.W., and Kress, W.H., 2021a, Altitude of the potentiometric surface in the Mississippi River Valley alluvial aquifer, spring 2020: U.S. Geological Survey Scientific Investigations Map 3478, 5 sheets, 14-p. pamphlet, accessed July 18, 2023, at <https://doi.org/10.3133/sim3478>.

McGuire, V.L., Seanor, R.C., Asquith, W.H., Strauch, K.R., Nottmeier, A.M., Thomas, J.C., Tollett, R.W., and Kress, W.H., 2021b, Datasets used to map the potentiometric surface, Mississippi River Valley alluvial aquifer, spring 2020: U.S. Geological Survey data release, accessed July 18, 2023, at <https://doi.org/10.5066/P9CXDIPL>.

McKay, L., Bondelid, T., Dewald, T., Johnston, J., Moore, R., and Rea, A., 2012, NHDPlus version 2—User guide [data model ver. 2.1]: U.S. Environmental Protection Agency, accessed September 17, 2018, at [http://www.horizon-systems.com/NHDPlus/NHDPlusV2\\_documentation.php](http://www.horizon-systems.com/NHDPlus/NHDPlusV2_documentation.php).

McKee, P.W., and Clark, B.R., 2003, Development and calibration of a ground-water flow model for the Sparta aquifer of southeastern Arkansas and north-central Louisiana and simulated response to withdrawals, 1998–2027: U.S. Geological Survey Water-Resources Investigations Report 2003–4132, 71 p. [Also available at <https://doi.org/10.3133/wri034132>.]

Miller, B.V., Wallace, D.S., and Kress, W.H., 2016, Water-borne continuous resistivity profiling data from select streams of the Mississippi Alluvial Plain in northwestern Mississippi: U.S. Geological Survey data release, accessed July 18, 2023, at <https://doi.org/10.5066/F7FT8J68>.

Minsley, B.J., Rigby, J.R., James, S.R., Burton, B.L., Knierim, K.J., Pace, M.D.M., Bedrosian, P.A., and Kress, W.H., 2021, Airborne geophysical surveys of the lower Mississippi valley demonstrate system-scale mapping of subsurface architecture: *Communications Earth & Environment*, v. 2, no. 1, art. 131, 14 p. [Also available at <https://doi.org/10.1038/s43247-021-00200-z>.]

Moss, R.H., Edmonds, J.A., Hibbard, K.A., Manning, M.R., Rose, S.K., van Vuuren, D.P., Carter, T.R., Emori, S., Kainuma, M., Kram, T., Meehl, G.A., Mitchell, J.F.B., Nakicenovic, N., Riahi, K., Smith, S.J., Stouffer, R.J., Thomson, A.M., Weyant, J.P., and Wilbanks, T.J., 2010, The next generation of scenarios for climate change research and assessment: *Nature*, v. 463, p. 747–756. [Also available at <https://doi.org/10.1038/nature08823>.]

Nielsen, M.G., and Westenbroek, S.M., 2023, Updated estimates of water budget components for the Mississippi embayment region using a Soil-Water-Balance model, 2000–2020: U.S. Geological Survey Scientific Investigations Report 2023–5080, 58 p., <https://doi.org/10.3133/sir20235080>.

Niswonger, R.G., Panday, S., and Ibaraki, M., 2011, MODFLOW-NWT, a Newton formulation for MODFLOW-2005: U.S. Geological Survey Techniques and Methods, book 6, chap. A37, 44 p. [Also available at <https://doi.org/10.3133/tm6A37>.]

Pielke, R., Jr., Burgess, M.G., and Ritchie, J., 2022, Plausible 2005–2050 emissions scenarios project between 2 °C and 3 °C of warming by 2100: *Environmental Research Letters*, v. 17, no. 2, art. 024027, 8 p. [Also available at <https://doi.org/10.1088/1748-9326/ac4ebf>.]

Pierce, D.W., Cayan, D.R., Maurer, E.P., Abatzoglou, J.T., and Hegewisch, K.C., 2015, Improved bias correction techniques for hydrological simulations of climate change: *Journal of Hydrometeorology*, v. 16, no. 6, p. 2421–2442. [Also available at <https://doi.org/10.1175/JHM-D-14-0236.1>.]

Pierce, D.W., Cayan, D.R., and Thrasher, B.L., 2014, Statistical downscaling using localized constructed analogs (LOCA): *Journal of Hydrometeorology*, v. 15, no. 6, p. 2558–2585. [Also available at <https://doi.org/10.1175/JHM-D-14-0082.1>.]

Pörtner, H.-O., Roberts, D.C., Poloczanska, E.S., Mintenbeck, K., Tignor, M., Alegría, A., Craig, M., Langsdorf, S., Löschke, S., Möller, V., and Okem, A., eds., 2022, Summary for policymakers, in Pörtner, H.-O., Roberts, D.C., Tignor, M., Poloczanska, E.S., Mintenbeck, K., Alegría, A., Craig, M., Langsdorf, S., Löschke, S., Möller, V., Okem, A., and Rama, B., eds., Climate change 2022—Impacts, adaptation, and vulnerability [Contribution of Working Group II to the Sixth Assessment Report of the Intergovernmental Panel on Climate Change]: Cambridge, United Kingdom and New York, United States, Cambridge University Press, p. 3–33. [Also available at <https://doi.org/10.1017/9781009325844.001>.]

Pugh, A.L., 2022, Hydrogeologic Aquifer Test dataset, Lower Mississippi-Gulf Water Science Center, December 2020: U.S. Geological Survey data release, accessed July 18, 2023 at <https://doi.org/10.5066/P9Q9SI92>.

Rateb, A., Scanlon, B.R., Pool, D.R., Sun, A., Zhang, Z., Chen, J., Clark, B., Faunt, C.C., Haugh, C.J., Hill, M., Hobza, C., McGuire, V.L., Reitz, M., Schmied, H.M., Sutanudjaja, E.H., Swenson, S., Wiese, D., Xia, Y., and Zell, W., 2020, Comparison of groundwater storage changes from GRACE satellites with monitoring and modeling of major U.S. aquifers: *Water Resources Research*, v. 56, no. 12, art. e2020WR027556, 19 p. [Also available at <https://doi.org/10.1029/2020WR027556>.]

Reed, T.B., 2003, Recalibration of a ground-water flow model of the Mississippi River Valley alluvial aquifer of northeastern Arkansas, 1918–1998, with simulations of water levels caused by projected ground-water withdrawals through 2049: U.S. Geological Survey Water-Resources Investigations Report 2003–4109, 58 p. [Also available at <https://doi.org/10.3133/wri034109>.]

Reitz, M., and Kress, W.H., 2019, The use of national data-sets to produce an average annual water budget for the Mississippi Alluvial Plain, 2000–13: U.S. Geological Survey Fact Sheet 2019–3001, 4 p., accessed July 18, 2023, at <https://doi.org/10.3133/fs20193001>.

Renken, R.A., 1998, Segment 5—Arkansas, Louisiana, Mississippi, chap. F of Groundwater Atlas of the United States: U.S. Geological Survey Hydrologic Investigations Atlas 730–F, 28 p. [Also available at <https://doi.org/10.3133/ha730F>.]

Saucier, R.T., 1994, Geomorphology and Quaternary geo-logic history of the Lower Mississippi Valley [volume I]: Vicksburg, Miss., Mississippi River Commission, prepared by U.S. Army Corps of Engineers Waterways Experiment Station, [variously paged].

Spiers, C.A., 1977, The Winona-Tallahatta aquifer in Mississippi: U.S. Geological Survey Water-Resources Investigations Report 77–125, 1 sheet. [Also available at <https://doi.org/10.3133/wri77125>.]

Torak, L.J., 2023, Digital surfaces and site data of well-screen top and bottom altitudes defining the irrigation production zone of the Mississippi River Valley alluvial aquifer within the Mississippi Alluvial Plain project region: U.S. Geological Survey data release, <https://doi.org/10.5066/P9TSDEAC>.

U.S. Army Corps of Engineers, 2022, Water levels of rivers and lakes: U.S. Army Corps of Engineers digital data, accessed July 18, 2023, at <https://riversgates.mvr.usace.army.mil/WaterControl/stationinfo2.cfm?sid=MS126>.

U.S. Geological Survey, 2021, USGS water data for the Nation: U.S. Geological Survey National Water Information System database, accessed November 20, 2021, at <https://doi.org/10.5066/F7P55KJN>.

Van Arsdale, R.B., and Cox, R.T., 2007, The Mississippi’s curious origins: *Scientific American*, v. 296, no. 1, p. 76–82. [Also available at <https://doi.org/10.1038/scientificamerican0107-76>.]

Villers, J.J., and Ladd, D.E., 2023, Soil-Water-Balance forecasted climate model output for simulations of water budget components in the Mississippi Embayment Regional Aquifer System, 2020 to 2055: U.S. Geological Survey data release, <https://doi.org/10.5066/P9BC6UB8>.

Warwick, P.D., SanFilipo, J.R., Crowley, S.S., Thomas, R.E., Freid, J., and Tully, J.K., 1997, Map showing outcrop of the coal-bearing units and land use in the Gulf Coast region: U.S. Geological Survey Open-File Report 97–172, 1 sheet, scale 1:2,000,000. [Also available at <https://doi.org/10.3133/ofr97172>.]

Weiss, J.S., 1992, Geohydrologic units of the coastal lowlands aquifer system, south-central United States: U.S. Geological Survey Professional Paper 1416–C, 32 p.

Westenbroek, S.M., Engott, J.A., Kelson, V.A., and Hunt, R.J., 2018, SWB version 2.0—A Soil-Water-Balance code for estimating net infiltration and other water-budget components: U.S. Geological Survey Techniques and Methods, book 6, chap. A59, 118 p., accessed October 2018 at <https://doi.org/10.3133/tm6A59>.

Westenbroek, S.M., Nielsen, M.G., and Ladd, D.E., 2021, Initial estimates of net infiltration and irrigation from a Soil-Water-Balance model of the Mississippi Embayment Regional Aquifer Study area: U.S. Geological Survey Open-File Report 2021–1008, 29 p., accessed July 18, 2023 at <https://doi.org/10.3133/ofr20211008>.

Westenbroek, S.M., Nielsen, M.G., and Trost, J.J., 2023, Model archive and output files for net infiltration, runoff, and irrigation water use for the Mississippi Embayment Regional Aquifer System, 2000 to 2020, simulated with the Soil-Water-Balance model: U.S. Geological Survey data release, <https://doi.org/10.5066/P97KK17G>.

White, J.T., 2018, A model-independent iterative ensemble smoother for efficient history-matching and uncertainty quantification in very high dimensions: *Environmental Modelling & Software*, v. 109, p. 191–201. [Also available at <https://doi.org/10.1016/j.envsoft.2018.06.009>.]

White, J.T., Fienen, M.N., and Doherty, J.E., 2016, A python framework for environmental model uncertainty analysis: *Environmental Modelling & Software*, v. 85, p. 217–228. [Also available at <https://doi.org/10.1016/j.envsoft.2016.08.017>.]

White, J.T., Hemmings, B., Fienen, M.N., and Knowling, M.J., 2021, Towards improved environmental modeling outcomes—Enabling low-cost access to high-dimensional, geostatistical-based decision-support analyses: *Environmental Modelling & Software*, v. 139, art. 105022, 9 p. [Also available at <https://doi.org/10.1016/j.envsoft.2021.105022>.]

White, J.T., Hunt, R.J., Fienen, M.N., and Doherty, J.E., 2020, Approaches to highly parameterized inversion—PEST++ Version 5, a software suite for parameter estimation, uncertainty analysis, management optimization and sensitivity analysis: U.S. Geological Survey Techniques and Methods, book 7, chap. C26, 52 p., accessed July 18, 2023, at <https://doi.org/10.3133/tm7C26>.

Wilson, J.L., 2021, Aquaculture and Irrigation Water-Use Model (AIWUM) version 1.0—An agricultural water-use model developed for the Mississippi Alluvial Plain, 1999–2017: U.S. Geological Survey Scientific Investigations Report 2021–5011, 36 p., accessed July 18, 2023, at <https://doi.org/10.3133/sir20215011>.

Woods, A.J., Foti, T.L., Chapman, S.S., Omernik, J.M., Wise, J.A., Murray, E.O., Prior, W.L., Pagan, J.B., Jr., Comstock, J.A., and Radford, M., 2004, Ecoregions of Arkansas (color poster with map, descriptive text, summary tables, and photographs): Reston, Va., U.S. Geological Survey, 4 sheets, scale 1:1,000,000, accessed August 16, 2018, at <https://www.epa.gov/eco-research/ecoregion-download-files-state-region-6>.

## Appendix 1. Groundwater Flow Model Constructions

Groundwater flow models were developed for the Mississippi Embayment Regional Aquifer Study (MERAS) and Mississippi Delta extents using MODFLOW 6 (version 6.3.0; Langevin and others, 2022). The new MERAS model (MERAS 3) represents a simplified representation of the Mississippi Embayment aquifer system that solves faster than previous MERAS models and is primarily aimed at providing boundary fluxes and heads for more detailed inset models within the MERAS area, such as the Mississippi Delta model described in this study. The Mississippi Delta model (or simply the “Delta model”) is intended to focus on groundwater sustainability in the Mississippi Delta region, at a higher level of detail than what is feasible at the scale of the MERAS. Base-case versions of each model were created for the history matching period of 2010 through 2018. Model parameters estimated from history matching were then applied to future scenario versions of the Mississippi Delta model, described in the “Future Climate Scenarios” section.

The models were constructed in two steps: an initial preprocessing step that focused on reformatting the data from various sources into common formats such as .csv, shapefiles, and rasters; and a second automated build step where the MODFLOW input files were generated from the preprocessed data using Modflow-setup (Leaf and Fienen, 2022). Model files and reproducible model construction workflows are provided in an associated data release (Leaf and others, 2023).

## Model Domains and Discretization

The MERAS 3 regional model covers the same extent as previous versions of the MERAS model (fig. 1, Clark and Hart, 2009; Haugh and others, 2020a, b; Hunt and others, 2021), at a 1-kilometer (km) uniform grid resolution that aligns with the U.S. Geological Survey (USGS) National Hydrogeologic Grid (NHG; Clark and others, 2018).

The Mississippi Delta model includes the geographic extent of the Mississippi Delta (fig. 1), extending from just west of the Mississippi River east to an arbitrary north/south line that encompasses the outlets of the flood control reservoirs in the Tallahatchie/Yazoo River system, and to the southeast, just past the Big Black River (fig. 1). The northern boundary of the model is an east-west line in the Albers conical equal area coordinate reference system (CRS) that is close to the Tennessee/Mississippi State line. The Mississippi Delta model has a uniform horizontal resolution of 500 meters that also is aligned with the NHG (Clark and others, 2018).

## Regional and Inset Model Layering

The MERAS 3 model layering distills the regional aquifer system into three components: the Mississippi River Valley alluvial aquifer (layer 1); a lumped confining unit consisting of the Vicksburg-Jackson confining unit, the Upper Claiborne aquifer, and the Middle Claiborne confining unit (layer 2); and a lumped lower aquifer (layer 3) that includes the Middle Claiborne aquifer and all underlying units in the Tertiary sequence (fig. 4). The bottom elevation of layer 1 where it represents the alluvial aquifer is based on the alluvial aquifer base elevation raster surface from James and Minsley (2021) developed from the airborne electromagnetic (AEM) survey (Minsley and others, 2021). Outside of the alluvial aquifer, the average thickness of the alluvial aquifer from the AEM survey was used to maintain continuity in the layer. Layer 2 (the lumped confining unit) is only present in the model where at least one of the member units is present. Where no member units are present, layer 2 consists of vertical passthrough cells (Langevin and others, 2017) of zero thickness. Where present, the bottom of layer 2 is based on the raster surfaces of Hart and others (2008). As in previous versions of the MERAS model, the bottom of MERAS 3 is formed by the top of the Midway confining unit developed by Hart and others (2008).

To make use of the AEM results, which are based on three-dimensional voxels instead of two-dimensional surfaces, the Mississippi Delta model uses mostly uniform layer thicknesses in areas with AEM data. Layers within the alluvial aquifer are uniformly 5 meters thick down to the base of the aquifer (James and Minsley, 2021), which is represented by the bottom of layer 8. In places where the alluvial aquifer bottom is shallower than 40 meters depth, the deepest layer(s) in the sequence were converted to zero thickness passthrough cells so that the last active layer coincided with the alluvial aquifer bottom and was between 5 to 10 meters thick; for example, if the alluvial aquifer bottom was at 31 meters depth, the layer bottoms would be 5, 10, 15, 20, 25, 31, and the last two layers would be zero-thickness passthrough cells. Below the alluvial aquifer bottom, an expanding uniform layer thickness with a multiplier of 1.5 (for example, 7.5 meters for layer 9, 11.25 meters for layer 10, and so on) is used to the maximum depth of AEM data (about represented by the bottom extent of the resistivity facies classes in fig. 5). Below the base of the AEM data, model layers are based on the original MERAS framework surfaces of Hart and others (2008), where present, with the Midway confining unit top constituting the model bottom (fig. 5).

## Time Discretization

The time discretization for the MERAS 3 and Mississippi Delta models is designed to simulate the full history of pumping from predevelopment conditions, while minimizing model runtimes and maximizing focus on the period since 2007, when the most accurate water use data are available. Both models use the same time discretization, which begins in 1900, with an initial, predevelopment steady-state period (without pumping), followed by 6 multiyear stress periods of three timesteps each extending to April (the start of the growing season) in 2007. The multiyear stress periods are structured to approximately align with step changes in the pumping history for previous MERAS models (Clark and Hart, 2009, fig. 10). Starting April 1, 2007, and extending to the history matching end time of January 1, 2019, the models have monthly stress periods of one timestep each ([table 1.1](#); Leaf and others, 2023).

**Table 1.1.** Time discretization in the Mississippi Embayment Regional Aquifer Study (MERAS) 3 regional and Mississippi Delta models.

[Dates are given in month/day/year]

Stress period number	Start date	End date <sup>1</sup>	Length, in days	Number of timesteps	Timestep multiplier
1	(Steady state)	1/1/1900	1	1	1
2	1/1/1900	12/31/1949	18,262	3	1.5
3	1/1/1950	12/31/1969	7,305	3	1.5
4	1/1/1970	3/31/1986	5,934	3	1.5
5	4/1/1986	9/30/1992	2,375	3	1.5
6	10/1/1992	3/31/1998	2,008	3	1.5
7	4/1/1998	3/31/2007	3,287	3	1.5
8	4/1/2007	4/30/2007	30	1	1.5
9	5/1/2007	5/31/2007	31	1	1.5
10	6/1/2007	6/30/2007	30	1	1.5
11	7/1/2007	7/31/2007	31	1	1.5
12	8/1/2007	8/31/2007	31	1	1.5
13	9/1/2007	9/30/2007	30	1	1.5
14	10/1/2007	10/31/2007	31	1	1.5
15	11/1/2007	11/30/2007	30	1	1.5
16	12/1/2007	12/31/2007	31	1	1.5
17	1/1/2008	1/31/2008	31	1	1.5
18	2/1/2008	2/29/2008	29	1	1.5
19	3/1/2008	3/31/2008	31	1	1.5
20	4/1/2008	4/30/2008	30	1	1.5
21	5/1/2008	5/31/2008	31	1	1.5
22	6/1/2008	6/30/2008	30	1	1.5
23	7/1/2008	7/31/2008	31	1	1.5
24	8/1/2008	8/31/2008	31	1	1.5
25	9/1/2008	9/30/2008	30	1	1.5
26	10/1/2008	10/31/2008	31	1	1.5
27	11/1/2008	11/30/2008	30	1	1.5
28	12/1/2008	12/31/2008	31	1	1.5
29	1/1/2009	1/31/2009	31	1	1.5
30	2/1/2009	2/28/2009	28	1	1.5
31	3/1/2009	3/31/2009	31	1	1.5
32	4/1/2009	4/30/2009	30	1	1.5
33	5/1/2009	5/31/2009	31	1	1.5
34	6/1/2009	6/30/2009	30	1	1.5
35	7/1/2009	7/31/2009	31	1	1.5
36	8/1/2009	8/31/2009	31	1	1.5
37	9/1/2009	9/30/2009	30	1	1.5
38	10/1/2009	10/31/2009	31	1	1.5
39	11/1/2009	11/30/2009	30	1	1.5
40	12/1/2009	12/31/2009	31	1	1.5
41	1/1/2010	1/31/2010	31	1	1.5
42	2/1/2010	2/28/2010	28	1	1.5

**Table 1.1.** Time discretization in the Mississippi Embayment Regional Aquifer Study (MERAS) 3 regional and Mississippi Delta models.—Continued

[Dates are given in month/day/year]

Stress period number	Start date	End date <sup>1</sup>	Length, in days	Number of timesteps	Timestep multiplier
43	3/1/2010	3/31/2010	31	1	1.5
44	4/1/2010	4/30/2010	30	1	1.5
45	5/1/2010	5/31/2010	31	1	1.5
46	6/1/2010	6/30/2010	30	1	1.5
47	7/1/2010	7/31/2010	31	1	1.5
48	8/1/2010	8/31/2010	31	1	1.5
49	9/1/2010	9/30/2010	30	1	1.5
50	10/1/2010	10/31/2010	31	1	1.5
51	11/1/2010	11/30/2010	30	1	1.5
52	12/1/2010	12/31/2010	31	1	1.5
53	1/1/2011	1/31/2011	31	1	1.5
54	2/1/2011	2/28/2011	28	1	1.5
55	3/1/2011	3/31/2011	31	1	1.5
56	4/1/2011	4/30/2011	30	1	1.5
57	5/1/2011	5/31/2011	31	1	1.5
58	6/1/2011	6/30/2011	30	1	1.5
59	7/1/2011	7/31/2011	31	1	1.5
60	8/1/2011	8/31/2011	31	1	1.5
61	9/1/2011	9/30/2011	30	1	1.5
62	10/1/2011	10/31/2011	31	1	1.5
63	11/1/2011	11/30/2011	30	1	1.5
64	12/1/2011	12/31/2011	31	1	1.5
65	1/1/2012	1/31/2012	31	1	1.5
66	2/1/2012	2/29/2012	29	1	1.5
67	3/1/2012	3/31/2012	31	1	1.5
68	4/1/2012	4/30/2012	30	1	1.5
69	5/1/2012	5/31/2012	31	1	1.5
70	6/1/2012	6/30/2012	30	1	1.5
71	7/1/2012	7/31/2012	31	1	1.5
72	8/1/2012	8/31/2012	31	1	1.5
73	9/1/2012	9/30/2012	30	1	1.5
74	10/1/2012	10/31/2012	31	1	1.5
75	11/1/2012	11/30/2012	30	1	1.5
76	12/1/2012	12/31/2012	31	1	1.5
77	1/1/2013	1/31/2013	31	1	1.5
78	2/1/2013	2/28/2013	28	1	1.5
79	3/1/2013	3/31/2013	31	1	1.5
80	4/1/2013	4/30/2013	30	1	1.5
81	5/1/2013	5/31/2013	31	1	1.5
82	6/1/2013	6/30/2013	30	1	1.5
83	7/1/2013	7/31/2013	31	1	1.5

**Table 1.1.** Time discretization in the Mississippi Embayment Regional Aquifer Study (MERAS) 3 regional and Mississippi Delta models.—Continued

[Dates are given in month/day/year]

Stress period number	Start date	End date <sup>1</sup>	Length, in days	Number of timesteps	Timestep multiplier
84	8/1/2013	8/31/2013	31	1	1.5
85	9/1/2013	9/30/2013	30	1	1.5
86	10/1/2013	10/31/2013	31	1	1.5
87	11/1/2013	11/30/2013	30	1	1.5
88	12/1/2013	12/31/2013	31	1	1.5
89	1/1/2014	1/31/2014	31	1	1.5
90	2/1/2014	2/28/2014	28	1	1.5
91	3/1/2014	3/31/2014	31	1	1.5
92	4/1/2014	4/30/2014	30	1	1.5
93	5/1/2014	5/31/2014	31	1	1.5
94	6/1/2014	6/30/2014	30	1	1.5
95	7/1/2014	7/31/2014	31	1	1.5
96	8/1/2014	8/31/2014	31	1	1.5
97	9/1/2014	9/30/2014	30	1	1.5
98	10/1/2014	10/31/2014	31	1	1.5
99	11/1/2014	11/30/2014	30	1	1.5
100	12/1/2014	12/31/2014	31	1	1.5
101	1/1/2015	1/31/2015	31	1	1.5
102	2/1/2015	2/28/2015	28	1	1.5
103	3/1/2015	3/31/2015	31	1	1.5
104	4/1/2015	4/30/2015	30	1	1.5
105	5/1/2015	5/31/2015	31	1	1.5
106	6/1/2015	6/30/2015	30	1	1.5
107	7/1/2015	7/31/2015	31	1	1.5
108	8/1/2015	8/31/2015	31	1	1.5
109	9/1/2015	9/30/2015	30	1	1.5
110	10/1/2015	10/31/2015	31	1	1.5
111	11/1/2015	11/30/2015	30	1	1.5
112	12/1/2015	12/31/2015	31	1	1.5
113	1/1/2016	1/31/2016	31	1	1.5
114	2/1/2016	2/29/2016	29	1	1.5
115	3/1/2016	3/31/2016	31	1	1.5
116	4/1/2016	4/30/2016	30	1	1.5
117	5/1/2016	5/31/2016	31	1	1.5
118	6/1/2016	6/30/2016	30	1	1.5
119	7/1/2016	7/31/2016	31	1	1.5
120	8/1/2016	8/31/2016	31	1	1.5
121	9/1/2016	9/30/2016	30	1	1.5
122	10/1/2016	10/31/2016	31	1	1.5
123	11/1/2016	11/30/2016	30	1	1.5
124	12/1/2016	12/31/2016	31	1	1.5

**Table 1.1.** Time discretization in the Mississippi Embayment Regional Aquifer Study (MERAS) 3 regional and Mississippi Delta models.—Continued

[Dates are given in month/day/year]

Stress period number	Start date	End date <sup>1</sup>	Length, in days	Number of timesteps	Timestep multiplier
125	1/1/2017	1/31/2017	31	1	1.5
126	2/1/2017	2/28/2017	28	1	1.5
127	3/1/2017	3/31/2017	31	1	1.5
128	4/1/2017	4/30/2017	30	1	1.5
129	5/1/2017	5/31/2017	31	1	1.5
130	6/1/2017	6/30/2017	30	1	1.5
131	7/1/2017	7/31/2017	31	1	1.5
132	8/1/2017	8/31/2017	31	1	1.5
133	9/1/2017	9/30/2017	30	1	1.5
134	10/1/2017	10/31/2017	31	1	1.5
135	11/1/2017	11/30/2017	30	1	1.5
136	12/1/2017	12/31/2017	31	1	1.5
137	1/1/2018	1/31/2018	31	1	1.5
138	2/1/2018	2/28/2018	28	1	1.5
139	3/1/2018	3/31/2018	31	1	1.5
140	4/1/2018	4/30/2018	30	1	1.5
141	5/1/2018	5/31/2018	31	1	1.5
142	6/1/2018	6/30/2018	30	1	1.5
143	7/1/2018	7/31/2018	31	1	1.5
144	8/1/2018	8/31/2018	31	1	1.5
145	9/1/2018	9/30/2018	30	1	1.5
146	10/1/2018	10/31/2018	31	1	1.5
147	11/1/2018	11/30/2018	30	1	1.5
148	12/1/2018	12/31/2018	31	1	1.5

<sup>1</sup>Stress periods end at midnight after the end date; for example, stress period 148 ends at midnight on 01/01/2019.

## Boundary Conditions

Boundary conditions in the MERAS 3 and Mississippi Delta models include terrestrial recharge originating from precipitation, groundwater/surface water interactions and pumping fluxes representing water use. Similar to past MERAS models, MERAS 3 assumes a no-flow boundary around its perimeter. The Mississippi Delta model perimeter consists of transient specified fluxes extracted from the independent MERAS 3 model solution. Figure 1.1 shows the boundary conditions used in the two models. Most boundary condition values were adjusted during history matching; appendix 2 describes the parametrization and adjustments made.

## Perimeter Boundaries

The Mississippi Delta model is connected to the MERAS 3 model via transient specified fluxes along its perimeter (fig. 1.1). Cell-by-cell flow values were extracted from the MERAS 3 solution at each inset model cell along the active area perimeter, at each stress period, using Modflow-setup (Leaf and Fienen, 2022), which uses a three-dimensional barycentric interpolation scheme similar to the griddata method in Scipy (Virtanen and others, 2020). The extracted fluxes were then applied to the Delta model using the Well (WEL) Package in MODFLOW 6.

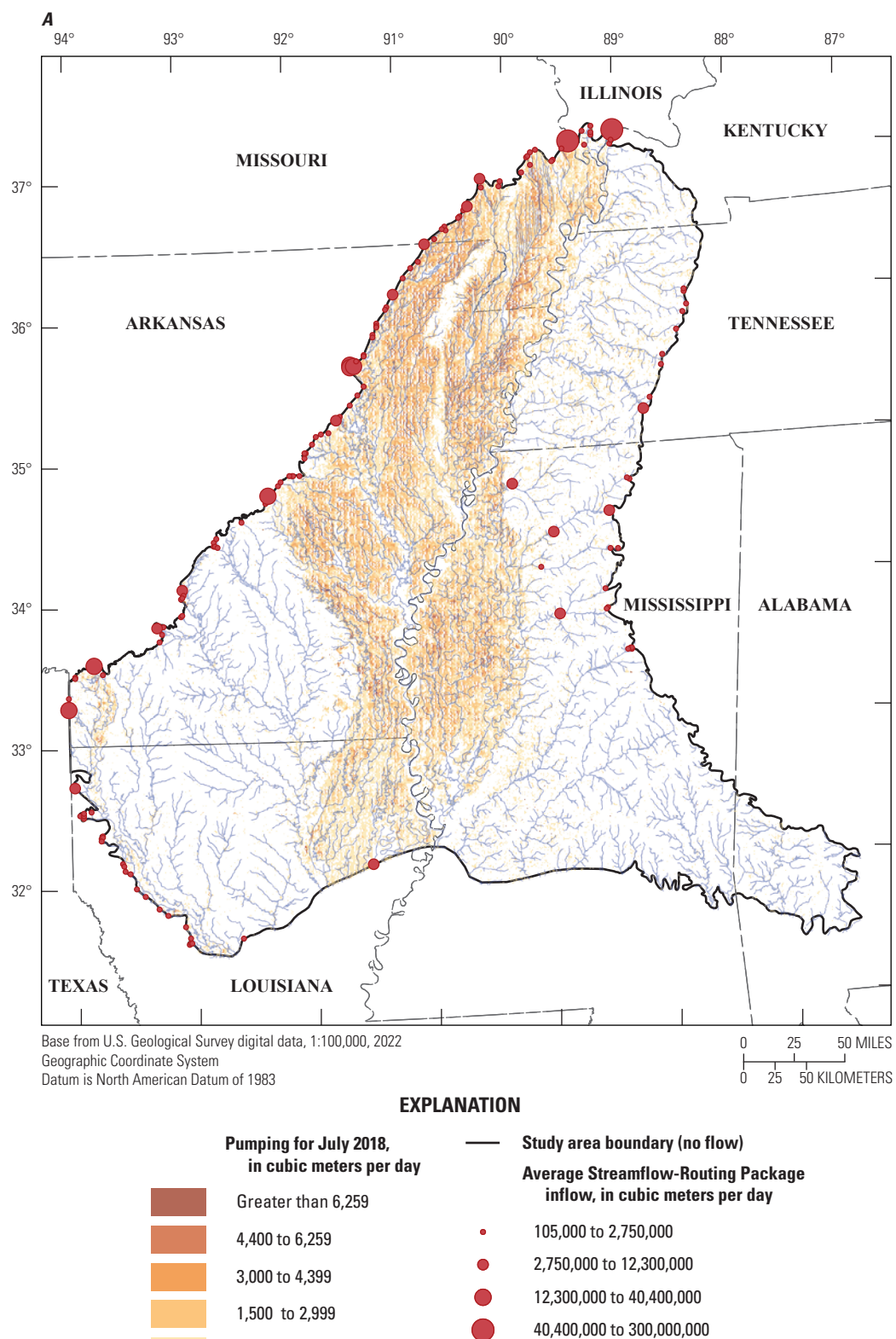


**Figure 1.1.** Boundary conditions in A, the Mississippi Embayment Regional Aquifer Study (MERAS) 3 and B, Mississippi Delta models.

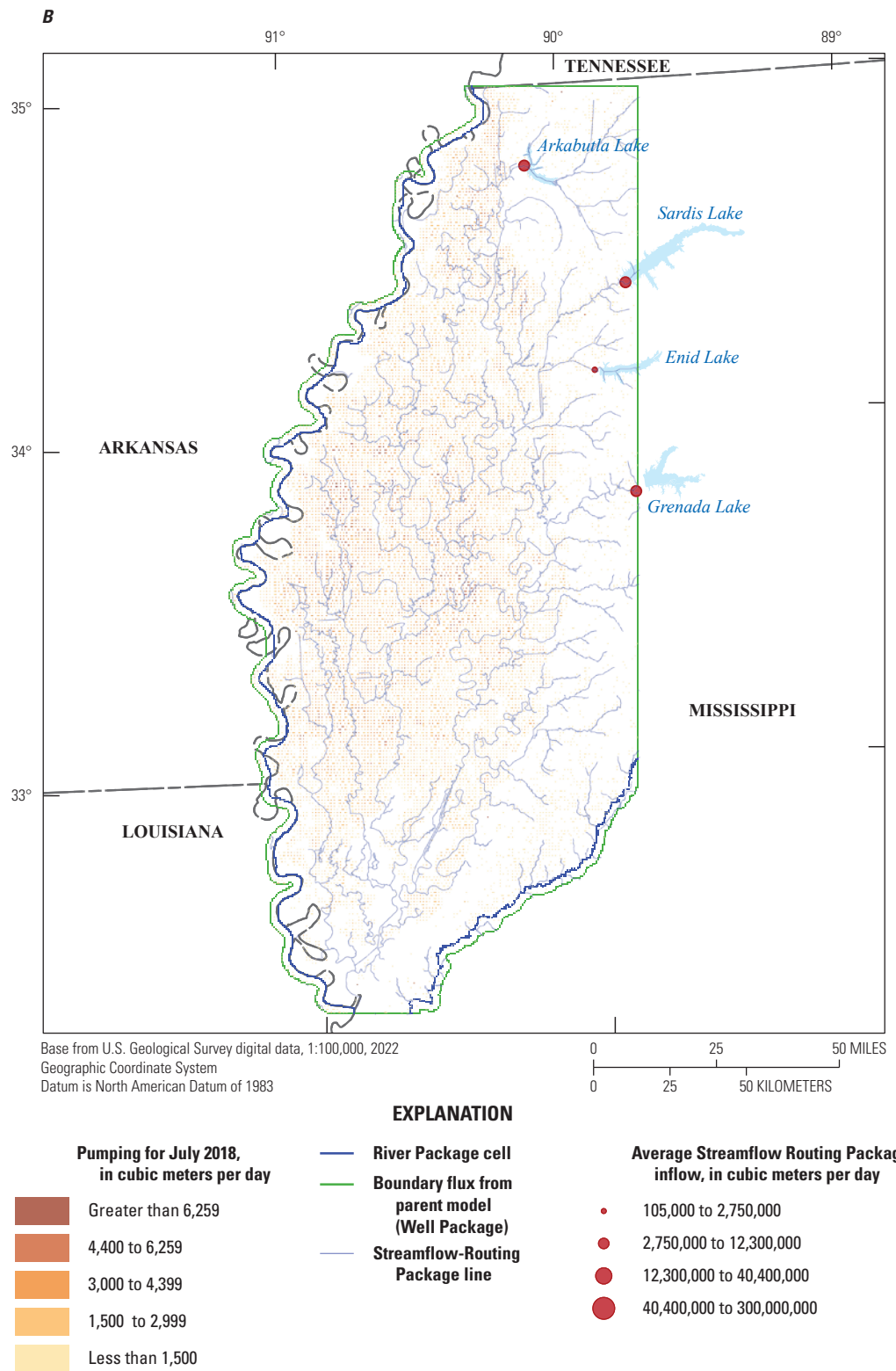


**Figure 1.1.** Boundary conditions in *A*, the Mississippi Embayment Regional Aquifer Study (MERAS) 3 and *B*, Mississippi Delta models.

## Recharge

Recharge input to the MERAS 3 and Mississippi Delta models was based on net infiltration results from the Soil-Water-Balance (SWB) simulation of Nielsen and Westenbroek (2023). Daily net infiltration values were averaged to monthly values and then resampled to the model grids using the nearest-neighbor option in Modflow-setup. As the SWB simulation also is aligned with the NHG (at a 1-km resolution), each model cell corresponds to a single SWB cell, meaning mass is conserved. In both models, average net infiltration values for the period of 1999 through 2018 were used for the initial steady-state stress period and subsequent multiyear stress periods before April 2007; monthly averages were used for the remaining stress periods. Recharge was simulated in MODFLOW 6 using the Recharge (RCH) Package with array-based input (Langevin and others, 2022). Recharge values were parametrized at multiple scales and adjusted during history matching (app. 2), in recognition of uncertainty in the quantity of net infiltration that ultimately reaches the regional water table.

## Surface Water

In both models, the surface water network was simulated using the Streamflow-Routing (SFR) Package in MODFLOW 6, except for the Mississippi and Big Black Rivers in the Delta model, which were simulated using the River Package (fig. 1.1). SFR input was developed from NHDPlus version 2 data (McKay and others, 2012) following the methods described in Leaf (2023), using SFRmaker (Leaf and others, 2021) and Modflow-setup (Leaf and Fienen, 2022). Unlike previous versions of the MERAS model, which only included the 42 largest streams, MERAS 3 includes most streams in the Mississippi Embayment that are likely to flow for at least a few months each year—several thousand streams in total or about 24 percent of the flowlines mapped in NHDPlus version 2 (Leaf, 2023). Drainage lakes connected to the stream network are represented as linear features based on the NHDPlus flowlines that pass through them (McKay and others, 2012). Seepage lakes that are unconnected to the stream network are not explicitly represented. Given the regional scale of both the MERAS 3 and Delta models, such simplifications are considered reasonable (see for example the discussion of St. Venant's Principle in Haitjema, 1995). The same preprocessed stream network was used for the MERAS 3 and Mississippi Delta models.

The SFR packages in the MERAS 3 and Mississippi Delta models simulate a water balance for each stream reach, accounting for flow accumulated from upstream, groundwater/surface water interactions within the reach, and surface water runoff (as overland flow) estimated from the SWB simulation (Nielsen and Westenbroek, 2023). Other potentially important streamflow generation processes such as subsurface interflow, perched groundwater, bank storage and irrigation return flow

are not accounted for. Comparison of simulated and observed streamflow and stages indicated that inclusion of surface water runoff was critical for realistic simulation of surface water availability and groundwater/surface water gradients, consistent with the large part of runoff in the surface water balance. Leaf (2023) describes the methods used to aggregate daily gridded SWB runoff to monthly runoff at each stream reach.

Monthly total stream inflows at 44 sites along the MERAS perimeter were estimated from climate and watershed characteristics and flows measured at gaging sites, using a random forest regression model (Dietsch and others, 2022; fig. 1.14). For the Mississippi Delta model, inflows to the Tallahatchie/Yazoo system were derived from measured daily outflows at the four major flood control reservoirs (Arkabutla, Enid, Sardis and Grenada Lakes; Tim Rodgers, U.S. Army Corps of Engineers, written commun., March 19, 2020; fig. 1.1B). Inflow rates were averaged to the periods represented by each model stress period and specified in the period data blocks of the SFR Package input file. Since the flood control reservoir outlets are downstream from the Mississippi Delta model perimeter, corresponding outlets were specified in the SFR Package immediately upstream from the inflows, to intercept all flow accumulated from upstream (so that streamflow was 100 percent specified at the reservoir outlets). Stress periods without inflows were filled with average values across the record for a particular site (typically July 2000 to January 2019 for the random forest model estimates, and April 1998 to January 2020 for the flood control reservoirs).

## Water Use

Agricultural water use for the monthly history matching stress periods (April 1, 2007, through 2018) was estimated using the Aquaculture and Irrigation Water-Use Model (AIWUM), version 1.1. (Bristow and Wilson, 2023; Wilson, 2021). Volumetric water use rates (cubic meters for each 1-square-kilometer NHG cell) from the AIWUM output were averaged for each monthly stress period and resampled to the model grids using the nearest neighbor method in Modflow-setup. Agricultural water-use estimates for 2019 and future years out to 2056 were based on crop water demand from the SWB simulation of Nielsen and Westenbroek (2023), and a future version of that simulation driven by downscaled General Circulation (climate) Model outputs (see the “Future Climate Scenarios” section). Daily gridded water use estimates from the SWB simulations were averaged to the monthly stress periods and resampled to the model grid using a nearest neighbor approach. AIWUM and SWB-based pumping rates were located vertically in the model using geostatistical estimates for the top and bottom of irrigation production zone in the alluvial aquifer developed by Torak (2023).

Nonagricultural water use for the monthly stress periods was compiled from the USGS Site-Specific Water Use Data System (SWUDs) and national estimates for water use associated with thermoelectric power generation in 2010 and 2015

(Diehl and Harris, 2014; Harris and Diehl, 2019a, b). Together, these two data sources are assumed to represent most nonagricultural water use within the Mississippi Embayment (for example, Lovelace and others, 2020). For each monthly stress period (after April 1, 2007), the closest available rate (backward or forward in time) was applied at each pumping location in the two databases. Nonagricultural pumping was located vertically using open intervals or estimated production zones from Knierim and others (2019).

Water use before April 2007 was taken from the MERAS 2.2 model (Haugh and others, 2020a). Pumping rates were read from the Multinode Well (MNW1) Package and located in space using FloPy (Bakker and others, 2022), and then mapped to the MERAS 3 and Delta model discretizations using Modflow-setup. In instances where multiple MERAS 2.2 stress periods overlapped a single MERAS 3 or Delta model stress period, average values were applied.

All water use was simulated in the MERAS 3 and Mississippi Delta models using the Well Package in MODFLOW 6. After constructing the model, input water use rates were adjusted by source dataset, stress period, and geographic region ([fig. 2](#)) or use category (crop type or nonagricultural), as described in the “Parameter Estimation” section. [Figure 1.2](#) compares water use from the various sources to the inputs used in the two models. Differences between the fluxes estimated by the AIWUM and the rates ultimately applied to the Well Package (after history matching; see [app. 2](#)) reflect both uncertainty in the AIWUM rates (Wilson, 2021) and correlation with the groundwater recharge input, which also is uncertain; for example, lower pumping rates in the MERAS 3 model relative to the AIWUM estimates could be at least in part an artifact of lower recharge rates estimated for the Mississippi Alluvial Plain in MERAS 3 compared to the Delta model.

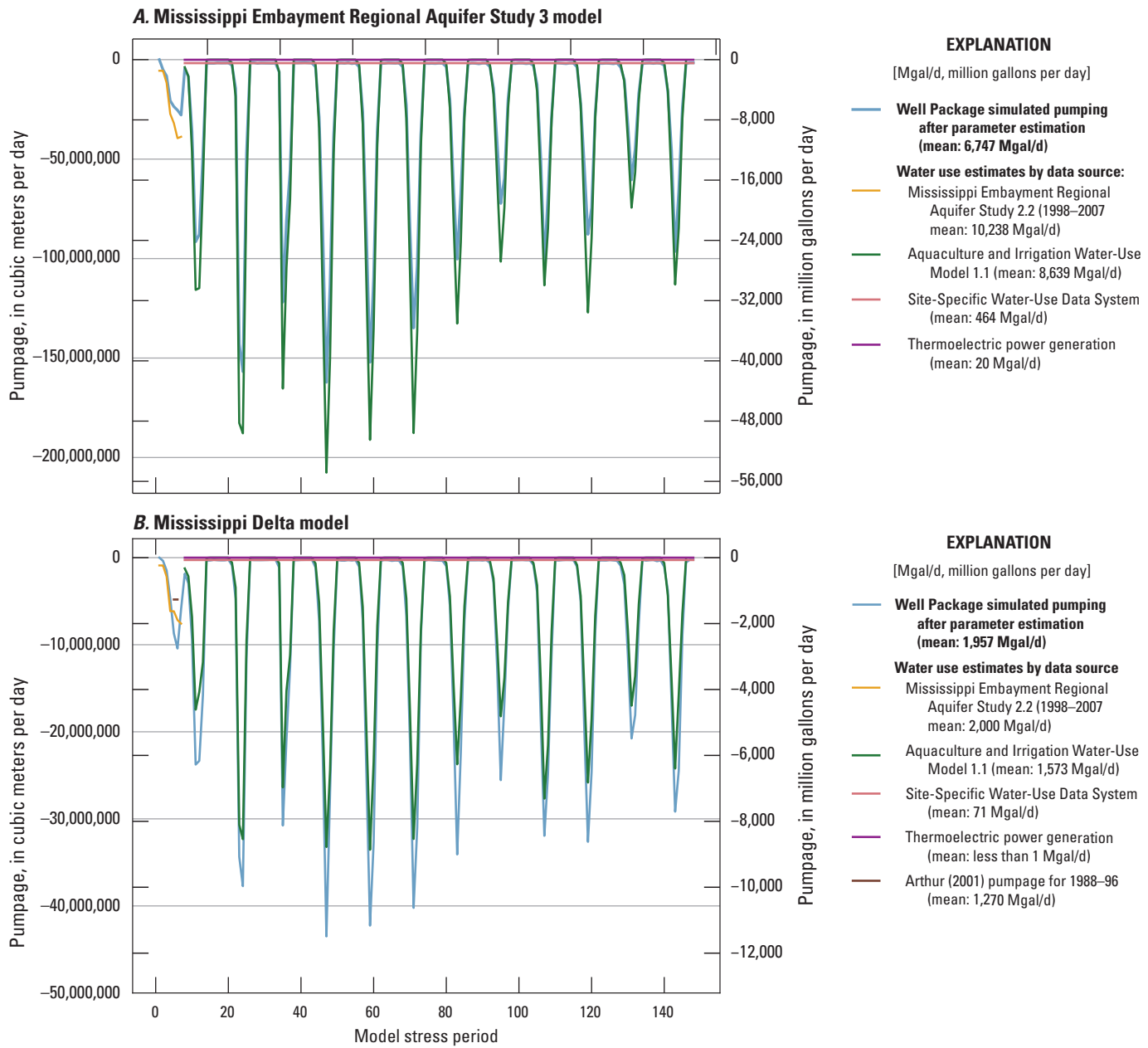


**Figure 1.2.** Water use estimates by data source compared to model input A, for the Mississippi Embayment Regional Aquifer Study (MERAS) 3 model; B, for the Mississippi Delta model. To facilitate comparison with the model input, values from each source were summed across the model area, and then averaged to each stress period.

## Subsurface Properties

Aquifer hydraulic conductivity and storage properties were represented structurally in the MERAS 3 and Mississippi Delta models at multiple scales, using a blend of the conceptual models produced by the AEM survey of Minsley and others (2021), and the original MERAS characterization of Hart and others (2008).

### Aquifer Properties in the MERAS 3 Model

The MERAS 3 model consists of three layers: the Mississippi River Valley alluvial aquifer (layer 1); a lumped confining unit consisting of the Vicksburg-Jackson confining unit, the Upper Claiborne aquifer, and the Middle Claiborne confining unit (layer 2); and a lumped lower aquifer (layer 3) that includes the Middle Claiborne aquifer and all underlying units in the Tertiary sequence (fig. 4). At the coarsest level, aquifer properties in layer 1 were zoned based on logarithmically binned classes of vertically averaged electrical resistivity within the alluvial aquifer (Minsley and others, 2021; James and Minsley, 2021), shown as the blue-green-yellow tones in figure 4. In the model parametrization for history matching, the electrical resistivity-based zones were further subdivided by geographic region (fig. 2, table 2.5). Outside of the alluvial plain, aquifer properties in layer 1 were zoned based on the relation of the model cell centers to the hydrostratigraphic surfaces of Hart and others (2008); for example, cells with centers between the top and bottom surfaces for the Middle Claiborne aquifer were classified as Middle Claiborne (zone 15 in fig. 1.3). Layers 2 and 3 are defined based on the hydrostratigraphic surfaces of Hart and others (2008), with each having a single zone. Additional cell to cell variability within all zones was incorporated using pilot points (Doherty, 2003), as described in appendix 2.

### Aquifer Properties in the Mississippi Delta Model

Layers in the Delta model were uniformly discretized to 5 meters thickness within the alluvial aquifer, except along the alluvial aquifer bottom, where extruding layers were either

pinched out or consolidated with the overlying layer (see the Regional and inset model layering section). Below the alluvial aquifer, thickness increases by 50 percent with each successive layer, starting with a thickness of 7.5 meters, and extending to the base of the AEM data. At the coarsest level, aquifer properties in the cells containing AEM data were zoned, based on the logarithmically binned electrical resistivity “facies classes” of Minsley and others (2021) and James and Minsley (2021). Similar to the MERAS 3 model, cells outside the extent of the AEM data were assigned a zone corresponding to the position of their center point with respect to the hydrostratigraphic surfaces of Hart and others (2008). Figure 1.4 shows the aquifer property zones by layer.

Similar to the regional MERAS 3 model, additional cell to cell variability in horizontal and vertical hydraulic conductivity, and specific yield (in the AEM based zones only) was incorporated within zones using pilot points, as described in the parameter estimation section. Specific storage and specific yield below the AEM data extent were only represented with piecewise-constant zones (no sub-zone heterogeneity was included).

### Streambed Leakance

The streambed vertical hydraulic conductivity input to the SFR Package ( $rhk$ ; Langevin and others, 2022) was specified as streambed leakance, by specifying a uniform streambed thickness of 1 meter. Specifying leakance (streambed vertical hydraulic conductivity divided by streambed thickness) is advantageous in that it represents a single integrated term that can potentially be estimated from aquifer heads and stream stages, without direct knowledge of streambed thickness, which is difficult or impossible to adequately characterize in the field. Initial streambed leakance values were estimated on a cell-by-cell basis using results from waterborne surveys of subsurface electrical resistivity (Leaf, 2023, fig. 11; fig. 2.21 in this report).

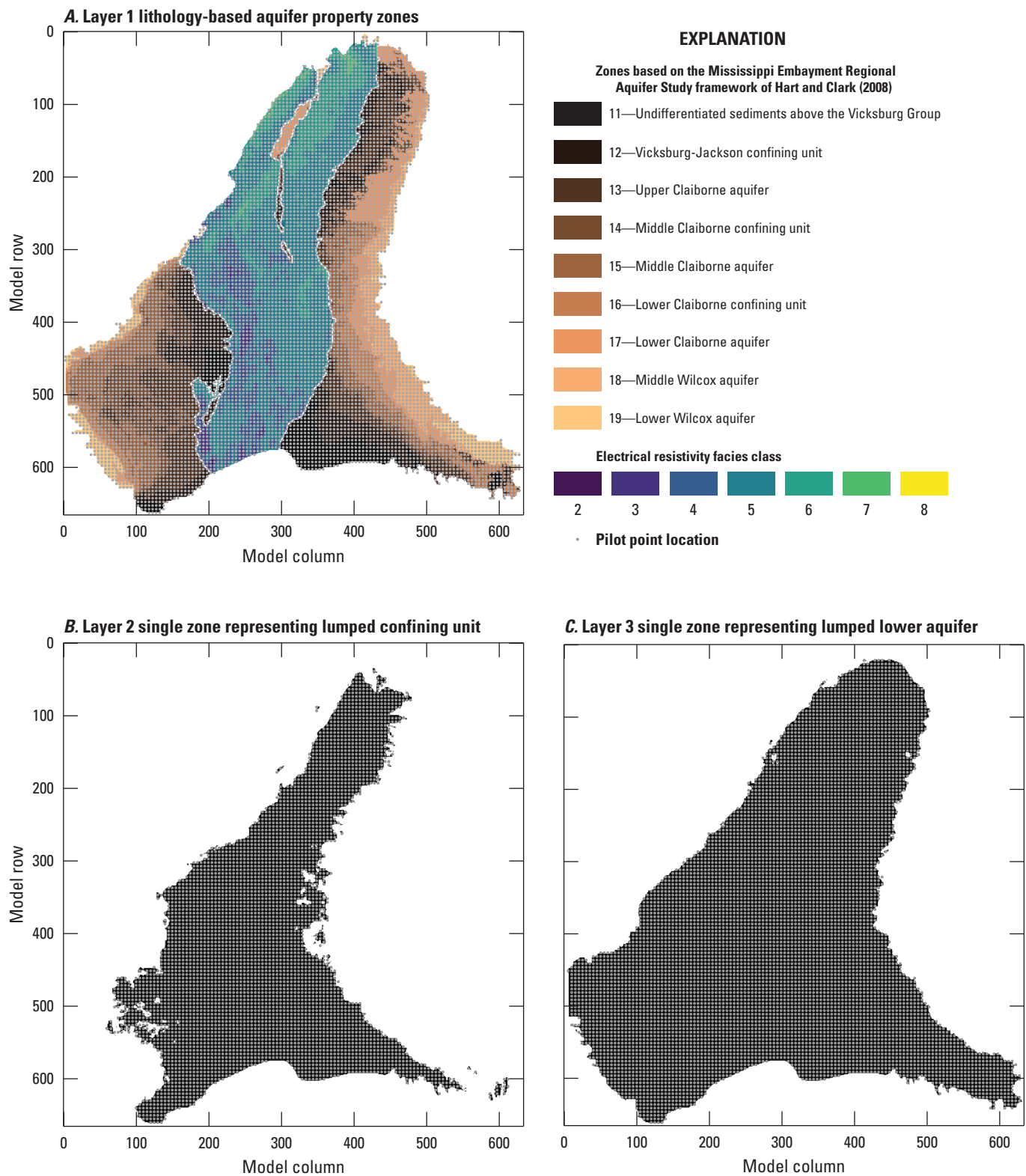


**Figure 1.3.** Lithology-based aquifer property zones in the Mississippi Embayment Regional Aquifer Study 3 model with pilot point locations.

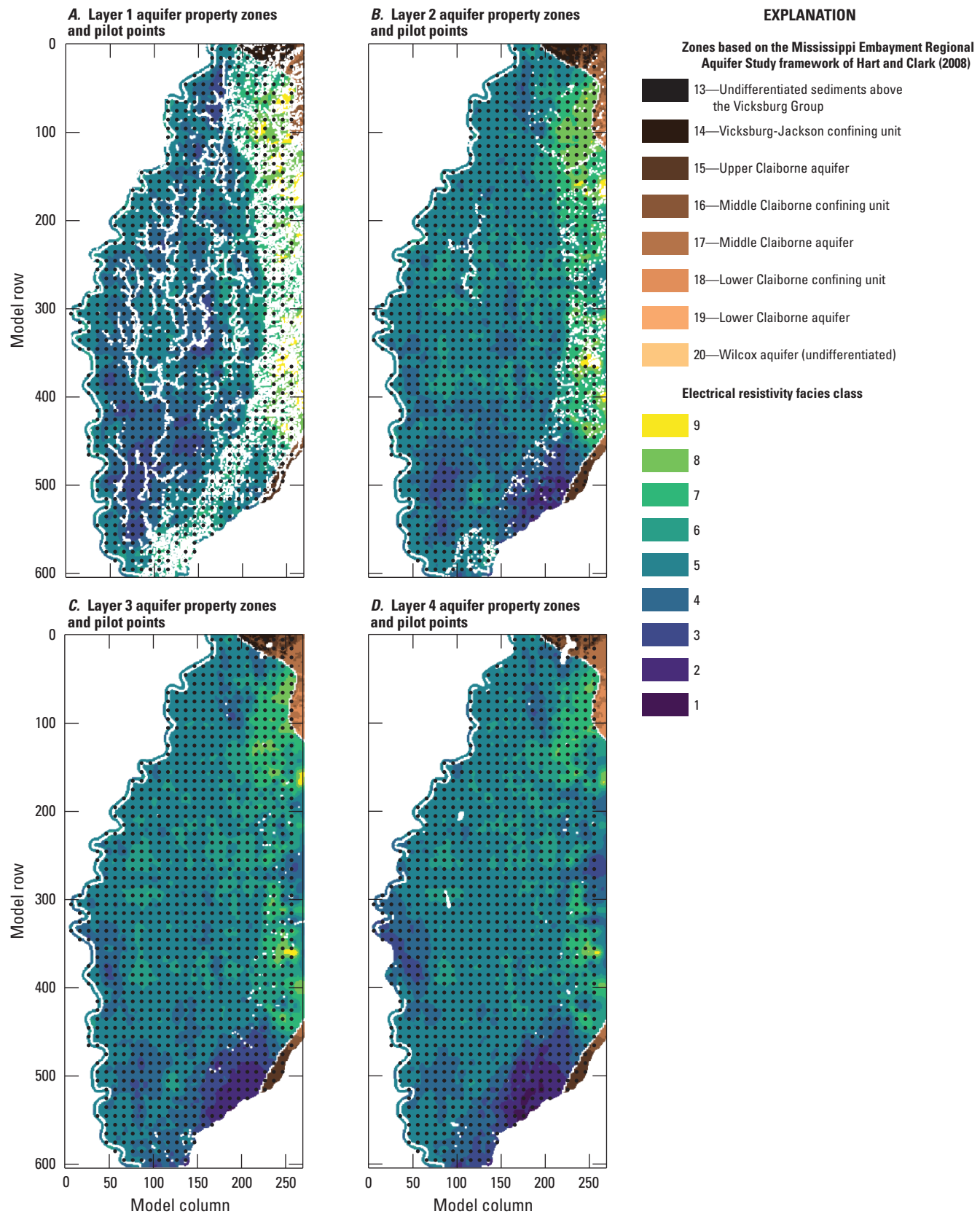


Figure 1.4. Aquifer property zones in the Mississippi Delta model, by layer, with pilot point locations.

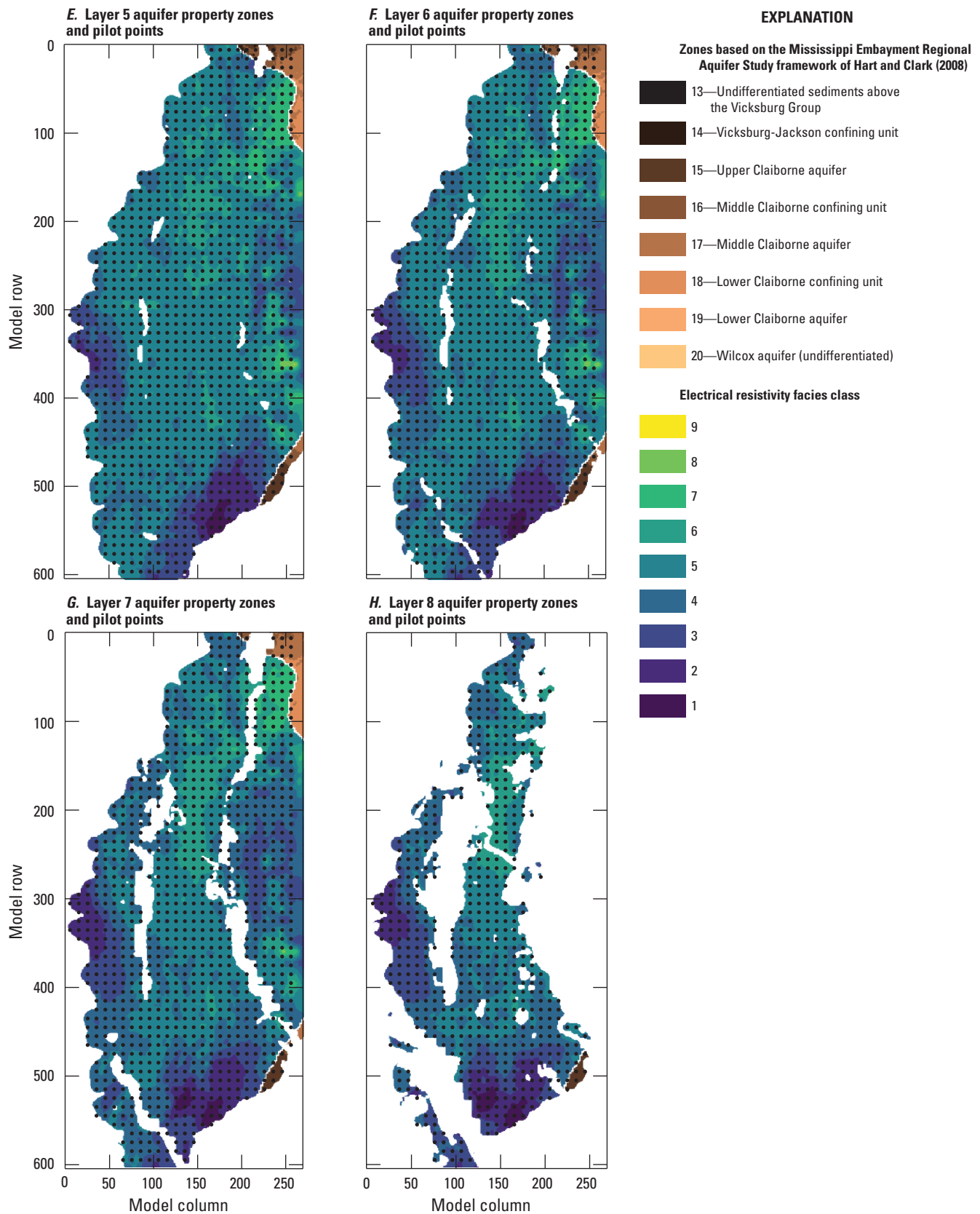


Figure 1.4. Aquifer property zones in the Mississippi Delta model, by layer, with pilot point locations.

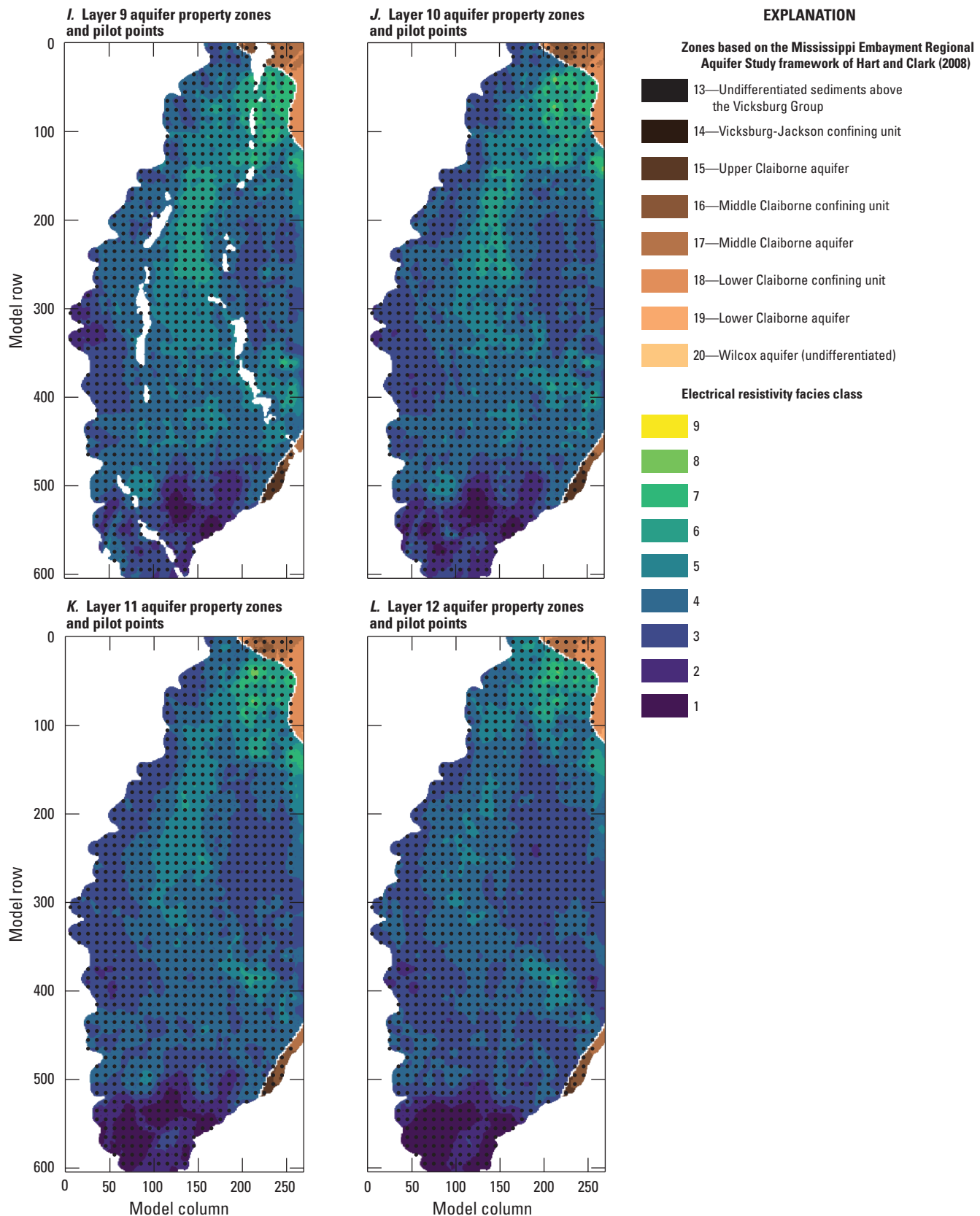


Figure 1.4. Aquifer property zones in the Mississippi Delta model, by layer, with pilot point locations.

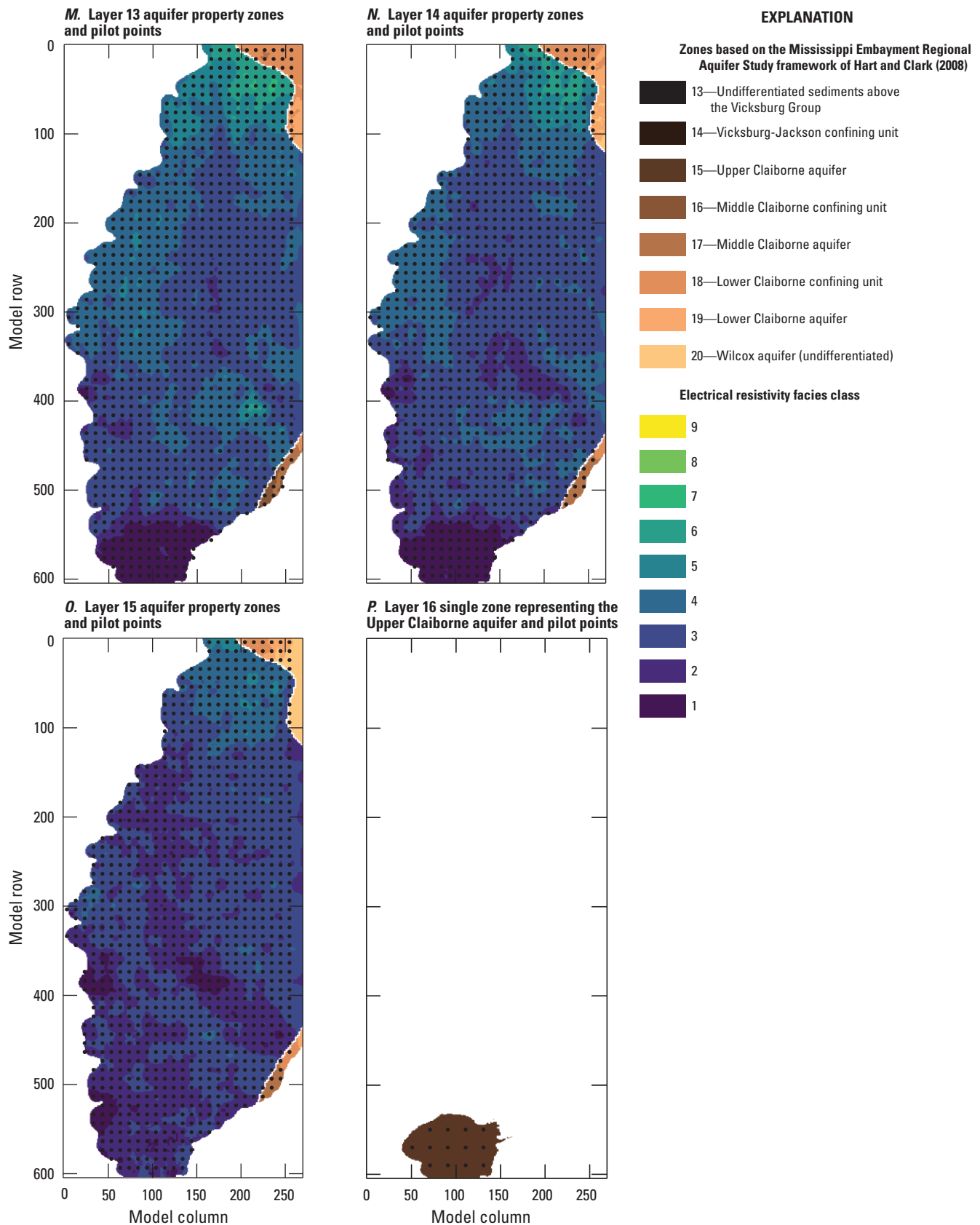


Figure 1.4. Aquifer property zones in the Mississippi Delta model, by layer, with pilot point locations.

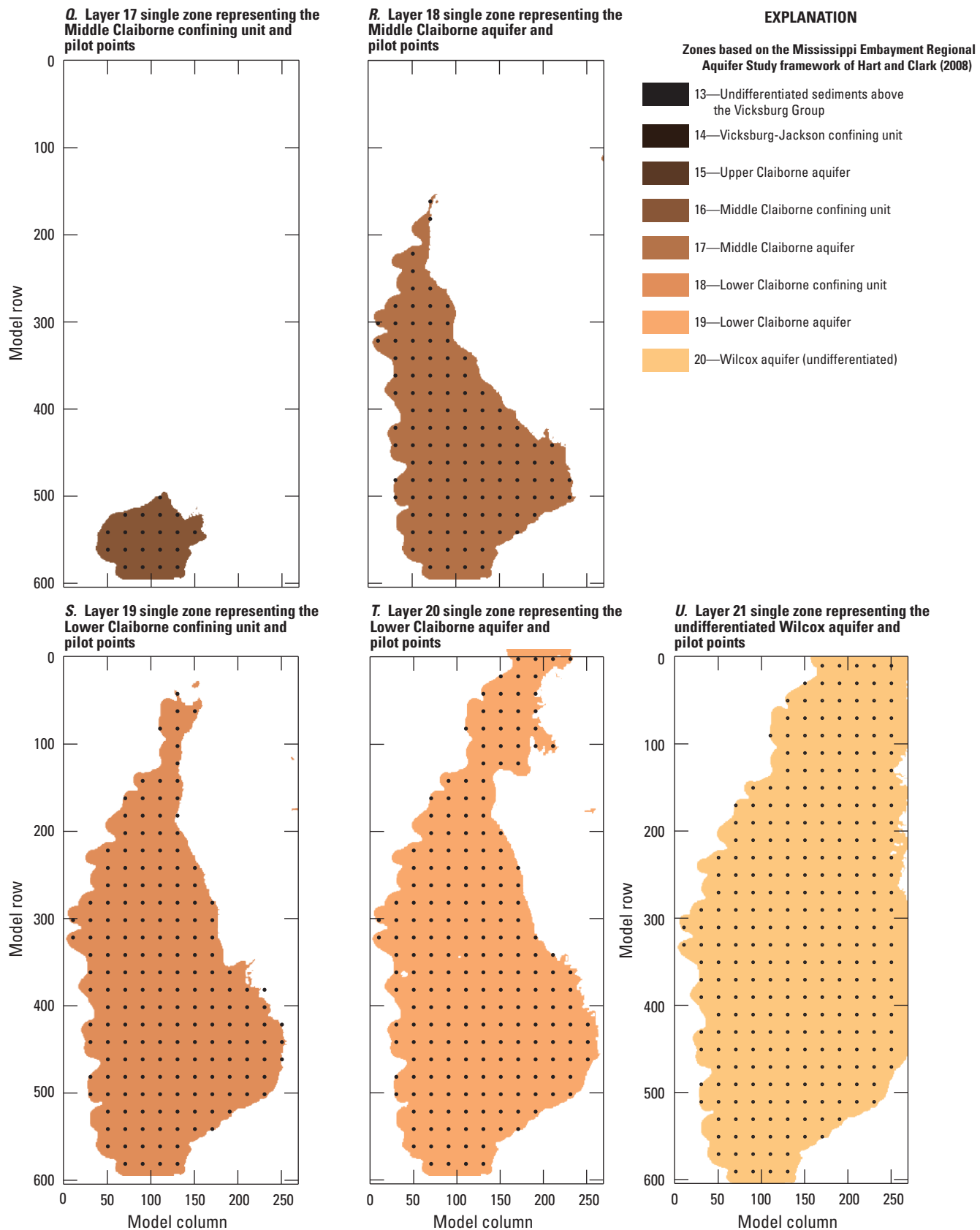


Figure 1.4. Aquifer property zones in the Mississippi Delta model, by layer, with pilot point locations.

## Model Solver

The systems of equations for the MERAS 3 and Mississippi Delta models were developed using the Newton-Raphson formulation in MODFLOW 6 (Langevin and others, 2017). The two models were solved independently using the Integrated Model Solution (IMS) Package with the “complex” setting (Langevin and others, 2022). Solution times for the two models are sensitive to the model input values. Using the “best” parameter sets (described in the Parameter Estimation section), solution times for the spin-up and history matching period of 1900 through 2018 (148 stress periods) are about 1.5 hours for the MERAS 3 model and 2 hours for the Mississippi Delta model.

## References Cited

Bakker, M., Post, V., Hughes, J.D., Langevin, C.D., White, J.T., Leaf, A.T., Paulinski, S.R., Bellino, J.C., Morway, E.D., Toews, M.W., Larsen, J.D., Fienen, M.N., Starn, J.J., and Brakenhoff, D., 2022, FloPy v3.3.5—Release candidate: U.S. Geological Survey software release, accessed July 18, 2023, at <https://doi.org/10.5066/F7BK19FH>.

Bristow, E., and Wilson, J.L., 2023, Aquaculture and irrigation water-use model (AIWUM) version 1.1 estimates and related datasets for the Mississippi Alluvial Plain: U.S. Geological Survey data release, <https://doi.org/10.5066/P9RGZOBZ>.

Clark, B.R., Barlow, P.M., Peterson, S.M., Hughes, J.D., Reeves, H.W., and Viger, R.J., 2018, National-scale grid to support regional groundwater availability studies and a national hydrogeologic database: U.S. Geological Survey data release, accessed July 18, 2023, at <https://doi.org/10.5066/F7P84B24>.

Clark, B.R., and Hart, R.M., 2009, The Mississippi Embayment Regional Aquifer Study (MERAS)—Documentation of a groundwater-flow model constructed to assess water availability in the Mississippi embayment: U.S. Geological Survey Scientific Investigations Report 2009–5172, 61 p., accessed July 18, 2023, at <https://doi.org/10.3133/sir20095172>.

Diehl, T.H., and Harris, M.A., 2014, Withdrawal and consumption of water by thermoelectric power plants in the United States, 2010: U.S. Geological Survey Scientific Investigations Report 2014–5184, 28 p. [Also available at <https://doi.org/10.3133/sir20145184>.]

Dietsch, B., Asquith, W.H., Breaker, B.K., Westenbroek, S.M., and Kress, W.H., 2022, Simulation of monthly mean and monthly base flow of streamflow using random forests for the Mississippi River Alluvial Plain, 1901 to 2018: U.S. Geological Survey Scientific Investigations Report 2022–5079, 17 p., accessed July 18, 2023, at <https://doi.org/10.3133/sir20225079>.

Doherty, J., 2003, Ground water model calibration using pilot points and regularization: *Groundwater*, v. 41, no. 2, p. 170–177. [Also available at <https://doi.org/10.1111/j.1745-6584.2003.tb02580.x>.]

Haitjema, H.M., 1995, Analytic element modeling of groundwater flow: San Diego, Calif., Academic Press, 394 p.

Harris, M.A., and Diehl, T.H., 2019a, Water withdrawal and consumption estimates for thermoelectric power plants in the United States, 2015: U.S. Geological Survey data release, accessed July 18, 2023, at <https://doi.org/10.5066/P9V0T04B>.

Harris, M.A., and Diehl, T.H., 2019b, Withdrawal and consumption of water by thermoelectric power plants in the United States, 2015: U.S. Geological Survey Scientific Investigations Report 2019–5103, 15 p. [Also available at <https://doi.org/10.3133/sir20195103>.]

Hart, R.M., Clark, B.R., and Bolyard, S.E., 2008, Digital surfaces and thicknesses of selected hydrogeologic units within the Mississippi Embayment Regional Aquifer Study (MERAS): U.S. Geological Survey Scientific Investigations Report 2008–5098, 33 p., accessed July 18, 2023, at <https://doi.org/10.3133/sir20085098>.

Haugh, C.J., Killian, C.D., and Barlow, J.R.B., 2020a, MODFLOW–2005 model used to evaluate water-management scenarios for the Mississippi Delta: U.S. Geological Survey data release, accessed July 18, 2023, at <https://doi.org/10.5066/P906VM5>.

Haugh, C.J., Killian, C.D., and Barlow, J.R.B., 2020b, Simulation of water-management scenarios for the Mississippi Delta: U.S. Geological Survey Scientific Investigations Report 2019–5116, 15 p. [Also available at <https://doi.org/10.3133/sir20195116>.]

Hunt, R.J., White, J.T., Duncan, L.L., Haugh, C.J., and Doherty, J., 2021, Evaluating lower computational burden approaches for calibration of large environmental models: *Groundwater*, v. 59, no. 6, p. 788–798. [Also available at <https://doi.org/10.1111/gwat.13106>.]

James, S.R., and Minsley, B.J., 2021, Combined results and derivative products of hydrogeologic structure and properties from airborne electromagnetic surveys in the Mississippi Alluvial Plain: U.S. Geological Survey data release, accessed July 18, 2023, at <https://doi.org/10.5066/P9382RCI>.

Knierim, K.J., Kingsbury, J.A., and Haugh, C.J., 2019, Groundwater withdrawal zones for drinking water from the Mississippi River Valley alluvial aquifer and Mississippi embayment aquifers: U.S. Geological Survey data release, accessed July 18, 2023, at <https://doi.org/10.5066/P9FZV4ED>.

Langevin, C.D., Hughes, J.D., Banta, E.R., Niswonger, R.G., Panday, S., and Provost, A.M., 2017, Documentation for the MODFLOW 6 Groundwater Flow Model: U.S. Geological Survey Techniques and Methods, book 6, chap. A55, [variously paged], accessed July 18, 2023, at <https://doi.org/10.3133/tm6A55>.

Langevin, C.D., Hughes, J.D., Provost, A.M., Russcher, M.J., Niswonger, R.G., Panday, S., Merrick, D., and Banta, E.R., 2022, MODFLOW 6 Modular Hydrologic Model (ver. 6.3.0): U.S. Geological Survey software release, accessed July 18, 2023, at <https://doi.org/10.5066/P97FFF9M>.

Leaf, A.T., 2023, Automated construction of Streamflow-Routing networks for MODFLOW—Application in the Mississippi Embayment region: U.S. Geological Survey Scientific Investigations Report 2023–5051, 27 p., <https://doi.org/10.3133/sir20235051>.

Leaf, A.T., Duncan, L.L., and Haugh, C.J., 2023, MODFLOW 6 models for simulating groundwater flow in the Mississippi Embayment with a focus on the Mississippi Delta: U.S. Geological Survey data release, <https://doi.org/10.5066/P971LPOB>.

Leaf, A.T., and Fienen, M.N., 2022, Modflow-setup—Robust automation of groundwater model construction: *Frontiers in Earth Science*, v. 10, art. 903965, 11 p. [Also available at <https://doi.org/10.3389/feart.2022.903965>.]

Leaf, A.T., Fienen, M.N., and Reeves, H.W., 2021, SFRmaker and Linesink-maker—Rapid construction of streamflow routing networks from hydrography data: *Groundwater*, v. 59, no. 5, p. 761–771. [Also available at <https://doi.org/10.1111/gwat.13095>.]

Lovelace, J.K., Nielsen, M.G., Read, A.L., Murphy, C.J., and Maupin, M.A., 2020, Estimated groundwater withdrawals from principal aquifers in the United States, 2015 (ver. 1.2, October 2020): U.S. Geological Survey Circular 1464, 70 p. [Also available at <https://doi.org/10.3133/cir1464>.]

McKay, L., Bondelid, T., Dewald, T., Johnston, J., Moore, R., and Rea, A., 2012, NHDPlus version 2—User guide [data model ver. 2.1]: U.S. Environmental Protection Agency, accessed September 17, 2018, at [http://www.horizon-systems.com/NHDPlus/NHDPlusV2\\_documentation.php](http://www.horizon-systems.com/NHDPlus/NHDPlusV2_documentation.php).

Minsley, B.J., Rigby, J.R., James, S.R., Burton, B.L., Knierim, K.J., Pace, M.D.M., Bedrosian, P.A., and Kress, W.H., 2021, Airborne geophysical surveys of the lower Mississippi valley demonstrate system-scale mapping of subsurface architecture: *Communications Earth & Environment*, v. 2, no. 1, art. 131, 14 p. [Also available at <https://doi.org/10.1038/s43247-021-00200-z>.]

Nielsen, M.G., and Westenbroek, S.M., 2023, Updated estimates of water budget components for the Mississippi embayment region using a Soil-Water-Balance model, 2000–2020: U.S. Geological Survey Scientific Investigations Report 2023–5080, 58 p., <https://doi.org/10.3133/sir20235080>.

Torak, L.J., 2023, Digital surfaces and site data of well-screen top and bottom altitudes defining the irrigation production zone of the Mississippi River Valley alluvial aquifer within the Mississippi Alluvial Plain project region: U.S. Geological Survey data release, <https://doi.org/10.5066/P9TSDEAC>.

Virtanen, P., Gommers, R., Oliphant, T.E., Haberland, M., Reddy, T., Cournapeau, D., Burovski, E., Peterson, P., Weckesser, W., Bright, J., van der Walt, S.J., Brett, M., Wilson, J., Millman, K.J., Mayorov, N., Nelson, A.R.J., Jones, E., Kern, R., Larson, E., Carey, C.J., Polat, I., Feng, Y., Moore, E.W., and VanderPlas, J., 2020, SciPy 1.0—Fundamental algorithms for scientific computing in Python: *Nature Methods*, v. 17, no. 3, p. 261–272. [Also available at <https://doi.org/10.1038/s41592-019-0686-2>.]

Wilson, J.L., 2021, Aquaculture and Irrigation Water-Use Model (AIWUM) version 1.0—An agricultural water-use model developed for the Mississippi Alluvial Plain, 1999–2017: U.S. Geological Survey Scientific Investigations Report 2021–5011, 36 p., accessed July 18, 2023, at <https://doi.org/10.3133/sir20215011>.

## Appendix 2. Parameter Estimation and Uncertainty Analysis

After construction, the models were parameterized, and history matching (Anderson and others, 2015, chap. 9) was performed, in which model input parameter values were systematically adjusted within reasonable (prior) ranges to improve model fit to field observations. The overall approach to history matching is similar to the detailed description given by Corson-Dosch and others (2022) and Fienen and others (2022). Parametrization followed a multiscale, high-dimensional approach, where both coarse- and fine-scale parameters were used with the tools of White and others (2021). Field observations of aquifer heads and stream flows were processed into multiyear or monthly averages corresponding to model stress periods. Initial trial-and-error model runs focused on manual adjustment of coarse-scale parameters to improve history matching and gain insight about the key aspects of the groundwater flow system. The iterative Ensemble Smoother (iES) algorithm implemented in PEST++; (White, 2018; White and others, 2020) was then used to formally estimate both coarse and fine scale parameters. In iES, an ensemble of parameter sets (realizations) is carried through the analysis. At each step, empirical correlations between the parameter ensemble and changes in observation values are used to iteratively improve model fit to observations (that is, minimize the objective function) while constraining the parameter values (reducing model uncertainty). The iES results therefore provide estimates of model uncertainty through the parameter values and observation outputs of the ensemble members. A “base” ensemble member that approximates the minimum error variance solution can be used as a “best” model. Parameter estimation files and reproducible workflows for setting up the parameter estimation are provided in an associated data release (Leaf and others, 2023).

## Observations

Field observation data included groundwater levels, streamflow, and estimates of aquifer transmissivity derived from pumping tests. Raw field observations were aggregated as described below to best match simulated equivalents in the model, and then further processed into derivative observations aimed at capturing spatial and temporal gradients. [Table 2.1](#) summarizes the various observations by group.

## Head Observation Data

Monthly head observations for 3,436 wells in the MERAS study area (717 wells within the Mississippi Delta model area) were produced from the National Water

Information System (NWIS) database using the methods of Asquith and Seanor (2019) and Asquith and others (2020). In instances of multiple observations at a site within the same month, the last observation was used, as this represents the observed system at a state closest to the simulated system state at the end of a stress period (when all stresses for that period have been applied). A similar approach was taken for the multiyear spin-up stress periods, where observation values were computed as the mean of observed values during the last two years of the stress period, where two or more values were present. No observations were included for the initial steady-state period. [Figure 2.1](#) shows a map of head observation sites with weighted observations that were formally included in the history matching. In most wells, head observations were available biannually at the typical seasonal high point of April and typical low point in October.

## Streamflow and Stage Observation Data

Monthly observations of total streamflow and stream stage were produced from the NWIS database and the random forest regression model of Dietsch and others (2022). Daily values at 182 continuous record sites within the MERAS study area (30 sites within the Mississippi Delta model area) were downloaded and aggregated to monthly values by taking the mean. Given the short timeframes at which total stream flows and stages can vary, mean values (as opposed to the last values used for heads) were seen as most representative of the overall system mass balance at a monthly timescale. Monthly means of measured values were also consistent with the random forest regression model of Dietsch and others (2022), which estimates monthly mean total flows. Monthly streamflow estimates from the random forest regression model (Dietsch and others, 2022; “flux\_estimated” observation group) were mostly used to fill gaps in the 2010 through 2018 measurement record at existing sites, with the exception of estimates from two ungaged locations used in the MERAS 3 model history matching. Observations derived from estimates were generally given lower weight ([table 2.1](#)), to reflect greater uncertainty. [Figure 2.2](#) shows a map of stream observation sites.

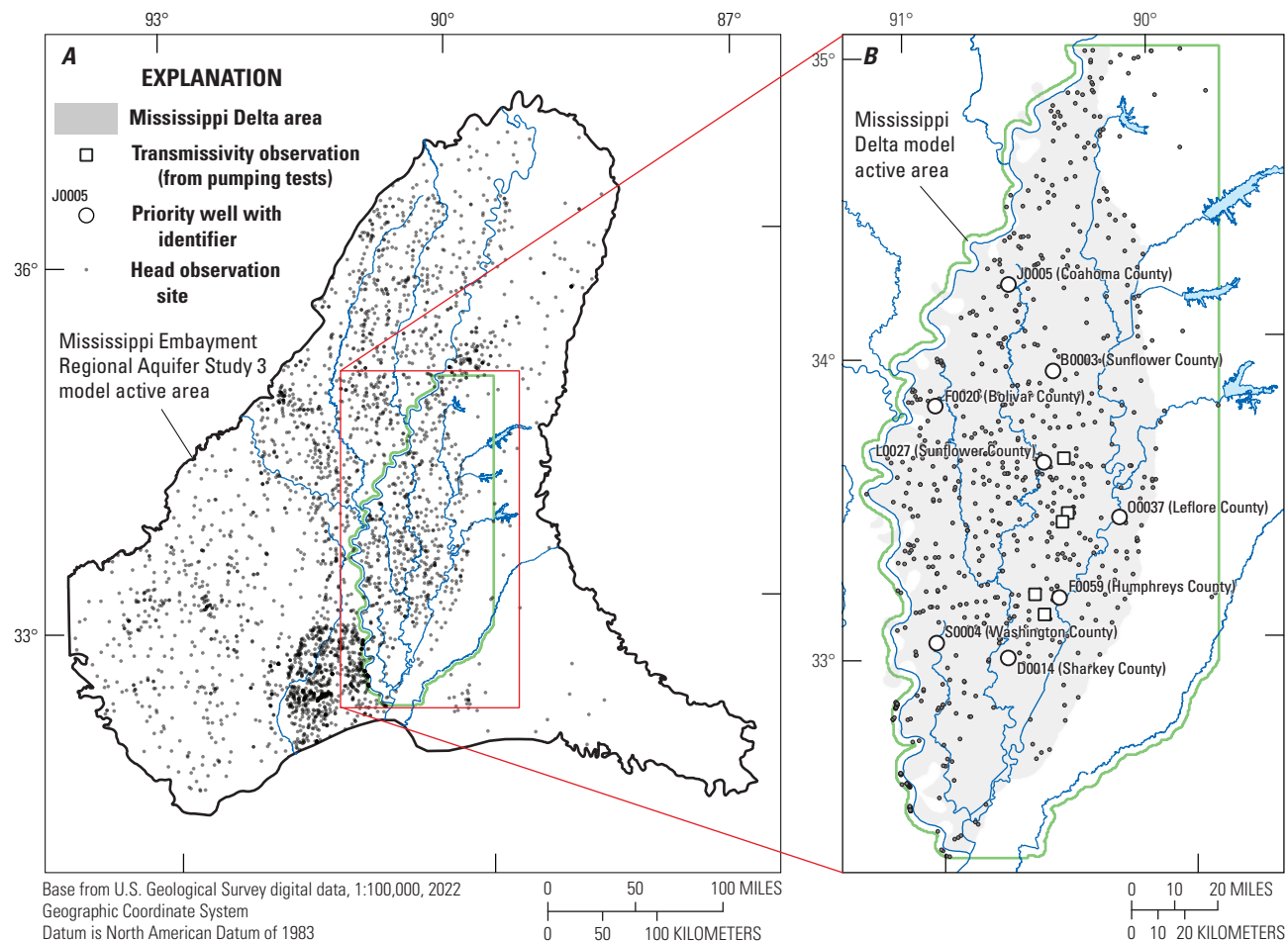


**Figure 2.1.** Head and transmissivity observation sites with weighted observations for *A*, the regional model; and *B*, the Mississippi Delta model.

## Aquifer Transmissivities

Pumping test estimates of aquifer transmissivity in the Mississippi River Valley alluvial aquifer were obtained from the Mississippi Department of Environmental Quality (James Hoffman, Geologist, written commun., May 27, 2020) and included as PEST observations in comparison to equivalent transmissivities in the model. Figure 2.1 shows the locations of the pumping tests.

## Derivative Observations

In addition to observations of head and streamflow, observations that are derived from these absolute quantities, including temporal and spatial differences, were computed using the Modflow-obs python package (<https://github.com/aleaf/modflow-obs>) developed in part for this study. Temporal difference observations, or changes in head or streamflow between time periods, were computed at all sites; spatial

difference observations (to assess computed hydraulic gradients or streamflow loss/gain, for example) were computed for select pairs of sites. Long-term trends in water levels for some wells from 2010 to 2019 also were input as derivative observations. To ensure consistency, all derivatives for the aggregated field observations and simulated equivalents were computed in tandem as part of a forward model run. Table 2.1 summarizes the various types and numbers of derivative observations that were ultimately given weight in the history matching for the two models.

## Temporal Differences

Two types of temporal differences were computed. Successive temporal differences, in which the previous observation value was subtracted from each observation, were computed to provide more direct information on aquifer storage (a function of the change in head with time). Displacement observations, in which each observation in a timeseries was subtracted from a datum or reference observation value, were computed to remove the bias of systematic errors, especially

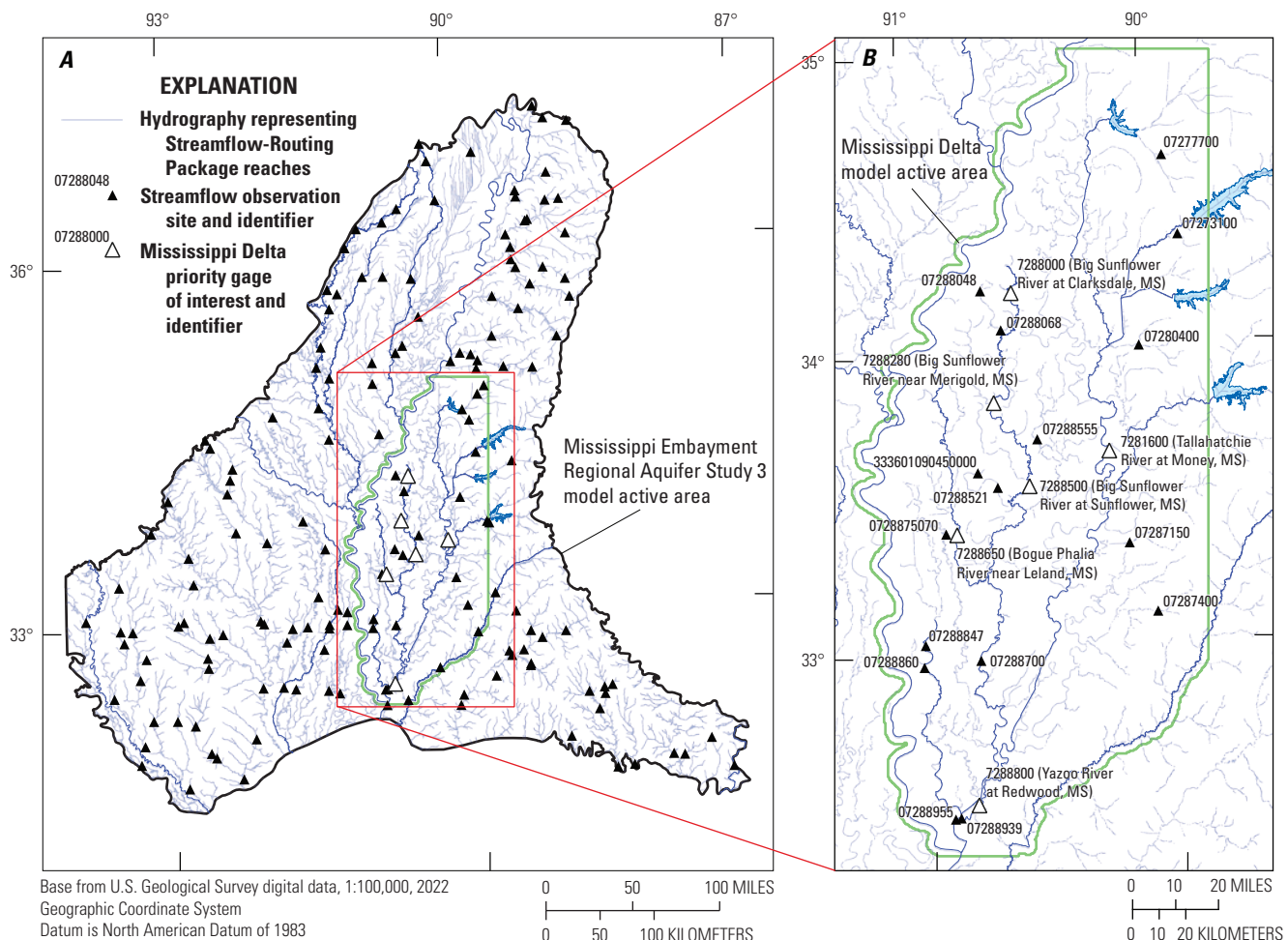


**Figure 2.2.** Streamflow observation sites for A, the regional model; and B, the Mississippi Delta model.

those related to the model spin-up, that might affect the simulation of absolute quantities but not trends with time (for example, Doherty and Hunt, 2010, p. 13).

## Spatial Differences

Spatial difference observations were computed at selected pairs of sites where the difference in the observed quantity was thought to provide information about a key aspect of the system. These included pairs of wells spanning the horizontal gradients into the depression cone in the central Delta area (figs. 2, 3), in addition to pairs of wells close to one another, but with different open intervals (for assessing vertical gradients). Gains or losses in streamflow between gaging locations are especially useful for directly measuring the net flux between the stream and groundwater system along the intervening stream reaches. Streamflow differences included the Merigold (07288280) and Sunflower (07288500) sites on the Big Sunflower River, the Money (07281600) and Redwood (07288800) sites on the Tallahatchie/Yazoo River, the Redwood and below Steel Bayou (07288955) sites on

the Yazoo River (to gage the total flow coming out of Steel Bayou), and the Tallahatchie at Money gage (07281600) subtracted from the total outflows from the four flood control reservoirs (figs. 1, 2.2). Spatial difference observations for each pair of sites were computed for all stress periods where both flows were available.

## Head Trend Observations

Longer-term water level trends, which are often approximately linear in the alluvial aquifer (see for example the hydrograph for NWIS site 335540090273001), were captured by computing linear regressions on measured heads and their simulated equivalents, for the period of 2010 to 2019. The estimated slopes for the measured and simulated trend lines were then treated as observations by PEST, for each site with at least 10 measurements from 2010 to 2019. While some wells exhibited a v-shaped recovery during this time period (for example, site 333742090303801), comparison of linear trends can still provide useful information for history matching; for example, if only absolute heads are

compared, a simulated time series with a trend opposite that of the observed data might still produce a model “best fit” (that minimizes the sum of squared, weighted residuals), especially with the inevitable trade-offs in history matching that result from model structural error(s). In this case, a somewhat worse absolute fit might be preferable if model match to the overall trend in water levels is improved.

## Observation Weighting

Observations were formally compared to simulated equivalents in an objective function (phi) consisting of the sum of squared, weighted residuals (differences between simulated and observed values). Initial observation weights were based on estimated measurement uncertainty, following the methods described by Hunt and others (2013). Observations were then grouped by geographic area and observation type, and the observation weights adjusted uniformly within each group to achieve a desired fraction of total phi for that group (Doherty and Hunt, 2010, p. 12). A subset of head observation sites representing various counties and hydrogeologic settings around the Mississippi Delta were selected by stakeholders as “priority wells” of focus in evaluating and comparing model results (fig. 2.2). Similar groups were developed for the Cache and Grand Prairie regions in Arkansas.

Observation groups and weighting for groups with at least one weighted observation are summarized in [table 2.1](#). Information on zero-weighted observations is available from Leaf and others (2023). Observation weighting for the regional MERAS 3 model focused on the alluvial aquifer, and on distributing the initial phi (with the starting parameter values) among the major geographic subregions ([fig. 2](#)). The majority of initial phi was distributed to absolute heads from 2010 through 2018, spatial differences in streamflow (that is, loss or gain between sites), and head trends ([table 2.1](#)). Lesser amounts of phi were distributed to absolute stream flows, aquifer transmissivities, heads during the multidecadal spin-up stress periods before April 2007 and various derivative observations. Head observations in Tertiary units were not weighted, after preliminary trial and error and formal parameter estimation runs failed to match those values.

In the Mississippi Delta model, observation weighting focused on head trends and absolute head values from 2010 through 2018, especially those within the cone of depression. Both the alluvial aquifer and Tertiary units were included in the weighting. In both the regional and Mississippi Delta models, streamflow observations were assigned a relatively small weight, as they mostly reflect specified inflows or runoff processes that are only approximated in the model (by the runoff estimates from SWB). Streamflow observations in the “flux\_estimated” group were estimated by a random forest statistical model, from basin characteristics and measured values at other locations and times and are therefore even less certain.

**Table 2.1.** Summary of observation data by group, including weighting and phi contribution for the Mississippi Embayment Regional Aquifer Study (MERAS) 3 model.

[PEST, parameter estimation software iES, iterative Ensemble Smoother; MS, Mississippi; AR: Arkansas; MO, Missouri; LA, Louisiana; m, meter; %, percent; cv, coefficient of variance; NA, not applicable]

PEST observation group	Observation type	Geographic region	Time period	Number of weighted observations	Weight	Equivalent error	Initial phi contribution	Initial relative phi contribution	iES iteration 2 phi contribution (base)	iES iteration 2 relative phi contribution (base)
delta_heads	Hydraulic head	MS Delta	2010–18	6,039	4.5 to 0.88	0.22 to 1.1 (m)	241,348	13.74%	71,890	10.76%
cache_heads	Hydraulic head	Cache, AR/MO	2010–18	2,528	0.89 to 0.32	1.1 to 3.1 (m)	208,239	11.86%	24,022	3.60%
gp_heads	Hydraulic head	Grand Prairie, AR	2010–18	1,927	1.1 to 0.5	0.9 to 2 (m)	195,586	11.14%	25,179	3.77%
flux_measured_sdiff	Streamflow loss/gain	All regions	2010–18	460	$1.5 \times 10^{-5}$ to $2.1 \times 10^{-8}$ (cv)	0.027 to 0.16	175,772	10.01%	126,889	18.99%
head_trend	Linear trend (slope) in head since 2010-01-01	All regions	2010–18	562	$2.5 \times 10^4$ to $2.5 \times 10^4$	$3.9 \times 10^{-5}$ to $3.9 \times 10^{-5}$	175,772	10.01%	85,704	12.83%
stfrancis_heads	Hydraulic head	St. Francis, AR/MO	2010–18	1,224	2.3 to 0.85	0.43 to 1.2 (m)	149,787	8.53%	11,301	1.69%
boeuf_heads	Hydraulic head	Boeuf, AR/LA	2010–18	2,053	3.6 to 1.2	0.28 to 0.83 (m)	126,811	7.22%	61,244	9.17%
priority_flux	Total streamflow	All regions	2010–18	1,582	$4.7 \times 10^{-5}$ to $2.7 \times 10^{-7}$ (cv)	0.085 to 0.18	87,886	5.00%	79,473	11.89%
delta_heads_spinup	Hydraulic head	MS Delta	Multiyear averages before April 2007	1,357	4.2 to 0.92	0.24 to 1.1 (m)	64,728	3.69%	23,172	3.47%
Transmissivity	Aquifer transmissivity	MS Delta	NA	5	0.047 to 0.047	0.004 to 0.004 (cv)	52,731	3.00%	10,377	1.55%
gp_heads_spinup	Hydraulic head	Grand Prairie, AR	Multiyear averages before April 2007	720	2.5 to 0.53	0.4 to 1.9 (m)	48,145	2.74%	27,782	4.16%
boeuf_heads_spinup	Hydraulic head	Boeuf, AR/LA	Multiyear averages before April 2007	456	6 to 1.3	0.17 to 0.79 (m)	43,611	2.48%	16,150	2.42%
cache_heads_spinup	Hydraulic head	Cache, AR/MO	Multiyear averages before April 2007	923	1.1 to 0.34	0.88 to 2.9 (m)	38,661	2.20%	10,861	1.63%
flux_measured	Total streamflow	All regions	2010–18	9,570	$6.3 \times 10^{-5}$ to $8.3 \times 10^{-10}$ (cv)	0.27 to 1.1	23,841	1.36%	23,148	3.46%

**Table 2.1.** Summary of observation data by group, including weighting and phi contribution for the Mississippi Embayment Regional Aquifer Study (MERAS) 3 model.—Continued

[PEST, parameter estimation software iES, iterative Ensemble Smoother; MS, Mississippi; AR: Arkansas; MO, Missouri; LA, Louisiana; m, meter; %, percent; cv, coefficient of variance; NA, not applicable]

PEST observation group	Observation type	Geographic region	Time period	Number of weighted observations	Weight	Equivalent error	Initial phi contribution	Initial relative phi contribution	iES iteration 2 phi contribution (base)	iES iteration 2 relative phi contribution (base)
stfrancis_heads_spinup	Hydraulic head	St. Francis, AR/MO	Multiyear averages before April 2007	402	2.3 to 0.9	0.43 to 1.1 (m)	22,837	1.30%	5,566	0.83%
delta_cha_heads	Hydraulic head	MS Delta	2010–18	482	2.6 to 0.88	0.38 to 1.1 (m)	13,974	0.80%	8,741	1.31%
gp_priority_wells	Hydraulic head	Grand Prairie, AR	2010–18	127	1.1 to 0.5	0.9 to 2 (m)	13,815	0.79%	3,285	0.49%
cache_priority_wells	Hydraulic head	Cache, AR/MO	2010–18	233	0.65 to 0.32	1.5 to 3.1 (m)	12,085	0.69%	7,164	1.07%
delta_heads_disp	Cumulative change in head	MS Delta	2010–18	5,221	1.7 to 0.44	0.61 to 2.3 (m)	11,932	0.68%	7,200	1.08%
delta_heads_tdiff	Temporal change in head	MS Delta	2010–18	6,754	2.2 to 0.44	0.45 to 2.3 (m)	8,423	0.48%	8,410	1.26%
delta_priority_wells	Hydraulic head	MS Delta	2010–18	100	3.1 to 1.8	0.32 to 0.57 (m)	6,718	0.38%	3,010	0.45%
flux_measured_tdiff	Temporal change in streamflow	All regions	2010–18	10,511	$3.2 \times 10^{-5}$ to $4.1 \times 10^{-10}$	1.1 to 6 (cv)	6,085	0.35%	6,181	0.92%
gp_priority_wells_spinup	Hydraulic head	Grand Prairie, AR	Multiyear averages before April 2007	32	1.2 to 0.54	0.81 to 1.9 (m)	3,471	0.20%	1,385	0.21%
boeuf_heads_disp	Cumulative change in head	Boeuf, AR/LA	2010–18	871	1.8 to 0.6	0.56 to 1.7 (m)	3,300	0.19%	2,630	0.39%
flux_estimated	Total streamflow	All regions	2010–18	4,943	$4.8 \times 10^{-6}$ to $1.4 \times 10^{-8}$	0.37 to 2.7 (cv)	3,206	0.18%	3,126	0.47%
boeuf_heads_tdiff	Temporal change in head	Boeuf, AR/LA	2010–18	1,294	2.5 to 0.6	0.4 to 1.7 (m)	2,050	0.12%	2,349	0.35%
cache_priority_wells_spinup	Hydraulic head	Cache, AR/MO	Multiyear averages before April 2007	54	0.8 to 0.34	1.3 to 2.9 (m)	2,019	0.11%	2,478	0.37%
stfrancis_heads_tdiff	Temporal change in head	St. Francis, AR/MO	2010–18	1,336	1.2 to 0.43	0.85 to 2.3 (m)	1,848	0.11%	1,072	0.16%
delta_cha_heads_spinup	Hydraulic head	MS Delta	Multiyear averages before April 2007	79	3.6 to 0.92	0.28 to 1.1 (m)	1,798	0.10%	1,431	0.21%
cache_heads_tdiff	Temporal change in head	Cache, AR/MO	2010–18	2,957	0.45 to 0.16	2.2 to 6.2 (m)	1,549	0.09%	517	0.08%

**Table 2.1.** Summary of observation data by group, including weighting and phi contribution for the Mississippi Embayment Regional Aquifer Study (MERAS) 3 model.—Continued

[PEST, parameter estimation software iES, iterative Ensemble Smoother; MS, Mississippi; AR: Arkansas; MO, Missouri; LA, Louisiana; m, meter; %, percent; cv, coefficient of variance; NA, not applicable]

PEST observation group	Observation type	Geographic region	Time period	Number of weighted observations	Weight	Equivalent error	Initial phi contribution	Initial relative phi contribution	iES iteration 2 phi contribution (base)	iES iteration 2 relative phi contribution (base)
delta_priority_wells_spinup	Hydraulic head	MS Delta	Multiyear averages before April 2007	23	4.4 to 2.1	0.23 to 0.48 (m)	1,373	0.08%	658	0.10%
gp_heads_tdiff	Temporal change in head	Grand Prairie, AR	2010–18	2,100	0.68 to 0.25	1.5 to 4 (m)	1,372	0.08%	780	0.12%
stfrancis_heads_disp	Cumulative change in head	St. Francis, AR/ MO	2010–18	894	1.2 to 0.43	0.85 to 2.3 (m)	1,300	0.07%	753	0.11%
gp_heads_disp	Cumulative change in head	Grand Prairie, AR	2010–18	1,599	0.53 to 0.25	1.9 to 4 (m)	1,042	0.06%	797	0.12%
cache_heads_disp	Cumulative change in head	Cache, AR/MO	2010–18	1,983	0.45 to 0.16	2.2 to 6.2 (m)	880	0.05%	645	0.10%
delta_heads_sdiff	Spatial difference in head	MS Delta	2010–18	109	1.3 to 0.58	0.74 to 1.7 (m)	568	0.03%	438	0.07%
flux_estimated_tdiff	Temporal change in streamflow	All regions	2010–18	5,458	$2.4 \times 10^{-6}$ to $6.8 \times 10^{-9}$ (cv)	0.99 to 8.3	513	0.03%	552	0.08%
delta_priority_wells_tdiff	Temporal change in head	MS Delta	2010–18	117	2.2 to 0.88	0.46 to 1.1 (m)	243	0.01%	183	0.03%
delta_cha_heads_tdiff	Temporal change in head	MS Delta	2010–18	511	1.8 to 0.44	0.55 to 2.3 (m)	223	0.01%	858	0.13%
gp_priority_wells_tdiff	Temporal change in head	Grand Prairie, AR	2010–18	147	0.61 to 0.25	1.6 to 4 (m)	170	0.01%	97	0.01%
delta_cha_heads_disp	Cumulative change in head	MS Delta	2010–18	420	1.3 to 0.44	0.76 to 2.3 (m)	146	0.01%	426	0.06%
cache_priority_wells_tdiff	Temporal change in head	Cache, AR/MO	2010–18	264	0.39 to 0.16	2.6 to 6.2 (m)	137	0.01%	52	0.01%
cache_priority_wells_disp	Cumulative change in head	Cache, AR/MO	2010–18	185	0.32 to 0.16	3.1 to 6.2 (m)	88	0.00%	60	0.01%
delta_priority_wells_disp	Cumulative change in head	MS Delta	2010–18	88	1.4 to 0.88	0.71 to 1.1 (m)	69	0.00%	78	0.01%
gp_priority_wells_disp	Cumulative change in head	Grand Prairie, AR	2010–18	95	0.53 to 0.25	1.9 to 4 (m)	57	0.00%	65	0.01%
<b>Total</b>	NA	NA	NA	<b>59,082</b>	NA	NA	<b>1,756,207</b>	<b>100.00%</b>	<b>668,179</b>	<b>100.00%</b>

**Table 2.2.** Summary of observation data by group, including weighting and phi contribution for the Mississippi Delta model.

[PEST, parameter estimation software; iES, iterative Ensemble Smoother; MS, Mississippi; AR: Arkansas; MO, Missouri; LA, Louisiana; %, percent; m, meter; cv, coefficient of variance; NA, not applicable]

PEST observation group	Description	Time period	Number of weighted observations	Weight	Equivalent error	Initial phi contribution	Initial relative phi contribution	iES iteration 2 phi contribution (base)	iES iteration 2 relative phi contribution (base)
cha_heads_msembm	Hydraulic Head in the Tertiary units (central Delta)	2010–18	839	4.1 to 2.7	0.24 to 0.37 (m)	173,889	35.74%	5,758	8.88%
cha_heads_center	Hydraulic Head (center of central Delta)	2010–18	300	4 to 2.7	0.25 to 0.37 (m)	103,536	21.28%	2,882	4.44%
cha_heads_margin	Hydraulic Head (edges of central Delta)	2010–18	184	5.4 to 3.6	0.19 to 0.28 (m)	70,258	14.44%	4,220	6.51%
head_trend	Linear trend (slope) in head	2010–18	425	$3.3 \times 10^4$ to $3.3 \times 10^4$	3e-05 to 3e-05	64,189	13.19%	24,557	37.87%
priority_wells	Hydraulic Head in selected wells of focus	2010–18	171	5.3 to 2.2	0.19 to 0.45 (m)	24,184	4.97%	2,368	3.65%
delta_heads_msembm	Hydraulic Head in the Tertiary units (within the Delta)	2010–18	4102	1.7 to 0.5	0.59 to 2 (m)	22,054	4.53%	11,073	17.08%
delta_heads	Hydraulic Head in the MRVA	2010–18	2413	2.2 to 0.74	0.45 to 1.3 (m)	20,029	4.12%	9,124	14.07%
tertiary_heads	Hydraulic Head in the MRVA	2010–18	106	1.4 to 0.69	0.73 to 1.5 (m)	4,462	0.92%	1,842	2.84%
flux_measured	Measured total streamflow	2010–18	1218	$4.2 \times 10^{-5}$ to $3.1 \times 10^{-8}$	0.74 to 1.1 (cv)	1,319	0.27%	1,221	1.88%
transmissivity	Aquifer transmissivity	--	5	0.0047 to 0.0047	0.04 to 0.04 (cv)	1,232	0.25%	493	0.76%
flux_measured_sdiff	Streamflow loss/gain	2010–18	339	$1.2 \times 10^{-5}$ to $9.6 \times 10^{-8}$	0.27 to 1 (cv)	1,197	0.25%	1,181	1.82%
flux_estimated	Estimated total streamflow	2010–18	878	$1.3 \times 10^{-6}$ to $2.7 \times 10^{-8}$	2.2 to 2.5 (cv)	134	0.03%	116	0.18%
<b>Total</b>			<b>NA</b>	<b>NA</b>	<b>10,980</b>	<b>NA</b>	<b>NA</b>	<b>486,483</b>	<b>100.00%</b>
								<b>64,837</b>	<b>100.00%</b>

## Parametrization

Parametrization of the models followed a multiscale approach as described in White and others (2021) and references therein. At the coarsest scale, piecewise-constant parameter values were estimated for zones covering large areas of the model. At successively finer scales, one or more multiplier parameters were then applied cumulatively on top of the coarse scale parameters. This approach appports model input uncertainty at different scales, which can improve history matching while avoiding overfitting, and also improve detection of model error phenomena such as parameter compensation (White and others, 2021); for example, the coarse scale parameters address large-scale biases in the model input, while the finer multipliers can address the effects of local-scale heterogeneity. Setup of the multiscale parameterization was enabled by the `PstFrom` routines in the `pyEMU` Python package (White and others, 2021; White and others, 2016). Although the parameterization workflows used for the two models were very similar, the history matching parameter adjustments for each model were done independently. Parametrization is summarized by group in [table 2.3](#).

## Aquifer Properties

At the coarsest level, piecewise-constant, “direct” or absolute values of horizontal hydraulic conductivity ( $K_h$ ), hydraulic conductivity vertical anisotropy ( $K_{v/h}$ ), specific yield ( $S_y$ ) and specific storage ( $S_s$ ) were estimated for zones corresponding to the electrical resistivity facies of Minsley and others (2021; with facies within and outside of the alluvial aquifer and combined), and the hydrostratigraphic units of Hart and others (2008; [figs. 1.3, 1.4](#)). In the MERAS 3 model, the laterally extensive electrical resistivity facies of Minsley and others (2021) were further subdivided by geographic region; for example, resistivity facies 4 is represented by zone 204 in the Boeuf region and zone 304 in the Mississippi Delta. Zone designations are summarized in [table 2.5](#); digital representations of the zones are available from Leaf and others (2023).

Use of coarse-scale zones allowed mean property values for the represented units (and geographic regions), which are not well characterized by field data, to be directly estimated from the observations. At the intermediate level, multiplier parameters were applied to each instance of a zone in each layer, allowing for variation in the property estimates with depth. Finally, a uniform network of individual pilot point multiplier parameters (kriged together within a single zone) was applied, to allow for finer-scale heterogeneity to be represented. In the regional model, pilot points were added to each layer for  $K_h$ ,  $K_{v/h}$ , and  $S_y$ . In the Mississippi Delta model, pilot points were added to each layer for  $K_h$  and  $K_{v/h}$ , and layers 1–15 for  $S_y$ . Pilot points (Doherty 2003) in the regional model were spaced every 5 cells (5 km; [fig. 1.3](#)).

In the Mississippi Delta model, pilot points were spaced every 10 cells (5 km) in layers 1–15, and every 20 cells (10 km) in layers 15–21 ([fig. 1.4](#)). The resulting model input value in a given cell was therefore the product of the direct value estimated for the zone, multiplied by the layer-zone and pilot point-based multipliers. To avoid unreasonable parameter values, “ultimate” upper and lower bounds were set for each property type; any resulting property values outside of these bounds were reset to the bound value (for example, White and others, 2021).

## Recharge

Aquifer recharge was parameterized at the coarsest level with multipliers on the Soil Water Balance Code (SWB) results of Nielsen and Westenbroek (2023) for the surficial connectivity zones developed by Minsley and others (2021; [fig. 2](#)), subdivided by geographic region ([fig. 2.3](#)). The surficial connectivity zones were assigned ending numbers reflecting the surficial connectivity zone developed by Minsley and others (2021) and starting numbers reflecting the geographic region; for example, in the MERAS 3 model, surficial connectivity zone 1 is represented by zone 11 in the central Delta area, zone 21 in the Boeuf region, and 71 in the Cache region. In the Delta model, surficial connectivity zone 1 is represented by zone 1 in the larger Delta, zone 11 in the central Delta, and zone 21 in the Bluff hills (east of the Delta). [Tables 2.3](#) and [2.4](#) list the surficial connectivity zones associated with each region.

Multipliers by surficial connectivity zone allow for the effects of shallow confining units that are below the soil zone (and therefore not considered by SWB) to be accounted for in the estimation of aquifer recharge. Global multiplier parameters (for the whole model area) were then applied by stress period, to account for any seasonal or wet or dry weather biases in the SWB simulation. Finally, a uniform network of pilot point parameters (kriged together in a single zone) was applied across the model area (through all stress periods), to account for finer-scale heterogeneity (in the makeup of the surficial confining unit, for example) that might affect recharge locally ([fig. 2.3](#)).

## Surface Runoff

Surface runoff estimates from the SWB results of Nielsen and Westenbroek (2023) were parameterized similar to recharge, in recognition of the inverse correlation between the two components (nonevapotranspiration output in SWB is partitioned into recharge or runoff). Multiplier parameters were applied by surficial connectivity zone and geographic area, following the same system used for recharge and SFR leakage ([fig. 2.3](#)), and by stress period, meaning each surficial connectivity zone within each geographic area was given a parameter for each model stress period.

**Table 2.3.** Summary of model for the Mississippi Embayment Regional Aquifer Study (MERAS) 3 model.

[--, not applicable; AEM, airborne electromagnetic; MERAS: Mississippi Embayment Regional Aquifer Study; SFR, Streamflow-Routing; NHDPlus v2, National Hydrography Dataset Plus version 2; COMID, NHDPlus Common Identifier; AWIUM, Aquaculture and Irrigation Water User Model; SWUDS, site-specific water-use data system; USGS, U.S. Geological Survey]

Parameter group	Description	Transform	Aquifer property zone <sup>1</sup>	Surficial connectivity zone <sup>2</sup>	Count	Initial value	Lower bound	Upper bound
k_pp_layer0	Pilot point multiplier on horizontal hydraulic conductivity: layer 0	Log	--	--	8,029	1	0.001	1,000
k_pp_layer1	Pilot point multiplier on horizontal hydraulic conductivity: layer 1	Log	--	--	8,029	1	0.001	1,000
k_pp_layer2	Pilot point multiplier on horizontal hydraulic conductivity: layer 2	Log	--	--	8,029	1	0.001	1,000
k_zone_direct <sup>1</sup>	Hydraulic conductivity by aquifer property zone	Log	2–7, 11–19, 200, 202–207, 303–307, 500, 502–507, 600, 603–607, 700, 703–708, 1,000, 2,000	--	50	10.0 to 130.0	1	30 to 300
kvani_pp_layer0	Pilot point multiplier on hydraulic conductivity vertical anisotropy	Log	--	--	8,029	1	0.001	1,000
kvani_pp_layer1	Pilot point multiplier on hydraulic conductivity vertical anisotropy	Log	--	--	8,029	1	0.001	1,000
kvani_pp_layer2	Pilot point multiplier on hydraulic conductivity vertical anisotropy	Log	--	--	8,029	1	0.001	1,000

**Table 2.3.** Summary of model for the Mississippi Embayment Regional Aquifer Study (MERAS) 3 model.—Continued

[--, not applicable; AEM, airborne electromagnetic; MERAS: Mississippi Embayment Regional Aquifer Study; SFR, Streamflow-Routing; NHDPlus v2, National Hydrography Dataset Plus version 2; COMID, NHDPlus Common Identifier; AWIUM, Aquaculture and Irrigation Water User Model; SWUDS, site-specific water-use data system; USGS, U.S. Geological Survey]

Parameter group	Description	Transform	Aquifer property zone <sup>1</sup>	Surficial connectivity zone <sup>2</sup>	Count	Initial value	Lower bound	Upper bound
kvani_zone_direct <sup>1</sup>	Hydraulic conductivity vertical anisotropy by aquifer property zone	Log	2–7, 11–19, 200, 202–207, 303–307, 500, 502–507, 600, 603–607, 700, 703–708, 1,000, 2,000	--	50	30.0 to 1,000.0	1	100,000,000
rch_pp_mult	Pilot point multiplier on recharge	Log	--	--	2,485	1	0.1	10
rchspmult	Global recharge multiplier by stress period	Log	--	--	148	1	0.01	1.5
rzonemult-boeuf	Recharge multiplier by surficial connectivity zone, Boeuf region	Log	--	21–27	7	0.1 to 0.4	0.01	1.5
rzonemult-cache	Recharge multiplier by surficial connectivity zone, Cache region	Log	--	71–76	6	0.1 to 0.4	0.01	1.5
rzonemult-delta	Recharge multiplier by surficial connectivity zone, Delta region	Log	--	31–37	7	0.1 to 0.4	0.01	1.5
rzonemult-delta-cha	Recharge multiplier by surficial connectivity zone, central Delta area	Log	--	11–15	5	0.1 to 0.4	0.01	1.5
rzonemult-gp	Recharge multiplier by surficial connectivity zone, Grand Prairie region	Log	--	51–57	7	0.1 to 0.4	0.01	1.5

**Table 2.3.** Summary of model for the Mississippi Embayment Regional Aquifer Study (MERAS) 3 model.—Continued

[--, not applicable; AEM, airborne electromagnetic; MERAS: Mississippi Embayment Regional Aquifer Study; SFR, Streamflow-Routing; NHDPlus v2, National Hydrography Dataset Plus version 2; COMID, NHDPlus Common Identifier; AWIUM, Aquaculture and Irrigation Water User Model; SWUDS, site-specific water-use data system; USGS, U.S. Geological Survey]

Parameter group	Description	Transform	Aquifer property zone <sup>1</sup>	Surficial connectivity zone <sup>2</sup>	Count	Initial value	Lower bound	Upper bound
rzonemult-msemb-margins	Recharge multiplier by surficial connectivity zone, Mississippi Embayment areas within AEM survey area	Log	--	1–6	6	0.1 to 0.4	0.01	1.5
rzonemult-stfrancis	Recharge multiplier by surficial connectivity zone, St. Francis region	Log	--	61–67	7	0.1 to 0.4	0.01	1.5
rzonemult-tertiary	Recharge multiplier by MERAS 2 framework unit, Mississippi Embayment areas outside of AEM survey area	Log	--	91–99	9	0	0.01	1.5
sfr_inflow_mult	SFR Package inflow multiplier by stream and stress period	Log	--	--	21,460	1	0.8	1.2
sfr_kv_mult	SFR Package leakance multipliers, by surficial connectivity zone and by NHDPlus v2 COMID	Log	--	--	19,072	0	0.0001	10
sfr_kv_mult-boeuf	SFR Package leakance multiplier by surficial connectivity zone, Boeuf region	Log	--	21–27	7	0	0.0001	10
sfr_kv_mult-cache	SFR Package leakance multiplier by surficial connectivity zone, Cache region	Log	--	71–76	6	0	0.0001	10
sfr_kv_mult-delta	SFR Package leakance multiplier by surficial connectivity zone, Delta region	Log	--	31–37	7	0	0.0001	10
sfr_kv_mult-delta-cha	SFR Package leakance multiplier by surficial connectivity zone, central Delta area	Log	--	11–15	5	0	0.0001	10

**Table 2.3.** Summary of model for the Mississippi Embayment Regional Aquifer Study (MERAS) 3 model.—Continued

[--, not applicable; AEM, airborne electromagnetic; MERAS: Mississippi Embayment Regional Aquifer Study; SFR, Streamflow-Routing; NHDPlus v2, National Hydrography Dataset Plus version 2; COMID, NHDPlus Common Identifier; AWIUM, Aquaculture and Irrigation Water User Model; SWUDS, site-specific water-use data system; USGS, U.S. Geological Survey]

Parameter group	Description	Transform	Aquifer property zone <sup>1</sup>	Surficial connectivity zone <sup>2</sup>	Count	Initial value	Lower bound	Upper bound
sfr_kv_mult-gp	SFR Package leakance multiplier by surficial connectivity zone, Grand Prairie region	Log	--	51–57	7	0	0.0001	10
sfr_kv_mult-msemb-margins	SFR Package leakance multiplier by surficial connectivity zone, Mississippi Embayment areas within AEM survey area	Log	--	1–6	7	1	0.0001	10
sfr_kv_mult-stfrancis	SFR Package leakance multiplier by surficial connectivity zone, St. Francis region	Log	--	61–67	7	0	0.0001	10
sfr_kv_mult-tertiary	SFR Package leakance multiplier by MERAS 2 framework unit Mississippi Embayment areas outside of AEM survey area	Log	--	91–99	9	1	0.0001	10
sfr_runoff_mult-boeuf	SFR Package runoff multiplier by surficial connectivity zone, Boeuf region	Log	--	21–27	1,036	1	0.3	3
sfr_runoff_mult-cache	SFR Package runoff multiplier by surficial connectivity zone, Cache region	Log	--	71–76	888	1	0.3	3
sfr_runoff_mult-delta	SFR Package runoff multiplier by surficial connectivity zone, Delta region	Log	--	31–37	1,036	1	0.3	3
sfr_runoff_mult-delta-cha	SFR Package runoff multiplier by surficial connectivity zone central Delta area	Log	--	11–15	740	1	0.3	3
sfr_runoff_mult-gp	SFR Package runoff multiplier by surficial connectivity zone, Grand Prairie region	Log	--	51–57	1,036	1	0.3	3

**Table 2.3.** Summary of model for the Mississippi Embayment Regional Aquifer Study (MERAS) 3 model.—Continued

[--, not applicable; AEM, airborne electromagnetic; MERAS: Mississippi Embayment Regional Aquifer Study; SFR, Streamflow-Routing; NHDPlus v2, National Hydrography Dataset Plus version 2; COMID, NHDPlus Common Identifier; AWIUM, Aquaculture and Irrigation Water User Model; SWUDS, site-specific water-use data system; USGS, U.S. Geological Survey]

Parameter group	Description	Transform	Aquifer property zone <sup>1</sup>	Surficial connectivity zone <sup>2</sup>	Count	Initial value	Lower bound	Upper bound
sfr_runoff_mult-msemb-margins	SFR Package runoff multiplier by surficial connectivity zone, Mississippi Embayment areas within AEM survey area	Log	--	1–6	1,036	1	0.3	3
sfr_runoff_mult-stfrancis	SFR Package runoff multiplier by surficial connectivity zone, St. Francis region	Log	--	61–67	1,036	1	0.3	3
sfr_runoff_mult-tertiary	SFR Package runoff multiplier by MERAS 2 framework unit Mississippi Embayment areas outside of AEM survey area	Log	--	91–99	1,332	1	0.3	3
ss_zone_direct <sup>1</sup>	Specific storage by aquifer property zone	Log	2–7, 11–19, 200, 202–207, 303–307, 500, 502–507, 600, 603–607, 700, 703–708, 1,000, 2,000	--	50	0	0.0000001	0.001
sy_pp_layer0	Pilot point multiplier on specific yield: layer 0	Log	--	--	8,029	1	0.001	1,000
sy_pp_layer1	Pilot point multiplier on specific yield: layer 1	Log	--	--	8,029	1	0.001	1,000
sy_pp_layer2	Pilot point multiplier on specific yield: layer 2	Log	--	--	8,029	1	0.001	1,000

**Table 2.3.** Summary of model for the Mississippi Embayment Regional Aquifer Study (MERAS) 3 model.—Continued

[--, not applicable; AEM, airborne electromagnetic; MERAS: Mississippi Embayment Regional Aquifer Study; SFR, Streamflow-Routing; NHDPlus v2, National Hydrography Dataset Plus version 2; COMID, NHDPlus Common Identifier; AWIUM, Aquaculture and Irrigation Water User Model; SWUDS, site-specific water-use data system; USGS, U.S. Geological Survey]

Parameter group	Description	Transform	Aquifer property zone <sup>1</sup>	Surficial connectivity zone <sup>2</sup>	Count	Initial value	Lower bound	Upper bound
sy_zone_direct <sup>1</sup>	Specific yield by aquifer property zone	Log	2–7, 11–19, 200, 202–207, 303–307, 500, 502–507, 600, 603–607, 700, 703–708, 1,000, 2,000	--	50	0	0.001	0.35
wel_datasource_mult	Pumping multiplier by data source (MERAS 2, AWIUM, SWUDS, or USGS thermoelectric data)	Log	--	--	4	1	0.5	1.25 to 1.5
wel_per_mult	Pumping multiplier by stress period	Log	--	--	147	1	0.8	1.2
wel_subregion_mult	Pumping multiplier by Mississippi Alluvial Plain sub-region	Log	--	--	8	1	0.5	1.5 to 2
<b>Total</b>		--	--	--	<b>124,034</b>	--	--	--

<sup>1</sup>See table 2.5 for additional explanation of aquifer property zone numbers.

<sup>2</sup>Surficial connectivity zones are numbered such that the first digit indicates the region (listed in the “Description” column) and the second digit indicates the surficial connectivity classification based on Minsley and others (2021), which ranges from 1 (least connected) to 6 (most connected). Zone 7 indicates areas that were unclassified by Minsley and others (2021).

**Table 2.4.** Summary of model parametrization by group for the Mississippi Delta model.

[--, not applicable; SFR, Streamflow-Routing; NHDPlus v2, National Hydrography Dataset Plus version 2; COMID, NHDPlus Common Identifier; MERAS, Mississippi Embayment Regional Aquifer Study; AWIUM, Aquaculture and Irrigation Water User Model; SWUDS, site-specific water-use data system; USGS, U.S. Geological Survey]

Parameter group	Description	Transform	Aquifer property zone	Surficial connectivity zone	Count	Initial value	Lower bound	Upper bound
k_pp_layer0	Pilot point multiplier on horizontal hydraulic conductivity: layer 0	Log	--	--	1,146	1	0.1	10
k_pp_layer1	Pilot point multiplier on horizontal hydraulic conductivity: layer 1	Log	--	--	1,146	1	0.1	10
k_pp_layer10	Pilot point multiplier on horizontal hydraulic conductivity: layer 10	Log	--	--	1,146	1	0.1	10
k_pp_layer11	Pilot point multiplier on horizontal hydraulic conductivity: layer 11	Log	--	--	1,146	1	0.1	10
k_pp_layer12	Pilot point multiplier on horizontal hydraulic conductivity: layer 12	Log	--	--	1,146	1	0.1	10
k_pp_layer13	Pilot point multiplier on horizontal hydraulic conductivity: layer 13	Log	--	--	1,146	1	0.1	10
k_pp_layer14	Pilot point multiplier on horizontal hydraulic conductivity: layer 14	Log	--	--	1,146	1	0.1	10
k_pp_layer15	Pilot point multiplier on horizontal hydraulic conductivity: layer 15	Log	--	--	285	1	0.1	10
k_pp_layer16	Pilot point multiplier on horizontal hydraulic conductivity: layer 16	Log	--	--	285	1	0.1	10
k_pp_layer17	Pilot point multiplier on horizontal hydraulic conductivity: layer 17	Log	--	--	285	1	0.1	10
k_pp_layer18	Pilot point multiplier on horizontal hydraulic conductivity: layer 18	Log	--	--	285	1	0.1	10

**Table 2.4.** Summary of model parametrization by group for the Mississippi Delta model.—Continued

[--, not applicable; SFR, Streamflow-Routing; NHDPlus v2, National Hydrography Dataset Plus version 2; COMID, NHDPlus Common Identifier; MERAS, Mississippi Embayment Regional Aquifer Study; AWIUM, Aquaculture and Irrigation Water User Model; SWUDS, site-specific water-use data system; USGS, U.S. Geological Survey]

Parameter group	Description	Transform	Aquifer property zone	Surficial connectivity zone	Count	Initial value	Lower bound	Upper bound
k_pp_layer19	Pilot point multiplier on horizontal hydraulic conductivity: layer 19	Log	--	--	285	1	0.1	10
k_pp_layer2	Pilot point multiplier on horizontal hydraulic conductivity: layer 2	Log	--	--	1,146	1	0.1	10
k_pp_layer20	Pilot point multiplier on horizontal hydraulic conductivity: layer 20	Log	--	--	285	1	0.1	10
k_pp_layer3	Pilot point multiplier on horizontal hydraulic conductivity: layer 3	Log	--	--	1,146	1	0.1	10
k_pp_layer4	Pilot point multiplier on horizontal hydraulic conductivity: layer 4	Log	--	--	1,146	1	0.1	10
k_pp_layer5	Pilot point multiplier on horizontal hydraulic conductivity: layer 5	Log	--	--	1,146	1	0.1	10
k_pp_layer6	Pilot point multiplier on horizontal hydraulic conductivity: layer 6	Log	--	--	1,146	1	0.1	10
k_pp_layer7	Pilot point multiplier on horizontal hydraulic conductivity: layer 7	Log	--	--	1,146	1	0.1	10
k_pp_layer8	Pilot point multiplier on horizontal hydraulic conductivity: layer 8	Log	--	--	1,146	1	0.1	10
k_pp_layer9	Pilot point multiplier on horizontal hydraulic conductivity: layer 9	Log	--	--	1,146	1	0.1	10
k_zone-lay_mult	Multiplier on hydraulic conductivity by aquifer property zone and layer	Log	1–9, 13–20	--	206	1	0.1	10
k_zone_direct	Hydraulic conductivity by aquifer property zone	Log	1–9, 13–20	--	18	0.1 to 90.0	0.01	500

**Table 2.4.** Summary of model parametrization by group for the Mississippi Delta model.—Continued

[--, not applicable; SFR, Streamflow-Routing; NHDPlus v2, National Hydrography Dataset Plus version 2; COMID, NHDPlus Common Identifier; MERAS, Mississippi Embayment Regional Aquifer Study; AWIUM, Aquaculture and Irrigation Water User Model; SWUDS, site-specific water-use data system; USGS, U.S. Geological Survey]

Parameter group	Description	Transform	Aquifer property zone	Surficial connectivity zone	Count	Initial value	Lower bound	Upper bound
kvani_pp_layer0	Pilot point multiplier on hydraulic conductivity vertical anisotropy	Log	--	--	1,146	1	0.1	10
kvani_pp_layer1	Pilot point multiplier on hydraulic conductivity vertical anisotropy	Log	--	--	1,146	1	0.1	10
kvani_pp_layer10	Pilot point multiplier on hydraulic conductivity vertical anisotropy	Log	--	--	1,146	1	0.1	10
kvani_pp_layer11	Pilot point multiplier on hydraulic conductivity vertical anisotropy	Log	--	--	1,146	1	0.1	10
kvani_pp_layer12	Pilot point multiplier on hydraulic conductivity vertical anisotropy	Log	--	--	1,146	1	0.1	10
kvani_pp_layer13	Pilot point multiplier on hydraulic conductivity vertical anisotropy	Log	--	--	1,146	1	0.1	10
kvani_pp_layer14	Pilot point multiplier on hydraulic conductivity vertical anisotropy	Log	--	--	1,146	1	0.1	10
kvani_pp_layer15	Pilot point multiplier on hydraulic conductivity vertical anisotropy	Log	--	--	285	1	0.1	10
kvani_pp_layer16	Pilot point multiplier on hydraulic conductivity vertical anisotropy	Log	--	--	285	1	0.1	10
kvani_pp_layer17	Pilot point multiplier on hydraulic conductivity vertical anisotropy	Log	--	--	285	1	0.1	10
kvani_pp_layer18	Pilot point multiplier on hydraulic conductivity vertical anisotropy	Log	--	--	285	1	0.1	10

**Table 2.4.** Summary of model parametrization by group for the Mississippi Delta model.—Continued

[--, not applicable; SFR, Streamflow-Routing; NHDPlus v2, National Hydrography Dataset Plus version 2; COMID, NHDPlus Common Identifier; MERAS, Mississippi Embayment Regional Aquifer Study; AWIUM, Aquaculture and Irrigation Water User Model; SWUDS, site-specific water-use data system; USGS, U.S. Geological Survey]

Parameter group	Description	Transform	Aquifer property zone	Surficial connectivity zone	Count	Initial value	Lower bound	Upper bound
kvani_pp_layer19	Pilot point multiplier on hydraulic conductivity vertical anisotropy	Log	--	--	285	1	0.1	10
kvani_pp_layer2	Pilot point multiplier on hydraulic conductivity vertical anisotropy	Log	--	--	1,146	1	0.1	10
kvani_pp_layer20	Pilot point multiplier on hydraulic conductivity vertical anisotropy	Log	--	--	285	1	0.1	10
kvani_pp_layer3	Pilot point multiplier on hydraulic conductivity vertical anisotropy	Log	--	--	1,146	1	0.1	10
kvani_pp_layer4	Pilot point multiplier on hydraulic conductivity vertical anisotropy	Log	--	--	1,146	1	0.1	10
kvani_pp_layer5	Pilot point multiplier on hydraulic conductivity vertical anisotropy	Log	--	--	1,146	1	0.1	10
kvani_pp_layer6	Pilot point multiplier on hydraulic conductivity vertical anisotropy	Log	--	--	1,146	1	0.1	10
kvani_pp_layer7	Pilot point multiplier on hydraulic conductivity vertical anisotropy	Log	--	--	1,146	1	0.1	10
kvani_pp_layer8	Pilot point multiplier on hydraulic conductivity vertical anisotropy	Log	--	--	1,146	1	0.1	10
kvani_pp_layer9	Pilot point multiplier on hydraulic conductivity vertical anisotropy	Log	--	--	1,146	1	0.1	10
kvani_zone-lay_mult	Multiplier on hydraulic conductivity by aquifer property zone and layer	Log	1–9, 13–20	--	206	1	0.1	10

**Table 2.4.** Summary of model parametrization by group for the Mississippi Delta model.—Continued

[--, not applicable; SFR, Streamflow-Routing; NHDPlus v2, National Hydrography Dataset Plus version 2; COMID, NHDPlus Common Identifier; MERAS, Mississippi Embayment Regional Aquifer Study; AWIUM, Aquaculture and Irrigation Water User Model; SWUDS, site-specific water-use data system; USGS, U.S. Geological Survey]

Parameter group	Description	Transform	Aquifer property zone	Surficial connectivity zone	Count	Initial value	Lower bound	Upper bound
kvani_zone_direct	Hydraulic conductivity vertical anisotropy by aquifer property zone	Log	1–9, 13–20	--	18	5.0 to 500.0	1	10,000
rch_pp_mult	Pilot point multiplier on recharge	Log	--	--	323	1	0.1	10
rchspmult	Global recharge multiplier by stress period	Log	--	--	148	1	0.01	1.5
riv_cond_mult	River Package conductance multiplier (Mississippi and Big Black Rivers)	Log	--	--	2	0	0.001	100
rzonemult	Recharge multiplier by surficial connectivity zone	Log	--	1–6, 11–15, 21–27	18	0.1 to 0.75	0.01	1.5
sfr_inflow_mult	SFR Package inflow multiplier by stream and stress period	Log	--	--	592	1	0.8	1.2
sfr_kv_mult	SFR Package leakance multipliers, by surficial connectivity zone and by NHDPlus v2 COMID	Log	--	1–6, 11–15, 21–27 (and by individual NHD-Plus COMIDs)	3,071	0.001 to 10.0	0.0001	10
sfr_runoff_mult-cha	SFR Package runoff multiplier by surficial connectivity zone, central Delta	Log	--	11–15	740	1	0.3	3
sfr_runoff_mult-mrva	SFR Package runoff multiplier by surficial connectivity zone, Mississippi Alluvial Plain outside of the central Delta	Log	--	1–6	888	1	0.3	3
sfr_runoff_mult-tertiary	SFR Package runoff multiplier by surficial connectivity zone, Mississippi Embayment areas outside of the Mississippi Alluvial Plain	Log	--	21–27	1,036	1	0.3	3
ss_zone-lay_mult	Multiplier on specific storage by aquifer property zone and layer	Log	1–9, 13–20	--	206	1	0.1	10
ss_zone_direct	Specific storage by aquifer property zone	Log	1–9, 13–20	--	18	0	0.0000001	0.00001
sy_pp_layer0	Pilot point multiplier on specific yield: layer 0	Log	--	--	1,146	1	0.1	10

**Table 2.4.** Summary of model parametrization by group for the Mississippi Delta model.—Continued

[--, not applicable; SFR, Streamflow-Routing; NHDPlus v2, National Hydrography Dataset Plus version 2; COMID, NHDPlus Common Identifier; MERAS, Mississippi Embayment Regional Aquifer Study; AWIUM, Aquaculture and Irrigation Water User Model; SWUDS, site-specific water-use data system; USGS, U.S. Geological Survey]

Parameter group	Description	Transform	Aquifer property zone	Surficial connectivity zone	Count	Initial value	Lower bound	Upper bound
sy_pp_layer1	Pilot point multiplier on specific yield: layer 1	Log	--	--	1,146	1	0.1	10
sy_pp_layer2	Pilot point multiplier on specific yield: layer 2	Log	--	--	1,146	1	0.1	10
sy_pp_layer3	Pilot point multiplier on specific yield: layer 3	Log	--	--	1,146	1	0.1	10
sy_pp_layer4	Pilot point multiplier on specific yield: layer 4	Log	--	--	1,146	1	0.1	10
sy_pp_layer5	Pilot point multiplier on specific yield: layer 5	Log	--	--	1,146	1	0.1	10
sy_pp_layer6	Pilot point multiplier on specific yield: layer 6	Log	--	--	1,146	1	0.1	10
sy_pp_layer7	Pilot point multiplier on specific yield: layer 7	Log	--	--	1,146	1	0.1	10
sy_pp_layer8	Pilot point multiplier on specific yield: layer 8	Log	--	--	1,146	1	0.1	10
sy_zone-lay_mult	Multiplier on specific yield by aquifer property zone and layer	Log	1–9, 13–20	--	206	1	0.1	10
sy_zone_direct	Specific yield by aquifer property zone	Log	1–9, 13–20	--	18	0.15 to 0.2	0.05	0.35
wel_croptype_mult	Pumping multiplier crop type and stress period	Log	--	--	897	1	0.5 to 0.7	1.4 to 10
wel_datasource_mult	Pumping multiplier by data-source (MERAS 2, AWIUM, SWUDS, or USGS thermoelectric data)	Log	--	--	4	1	0.5	1.25 to 2
<b>Total</b>	--	--	--	--	<b>56,729</b>	--	--	--

<sup>1</sup>See table 2.5 for additional explanation of aquifer property zone numbers.

**Table 2.5.** Additional explanation of parameter zone numbers.

[MERAS, Mississippi Embayment Regional Aquifer Study]

Model	Zone numbers	Geographic region	Description
MERAS 3	2–7	Mississippi Embayment	Electrical resistivity facies classes 2–7 <sup>1</sup>
MERAS 3	11–19	Mississippi Embayment	MERAS framework units of Hart and others (2008) <sup>1</sup>
MERAS 3	200	Boeuf	Undifferentiated
MERAS 3	202–207	Boeuf	Electrical resistivity facies classes 2–7 <sup>1</sup>
MERAS 3	300	Mississippi Delta	Undifferentiated
MERAS 3	303–307	Mississippi Delta	Electrical resistivity facies classes 3–7 <sup>1</sup>
MERAS 3	500	Grand Prairie	Undifferentiated
MERAS 3	502–507	Grand Prairie	Electrical resistivity facies classes 2–7 <sup>1</sup>
MERAS 3	600	St. Francis	Undifferentiated
MERAS 3	603–607	St. Francis	Electrical resistivity facies classes 3–7 <sup>1</sup>
MERAS 3	700	Cache	Cache region outside of the Mississippi Alluvial Plain
MERAS 3	703–708	Cache	Electrical resistivity facies classes 3–8 <sup>1</sup>
MERAS 3	1,000	Mississippi Embayment	Lumped confining unit in model layer 2
MERAS 3	2,000	Mississippi Embayment	Lumped lower aquifer in layer 3
Mississippi Delta	1–6	Mississippi Delta outside of central Delta	Surficial connectivity zones 1–6 <sup>2</sup>
Mississippi Delta	11–15	Central Delta	Surficial connectivity zones 1–5 <sup>2</sup>
Mississippi Delta	1–6	Bluff Hills	Surficial connectivity zones 1–7 <sup>2</sup>

<sup>1</sup>Based on the electrical resistivity facies from Minsley and others (2021); 2=low electrical resistivity/low hydraulic conductivity; 8=high electrical resistivity/high hydraulic conductivity.<sup>2</sup>Based on the surficial connectivity zones from Minsley and others (2021); 1=least connected; 6=most connected; 7=undefined.

## Surface Water Inflows

Specified inflows to the SFR network were parametrized with unique multipliers for each stream (fig. 2.3) and model stress period.

## Streambed Leakage

Initial estimates of streambed leakage derived from waterborne surveys of electrical resistivity (Killian, 2018; Adams and others, 2019; Leaf, 2023) were coarsely parametrized by the same zoned multipliers as surface runoff (by surficial connectivity zone and geographic area; fig. 2.3). At a fine scale, multiplier parameters were assigned by National Hydrography Dataset Plus (NHDPlus) version 2 Common

Identifier (COMID; McKay and others, 2012). On average there are about 4 SFR reaches per COMID in the 500-meter resolution Mississippi Delta model).

## Water Use

At the coarsest scale, to address any potential dataset-specific biases, multipliers on pumping rates were assigned by input dataset. This resulted in four parameters representing the MERAS 2.2 (Haugh and others, 2020a), USGS Site-Specific Water Use Data System, USGS estimates for thermoelectric power generation (for example, Harris and Diehl, 2019), and Aquaculture and Irrigation Water-Use Model (AIWUM; Wilson, 2021) data sources. In the MERAS 3 model, multipliers were also assigned by geographic region (fig. 2, table 2.3). Additional multipliers were then applied by stress period and in the Delta model, by crop type (table 2.4).

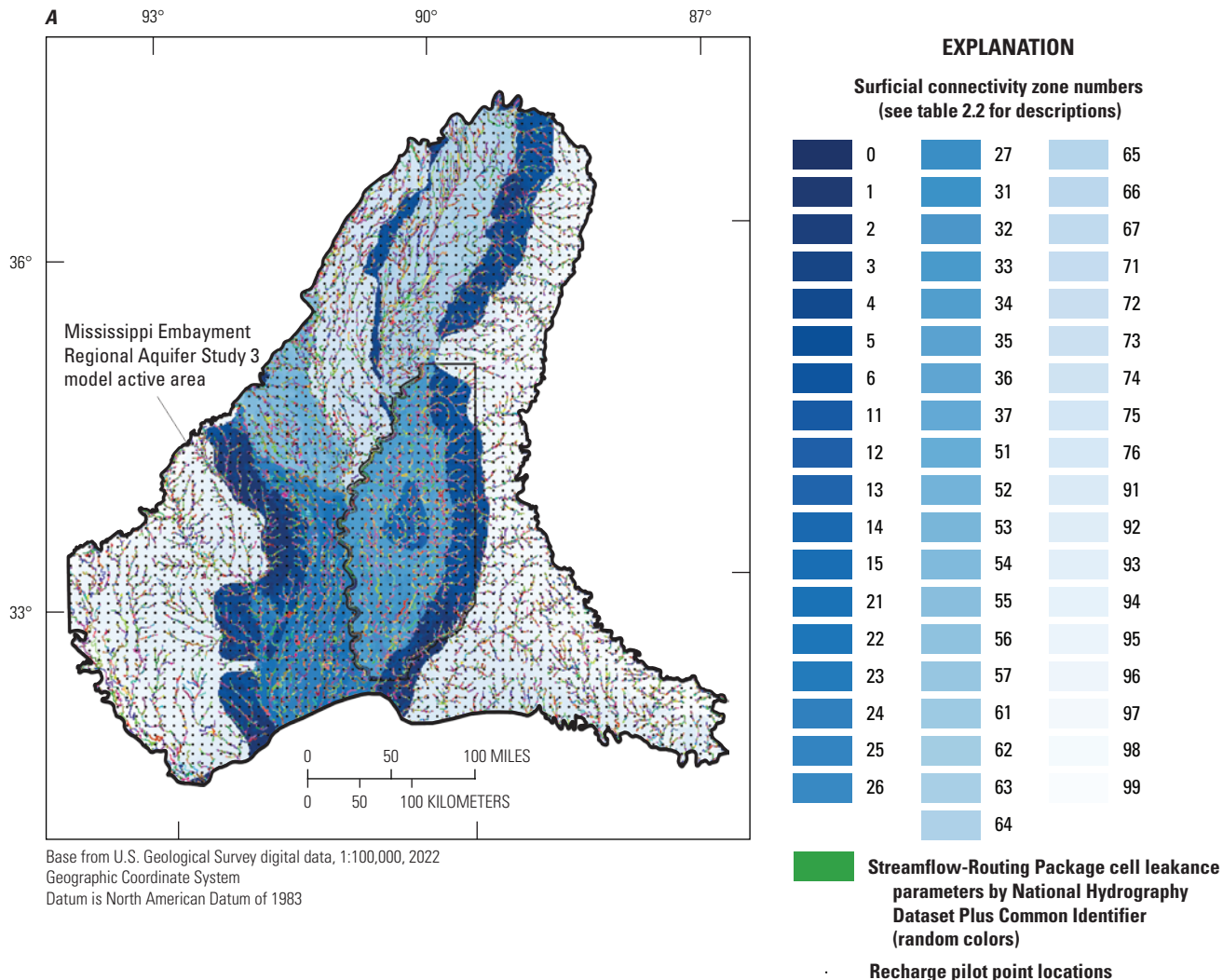


**Figure 2.3.** Spatial summary of model recharge, stream leakage and runoff parametrization, A, for the regional model; and B, for the Mississippi Delta model.

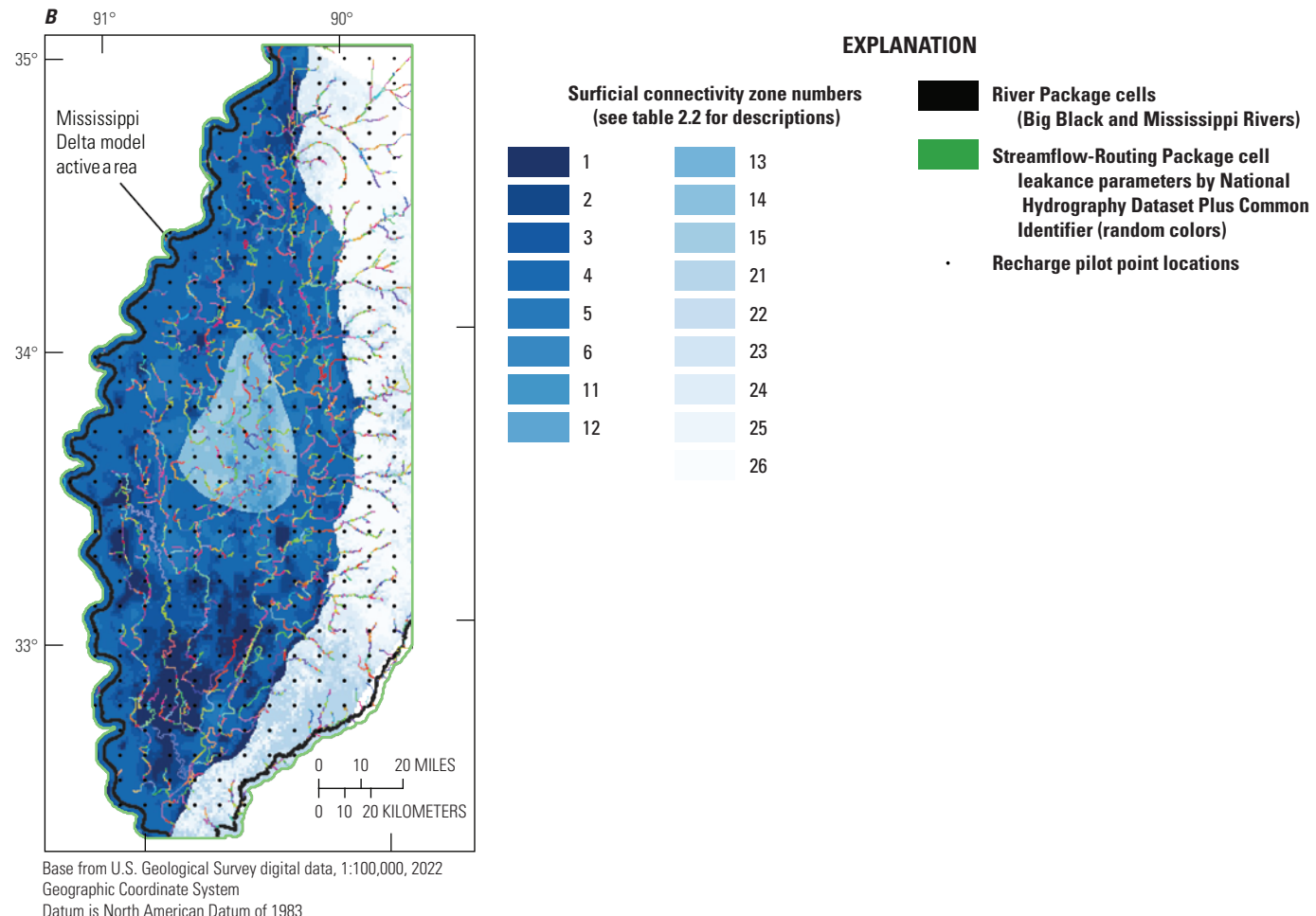


**Figure 2.3.** Spatial summary of model recharge, stream leakage and runoff parametrization, *A*, for the regional model; and *B*, for the Mississippi Delta model.

## Regional Model History Matching Results

The iES method results in an ensemble of objective function values for each iteration in the parameter estimation process, as well as a “base” set of model parameters that represents an approximation of the minimum error variance solution at that iteration. Typically, as an iES run progresses, the objective function values and their variance decrease as parameter adjustments are made to improve model fit to observations. At later iterations, the ensemble may collapse to have minimal variance among the members, and overfitting, where model parameters assume unrealistic values to improve fit to observation noise or compensate for deficiencies in the model structure, may occur. Figure 2.44 shows the MERAS 3 ensemble phi by iteration, and by iteration 3, the ensemble has collapsed. The modeler must decide which iES iteration to select for subsequent analyses, typically balancing a good

model fit with maintaining variability in the ensemble and avoiding overfitting. In this case, since the primary goal of the regional model is to provide perimeter boundaries for inset models, iteration two was selected for having a better model fit to head observations; furthermore, although the ensemble results provide an illustration of the effects of model parameter uncertainty, only results from the base realization of the regional model were used to produce perimeter boundary fluxes for the inset model forecasts.

A root mean squared error (RMSE) of 3.40 meters for all weighted head observations (in the alluvial aquifer) for the base ensemble member compares favorably to a previous RMSE of 4.31 meters reported by Clark and others (2013) for alluvial aquifer observations in the MERAS 2.0 model. As noted previously, head observations in the Tertiary units were not weighted, after preliminary trial and error and formal parameter estimation runs failed to meaningfully improve the model match of those values.

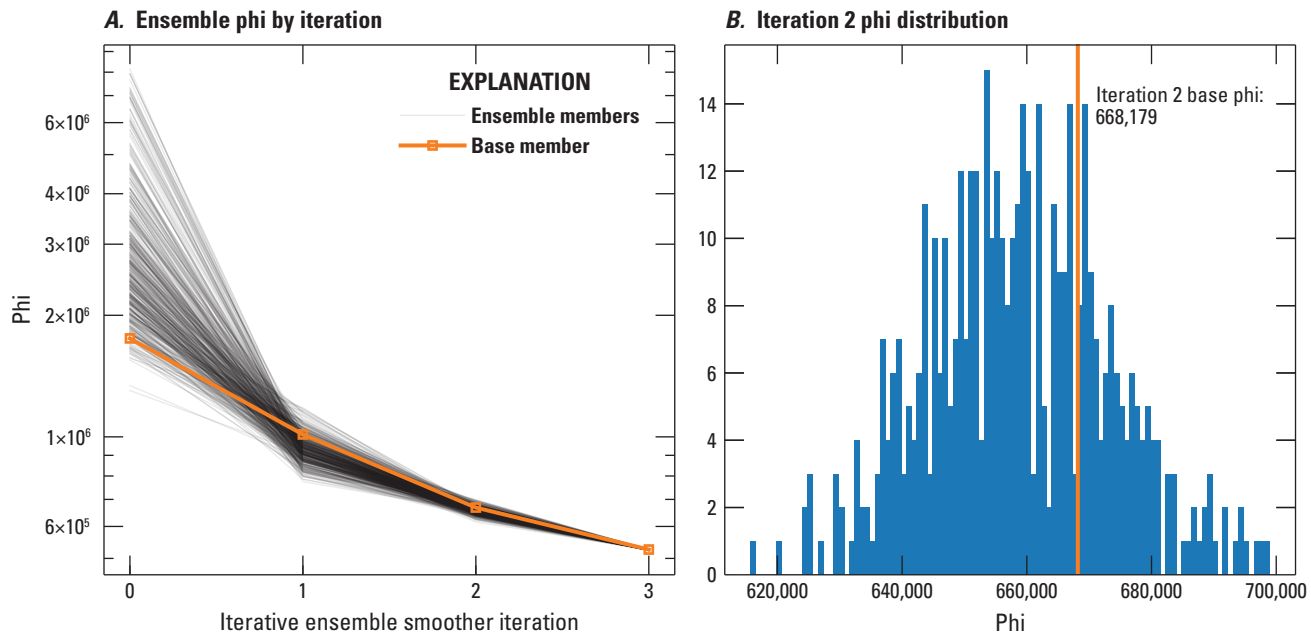


**Figure 2.4.** Ensemble objective function values for the regional model history matching.

## Comparison of Measured and Simulated Observations—By Observation Group

One-to-one scatter plots provide a qualitative overview of the match of model output to equivalent field observations. Figure 2.5 shows one-to-one scatter plot comparisons for weighted heads in the MAP regions of the MERAS 3 model (combining the “heads” and “priority\_wells” groups listed in table 2.1), measured stream flows (combining the “priority\_flux” and “flux\_measured” groups), streamflow gain/loss observations (“flux\_measured\_sdif” group), aquifer transmissivities, and head trends. Together, these observations account for 81 percent of phi for the base ensemble member at iES iteration 2. Simulated values from the base ensemble member are illustrated by the black dots. Model and measurement uncertainties are depicted respectively by the vertical and horizontal bars, which represent the 95-percent credible interval (plus or minus  $\pm 2$  standard deviations) of values from the ensemble, and the uncertainty implied by the inverse of the observation weights. Error bars were not included in the streamflow plots (F and G) because the low weight given to streamflow observations (which could only be approximated by the model) resulted in very wide bars that obscured the plots. Conversely, the transmissivity and head trend groups (H and I) were given disproportionately high weights so that they would be seen in the objective function; as a result, the implied measurement errors for these groups are too small to be visible in the plots.

## Fit Between Measured and Modeled Observations—Spatial Distributions

Spatial residuals plots provide a means of evaluating spatial bias in observation residuals (computed here as observed minus simulated), which can ultimately give insight into model structural error. Figure 2.6 shows mean spatial head residuals for 2010 through 2018 at each head observation site in the alluvial aquifer (fig. 2.6A), where observations were weighted and in the Tertiary system (fig. 2.6B), where observations were given zero weight.

Although the alluvial aquifer mean residuals in figure 2.6A are mostly well distributed between positive and negative, some clustering of negative residuals (indicating simulated heads greater than measured) is apparent near the drawdown cones in the Cache, Grand Prairie, and central Delta areas (see also fig. 2). Undersimulation of drawdown in these areas may be due to the representation of the alluvial deposits in the MERAS 3 regional model with a single layer. A surficial confining unit exists above the alluvial aquifer in many areas, including the primary drawdown cones (fig. 3). With the surficial confining unit, larger pumping drawdowns would be expected, because of specific storage (aquifer compression) and confining unit leakage being the dominant sources of water in early times, instead of specific yield (pore space drainage), which yields orders of magnitude more water. With a single layer representing the alluvium from the land surface to the base of the alluvial aquifer in the regional model, the confining unit is not represented, and MODFLOW generally uses the larger specific yield storage coefficient, unless cells are specified as confined a-priori, resulting in smaller simulated drawdowns compared to a confined case. Future versions of MERAS 3 may seek to explicitly represent the surficial confining unit as another layer.

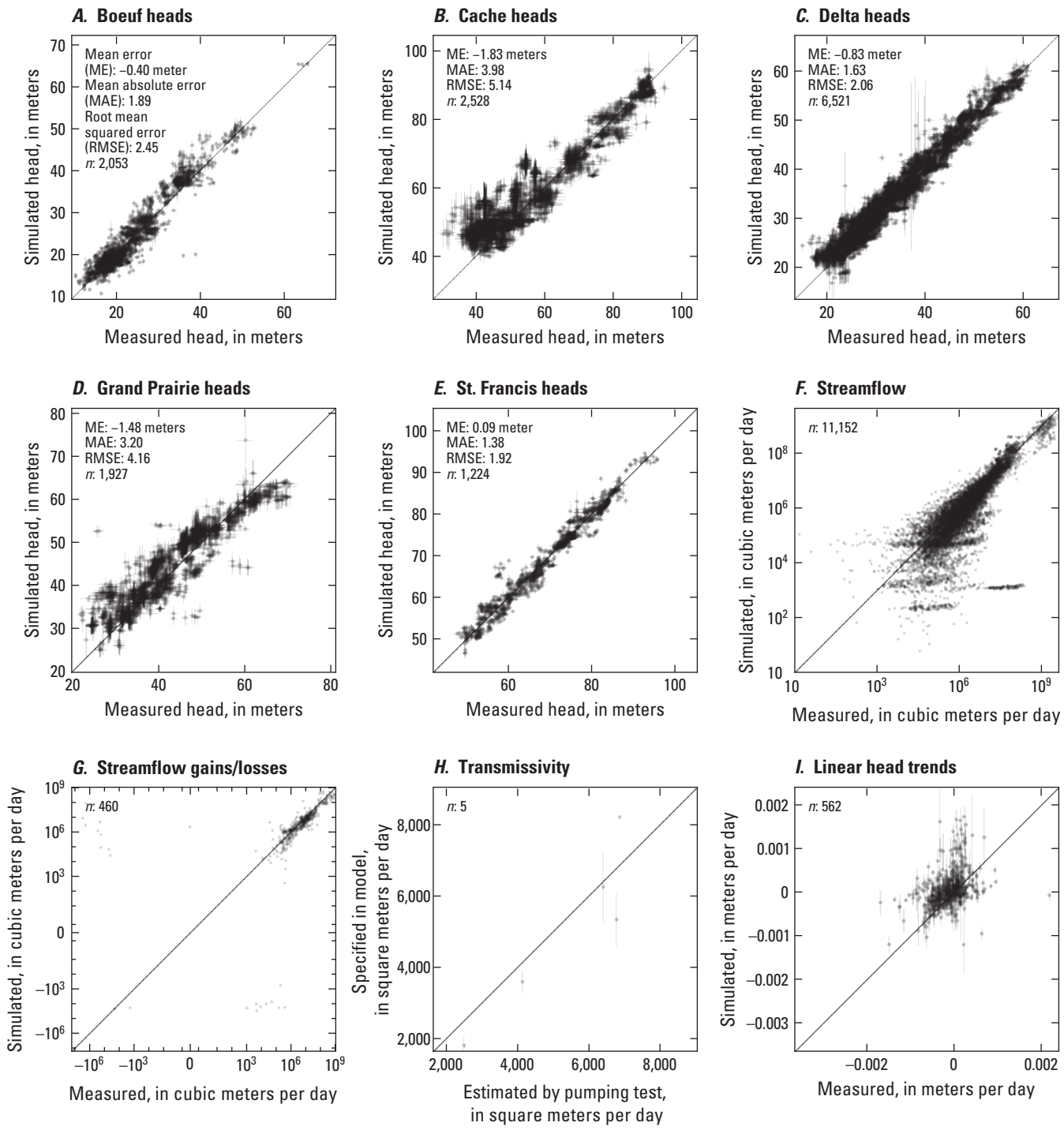


**Figure 2.5.** One-to-one comparison of Mississippi Embayment Regional Aquifer Study (MERAS) 3 model outputs to field observations, A–E, for absolute head values by geographic subregion; F, all measured stream flows; G, streamflow gains or losses between paired gages; H, model transmissivity values versus pumping test estimates; and I, head trends estimated by linear regression of simulated and observed head time series.

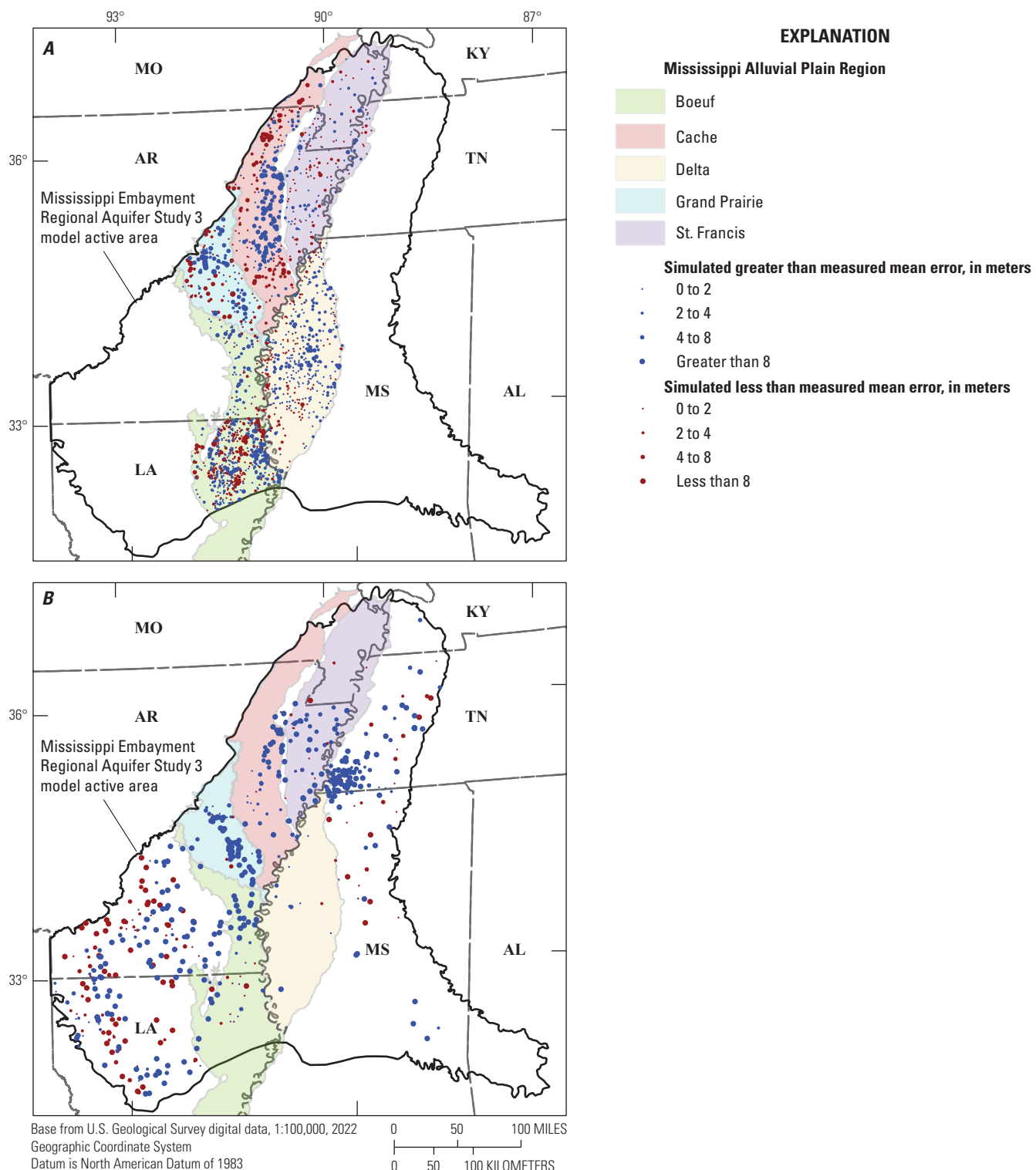


**Figure 2.6.** Spatial patterns of mean head residuals in the regional model. *A*, for weighted post-2010 head observations in the Mississippi River Valley alluvial aquifer; and *B*, for zero-weighted post-2010 head observations in the Tertiary system.

The zero-weighted residuals in the Tertiary system (fig. 2.6B) are generally large and biased in the negative direction (heads are simulated higher than observed), except along the western limb of the Mississippi Embayment in Arkansas and Louisiana. Large residuals and spatial bias in these areas may be due to inadequate representation of local geology (such as confining units and faults; for example, Clark and Hart, 2009; McKee and Clark, 2003) or misallocation of water use between the alluvial aquifer and Sparta. The AIWUM model used to estimate agricultural water use (Bristow and Wilson, 2023; Wilson, 2021) does not provide any information on the depth or aquifer from which the irrigation water is withdrawn. For simplicity, the MERAS 3 model assumes that all agricultural pumping occurs in the alluvial aquifer. This is generally the case in the Mississippi Delta, but in Arkansas, the Sparta (Middle Claiborne) aquifer also is used, and the distribution of agricultural pumping between the alluvial aquifer and Sparta is not well characterized (McKee and Clark, 2003). Incomplete representation of municipal and industrial pumping in the Memphis and southern Arkansas areas could also explain some of the negative residuals in these areas.

## Mississippi Delta Model History Matching Results

Figure 2.7 shows the iES ensemble phi by iteration for the Mississippi Delta model. Iteration 2 was selected as having a good fit to observations with reasonable parameter values and appreciable variability represented in the ensemble. A root mean squared error of 2.07 meters for all weighted head observations in the base ensemble member represents a 67% reduction in RMSE compared to the value of 6.31 meters reported by Haugh and others (2020b)

for the MERAS 2.1 model in the Mississippi Delta region. One-to-one scatter plots comparing field observations and their simulated equivalents are presented here, along with a map showing mean head residuals spatially, and time series comparing measured stream stages and their simulated equivalents. Time series of measured and simulated-equivalent heads at the priority wells of interest and flows at selected streamgages are shown in figures 6 through 8 and discussed in the main body of the report.

## Comparison of Measured and Simulated Observations by Observation Group

Figure 2.8 shows one-to-one scatter plot comparisons for weighted heads inside (fig. 2.8 and D) and outside of the central Delta area (figs. 2.8A, 2.8B; the “cha\_heads” and “delta\_heads” groups listed in table 2.2), as well as the “priority well” sites of focus (fig. 2.8E), measured stream flows (fig. 2.8G; the “flux\_measured” group), streamflow gain/loss observations (fig. 2.8F; “flux\_measured\_sdif” group), aquifer transmissivities (fig. 2.8H), and head trends (fig. 2.8I). Together, these observations account for 99.8 percent of phi for the base ensemble member at iES iteration 2. The one-to-one plots generally indicate a good fit to measured heads, though some areas and individual sites were matched better than others. In general, heads in the deepest parts of the drawdown cone in the central Delta area were difficult to match (figs. 2.8C, 2.8D), requiring parameter values that minimized the connection of the aquifer to net infiltration and surface water in that area. Smaller streamflow values are also often under-simulated (fig. 2.8G), presumably because of processes that are not represented in the model, such as irrigation return flows and discharge from bank storage or local perched aquifer systems, which may both in reality sustain base flow during low-flow periods.

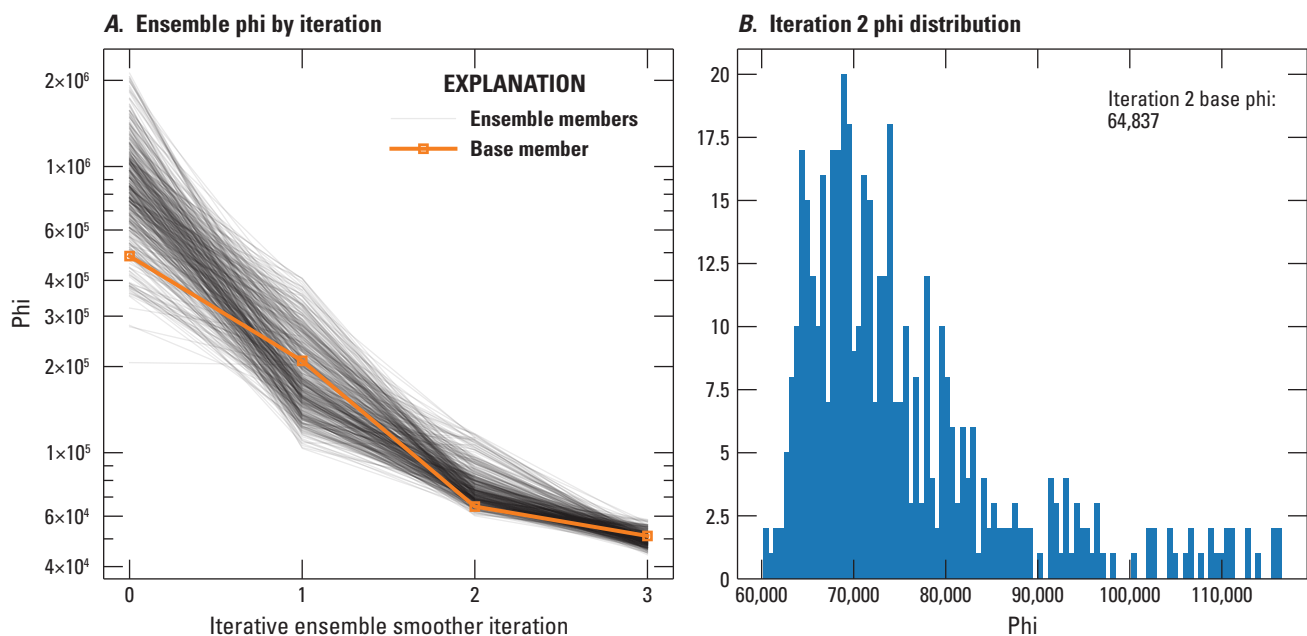
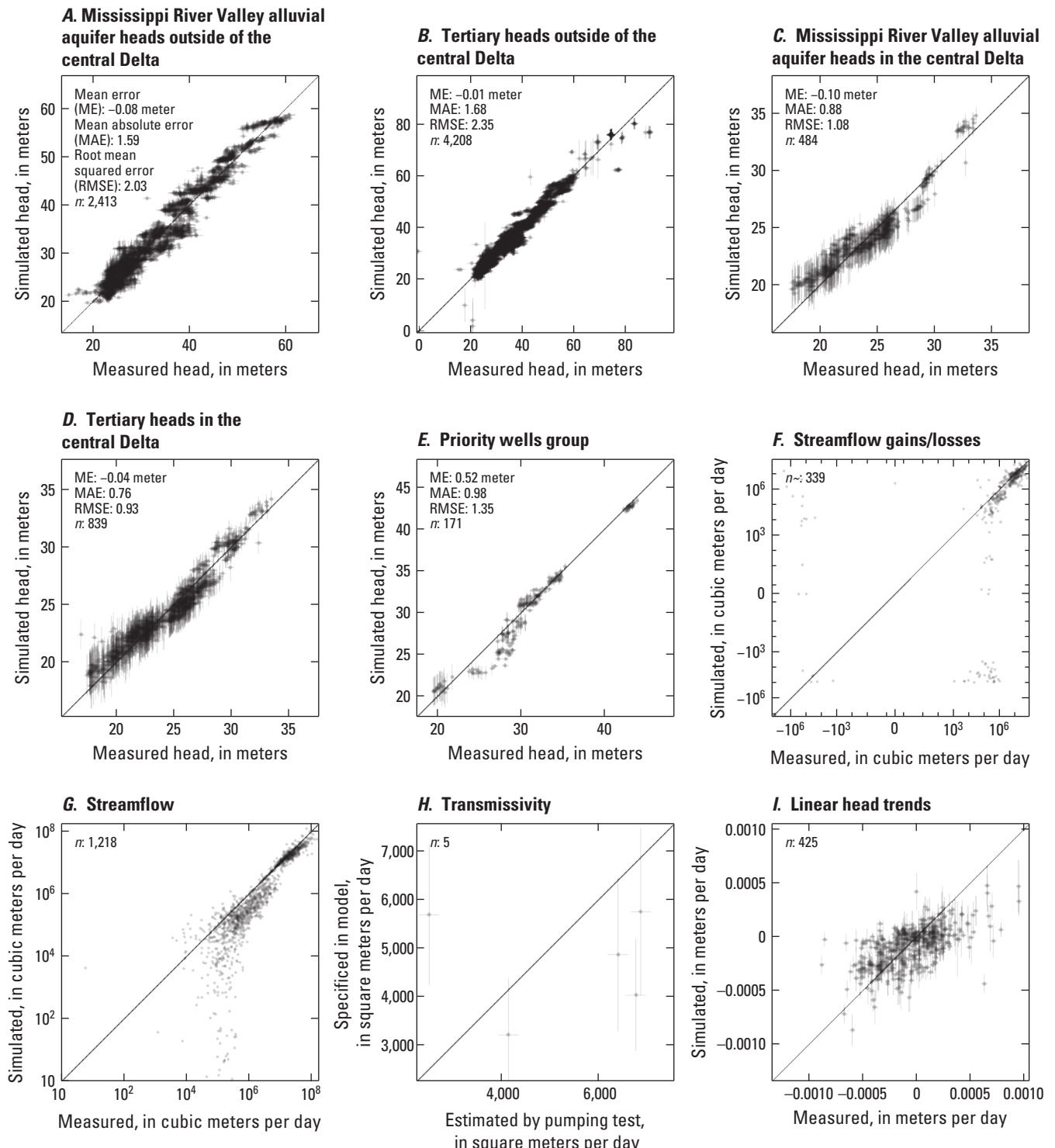


Figure 2.7. Ensemble objective function values for the Mississippi Delta model history matching.



**Figure 2.8.** One-to-one comparison of Delta model outputs to field observations for, A–D, absolute heads in the Mississippi River Valley alluvial aquifer and Sparta aquifers within and outside of the central Delta area of greatest drawdown, E, absolute heads at the “priority well” sites of focus, F, streamflow gains or losses between paired gages; G, all measured stream flows; H, model transmissivity values versus pumping test estimates; and I, head trends estimated by linear regression of simulated and observed head time series.

## Fit Between Measured and Modeled Observations—Spatial Distributions

Figure 2.9 shows mean residuals for all weighted heads plotted spatially. In general, the residuals are well distributed between positive and negative. The most notable exception is the far western part of the Delta between the Bogue Phalia River and the Mississippi River. In this area, the alluvial aquifer is thought to be relatively thin, with a higher bottom elevation than areas to the east. In the western part of the Delta, the alluvial aquifer also is separated from the Sparta Sand by several fine-grained or heterogeneous units, including the Yazoo Clay (for example, Arthur, 2001), which would limit connection with the underlying Sparta/Middle Claiborne aquifer system. These two factors may not be fully captured in the Mississippi Delta groundwater model.

## Fit Between Measured and Simulated Stream Stages

Figure 2.10 compares monthly mean stages to their simulated equivalents. As noted earlier, stages were not included formally in the model history matching, for the same reasons that streamflow were given low weights, and also because of the very approximate nature of the Manning's equation-based estimation of stream depth in the SFR Package (Pradic and others, 2004). Similar to streamflow, simulated stages are generally biased low by 1–2 meters, especially during low-flow periods, but are otherwise in good agreement with the measured monthly means.

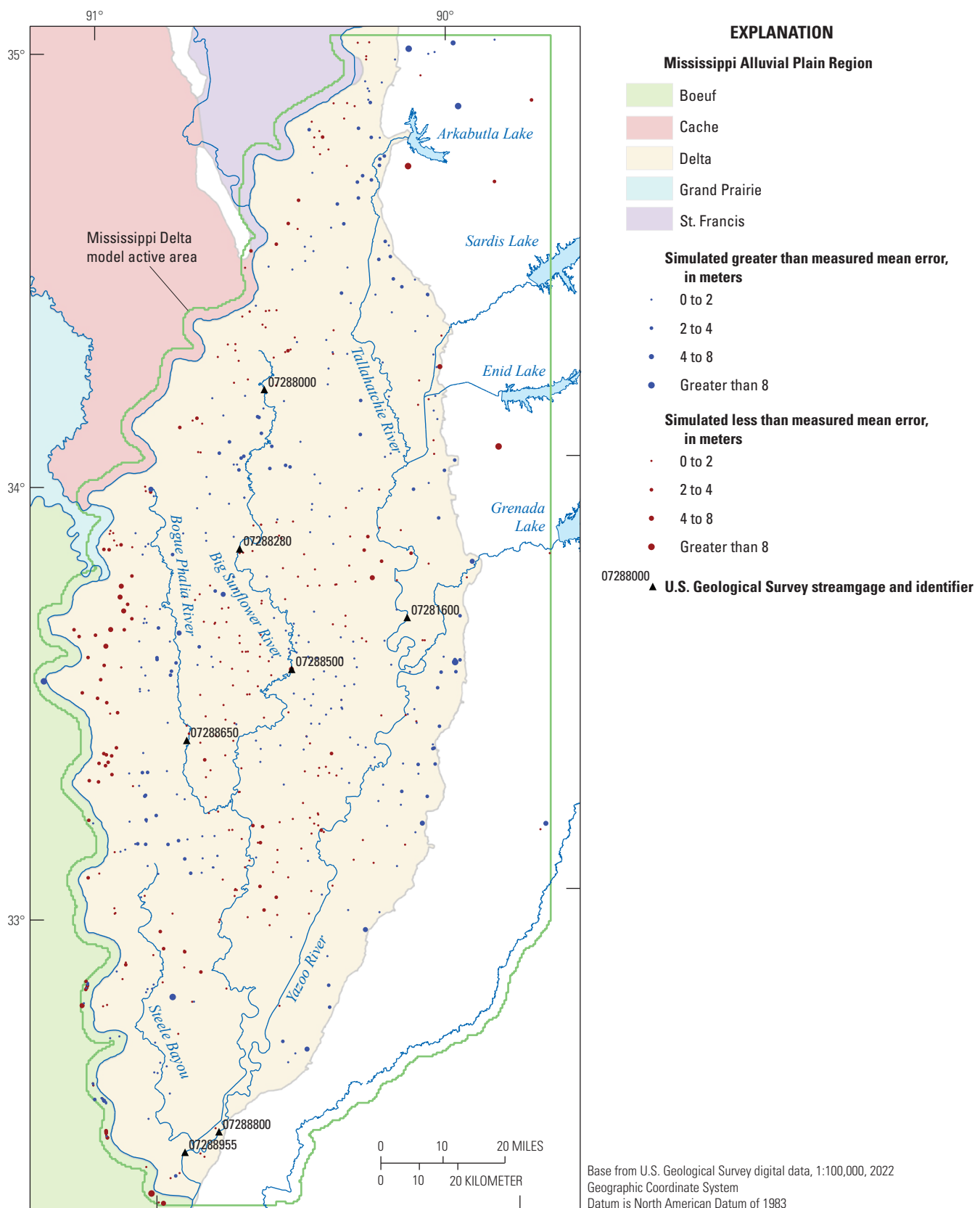


**Figure 2.9.** Spatial pattern of mean residuals for weighted head observations in the Delta model.

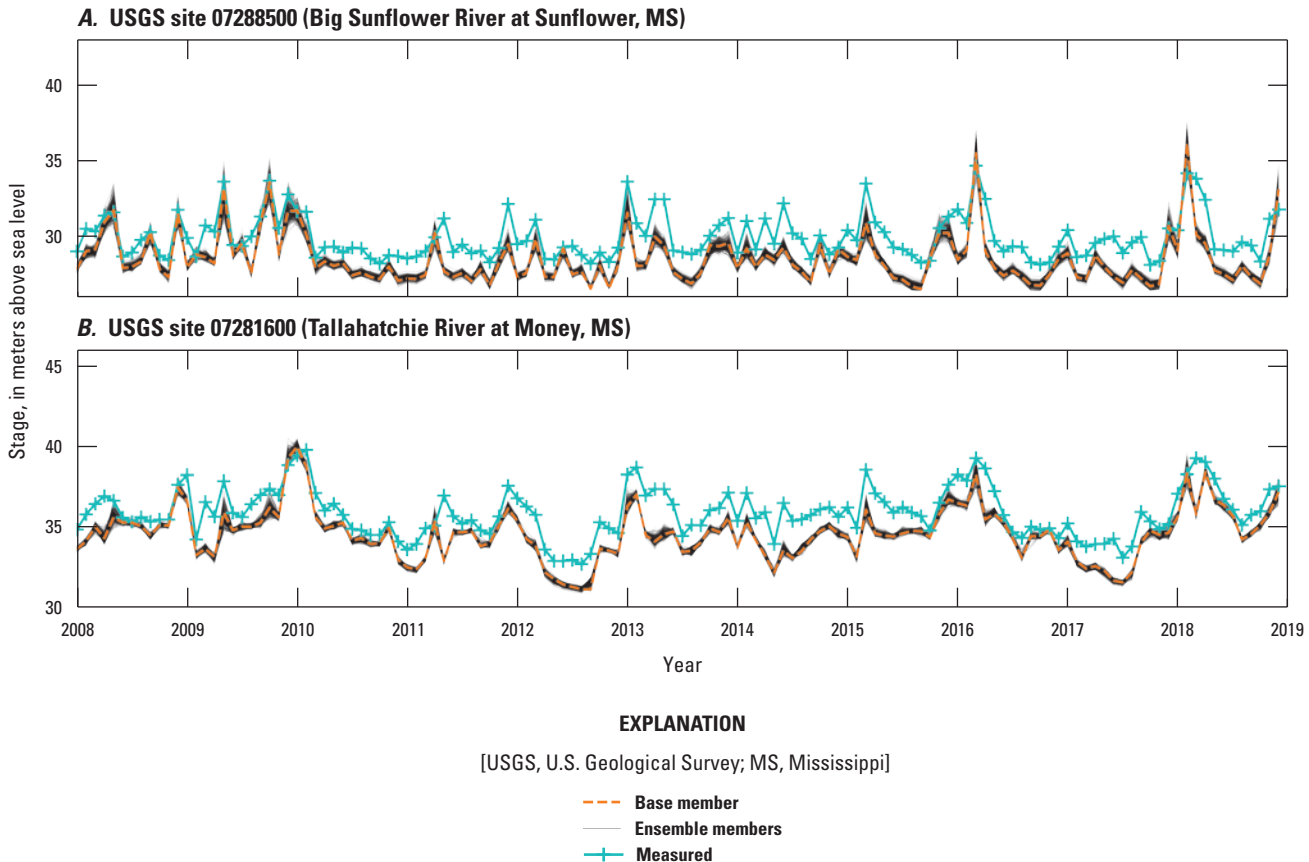


**Figure 2.10.** Times series of monthly averages of measured stream stages and simulated equivalents at selected gages.

## Regional Model Parameter Estimation Results

Estimated parameter values and resulting model inputs for aquifer properties, recharge and water use pumping rates are discussed here; other estimated parameter values and their associated model inputs are available in the companion data release (Leaf and others, 2023).

### Aquifer Properties

Figures 2.11, 2.12, 2.13, and 2.14 show estimated aquifer properties for the base member of the chosen second iteration of the iES history matching run. In general, the horizontal hydraulic ( $K_h$ ) conductivity estimates (fig. 2.11) are consistent with previous work indicating bulk  $K_h$  values in the alluvial aquifer of on the order of 100 meters per day, and bulk  $K_h$  in the Tertiary units of on the order of 1 to 10 meters per day (see the “Aquifer Properties” section for additional discussion and references). Hydraulic conductivity vertical anisotropy estimates (fig. 2.12) vary widely, reflecting the lumped nature of the regional model layers, which represent both aquifers and aquitards. In general, vertical hydraulic conductivity is difficult to assess because it is not easily measured in the field and more importantly, is scale-dependent. The somewhat rough

texture of the estimated specific yield fields (fig. 2.13) may indicate some overfitting, though specific yield is difficult to measure in the field, especially at the 1-km scale of the model cells. Because of the lumped nature of the regional model layers, low values of specific yield (down to 0.001) were allowed in the parameter estimation, to allow for the representation of leaky confined storage conditions that may occur at the sublayer scale.

### Recharge

Figure 2.15 compares estimated recharge in the regional model to the net infiltration estimates from the SWB model of Nielsen and Westenbroek (2023) that formed the basis for the initial parameter values. The spatial averages of about 2.5 inches per year are consistent with previous work (see the “Conceptual Model” section), though substantially lower than the SWB model estimates. The SWB model spatial average of 7.59 inches per year also reflects recent wet conditions between 2007 and 2018, compared to the 5.4-inch average for 1920–2017, reported by Westenbroek and others (2021) using an earlier version of the same model.

The discrepancy between the recharge values estimated through history matching and the net infiltration estimated by SWB could in part be the result of error in the partitioning of precipitation by SWB, where small errors in

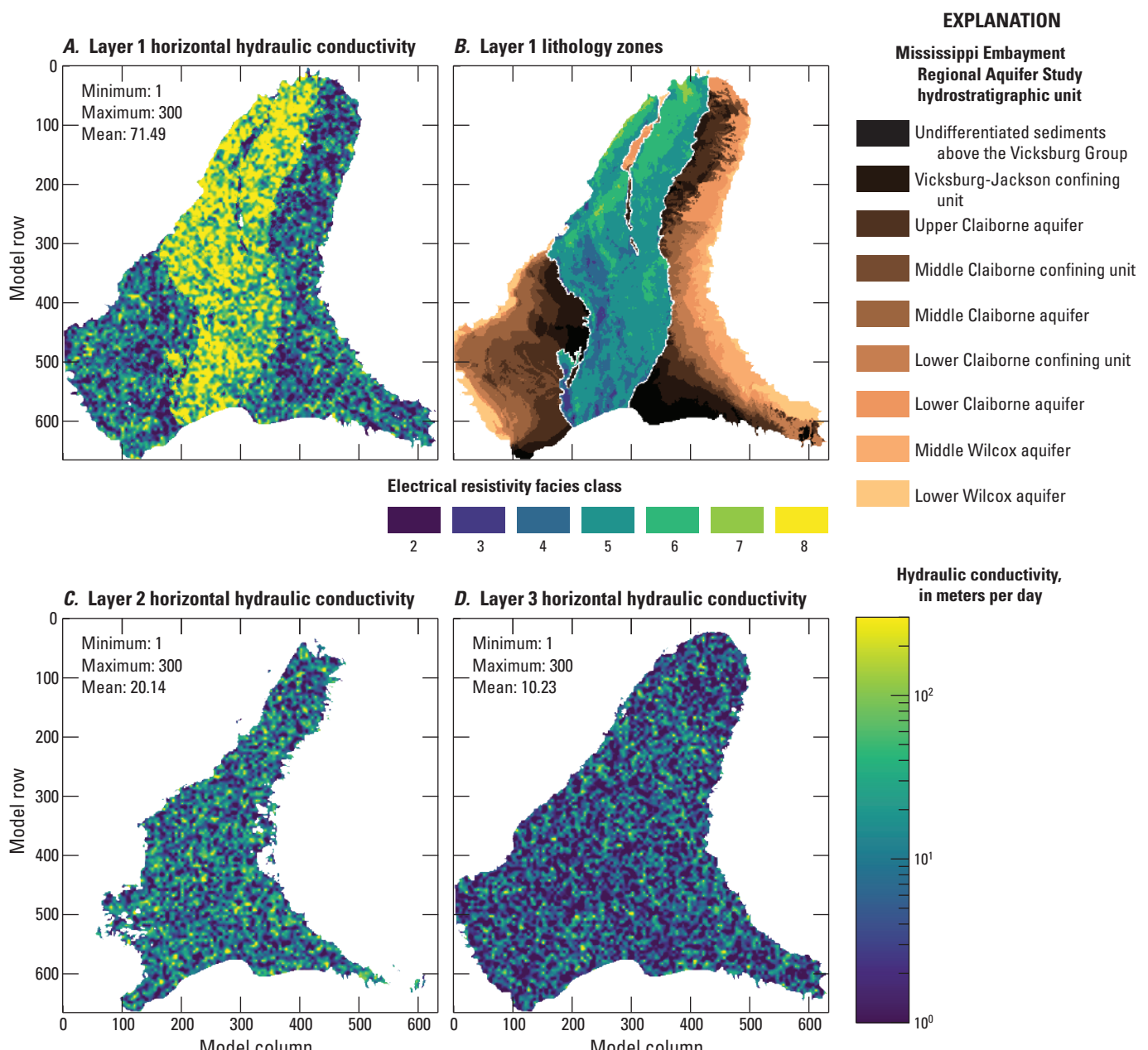


**Figure 2.11.** Horizontal hydraulic conductivity ( $K_h$ ) estimates for the regional model. *A*, horizontal hydraulic conductivity estimates in layer 1; *B*, “base” (lithology) zones used to parametrize horizontal hydraulic conductivity in layer 1; *C*, horizontal hydraulic conductivity estimates in layer 2; and *D*, horizontal hydraulic conductivity estimates in layer 3.

evapotranspiration or runoff could have a large effect on net infiltration, because of its small size as a component (about 5 percent). This explanation is supported by simulated stream flows that are generally biased low relative to measurements (fig. 2.5). The presence of a shallow confining unit in many parts of the alluvial plain provides an additional explanation. In places where the shallow confining unit is present to some degree, it may limit the connection between the soil zone and

the regional water table, causing net infiltration leaving the soil zone to run off to nearby streams, through interflow processes or perched groundwater (see the “Conceptual Model” section and also Nielsen and Westenbroek, 2023). In this way, net infiltration leaving the soil zone may not be equivalent to groundwater recharge to the alluvial aquifer in many parts of the alluvial plain.

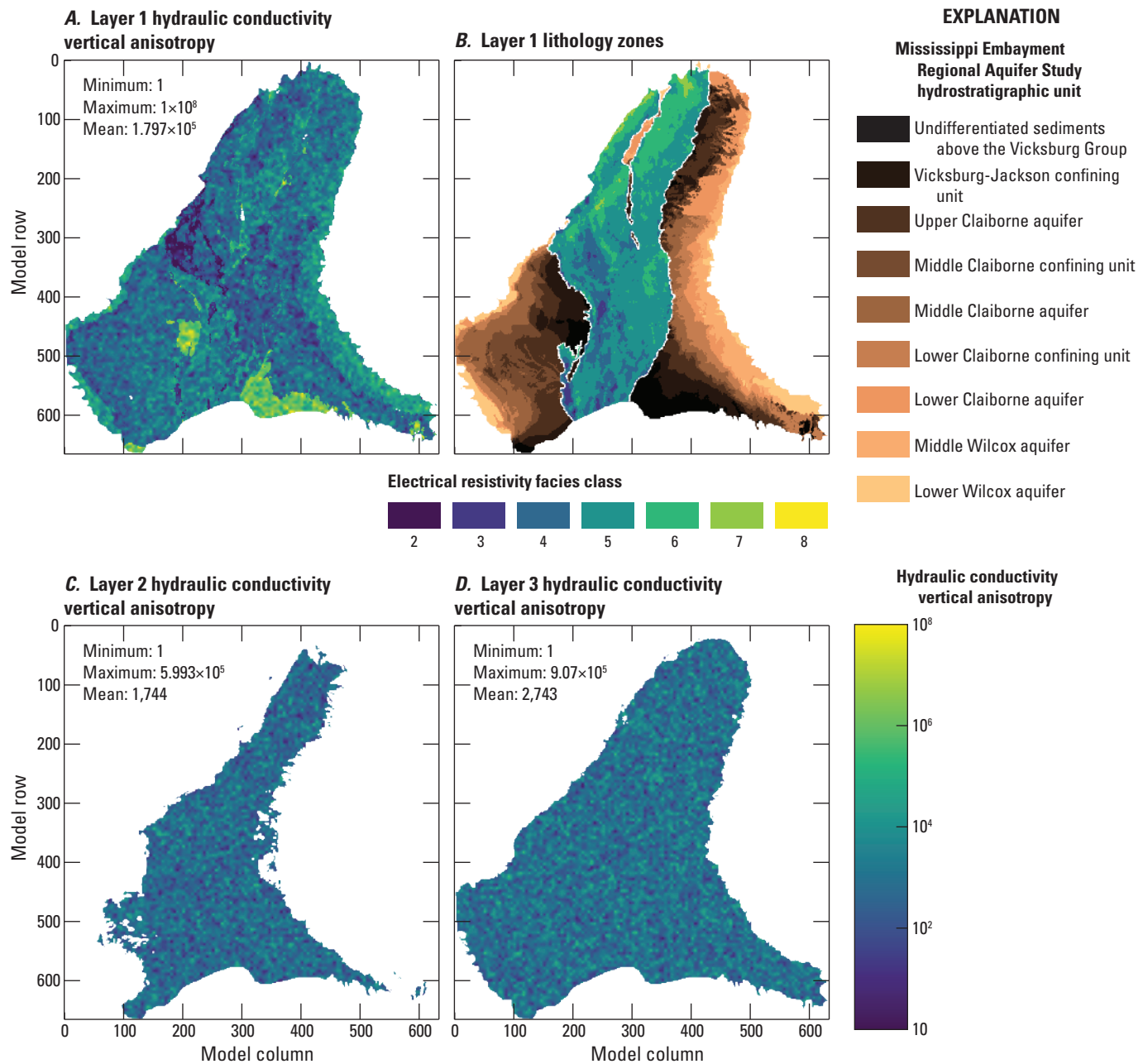


**Figure 2.12.** Hydraulic conductivity vertical anisotropy ( $K_h/K_v$ ) estimates for the regional model. *A*, Hydraulic conductivity vertical anisotropy estimates in layer 1; *B*, “base” (lithology) zones used to parametrize hydraulic conductivity vertical anisotropy in layer 1; *C*, hydraulic conductivity vertical anisotropy estimates in layer 2; and *D*, hydraulic conductivity vertical anisotropy estimates in layer 3.

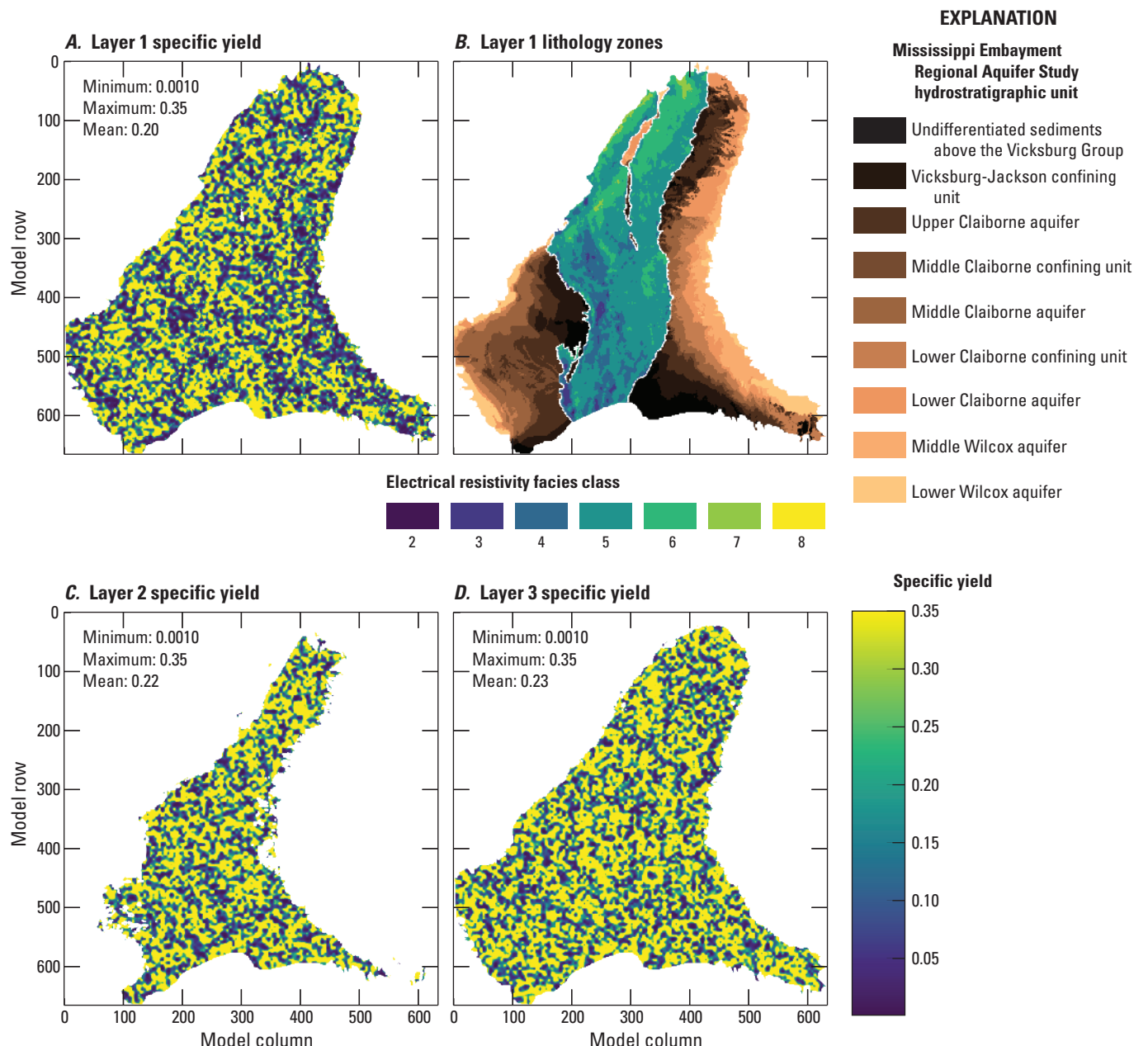


**Figure 2.13.** Specific yield ( $S_y$ ) estimates for the regional model. *A*, specific yield estimates in layer 1; *B*, “base” (lithology) zones used to parametrize specific yield in layer 1; *C*, specific yield estimates in layer 2; and *D*, specific yield estimates in layer 3.

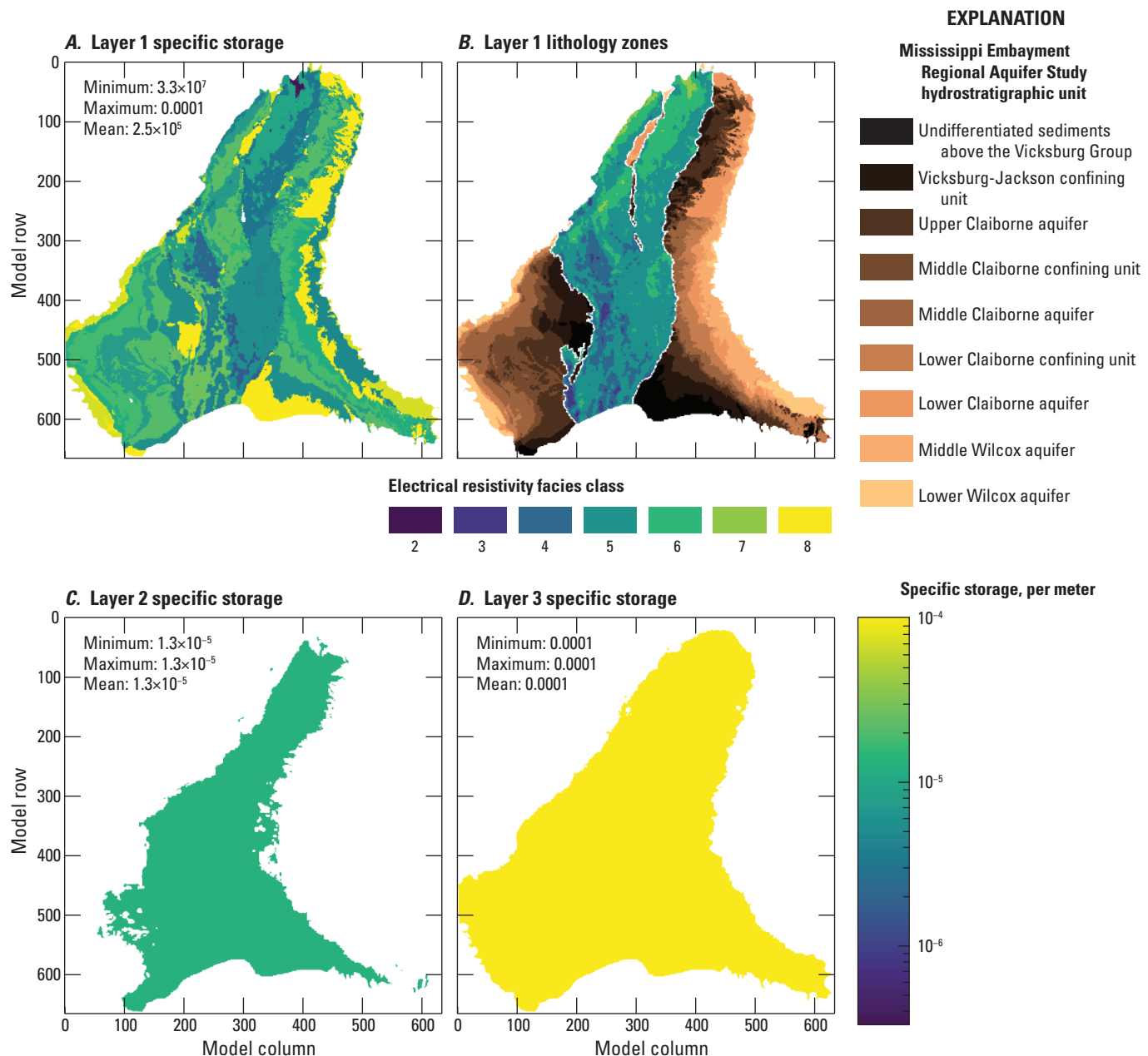


**Figure 2.14.** Specific storage ( $S_s$ ) estimates for the regional model. *A*, specific storage estimates in layer 1; *B*, “base” (lithology) zones used to parametrize specific storage in layer 1; *C*, specific storage estimates in layer 2; and *D*, specific storage estimates in layer 3.

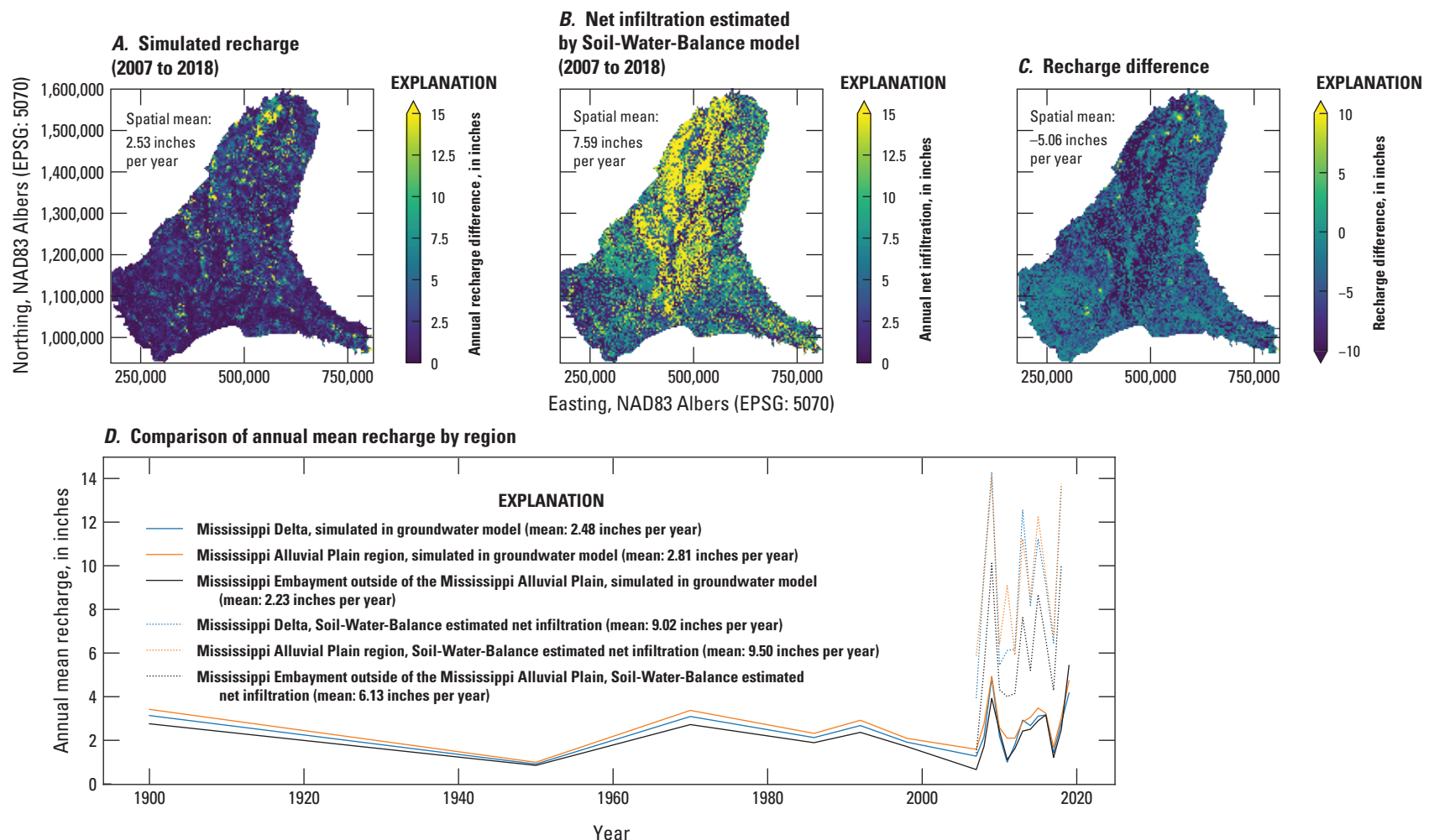


**Figure 2.15.** A, estimated mean annual recharge in the regional model compared to, B, net infiltration (leaving the soil zone) estimated by the Soil-Water-Balance code model of Nielsen and Westenbroek (2023), for 2007 through 2018; C, recharge difference; and D, compares regional average annual recharge values after model history matching to their equivalent net infiltration values estimated by Soil-Water-Balance code.

## Water Use

Water use parametrization for the MERAS 3 model history matching consisted of static multipliers for the pumping rates associated with each dataset, static multipliers for the pumping rates associated with each geographic region listed in [table 2.6](#), and dynamic multipliers for all pumping rates associated with each stress period; therefore, the estimated

pumping rate for each well in a given stress period was the product of the initial pumping rate, the two static rates, and the global dynamic rate for that stress period. Total estimated water use for the base ensemble member from the second iES history matching iteration is shown through time in [figure 1.2](#); [table 2.6](#) summarizes the static multiplier estimates from that model. Dynamic multiplier values are available in the companion data release (Leaf and others, 2023).

**Table 2.6.** Summary of static multiplier parameters applied to water use, simulated by the Well Package.

[MERAS, Mississippi Embayment Regional Aquifer Study; AIWUM, Aquiculture and Irrigation Water Use Model; SWUDS, site-specific water-use data system; --, not included in model parametrization]

Dataset	Geographic region	MERAS 3 model estimated multiplier	Mississippi Delta model estimated multiplier
MERAS 2 model	All	0.86	0.99
AIWUM	All	0.88	1.25
SWUDS	All	0.95	0.96
Estimated water use for thermoelectric power generation <sup>1</sup>	All	1.04	0.98
All datasets	Mississippi Delta	0.90	--
All datasets	Cache	0.95	--
All datasets	Western Mississippi Embayment outside of the Mississippi Alluvial Plain <sup>2</sup>	1.14	--
All datasets	Northeastern Mississippi Embayment outside of Mississippi Alluvial Plain <sup>3</sup>	1.28	--
All datasets	Grand Prairie	0.84	--
All datasets	Southeastern Mississippi Embayment outside of the Mississippi Alluvial Plain <sup>4</sup>	0.81	--
All datasets	Boeuf	0.86	--
All datasets	St. Francis	0.75	--

<sup>1</sup>Diehl and Harris (2014); Harris and Diehl (2019a, b)

<sup>2</sup>Model cells outside of the Mississippi Alluvial Plain west of column 250; primarily Arkansas and Louisiana.

<sup>3</sup>Model cells outside of the Mississippi Alluvial Plain east of column 250 and north of row 357; primarily Tennessee and Kentucky, including the Memphis area.

<sup>4</sup>Model cells outside of the Mississippi Alluvial Plain east of column 250 and south of row 357; primarily Mississippi.

## Mississippi Delta Model Parameter Estimation Results

Estimated parameter values and resulting model inputs for aquifer properties, recharge and water use pumping rates are discussed here; other estimated parameter values and their associated model inputs are available in the companion data release (Leaf and others, 2023).

### Aquifer Properties

Figures 2.16, 2.17, 2.18, and 2.19 show estimated aquifer properties for the base member of the chosen second iteration of the iES history matching run, in comparison to the electrical resistivity-based “facies classes” from the airborne electromagnetic (AEM) survey (Minsley and others, 2021; James and Minsley, 2021). In general, the horizontal hydraulic conductivity ( $K_h$ ) distributions in each layer compare well with the relative distributions of electrical resistivity facies, in that high and low values of hydraulic conductivity correspond to high and low electrical resistivity values. Although some of the correspondence between the distribution of hydraulic conductivity and the electrical resistivity facies may be supported by the observation data, results from initial history matching runs seemed to be sensitive to the starting (prior) parameter values; therefore, initial values were selected for the resistivity facies zones that respected the relative magnitudes of the electrical resistivities represented by the zones (that is, the starting value for zone 1 was set lower or at most equal to the value for zone 2).

In absolute terms, the range of hydraulic conductivity values reflects the heterogeneity that might be expected for a large alluvial system, at the 500-meter scale of the groundwater model, with areas of higher hydraulic conductivity being similar to bulk estimates produced by previous work ( $K_h$  on the order of 100 meters per day; see the “Conceptual Model” section). To improve model stability, and in recognition of the 500-meter scale of the model, an arbitrary lower bound of 1 meter per day was selected for  $K_h$ . Lower values certainly exist, but in general, the lower range of hydraulic conductivity is not well characterized by field data, as aquifer tests usually occur in productive intervals. At a 500-meter scale, there also is greater likelihood of preferential flow paths that would lead to higher bulk  $K_h$  values (for example, Freeze and Cherry, 1979). An upper bound of 500 meters per day was selected based on previous work, with the recognition that higher  $K_h$  may exist in this continental-scale alluvial system. In average terms, estimated values of horizontal hydraulic conductivity compare well with previous work (table 1).

Hydraulic conductivity vertical anisotropy, specific yield and specific storage are all relatively difficult to characterize in detail in the field, especially at the 500-meter scale of the model. Vertical hydraulic conductivity is especially scale

dependent; for example, vertical hydraulic conductivities in layers 1-8 in the Mississippi Delta model (5-meter thick cells) are not readily comparable to vertical hydraulic conductivities in the MERAS 3 or previous models that represented the alluvium with a single layer. The values shown in figures 2.17, 2.18 and 2.19 are generally consistent with previous work and literature values (for example, Clark and Hart, 2009; Clark and others, 2013; Arthur, 2001; table 1 in this report).

### Recharge

Figure 2.20 compares estimated recharge in the Mississippi Delta model to the net infiltration estimates from the SWB model of Nielsen and Westenbroek (2023) that formed the basis for the initial parameter values. Similar to the regional model, the spatial average here of 3.22 inches per year for the Mississippi Delta is consistent with previous work (see the Conceptual model section), but substantially lower than the SWB model estimates. The explanations for this discrepancy are likely the same as those given previously for the regional model—potentially error in the SWB simulation exacerbated by the small net infiltration component, or the shallow confining unit limiting the connection between net infiltration leaving the soil zone and the regional water table (Nielsen and Westenbroek, 2023). Very low multipliers (as low as 0.02) in the lower connectivity zones, especially in the central Delta area, are consistent with initial trial and error runs that required low recharge and stream leakage to reproduce observed drawdowns in the central Delta area.

### Streambed Leakage

Figure 2.21 shows estimated values of streambed leakage, compared to the initial values, which were based on waterborne surveys of subsurface electrical resistivity (Killian, 2018; Adams and others, 2019; Leaf, 2023). Similar to recharge, the spatial pattern of estimated values reflects the relative distribution of shallow confining unit thicknesses represented by the surficial connectivity zones. Very low values of leakage in the central Delta area are consistent with trial-and-error runs that required low levels of stream leakage and recharge to reproduce observed drawdowns in this area. The large discrepancy between the initial values and the lower range of estimated leakances could potentially be an artifact of how the waterborne resistivity-based estimates were developed. In many cases, the waterborne resistivity results may be integrating coarser aquifer sediments in addition to any interval(s) that provide shallow confinement, leading to leakage estimates that are biased high. It should also be noted that most of the stream reaches shown in figure 2.21A were not included in the waterborne electrical resistivity survey; initial values for these recharges were filled with the geometric mean for the whole dataset of Adams and others (2019; 1.2 days<sup>-1</sup>).

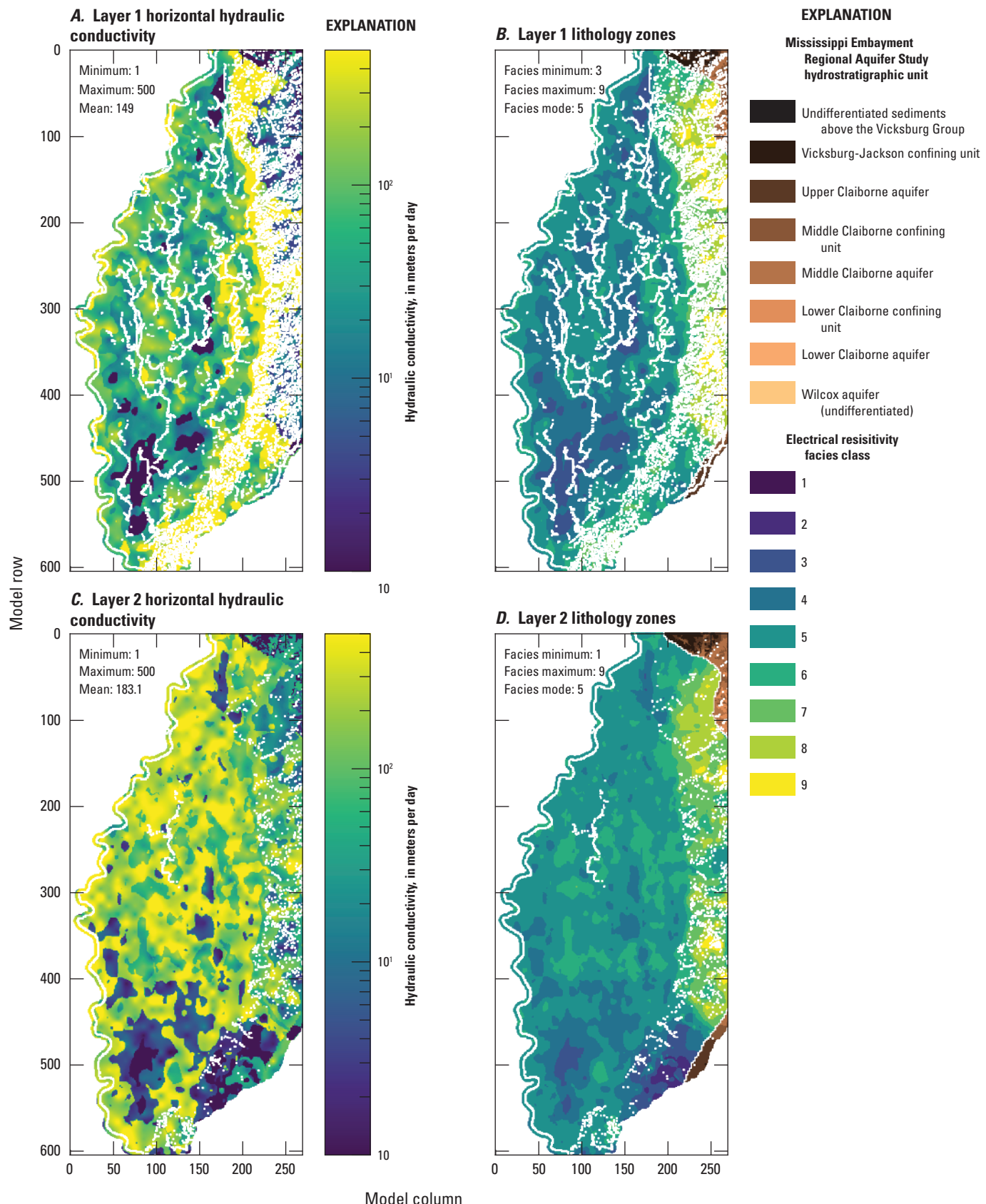


**Figure 2.16.** Horizontal hydraulic conductivity ( $K_h$ ) estimates for the Mississippi Delta model, compared to electrical resistivity-based “facies classes” from the airborne electromagnetic (AEM) survey (Minsley and others, 2021; James and Minsley, 2021). The AEM survey data extend to model layer 15; below that, each model layer represents a single unit from the Mississippi Embayment Regional Aquifer Study framework.

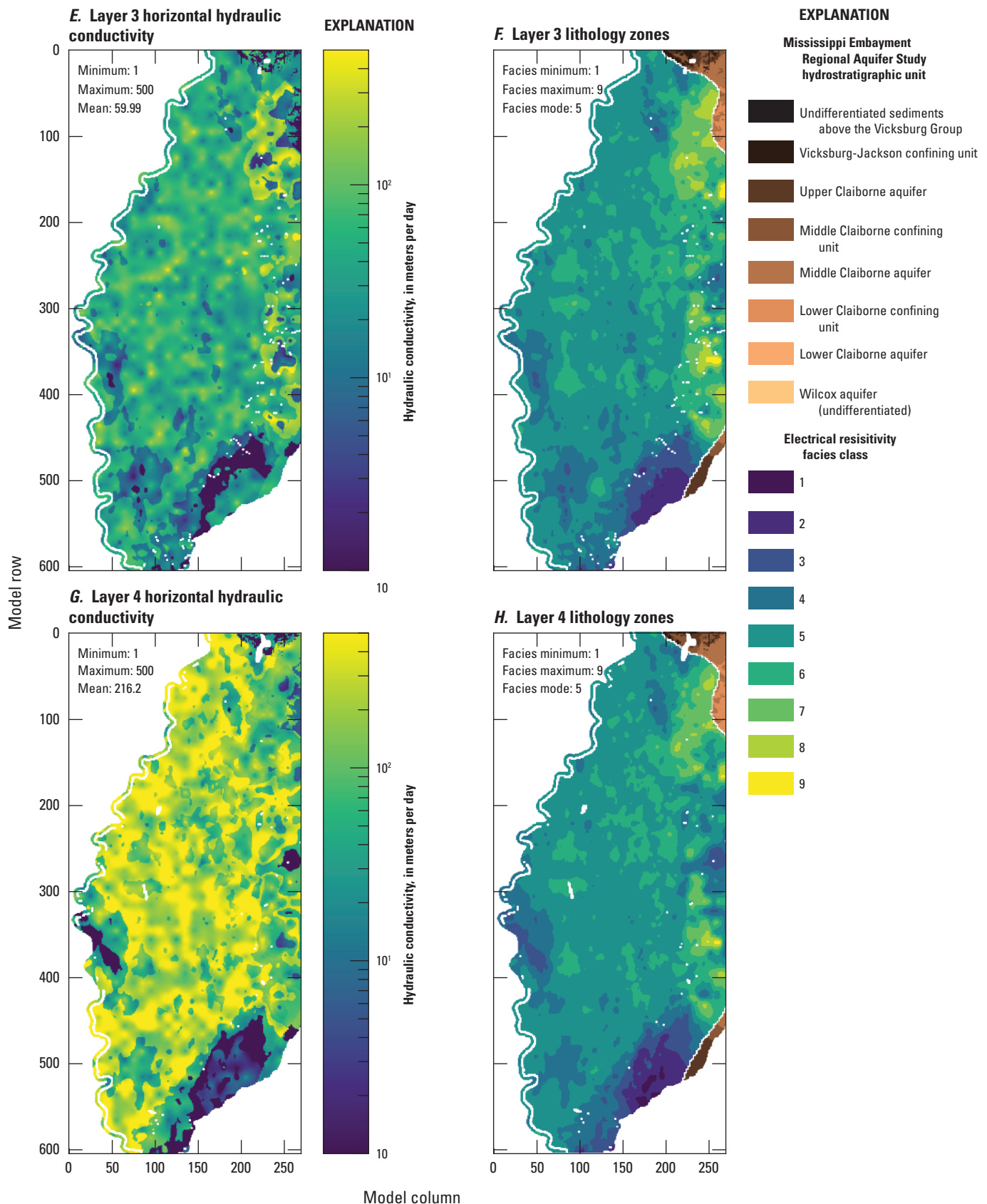


**Figure 2.16.** Horizontal hydraulic conductivity ( $K_h$ ) estimates for the Mississippi Delta model, compared to electrical resistivity-based “facies classes” from the airborne electromagnetic (AEM) survey (Minsley and others, 2021; James and Minsley, 2021). The AEM survey data extend to model layer 15; below that, each model layer represents a single unit from the Mississippi Embayment Regional Aquifer Study framework.

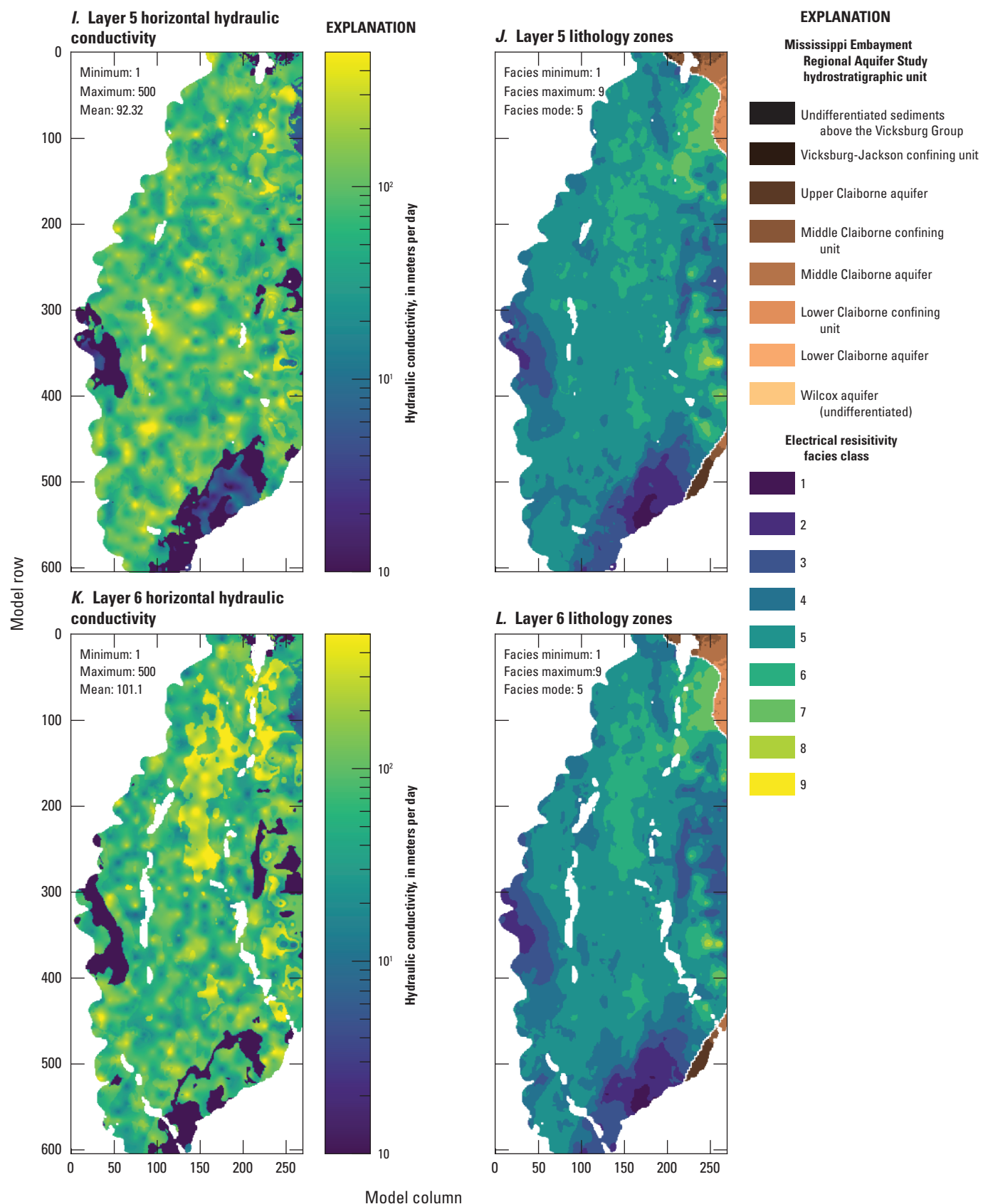


**Figure 2.16.** Horizontal hydraulic conductivity ( $K_h$ ) estimates for the Mississippi Delta model, compared to electrical resistivity-based “facies classes” from the airborne electromagnetic (AEM) survey (Minsley and others, 2021; James and Minsley, 2021). The AEM survey data extend to model layer 15; below that, each model layer represents a single unit from the Mississippi Embayment Regional Aquifer Study framework.

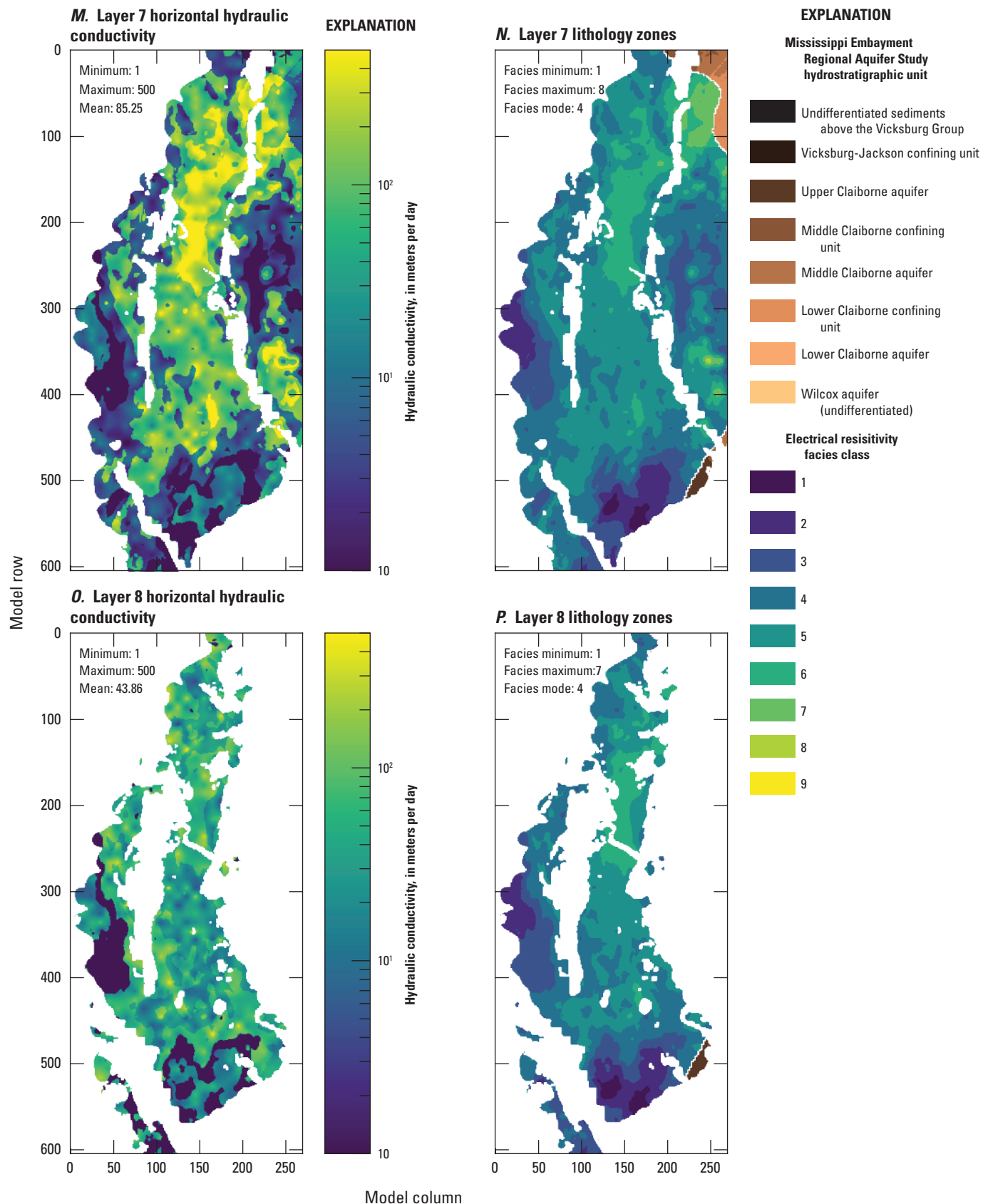


**Figure 2.16.** Horizontal hydraulic conductivity ( $K_h$ ) estimates for the Mississippi Delta model, compared to electrical resistivity-based “facies classes” from the airborne electromagnetic (AEM) survey (Minsley and others, 2021; James and Minsley, 2021). The AEM survey data extend to model layer 15; below that, each model layer represents a single unit from the Mississippi Embayment Regional Aquifer Study framework.

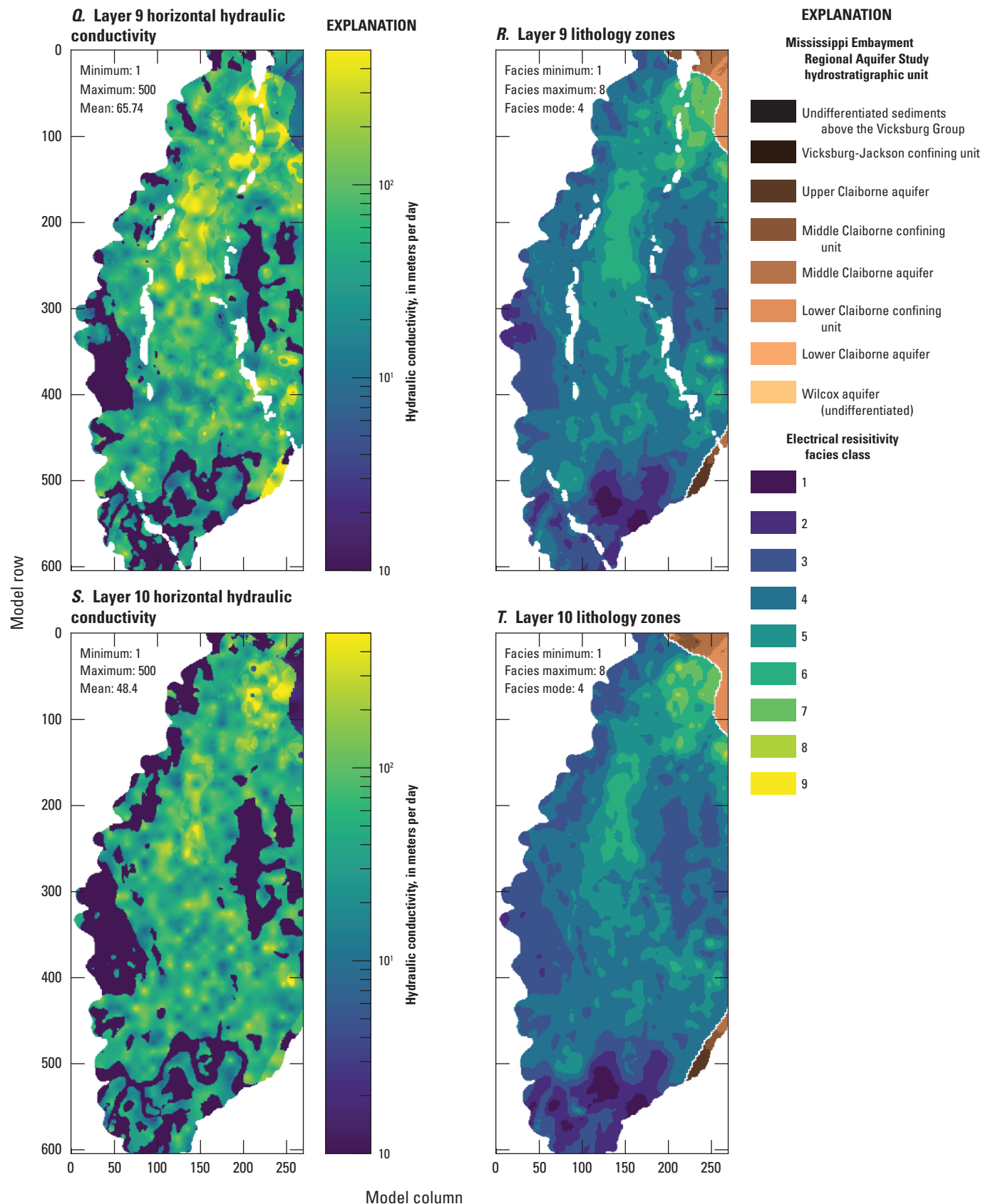


**Figure 2.16.** Horizontal hydraulic conductivity ( $K_h$ ) estimates for the Mississippi Delta model, compared to electrical resistivity-based “facies classes” from the airborne electromagnetic (AEM) survey (Minsley and others, 2021; James and Minsley, 2021). The AEM survey data extend to model layer 15; below that, each model layer represents a single unit from the Mississippi Embayment Regional Aquifer Study framework.

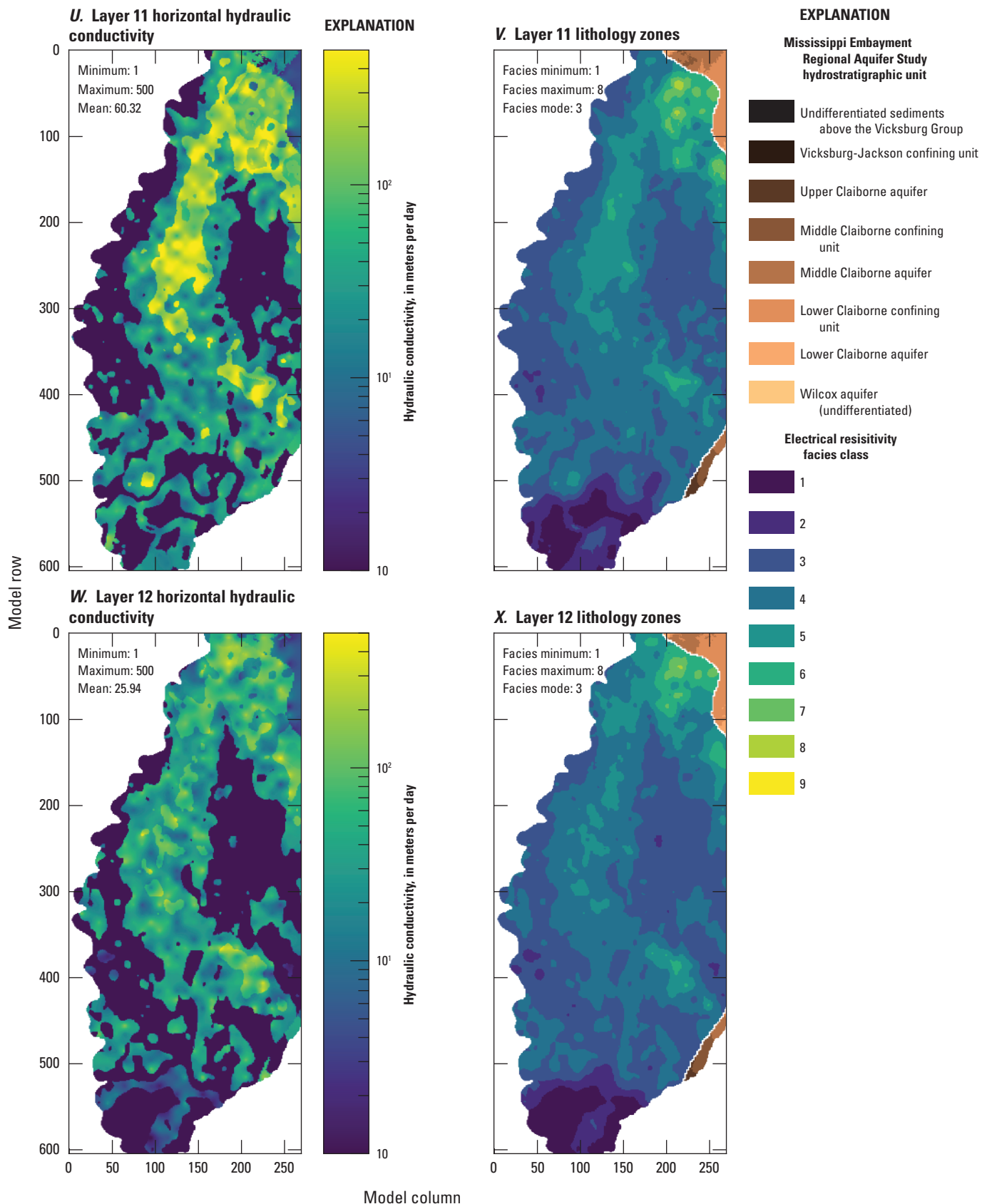


**Figure 2.16.** Horizontal hydraulic conductivity ( $K_h$ ) estimates for the Mississippi Delta model, compared to electrical resistivity-based “facies classes” from the airborne electromagnetic (AEM) survey (Minsley and others, 2021; James and Minsley, 2021). The AEM survey data extend to model layer 15; below that, each model layer represents a single unit from the Mississippi Embayment Regional Aquifer Study framework.

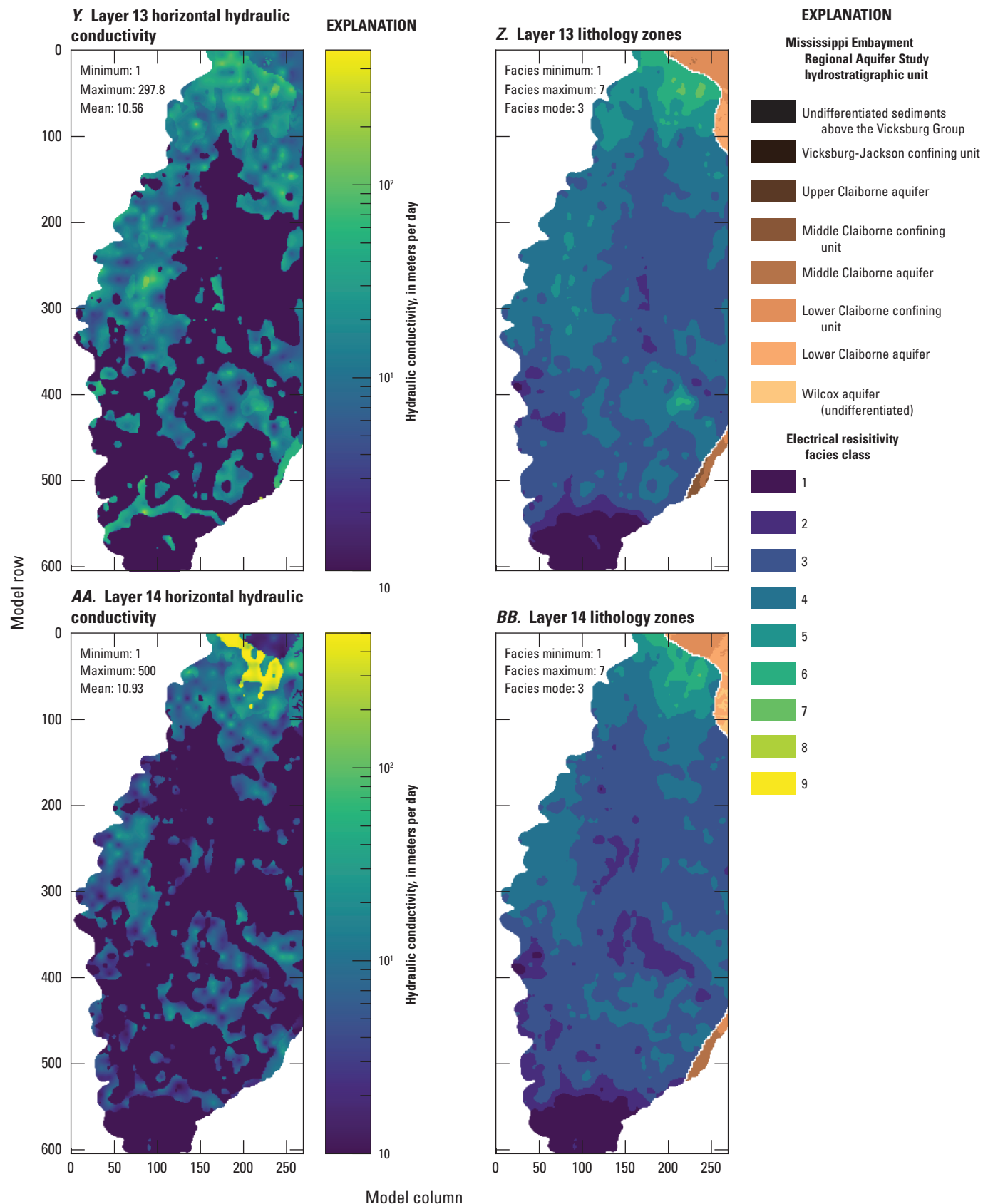


**Figure 2.16.** Horizontal hydraulic conductivity ( $K_h$ ) estimates for the Mississippi Delta model, compared to electrical resistivity-based “facies classes” from the airborne electromagnetic (AEM) survey (Minsley and others, 2021; James and Minsley, 2021). The AEM survey data extend to model layer 15; below that, each model layer represents a single unit from the Mississippi Embayment Regional Aquifer Study framework.

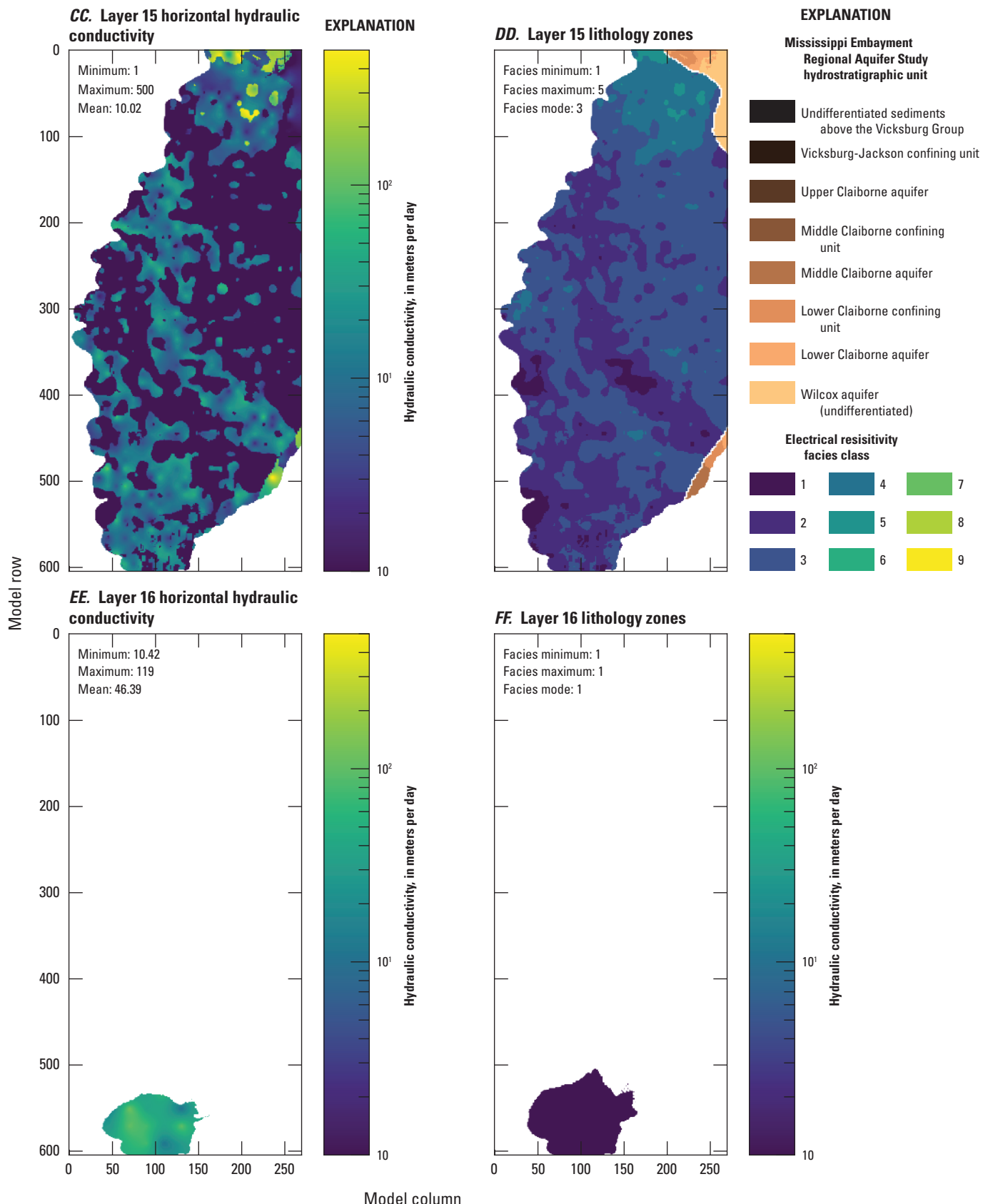


**Figure 2.16.** Horizontal hydraulic conductivity ( $K_h$ ) estimates for the Mississippi Delta model, compared to electrical resistivity-based “facies classes” from the airborne electromagnetic (AEM) survey (Minsley and others, 2021; James and Minsley, 2021). The AEM survey data extend to model layer 15; below that, each model layer represents a single unit from the Mississippi Embayment Regional Aquifer Study framework.

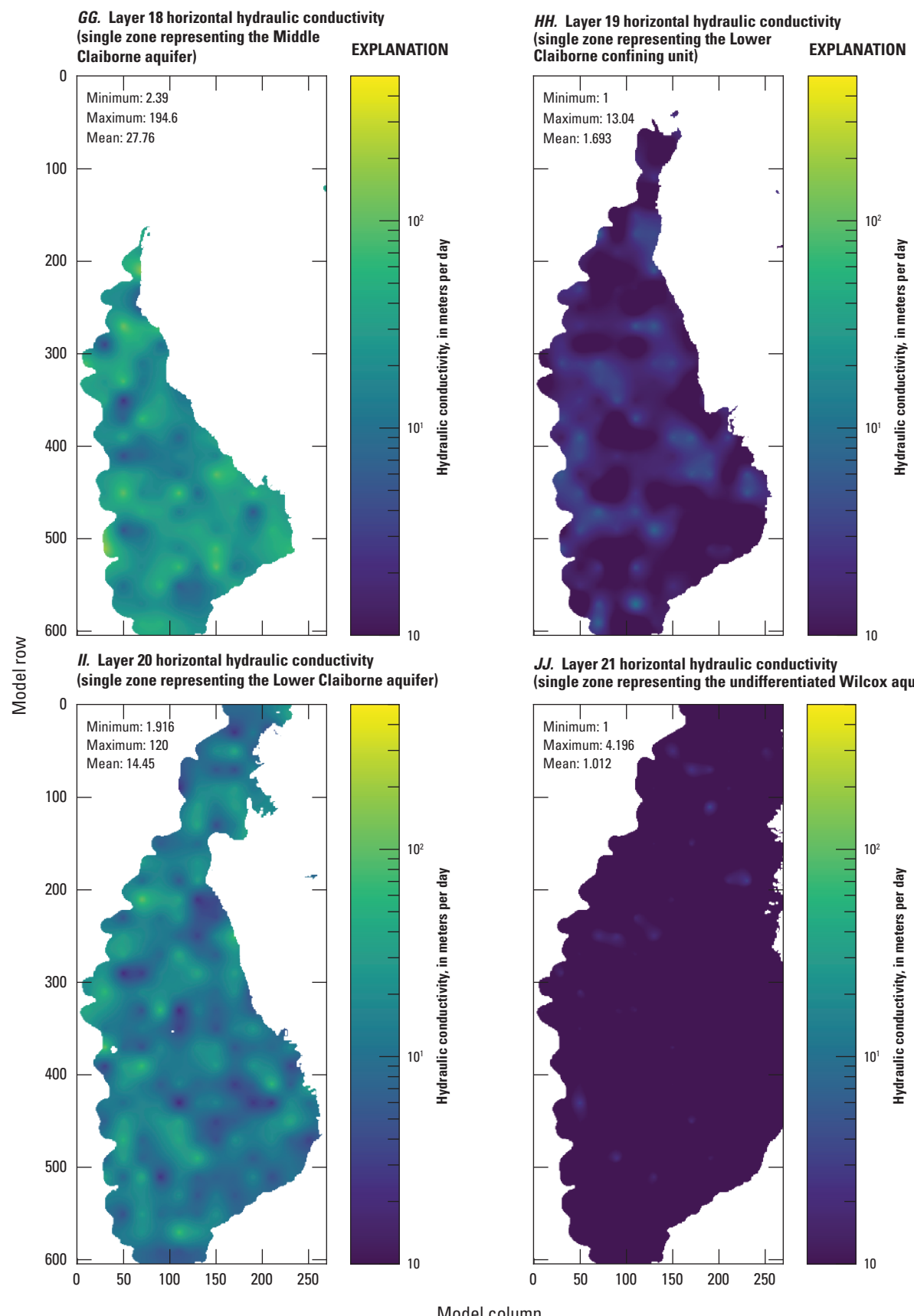


**Figure 2.16.** Horizontal hydraulic conductivity ( $K_h$ ) estimates for the Mississippi Delta model, compared to electrical resistivity-based “facies classes” from the airborne electromagnetic (AEM) survey (Minsley and others, 2021; James and Minsley, 2021). The AEM survey data extend to model layer 15; below that, each model layer represents a single unit from the Mississippi Embayment Regional Aquifer Study framework.

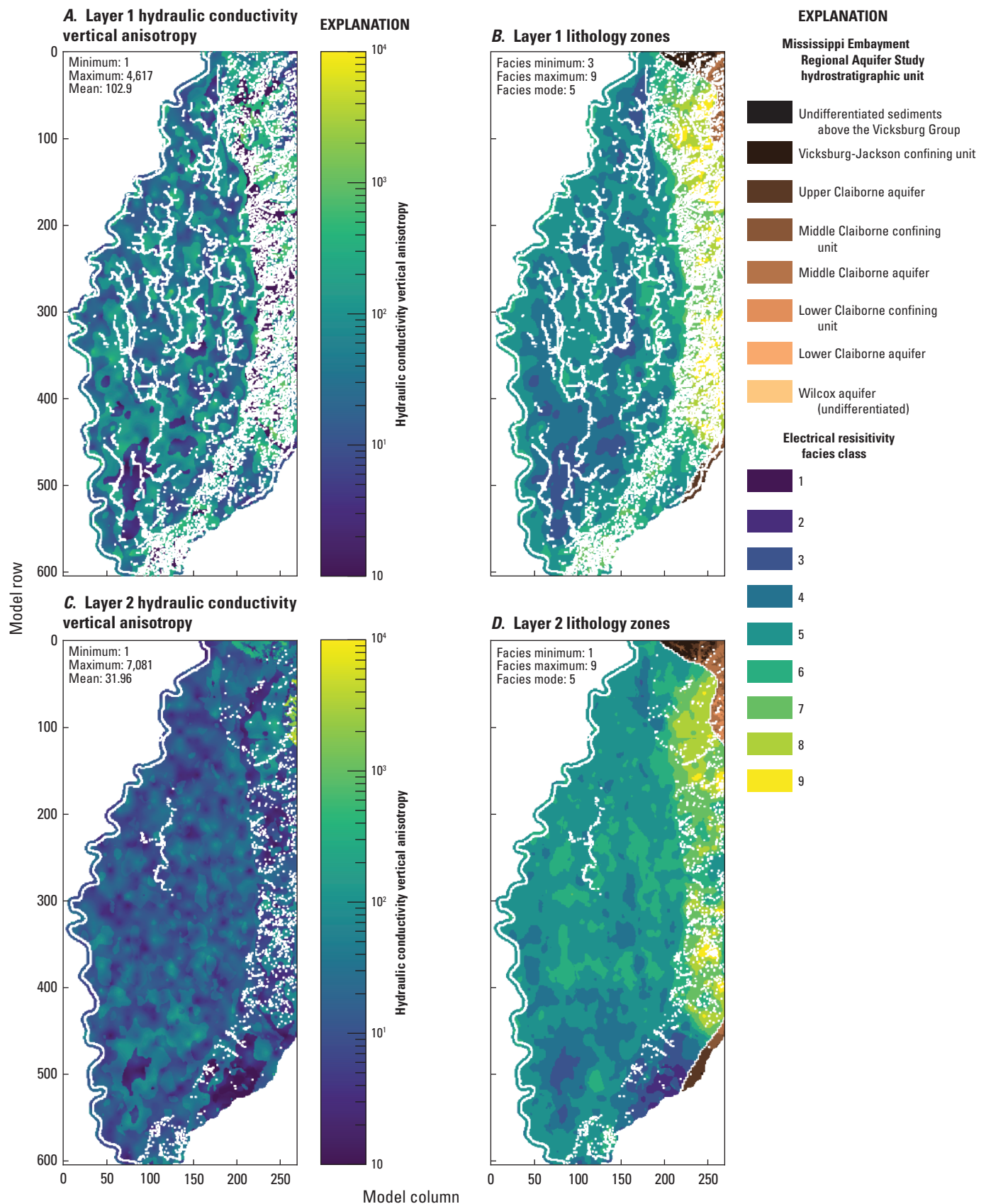


**Figure 2.17.** Hydraulic conductivity vertical anisotropy ( $K_h/K_v$ ) estimates for the Mississippi Delta model, compared to electrical resistivity-based “facies classes” from the airborne electromagnetic (AEM) survey (Minsley and others, 2021; James and Minsley, 2021).

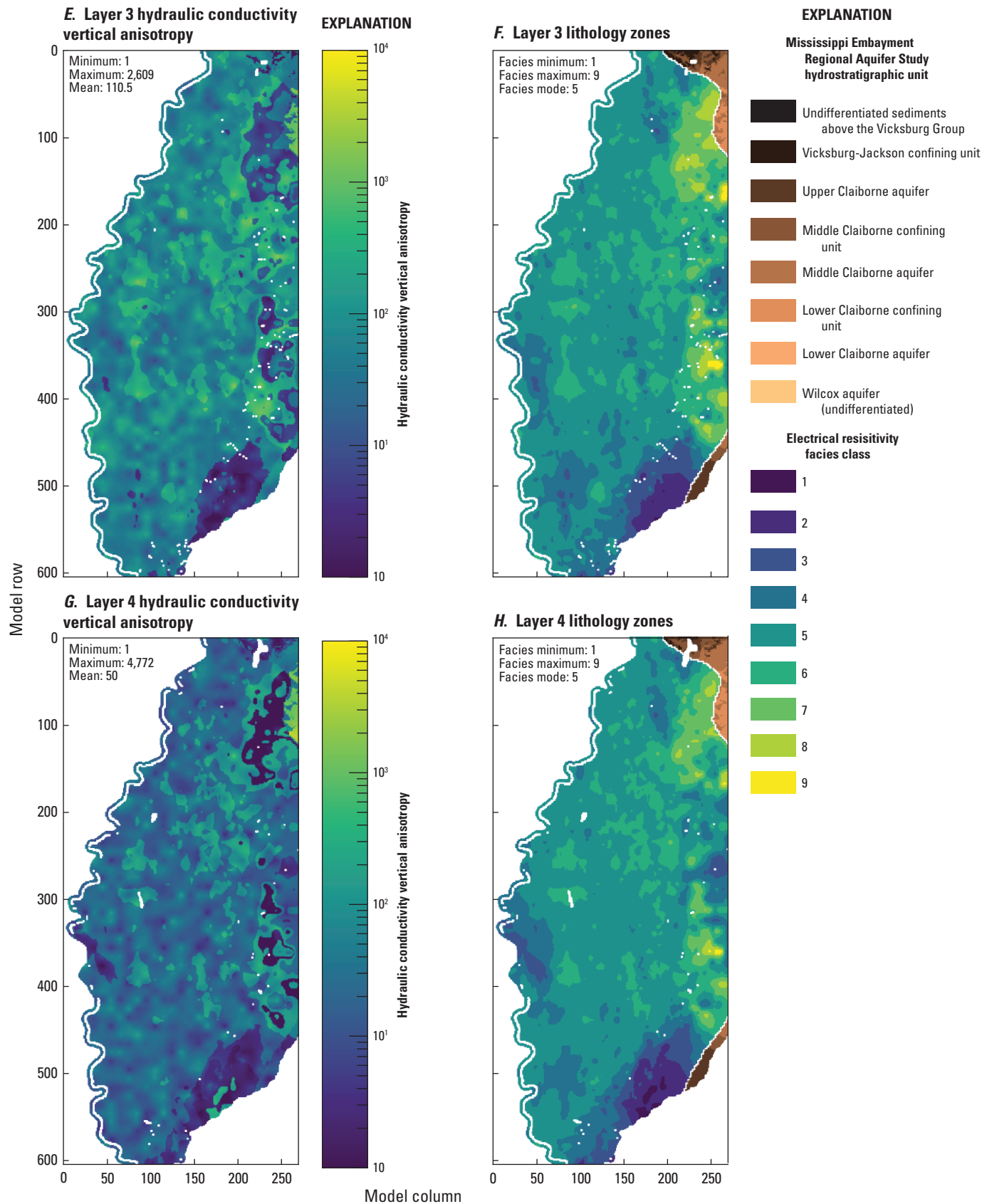


**Figure 2.17.** Hydraulic conductivity vertical anisotropy ( $K_h/K_v$ ) estimates for the Mississippi Delta model, compared to electrical resistivity-based “facies classes” from the airborne electromagnetic (AEM) survey (Minsley and others, 2021; James and Minsley, 2021).

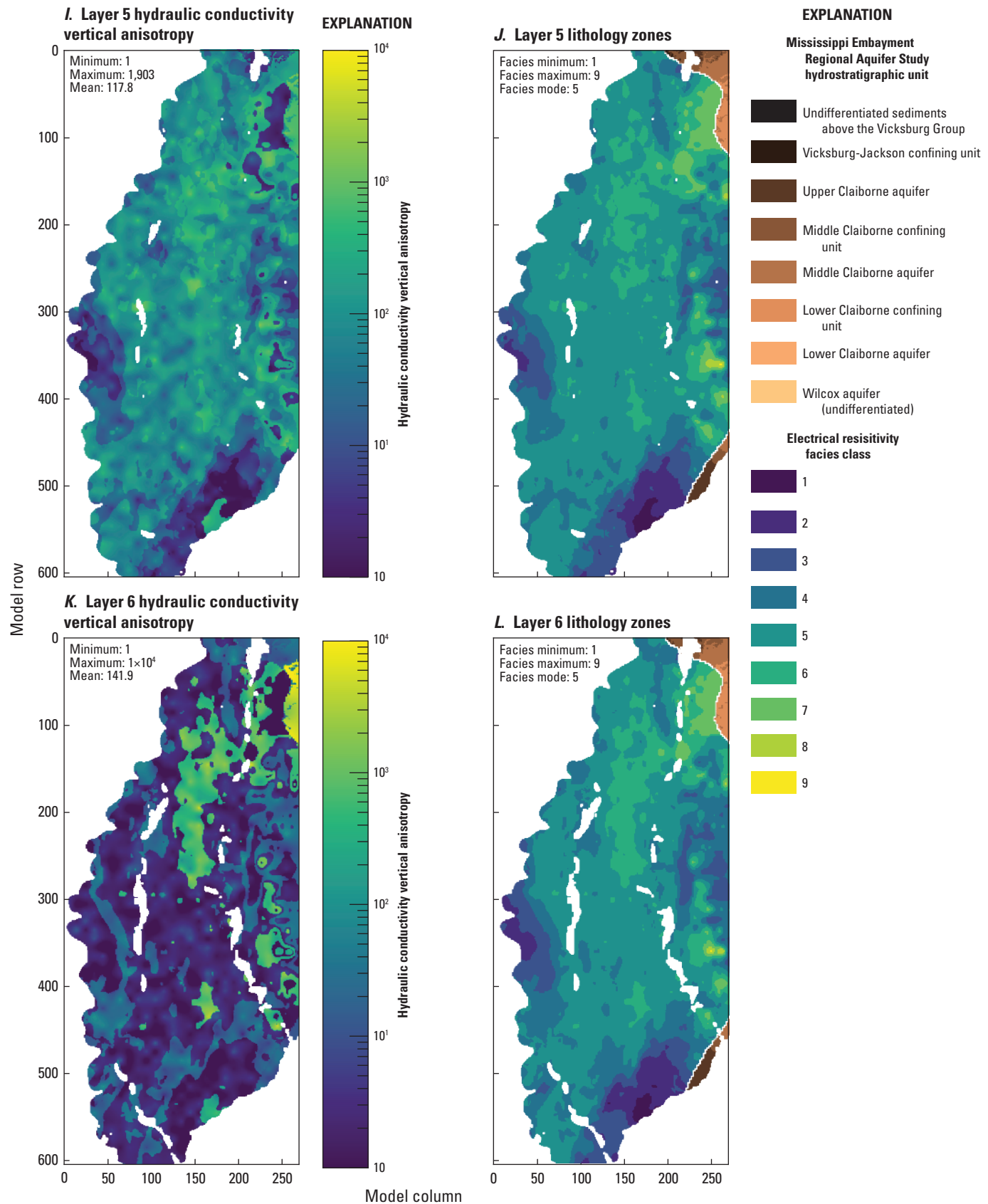


**Figure 2.17.** Hydraulic conductivity vertical anisotropy ( $K_h/K_v$ ) estimates for the Mississippi Delta model, compared to electrical resistivity-based “facies classes” from the airborne electromagnetic (AEM) survey (Minsley and others, 2021; James and Minsley, 2021).

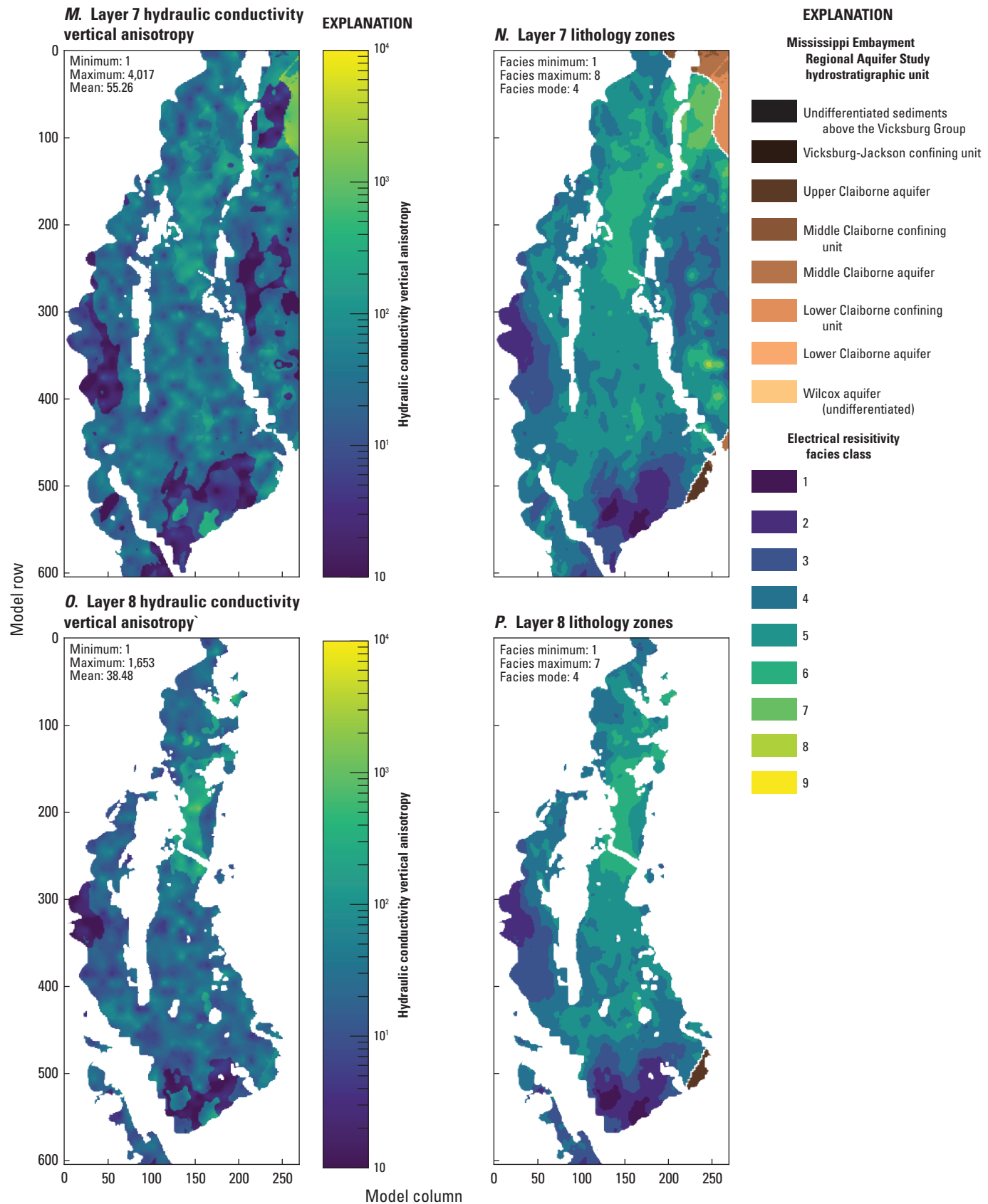
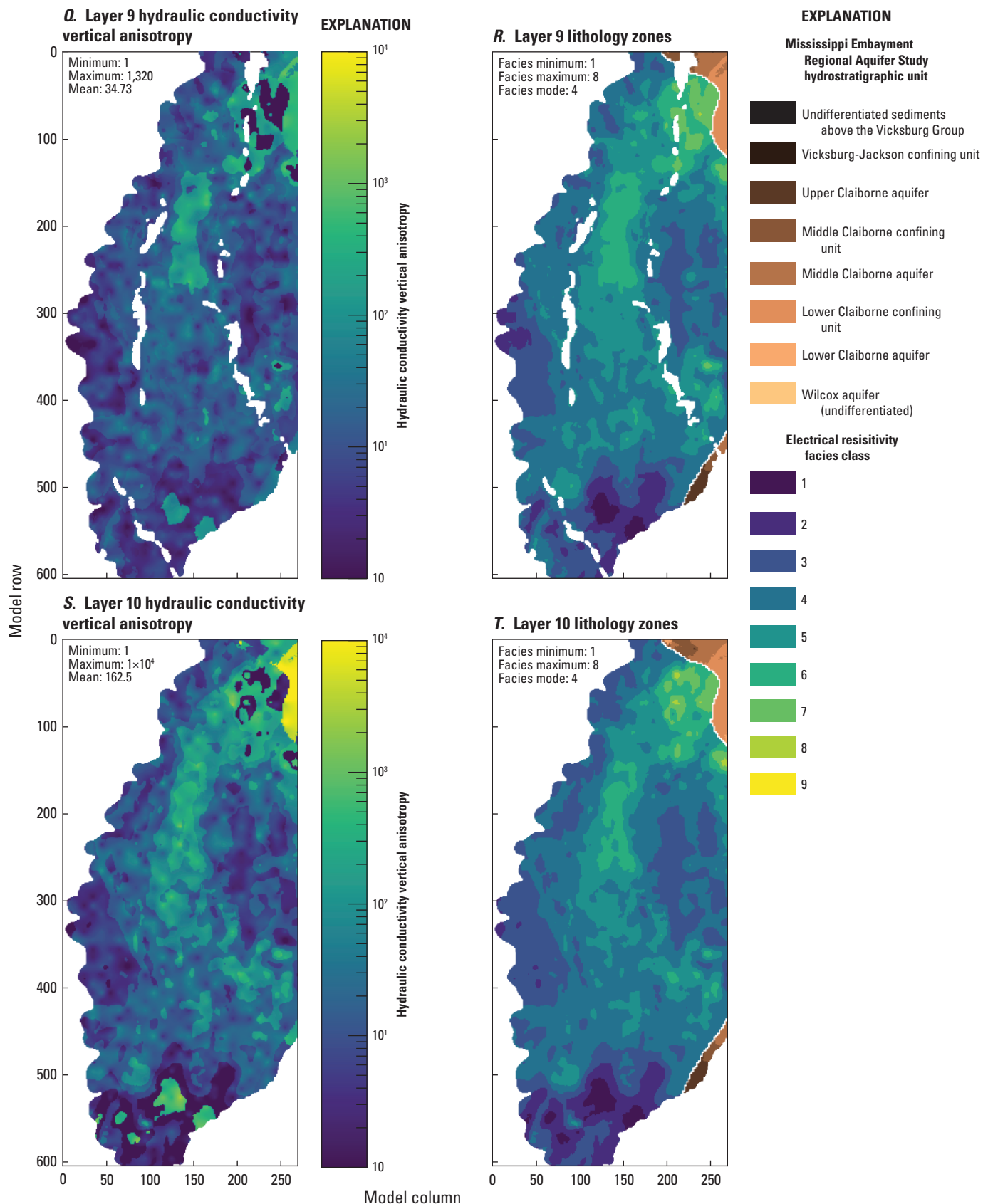


Figure 2.17. Hydraulic conductivity vertical anisotropy ( $K_h/K_v$ ) estimates for the Mississippi Delta model, compared to electrical resistivity-based “facies classes” from the airborne electromagnetic (AEM) survey (Minsley and others, 2021; James and Minsley, 2021).



**Figure 2.17.** Hydraulic conductivity vertical anisotropy ( $K_h/K_v$ ) estimates for the Mississippi Delta model, compared to electrical resistivity-based “facies classes” from the airborne electromagnetic (AEM) survey (Minsley and others, 2021; James and Minsley, 2021).

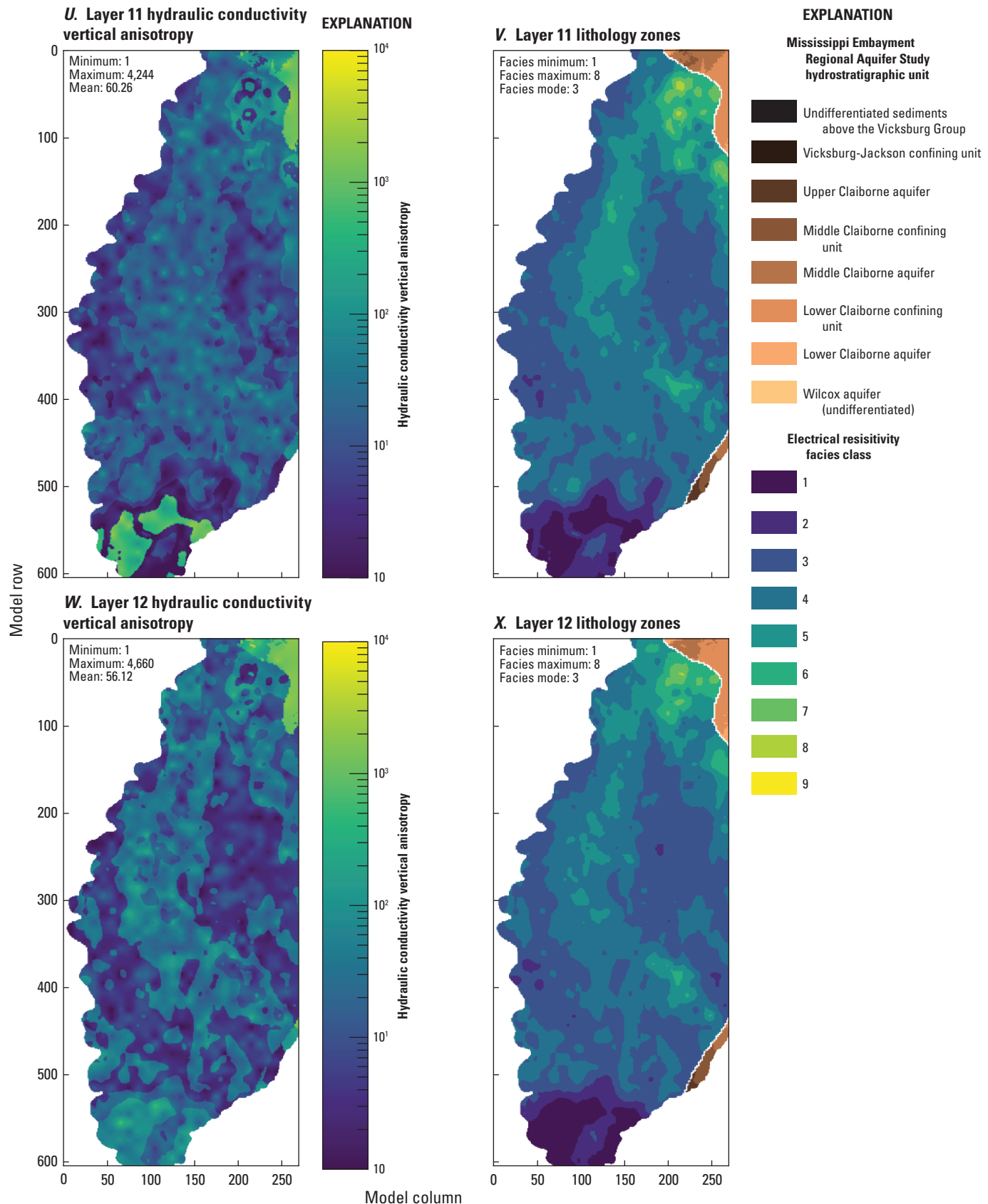
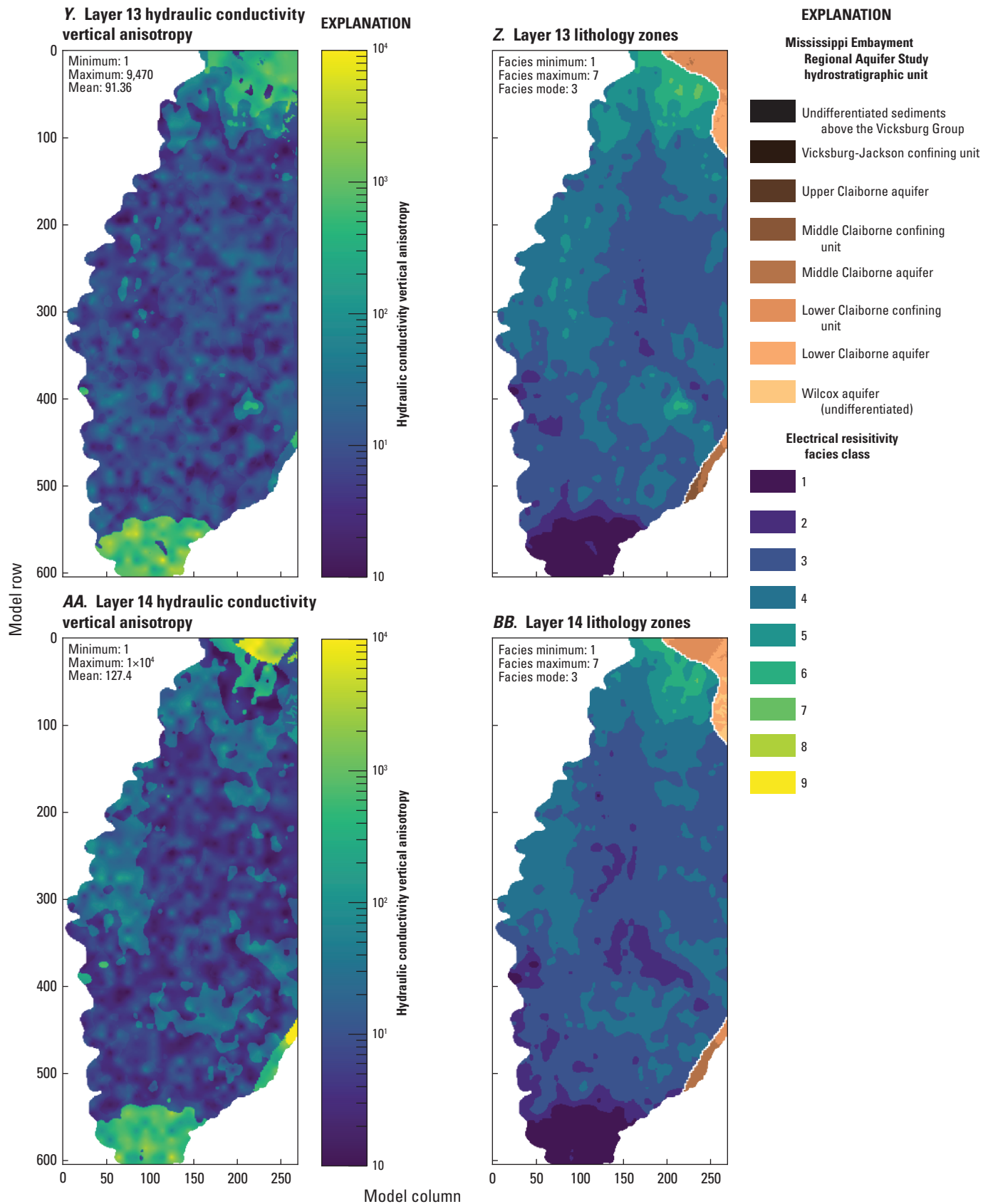
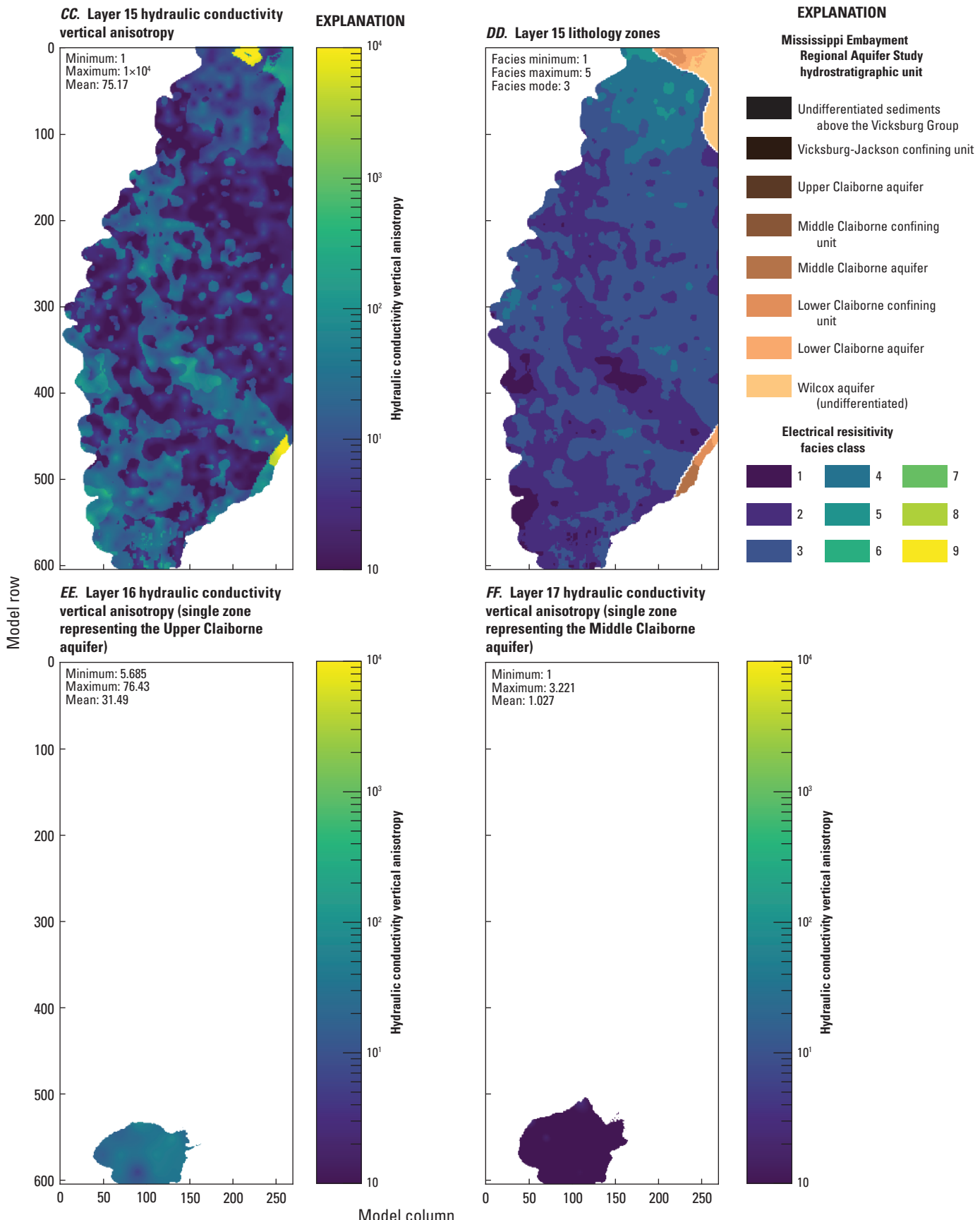


Figure 2.17. Hydraulic conductivity vertical anisotropy ( $K_h/K_v$ ) estimates for the Mississippi Delta model, compared to electrical resistivity-based “facies classes” from the airborne electromagnetic (AEM) survey (Minsley and others, 2021; James and Minsley, 2021).



**Figure 2.17.** Hydraulic conductivity vertical anisotropy ( $K_h/K_v$ ) estimates for the Mississippi Delta model, compared to electrical resistivity-based “facies classes” from the airborne electromagnetic (AEM) survey (Minsley and others, 2021; James and Minsley, 2021).



**Figure 2.17.** Hydraulic conductivity vertical anisotropy ( $K_h/K_v$ ) estimates for the Mississippi Delta model, compared to electrical resistivity-based “facies classes” from the airborne electromagnetic (AEM) survey (Minsley and others, 2021; James and Minsley, 2021).

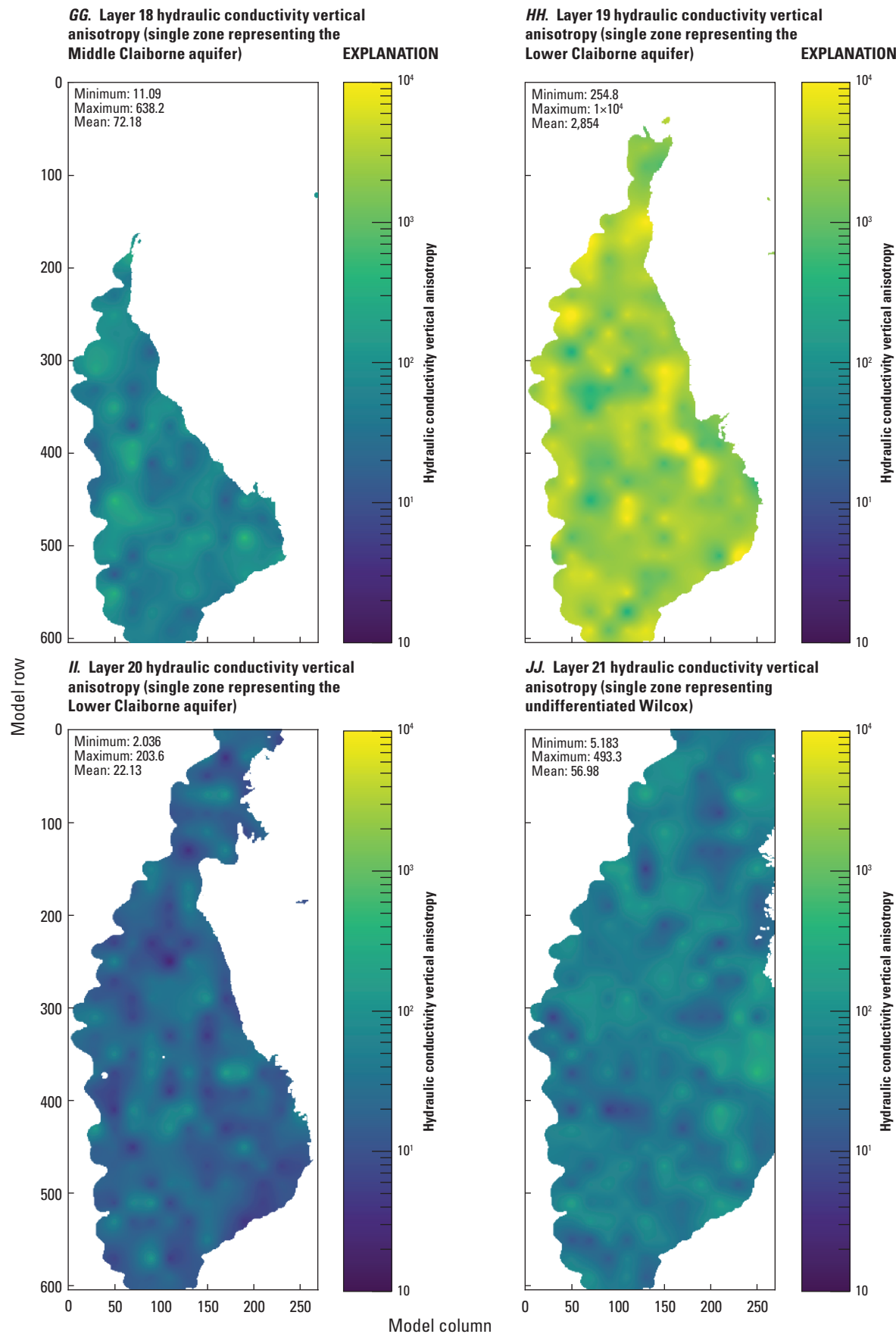


**Figure 2.17.** Hydraulic conductivity vertical anisotropy ( $K_h/K_v$ ) estimates for the Mississippi Delta model, compared to electrical resistivity-based “facies classes” from the airborne electromagnetic (AEM) survey (Minsley and others, 2021; James and Minsley, 2021).

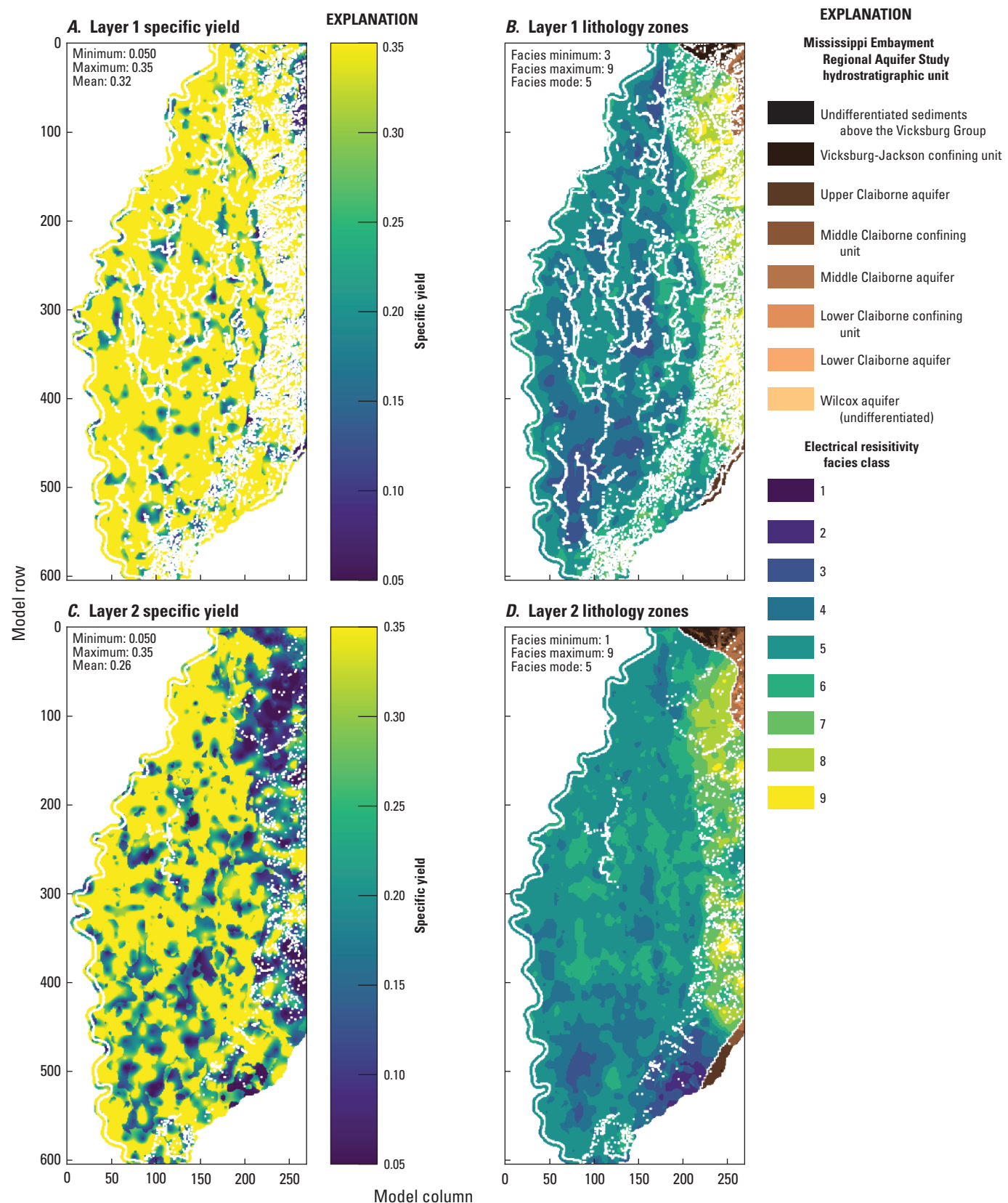
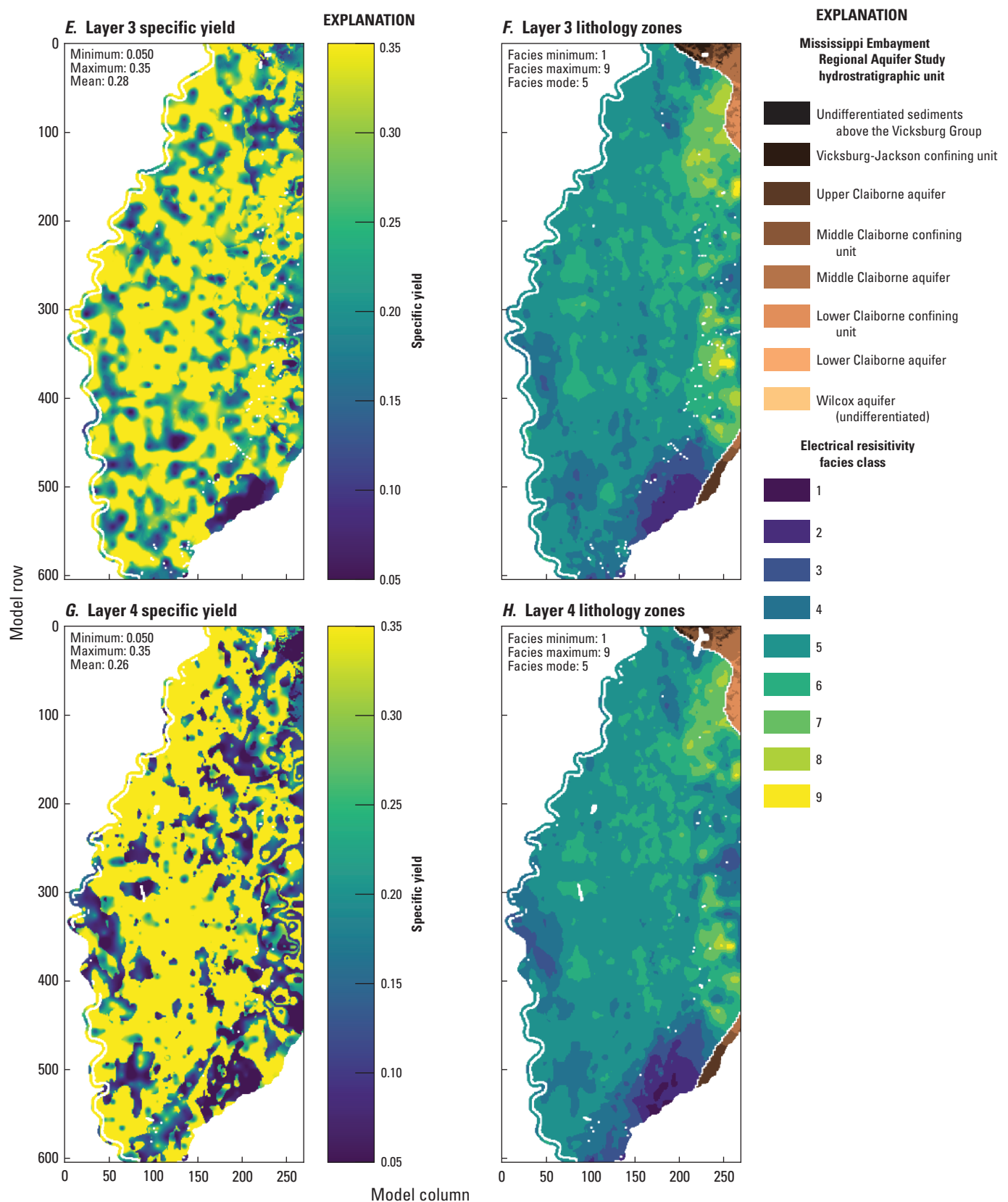
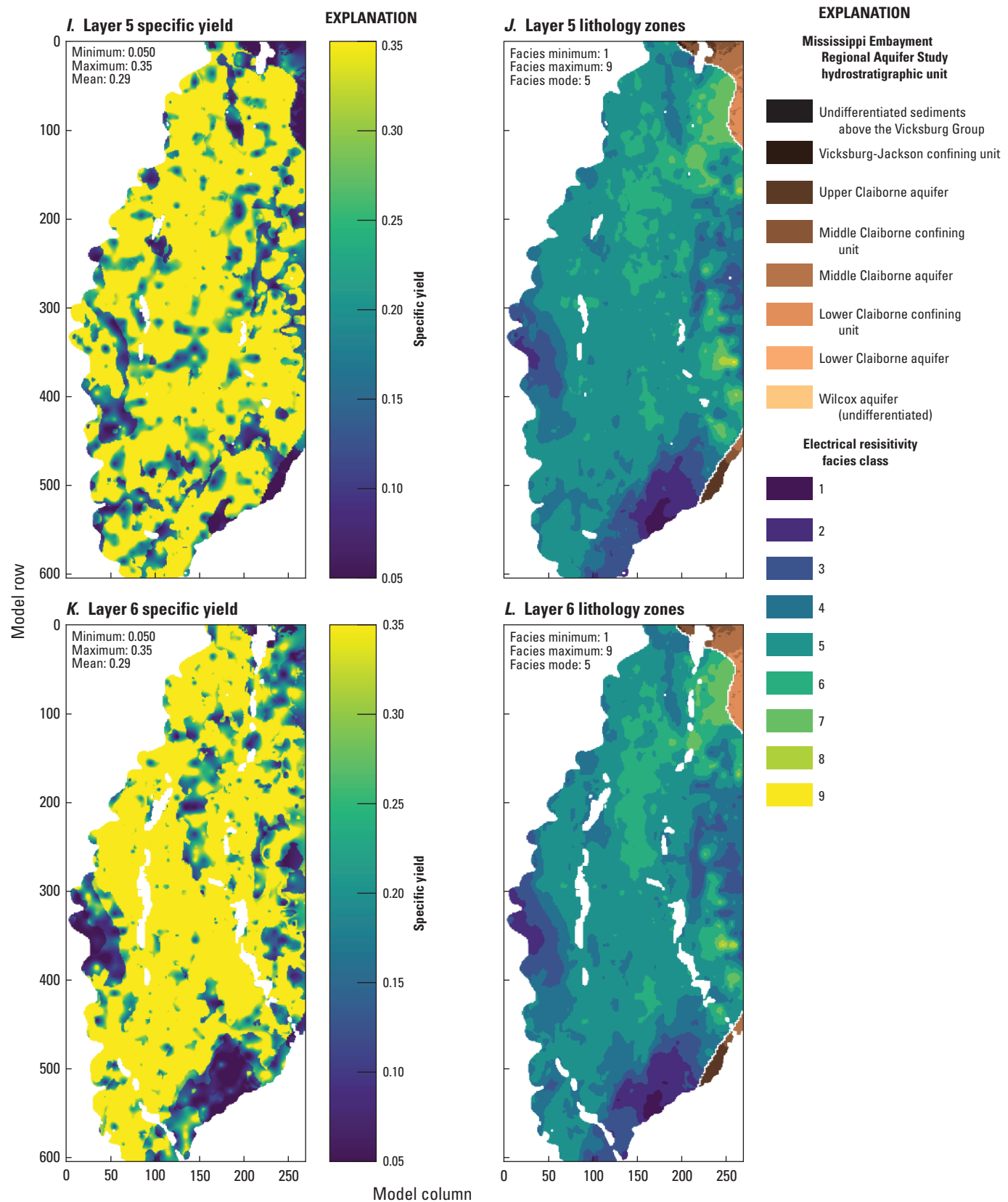


Figure 2.18. Specific yield ( $S_y$ ) estimates for the Mississippi Delta model, compared to electrical resistivity-based “facies classes” from the airborne electromagnetic (AEM) survey (Minsley and others, 2021; James and Minsley, 2021).



**Figure 2.18.** Specific yield ( $S_y$ ) estimates for the Mississippi Delta model, compared to electrical resistivity-based “facies classes” from the airborne electromagnetic (AEM) survey (Minsley and others, 2021; James and Minsley, 2021).



**Figure 2.18.** Specific yield ( $S_y$ ) estimates for the Mississippi Delta model, compared to electrical resistivity-based “facies classes” from the airborne electromagnetic (AEM) survey (Minsley and others, 2021; James and Minsley, 2021).

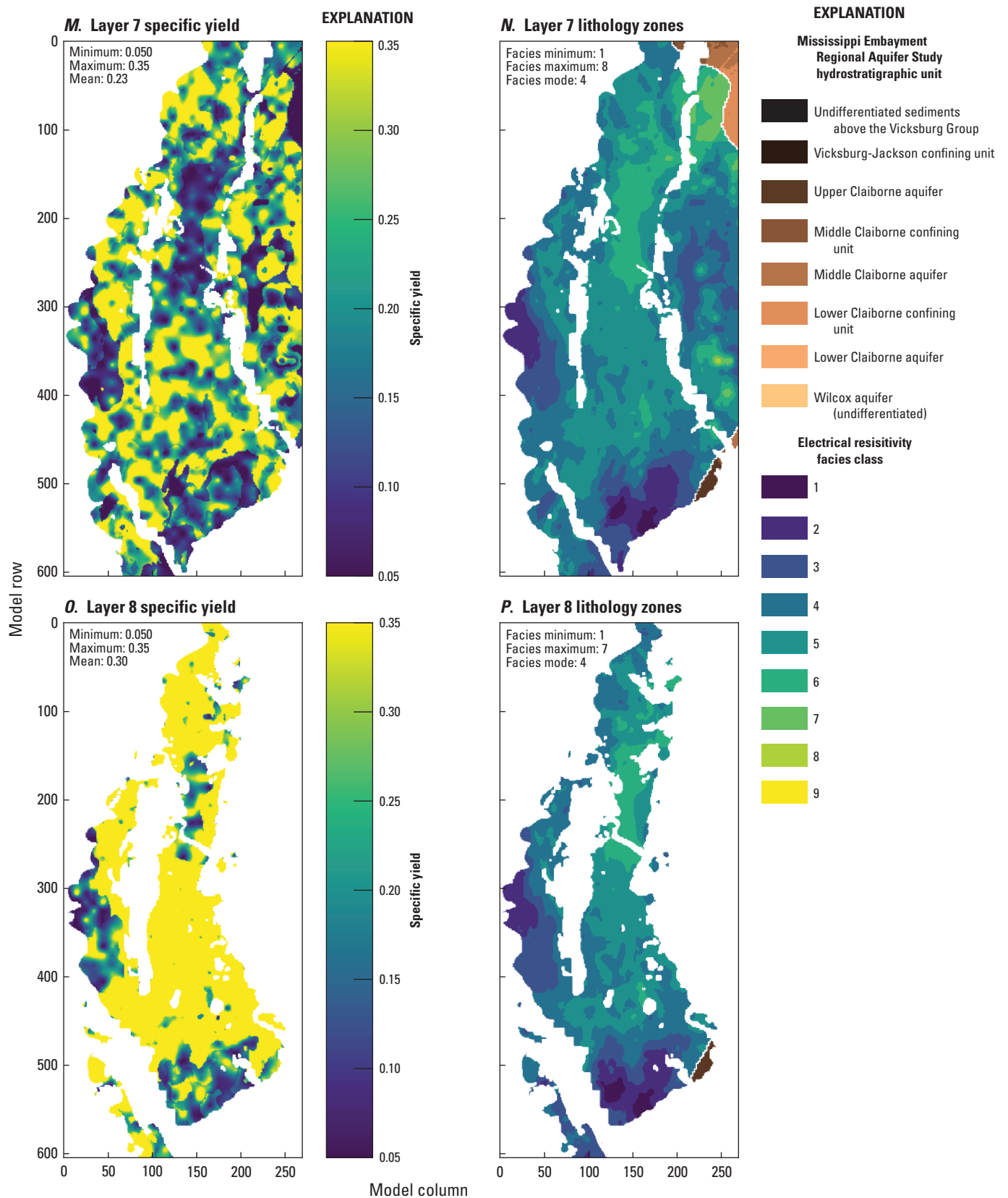


**Figure 2.18.** Specific yield ( $S_y$ ) estimates for the Mississippi Delta model, compared to electrical resistivity-based “facies classes” from the airborne electromagnetic (AEM) survey (Minsley and others, 2021; James and Minsley, 2021).

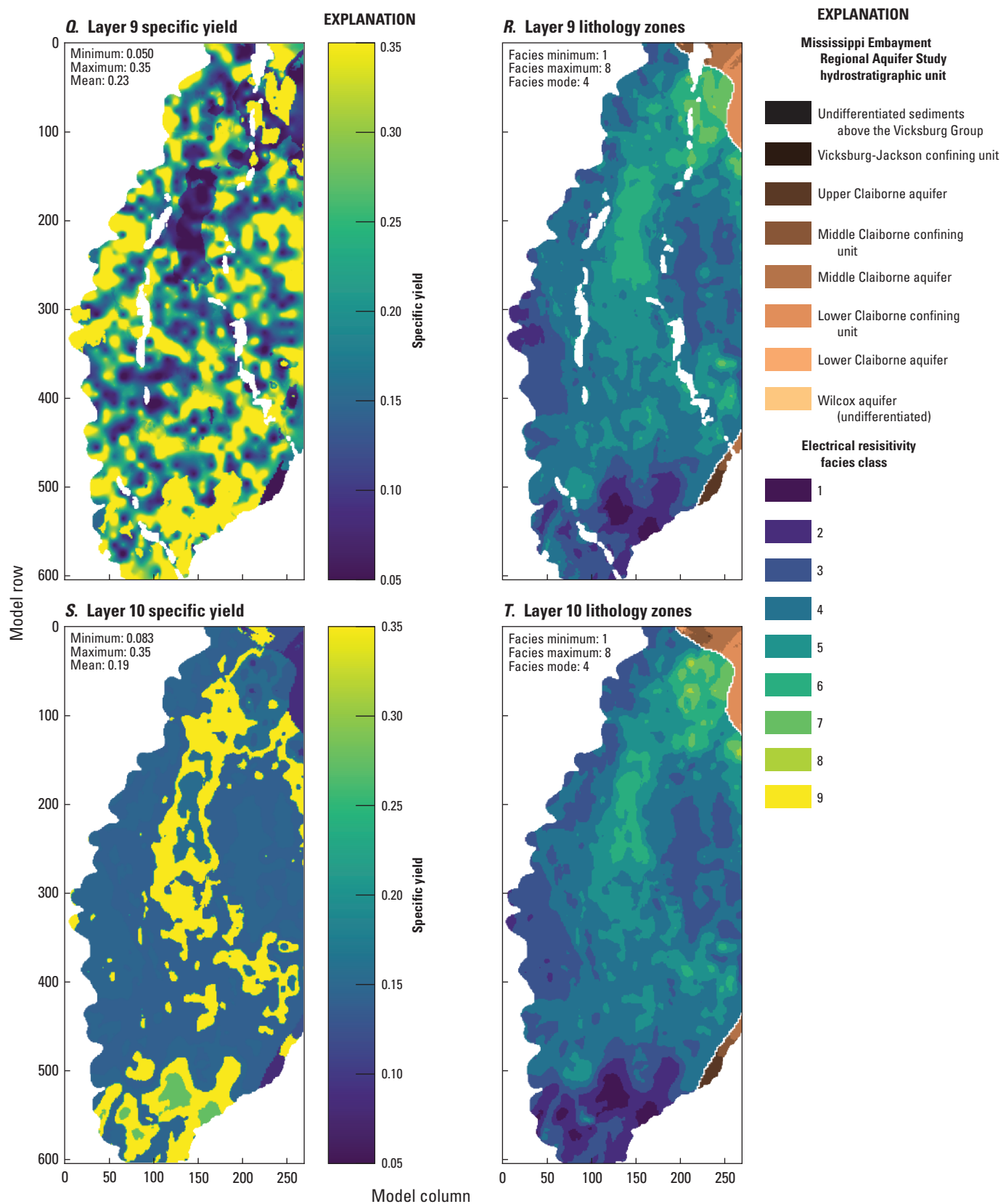


**Figure 2.18.** Specific yield ( $S_y$ ) estimates for the Mississippi Delta model, compared to electrical resistivity-based “facies classes” from the airborne electromagnetic (AEM) survey (Minsley and others, 2021; James and Minsley, 2021).

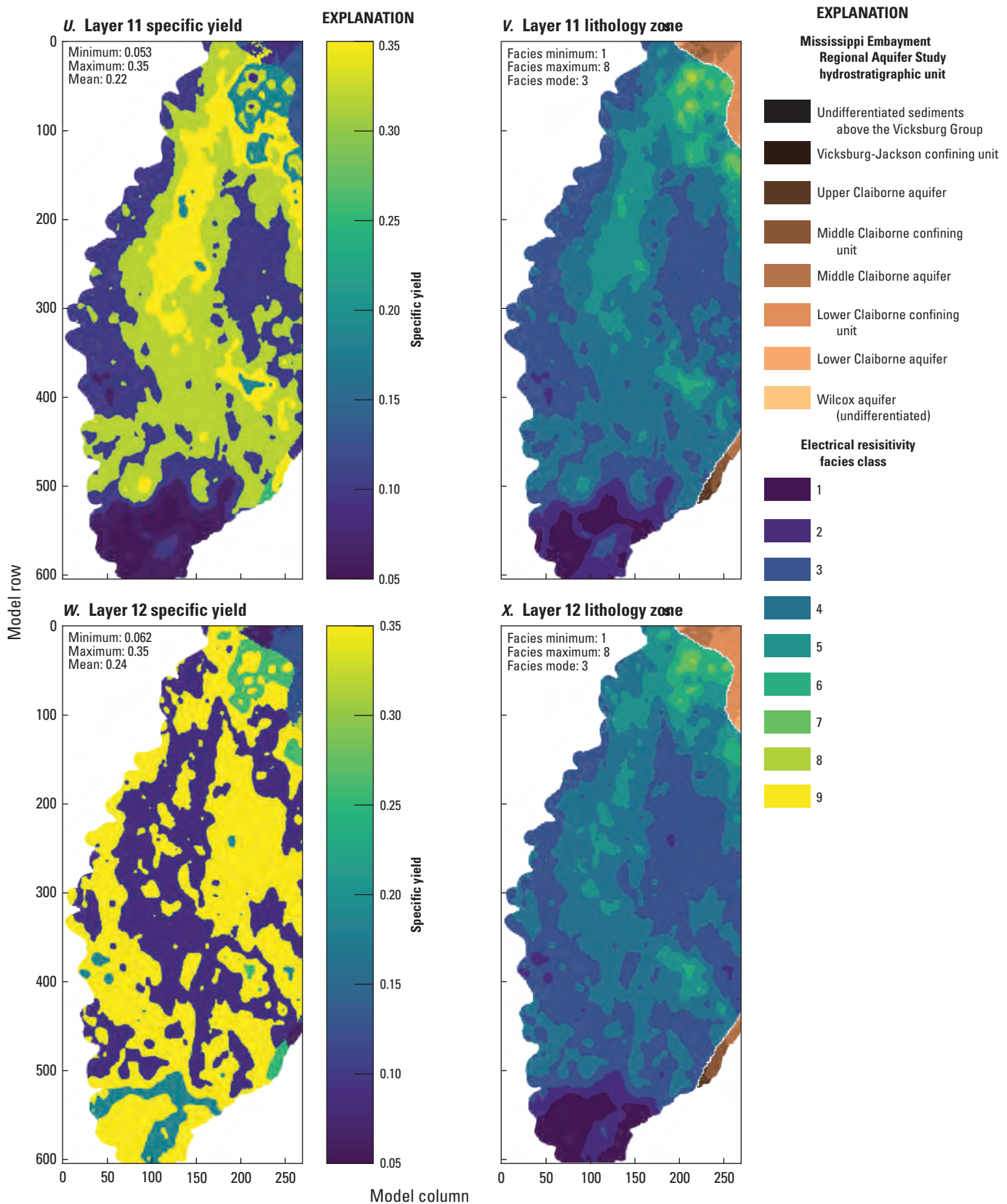


**Figure 2.18.** Specific yield ( $S_y$ ) estimates for the Mississippi Delta model, compared to electrical resistivity-based “facies classes” from the airborne electromagnetic (AEM) survey (Minsley and others, 2021; James and Minsley, 2021).

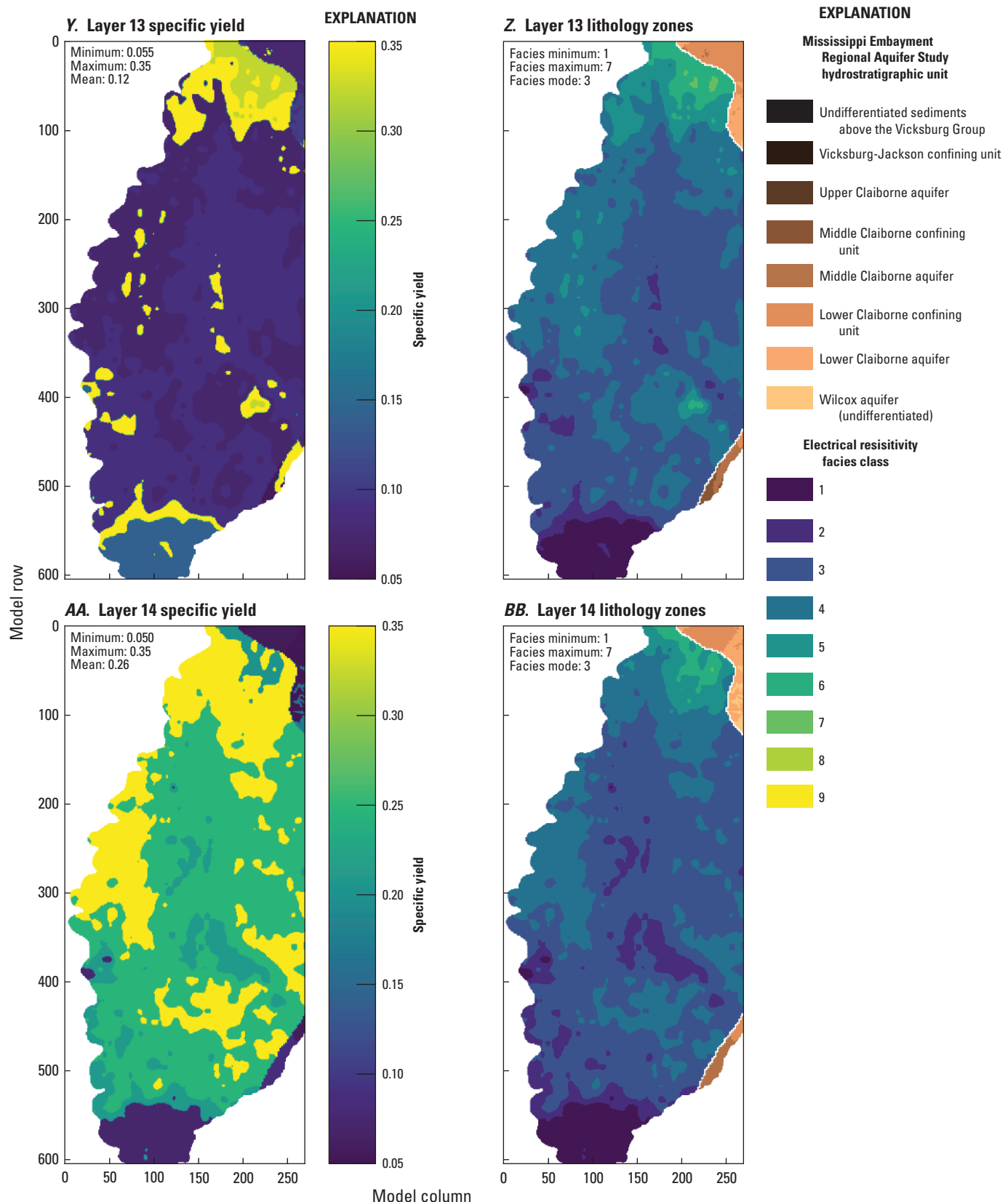
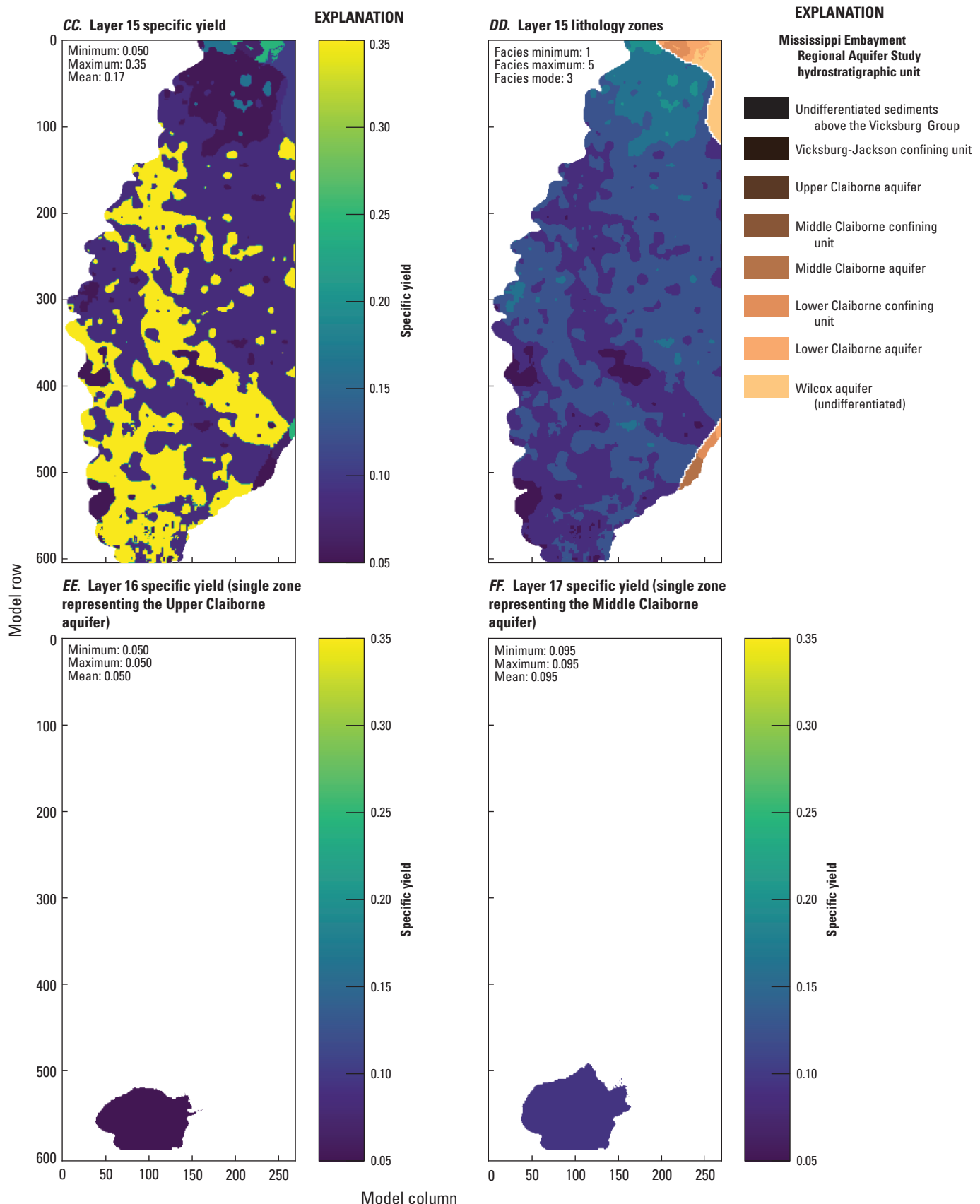
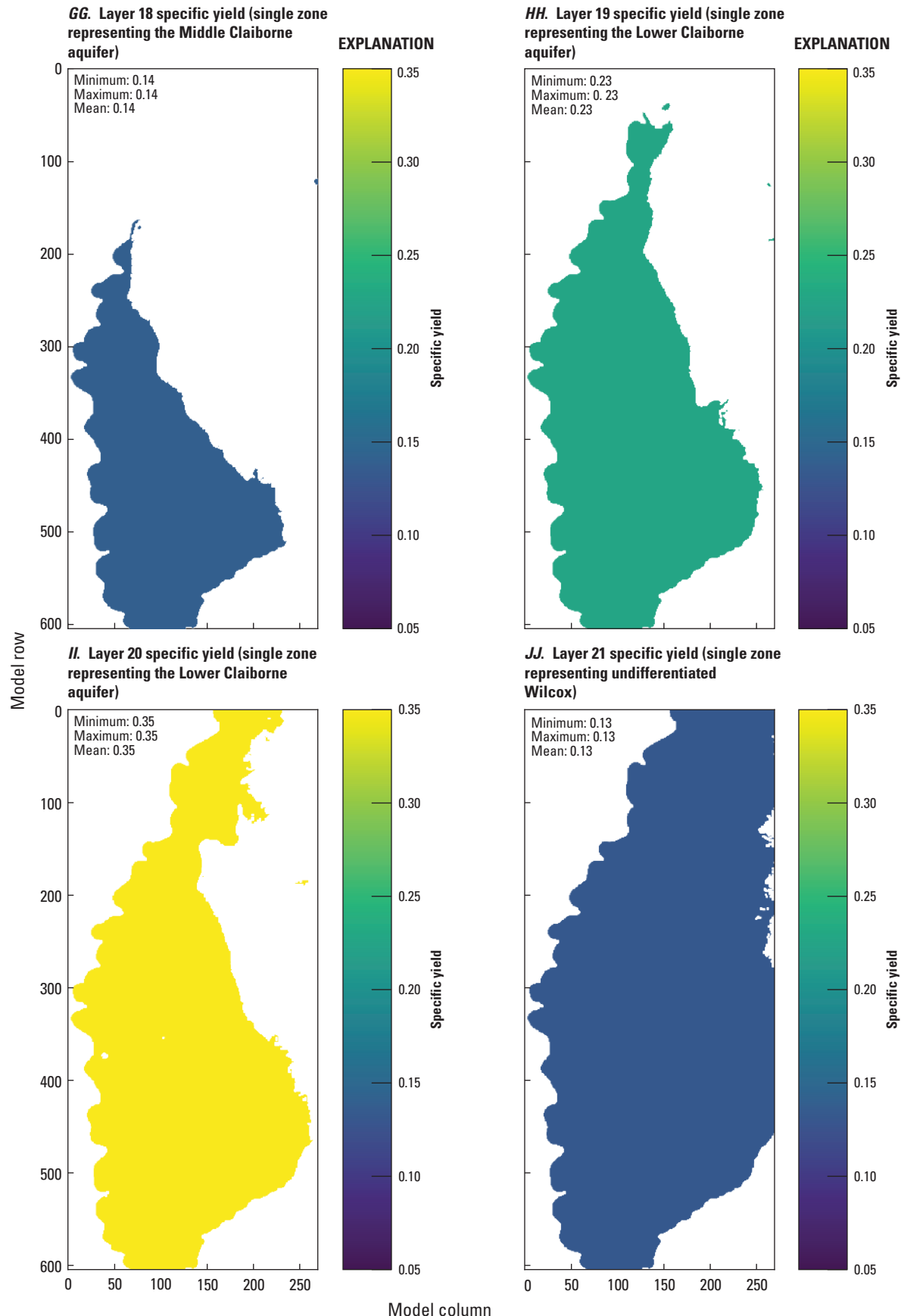


Figure 2.18. Specific yield ( $S_y$ ) estimates for the Mississippi Delta model, compared to electrical resistivity-based “facies classes” from the airborne electromagnetic (AEM) survey (Minsley and others, 2021; James and Minsley, 2021).



**Figure 2.18.** Specific yield ( $S_y$ ) estimates for the Mississippi Delta model, compared to electrical resistivity-based “facies classes” from the airborne electromagnetic (AEM) survey (Minsley and others, 2021; James and Minsley, 2021).



**Figure 2.18.** Specific yield ( $S_y$ ) estimates for the Mississippi Delta model, compared to electrical resistivity-based “facies classes” from the airborne electromagnetic (AEM) survey (Minsley and others, 2021; James and Minsley, 2021).

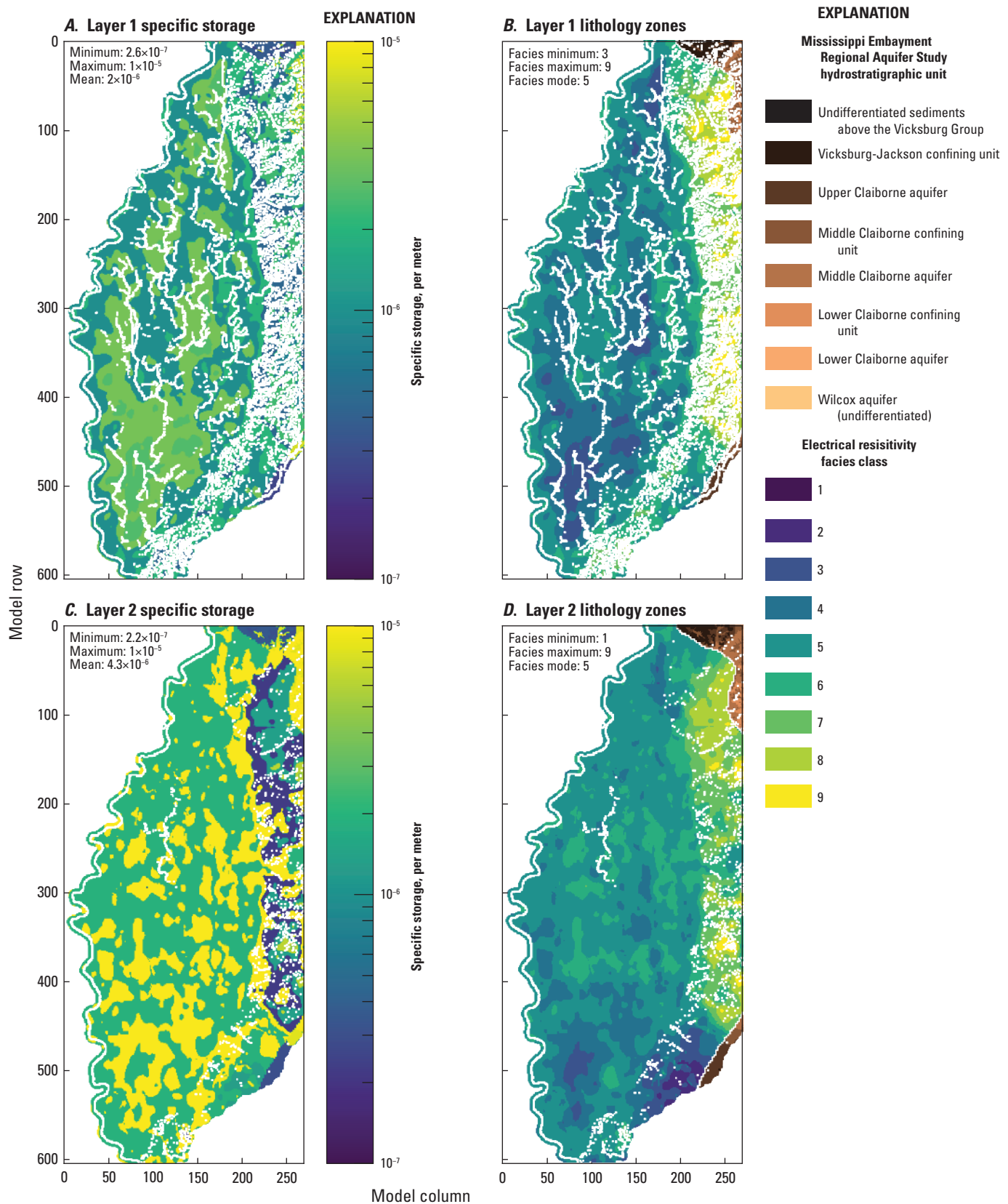


**Figure 2.19.** Specific storage ( $S_s$ ) estimates for the Mississippi Delta model, compared to electrical resistivity-based “facies classes” from the airborne electromagnetic (AEM) survey (Minsley and others, 2021; James and Minsley, 2021).

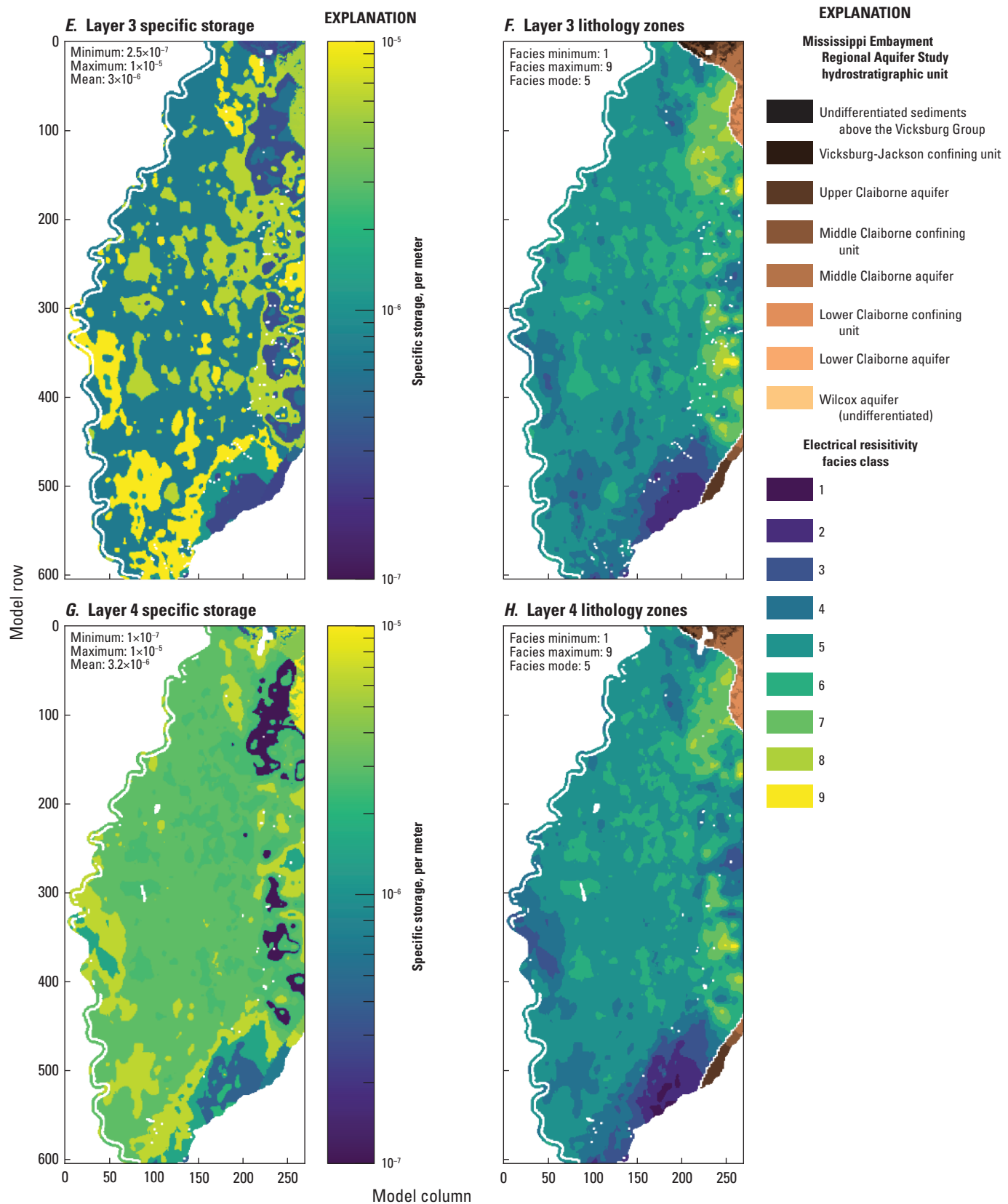
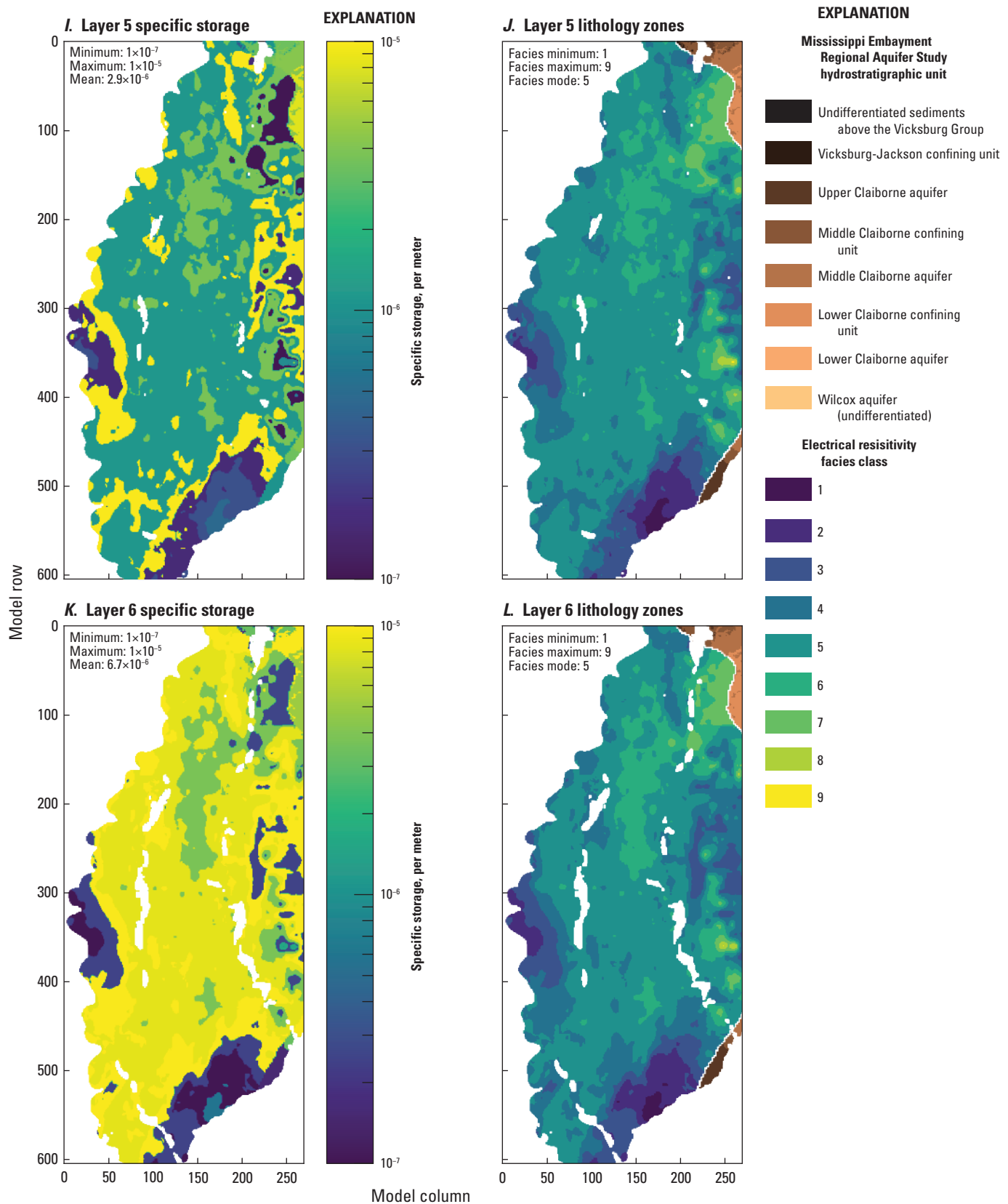


Figure 2.19. Specific storage ( $S_s$ ) estimates for the Mississippi Delta model, compared to electrical resistivity-based “facies classes” from the airborne electromagnetic (AEM) survey (Minsley and others, 2021; James and Minsley, 2021).



**Figure 2.19.** Specific storage ( $S_s$ ) estimates for the Mississippi Delta model, compared to electrical resistivity-based “facies classes” from the airborne electromagnetic (AEM) survey (Minsley and others, 2021; James and Minsley, 2021).

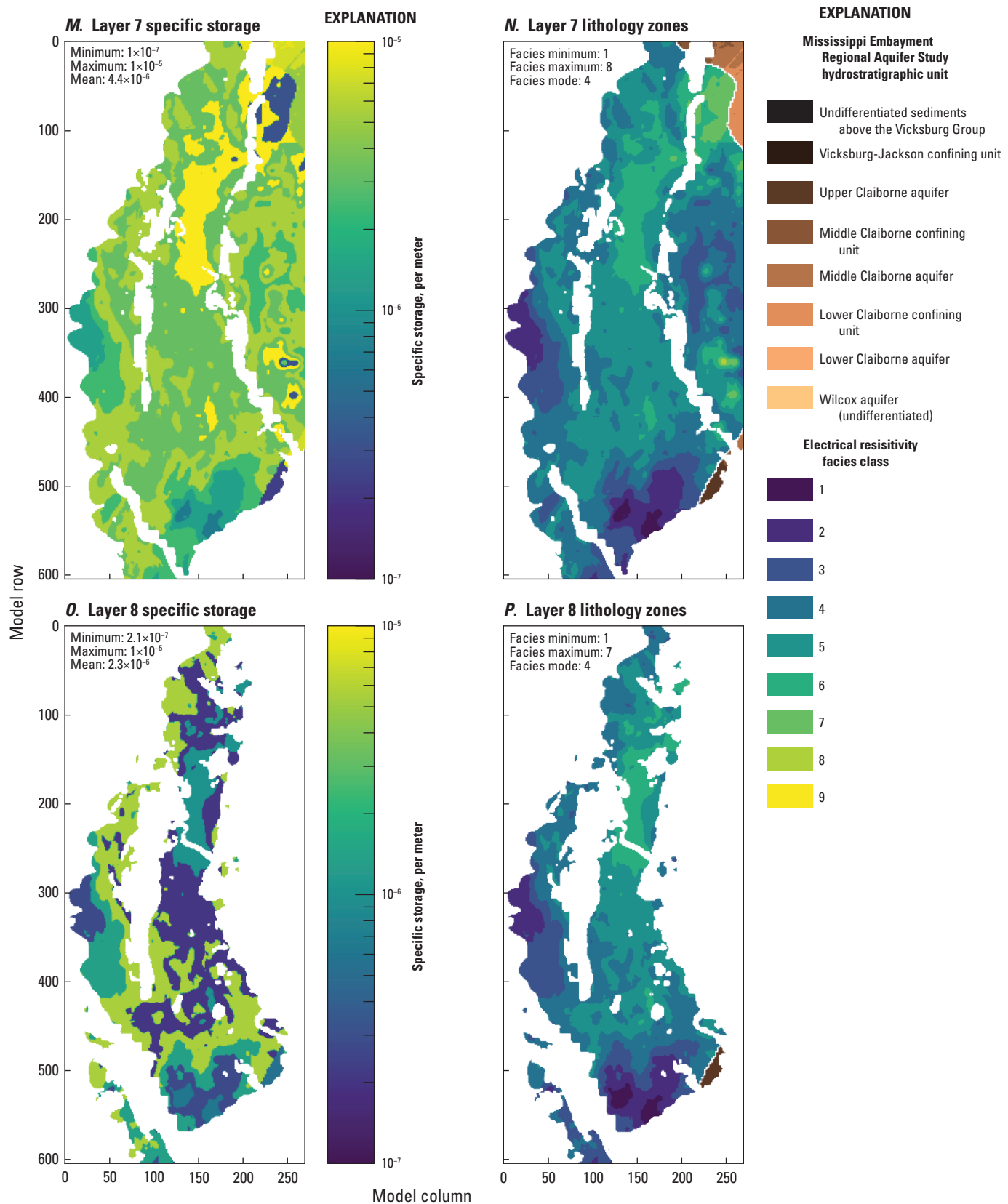
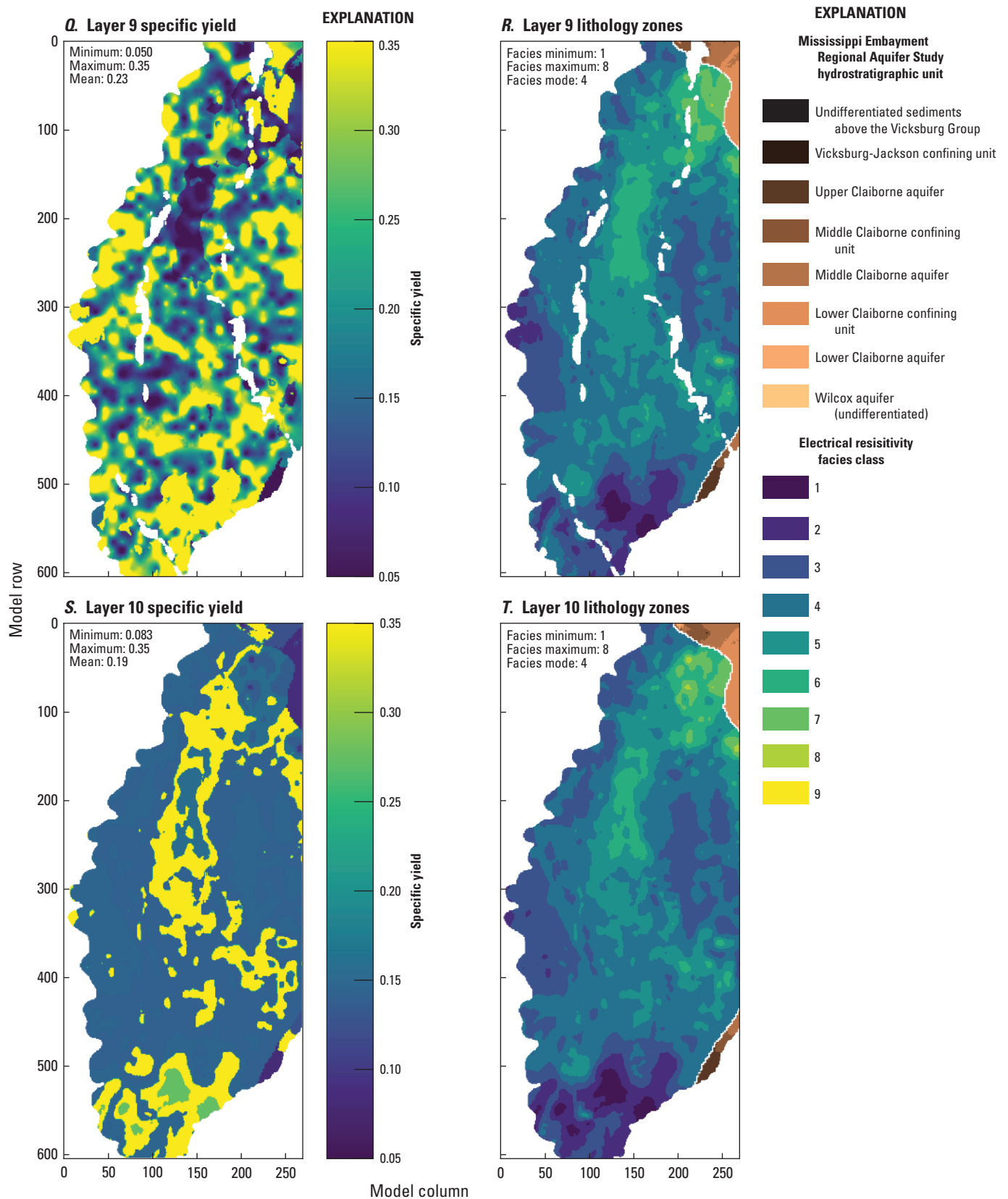


Figure 2.19. Specific storage ( $S_s$ ) estimates for the Mississippi Delta model, compared to electrical resistivity-based “facies classes” from the airborne electromagnetic (AEM) survey (Minsley and others, 2021; James and Minsley, 2021).



**Figure 2.19.** Specific storage ( $S_s$ ) estimates for the Mississippi Delta model, compared to electrical resistivity-based “facies classes” from the airborne electromagnetic (AEM) survey (Minsley and others, 2021; James and Minsley, 2021).

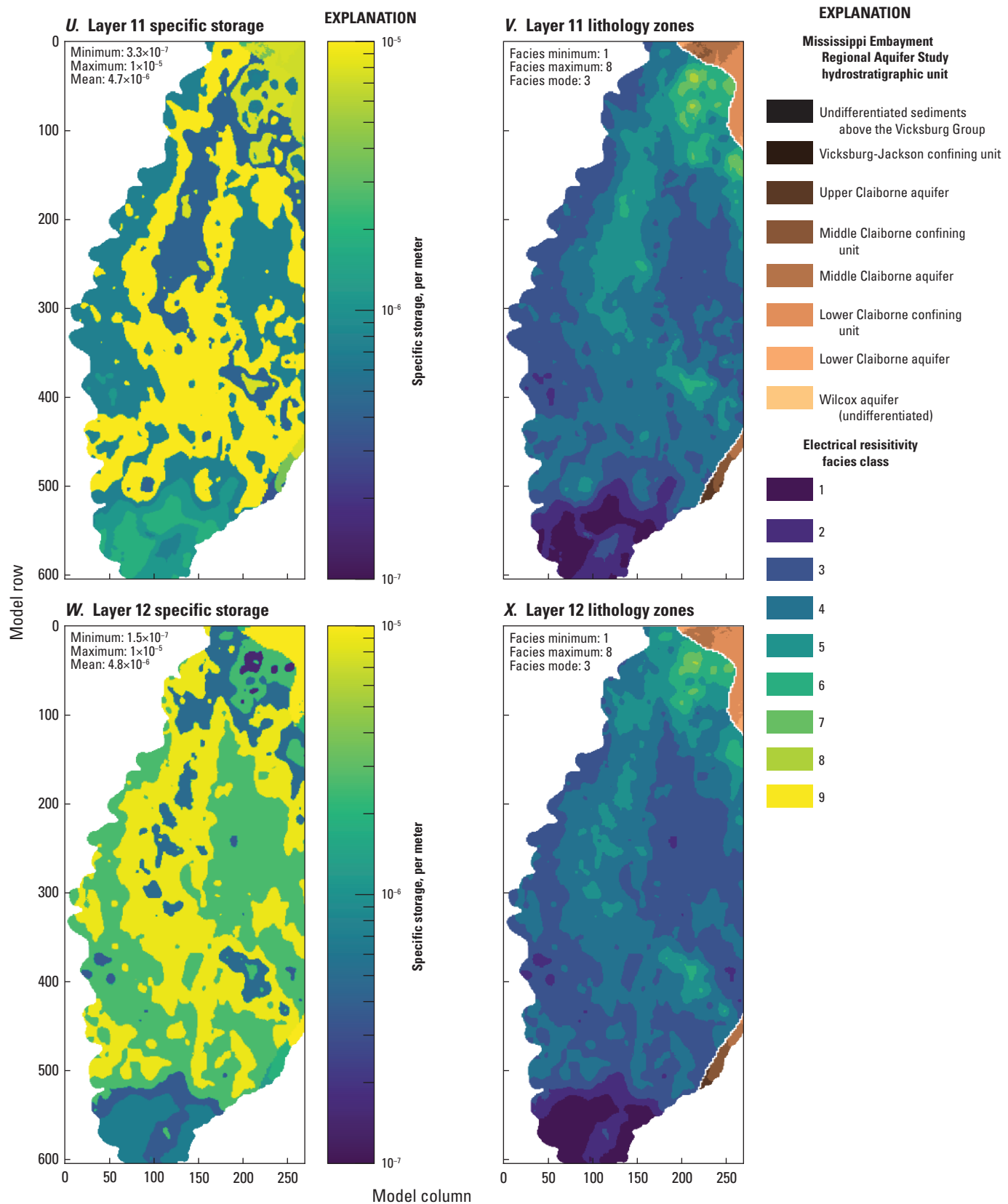
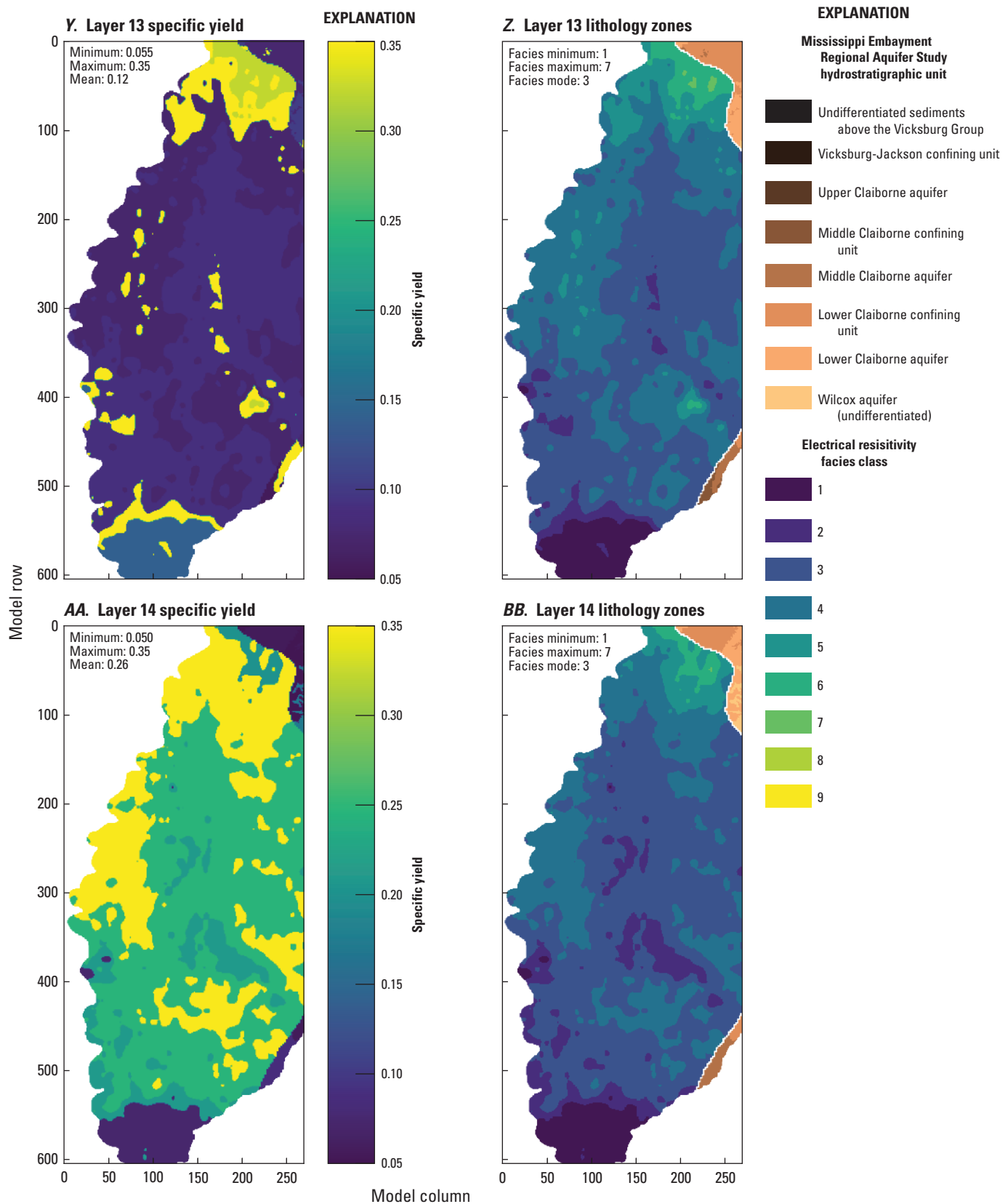
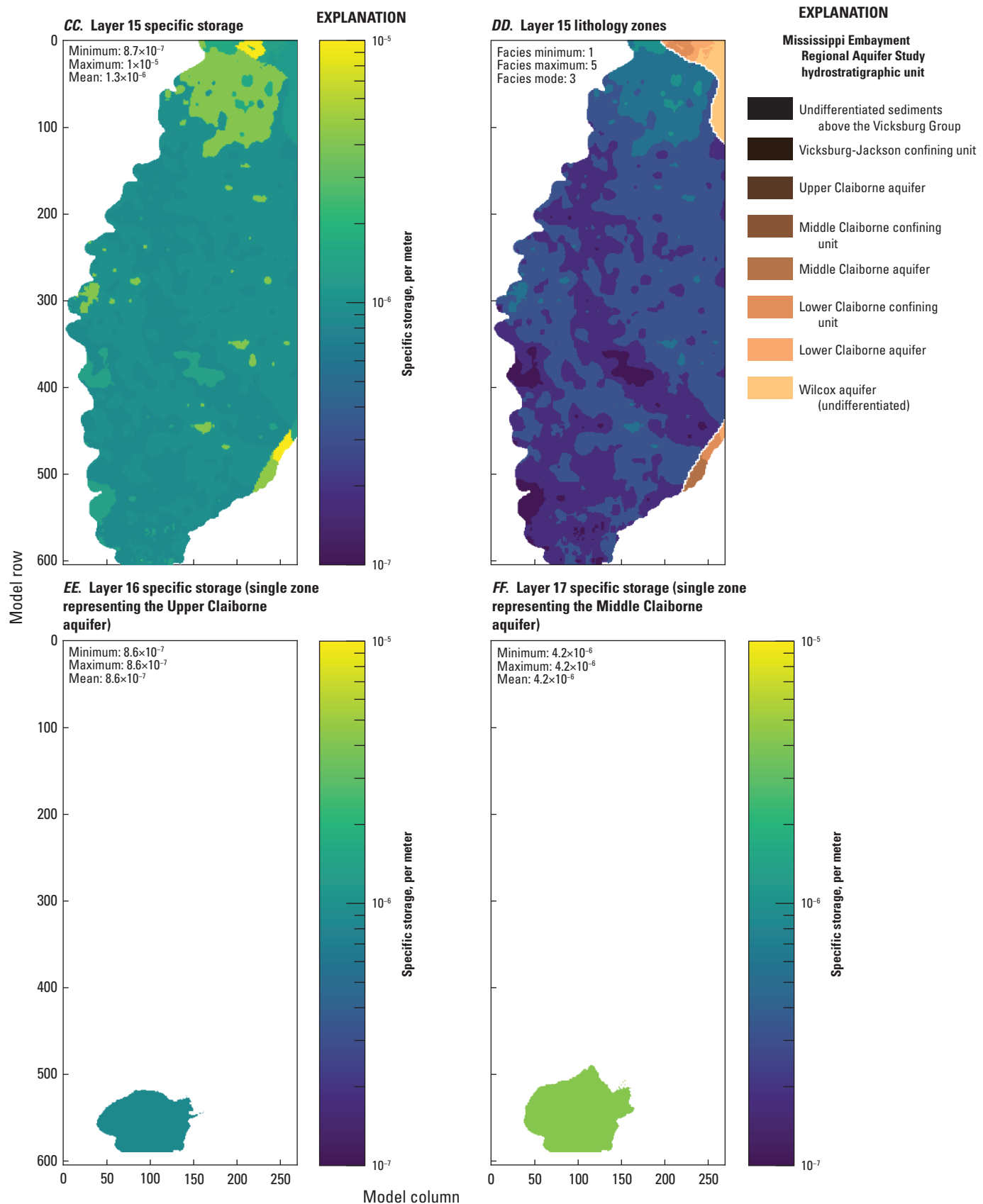


Figure 2.19. Specific storage ( $S_s$ ) estimates for the Mississippi Delta model, compared to electrical resistivity-based “facies classes” from the airborne electromagnetic (AEM) survey (Minsley and others, 2021; James and Minsley, 2021).



**Figure 2.19.** Specific storage ( $S_s$ ) estimates for the Mississippi Delta model, compared to electrical resistivity-based “facies classes” from the airborne electromagnetic (AEM) survey (Minsley and others, 2021; James and Minsley, 2021).



**Figure 2.19.** Specific storage ( $S_s$ ) estimates for the Mississippi Delta model, compared to electrical resistivity-based “facies classes” from the airborne electromagnetic (AEM) survey (Minsley and others, 2021; James and Minsley, 2021).

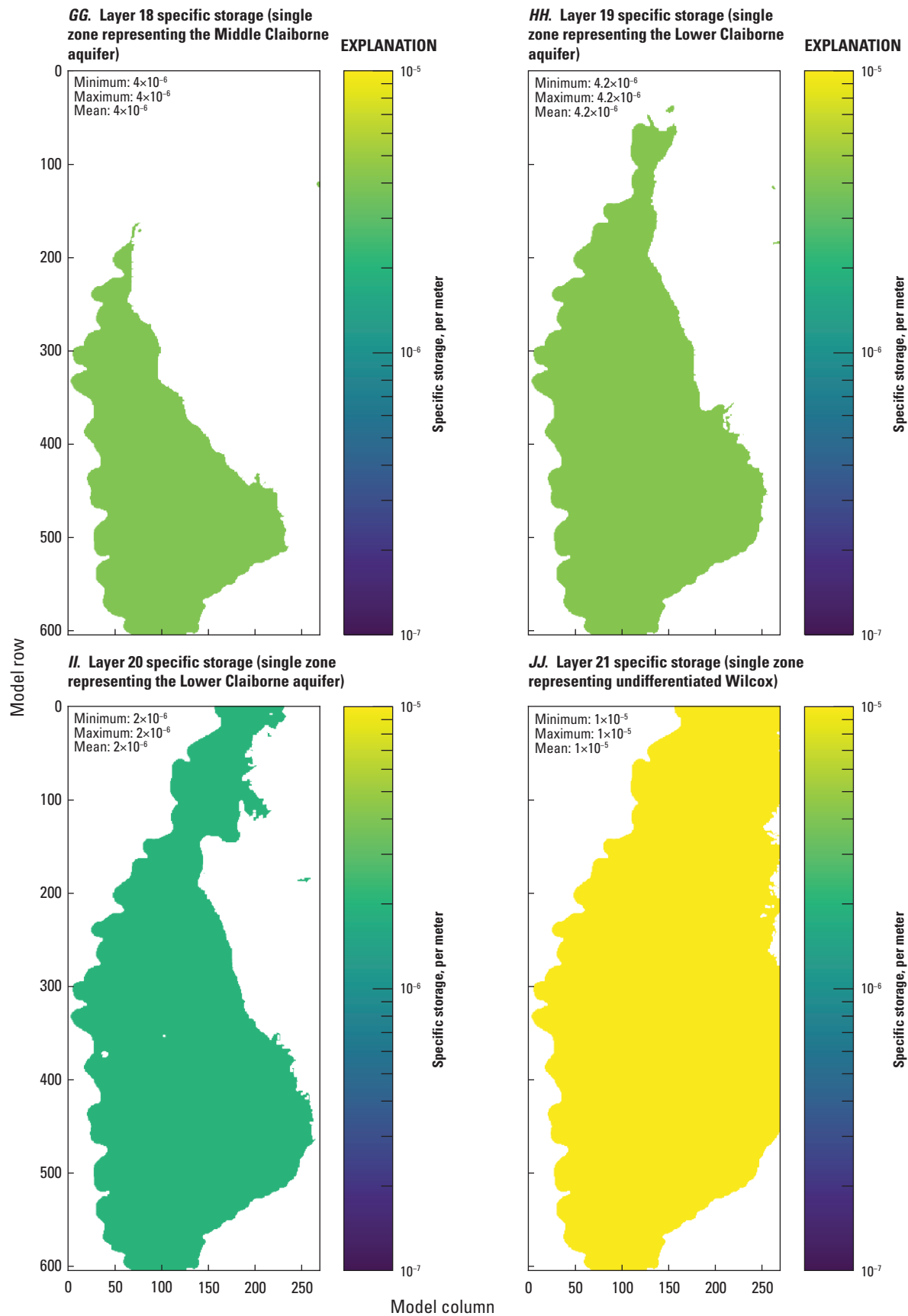


**Figure 2.19.** Specific storage ( $S_s$ ) estimates for the Mississippi Delta model, compared to electrical resistivity-based “facies classes” from the airborne electromagnetic (AEM) survey (Minsley and others, 2021; James and Minsley, 2021).

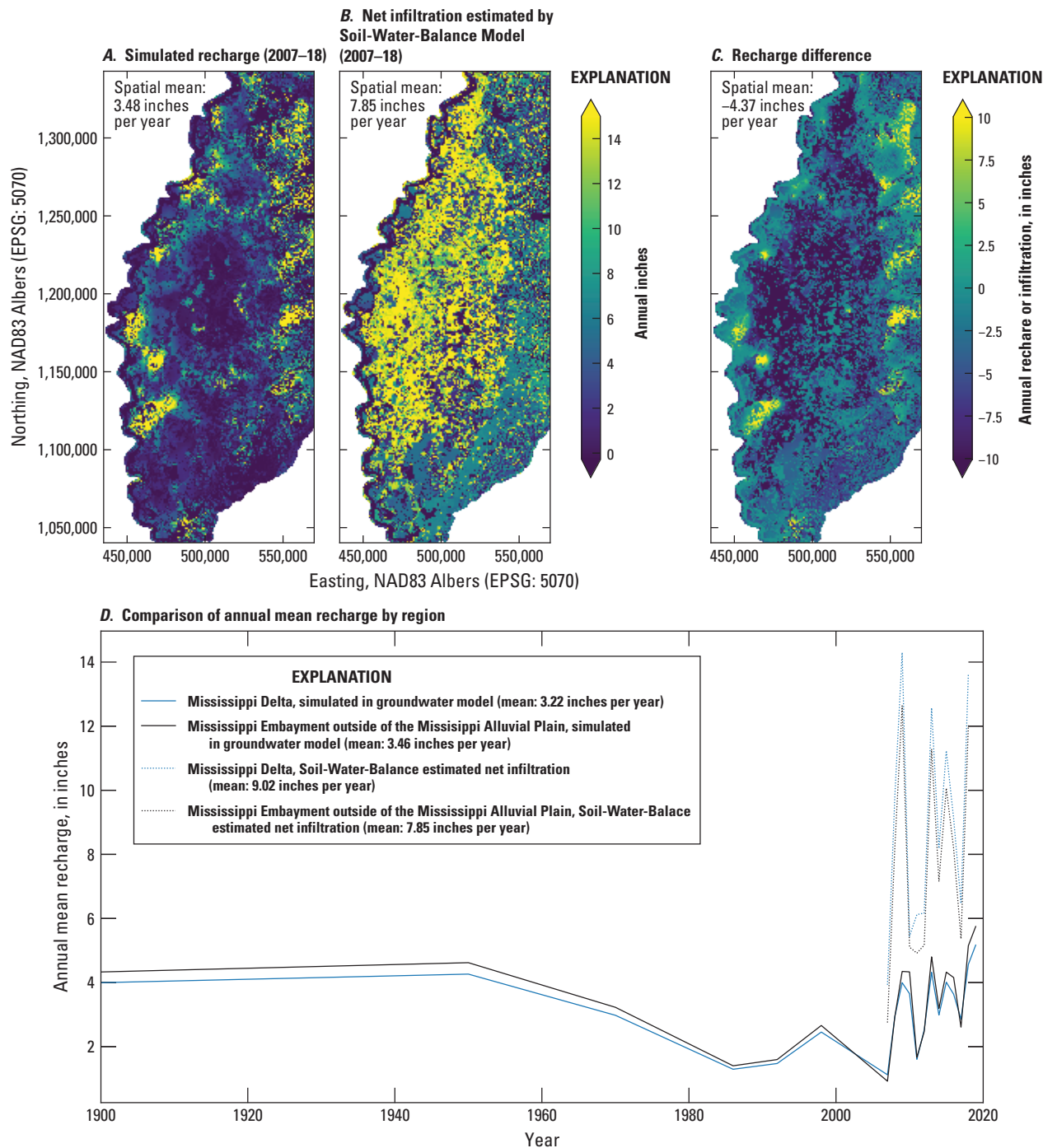


**Figure 2.20.** *A*, estimated mean annual recharge in the Mississippi Delta model compared to, *B*, net infiltration (leaving the soil zone) estimated by the Soil-Water-Balance code model of Nielsen and Westenbroek (2023); *C*, difference in recharge estimated by Soil-Water-Balance versus the Mississippi Delta model; and *D*, comparison of regional average annual recharge values after model history matching to their equivalent net infiltration values estimated by Soil-Water-Balance code.

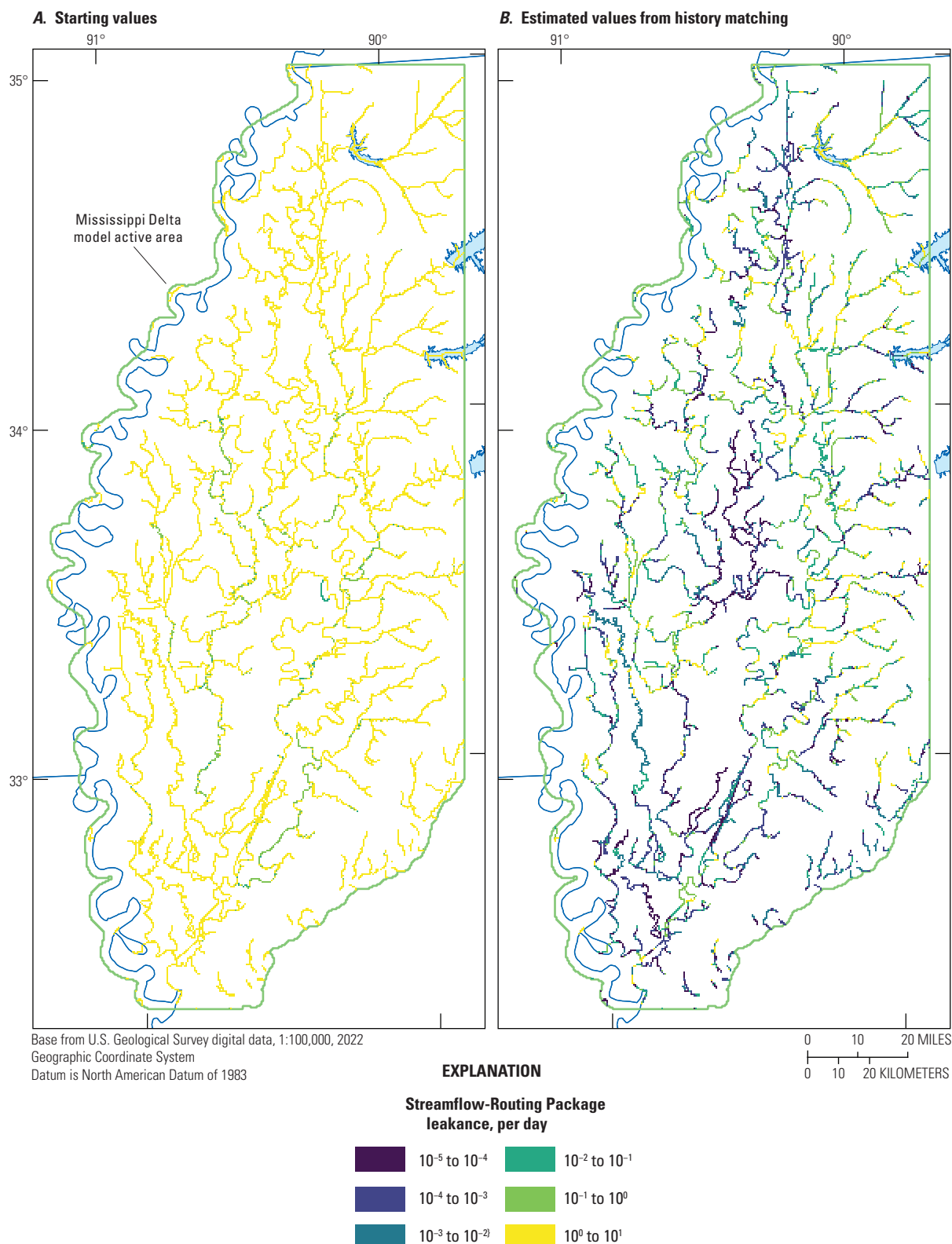


**Figure 2.21.** Estimates of streambed leakance in the Streamflow-Routing Package, A, initial values based on waterborne surveys of subsurface electrical resistivity (Leaf, 2023; Adams and others, 2019; Killian, 2018); and B, post-history matching values.

## Water Use

Water use parametrization for the Mississippi Delta model history matching consisted of static multipliers for the pumping rates associated with each dataset, and dynamic multipliers for pumping rates associated with each of the five major crop types (soybeans, cotton, corn, aquaculture and rice) as well as nonagricultural uses, for each stress period (table 2.4); therefore, the estimated pumping rate for each well in a given stress period was the product of the initial pumping rate, the static rate for that dataset, and the dynamic rate for the associated crop type and stress period. Total estimated water use for the base ensemble member from the second iES history matching iteration is shown through time in figure 1.2; table 2.6 summarizes the static multiplier estimates from that model. Dynamic multiplier values are available in the companion data release (Leaf and others, 2023).

## References Cited

Adams, R.F., Miller, B.V., and Kress, W.H., 2019, Waterborne resistivity inverted models, Mississippi Alluvial Plain, 2016–2018: U.S. Geological Survey data release, accessed July 18, 2023, at <https://doi.org/10.5066/P9WQPRFB>.

Anderson, M.P., Woessner, W.W., and Hunt, R.J., 2015, Applied groundwater modeling—Simulation of flow and advective transport (2d ed.): Academic Press, 564 p.

Arthur, J.K., 2001, Hydrogeology, model description, and flow analysis of the Mississippi River alluvial aquifer in northwestern Mississippi: U.S. Geological Survey Water-Resources Investigations Report 2001–4035, 47 p. [Also available at <https://doi.org/10.3133/wri014035>.]

Asquith, W.H., and Seanor, R.C., 2019, infoGW2visGWDB—An R groundwater data-processing utility for manipulating, checking the veracity, and converting an “infoGW” object to the “GWmaster” object for the visGWDB software with demonstration for the Mississippi River Valley alluvial aquifer: U.S. Geological Survey software release, accessed July 18, 2023, at <https://doi.org/10.5066/P9MK0B6L>.

Asquith, W.H., Seanor, R.C., McGuire, V.L., and Kress, W.H., 2020, Methods to quality assure, plot, summarize, interpolate, and extend groundwater-level information—Examples for the Mississippi River Valley alluvial aquifer: Environmental Modelling & Software, v. 134, art. 104758, 19 p. [Also available at <https://doi.org/10.1016/j.envsoft.2020.104758>.]

Bristow, E., and Wilson, J.L., 2023, Aquaculture and irrigation water-use model (AIWUM) version 1.1 estimates and related datasets for the Mississippi Alluvial Plain: U.S. Geological Survey data release, <https://doi.org/10.5066/P9RGZOBZ>.

Clark, B.R., and Hart, R.M., 2009, The Mississippi Embayment Regional Aquifer Study (MERAS)—Documentation of a groundwater-flow model constructed to assess water availability in the Mississippi embayment: U.S. Geological Survey Scientific Investigations Report 2009–5172, 61 p., accessed July 18, 2023, at <https://doi.org/10.3133/sir20095172>.

Clark, B.R., Westerman, D.A., and Fugitt, D.T., 2013, Enhancements to the Mississippi Embayment Regional Aquifer Study (MERAS) groundwater-flow model and simulations of sustainable water-level scenarios: U.S. Geological Survey Scientific Investigations Report 2013–5161, 29 p., accessed May 26, 2017, at <https://doi.org/10.3133/sir20135161>.

Corson-Dosch, N.T., Fienen, M.N., Finkelstein, J.S., Leaf, A.T., White, J.T., Woda, J., and Williams, J.H., 2022, Areas contributing recharge to priority wells in valley-fill aquifers in the Neversink River and Rondout Creek drainage basins, New York: U.S. Geological Survey Scientific Investigations Report 2021–5112, 50 p., accessed July 18, 2023, at <https://doi.org/10.3133/sir20215112>.

Diehl, T.H., and Harris, M.A., 2014, Withdrawal and consumption of water by thermoelectric power plants in the United States, 2010: U.S. Geological Survey Scientific Investigations Report 2014–5184, 28 p. [Also available at <https://doi.org/10.3133/sir20145184>.]

Dietsch, B., Asquith, W.H., Breaker, B.K., Westenbroek, S.M., and Kress, W.H., 2022, Simulation of monthly mean and monthly base flow of streamflow using random forests for the Mississippi River Alluvial Plain, 1901 to 2018: U.S. Geological Survey Scientific Investigations Report 2022–5079, 17 p., accessed July 18, 2023, at <https://doi.org/10.3133/sir20225079>.

Doherty, J., 2003, Ground water model calibration using pilot points and regularization: Groundwater, v. 41, no. 2, p. 170–177. [Also available at <https://doi.org/10.1111/j.1745-6584.2003.tb02580.x>.]

Doherty, J.E., and Hunt, R.J., 2010, Approaches to highly parameterized inversion—A guide to using PEST for groundwater-model calibration: U.S. Geological Survey Scientific Investigations Report 2010–5169, 59 p. [Also available at <https://doi.org/10.3133/sir20105169>.]

Fienen, M.N., Haserodt, M.J., Leaf, A.T., and Westenbroek, S.M., 2022, Simulation of regional groundwater flow and groundwater/lake interactions in the Central Sands, Wisconsin: U.S. Geological Survey Scientific Investigations Report 2022–5046, 111 p., accessed July 18, 2023, at <https://doi.org/10.3133/sir20225046>.

Freeze, R.A., and Cherry, J.A., 1979, Groundwater: Englewood Cliffs, N.J., Prentice-Hall, Inc., 604 p.

Harris, M.A., and Diehl, T.H., 2019a, Water withdrawal and consumption estimates for thermoelectric power plants in the United States, 2015: U.S. Geological Survey data release, accessed July 18, 2023, at <https://doi.org/10.5066/P9V0T04B>.

Harris, M.A., and Diehl, T.H., 2019b, Withdrawal and consumption of water by thermoelectric power plants in the United States, 2015: U.S. Geological Survey Scientific Investigations Report 2019–5103, 15 p. [Also available at <https://doi.org/10.3133/sir20195103>.]

Hart, R.M., Clark, B.R., and Bolyard, S.E., 2008, Digital surfaces and thicknesses of selected hydrogeologic units within the Mississippi Embayment Regional Aquifer Study (MERAS): U.S. Geological Survey Scientific Investigations Report 2008–5098, 33 p., accessed July 18, 2023, at <https://doi.org/10.3133/sir20085098>.

Haugh, C.J., Killian, C.D., and Barlow, J.R.B., 2020a, MODFLOW–2005 model used to evaluate water-management scenarios for the Mississippi Delta: U.S. Geological Survey data release, accessed July 18, 2023, at <https://doi.org/10.5066/P9906VM5>.

Haugh, C.J., Killian, C.D., and Barlow, J.R.B., 2020b, Simulation of water-management scenarios for the Mississippi Delta: U.S. Geological Survey Scientific Investigations Report 2019–5116, 15 p. [Also available at <https://doi.org/10.3133/sir20195116>.]

Hunt, R.J., Walker, J.F., Selbig, W.R., Westenbroek, S.M., and Regan, R.S., 2013, Simulation of climate-change effects on streamflow, lake water budgets, and stream temperature using GSFLOW and SNTEMP, Trout Lake Watershed, Wisconsin: U.S. Geological Survey Scientific Investigations Report 2013–5159, 118 p. [Also available at <https://doi.org/10.3133/sir20135159>.]

James, S.R., and Minsley, B.J., 2021, Combined results and derivative products of hydrogeologic structure and properties from airborne electromagnetic surveys in the Mississippi Alluvial Plain: U.S. Geological Survey data release, accessed July 18, 2023, at <https://doi.org/10.5066/P9382RCI>.

Killian, C., 2018, Characterizing spatial and temporal changes and driving factors of groundwater and surface-water interactions within the Mississippi portion of the Mississippi Alluvial Plain: Starkville, Miss., Mississippi State University, Ph.D. dissertation, 89 p., accessed April 8, 2019, at <https://scholarsjunction.msstate.edu/cgi/viewcontent.cgi?article=2043&context=td>.

Leaf, A.T., Duncan, L.L., and Haugh, C.J., 2023, MODFLOW 6 models for simulating groundwater flow in the Mississippi Embayment with a focus on the Mississippi Delta: U.S. Geological Survey data release, <https://doi.org/10.5066/P971LPOB>.

Leaf, A.T., 2023, Automated construction of Streamflow-Routing networks for MODFLOW—Application in the Mississippi Embayment region: U.S. Geological Survey Scientific Investigations Report 2023–5051, 27 p., <https://doi.org/10.3133/sir20235051>.

McKay, L., Bondelid, T., Dewald, T., Johnston, J., Moore, R., and Rea, A., 2012, NHDPlus version 2—User guide [data model ver. 2.1]: U.S. Environmental Protection Agency, accessed September 17, 2018, at [http://www.horizon-systems.com/NHDPlus/NHDPlusV2\\_documentation.php](http://www.horizon-systems.com/NHDPlus/NHDPlusV2_documentation.php).

McKee, P.W., and Clark, B.R., 2003, Development and calibration of a ground-water flow model for the Sparta aquifer of southeastern Arkansas and north-central Louisiana and simulated response to withdrawals, 1998–2027: U.S. Geological Survey Water-Resources Investigations Report 2003–4132, 71 p. [Also available at <https://doi.org/10.3133/wri034132>.]

Minsley, B.J., Rigby, J.R., James, S.R., Burton, B.L., Knierim, K.J., Pace, M.D.M., Bedrosian, P.A., and Kress, W.H., 2021, Airborne geophysical surveys of the lower Mississippi valley demonstrate system-scale mapping of subsurface architecture: *Communications Earth & Environment*, v. 2, no. 1, art. 131, 14 p. [Also available at <https://doi.org/10.1038/s43247-021-00200-z>.]

Nielsen, M.G., and Westenbroek, S.M., 2023, Updated estimates of water budget components for the Mississippi embayment region using a Soil-Water-Balance model, 2000–2020: U.S. Geological Survey Scientific Investigations Report 2023–5080, 58 p., <https://doi.org/10.3133/sir20235080>.

Pradic, D.E., Konikow, L.F., and Banta, E.R., 2004, A new Streamflow-Routing (SFR1) Package to simulate stream-aquifer interaction with MODFLOW-2000: U.S. Geological Survey Open-File Report 2004–1042, 95 p. [Also available at <https://doi.org/10.3133/ofr20041042>.]

Westenbroek, S.M., Nielsen, M.G., and Ladd, D.E., 2021, Initial estimates of net infiltration and irrigation from a Soil-Water-Balance model of the Mississippi Embayment Regional Aquifer Study area: U.S. Geological Survey Open-File Report 2021–1008, 29 p., accessed July 18, 2023, at <https://doi.org/10.3133/ofr20211008>.

White, J.T., 2018, A model-independent iterative ensemble smoother for efficient history-matching and uncertainty quantification in very high dimensions: *Environmental Modelling & Software*, v. 109, p. 191–201. [Also available at <https://doi.org/10.1016/j.envsoft.2018.06.009>.]

White, J.T., Fienen, M.N., and Doherty, J.E., 2016, A python framework for environmental model uncertainty analysis: *Environmental Modelling & Software*, v. 85, p. 217–228. [Also available at <https://doi.org/10.1016/j.envsoft.2016.08.017>.]

White, J.T., Hemmings, B., Fienen, M.N., and Knowling, M.J., 2021, Towards improved environmental modeling outcomes—Enabling low-cost access to high-dimensional, geostatistical-based decision-support analyses: *Environmental Modelling & Software*, v. 139, art. 105022, 9 p. [Also available at <https://doi.org/10.1016/j.envsoft.2021.105022>.]

White, J.T., Hunt, R.J., Fienen, M.N., and Doherty, J.E., 2020, Approaches to highly parameterized inversion—PEST++ Version 5, a software suite for parameter estimation, uncertainty analysis, management optimization and sensitivity analysis: U.S. Geological Survey Techniques and Methods, book 7, chap. C26, 52 p., accessed July 18, 2023, at <https://doi.org/10.3133/tm7C26>.

Wilson, J.L., 2021, Aquaculture and Irrigation Water-Use Model (AIWUM) version 1.0—An agricultural water-use model developed for the Mississippi Alluvial Plain, 1999–2017: U.S. Geological Survey Scientific Investigations Report 2021–5011, 36 p., accessed July 18, 2023, at <https://doi.org/10.3133/sir20215011>.

## Appendix 3. Additional Model Results

This appendix contains additional model results for the historical part of the model simulation. [Figure 3.1](#) shows water table elevations and groundwater/surface water interactions simulated in the Mississippi Alluvial Plain by the Mississippi Embayment Regional Aquifer Study (MERAS) 3 model. [Figure 3.2](#) shows water budgets for the Mississippi Alluvial Plain simulated by MERAS 3.

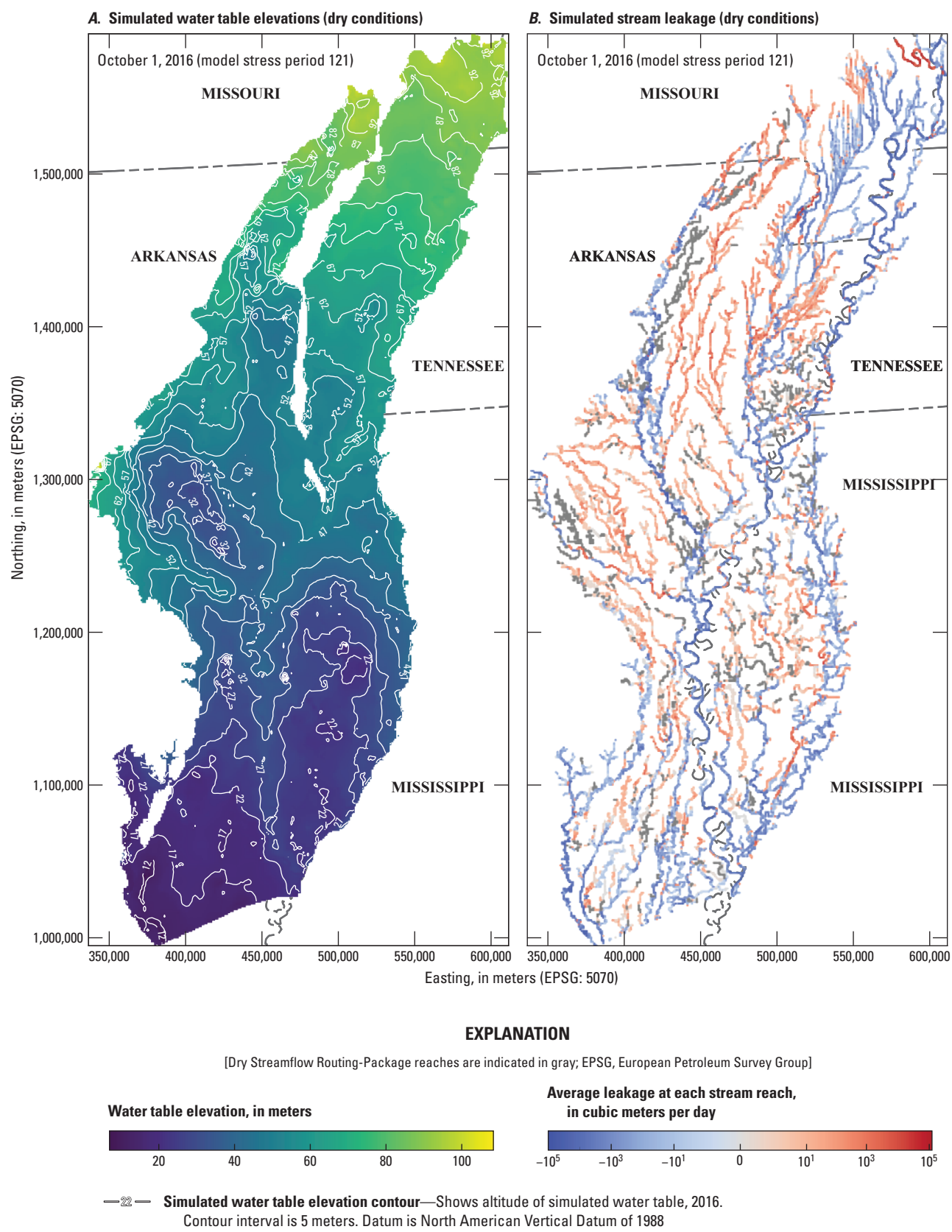


**Figure 3.1.** Water table elevations and stream leakage in the Mississippi Alluvial Plain, as simulated by the Mississippi Embayment Regional Aquifer Study (MERAS) 3 model under dry (A, B) and wet (C, D) conditions.

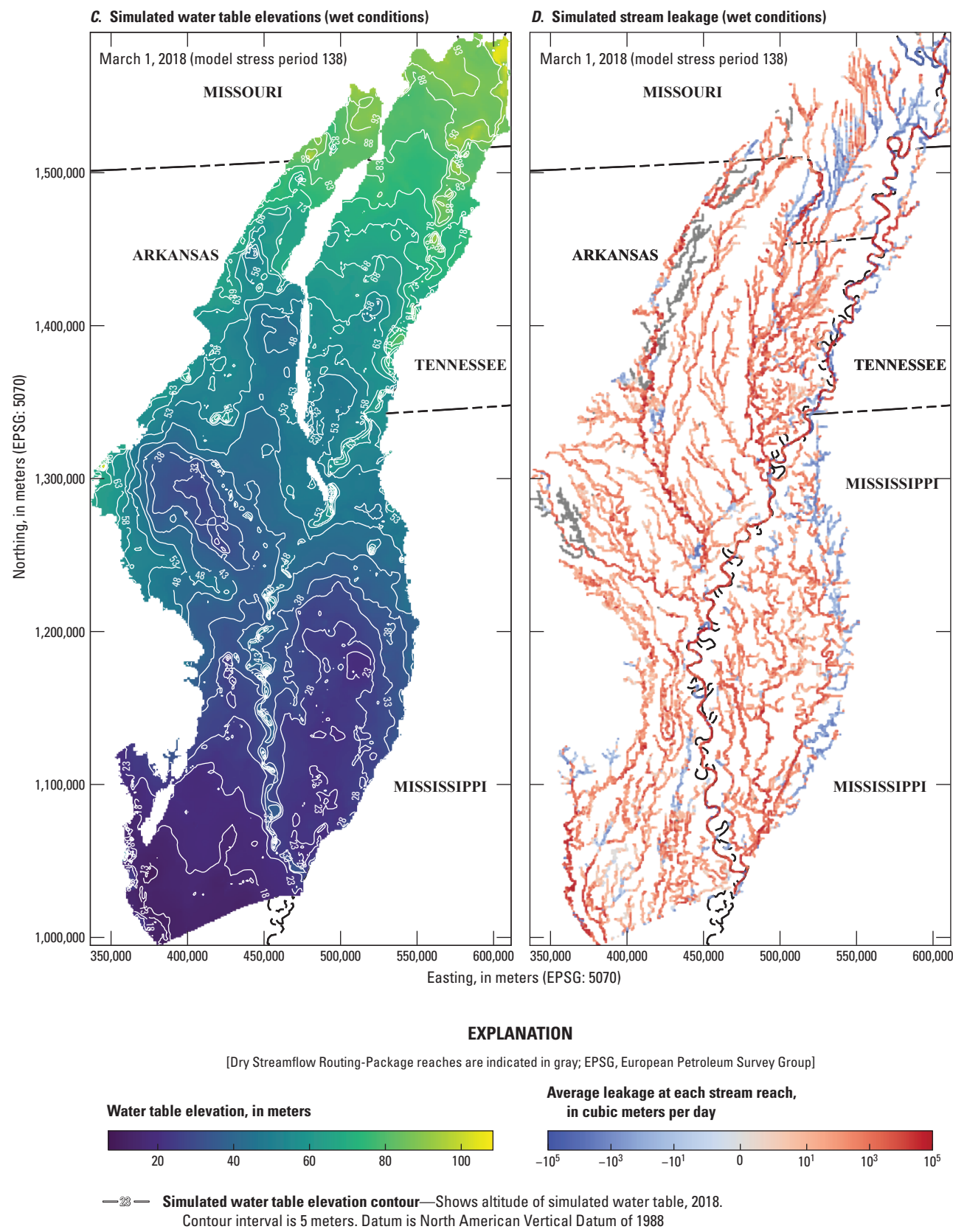


**Figure 3.1.** Water table elevations and stream leakage in the Mississippi Alluvial Plain, as simulated by the Mississippi Embayment Regional Aquifer Study (MERAS) 3 model under dry (A, B) and wet (C, D) conditions.

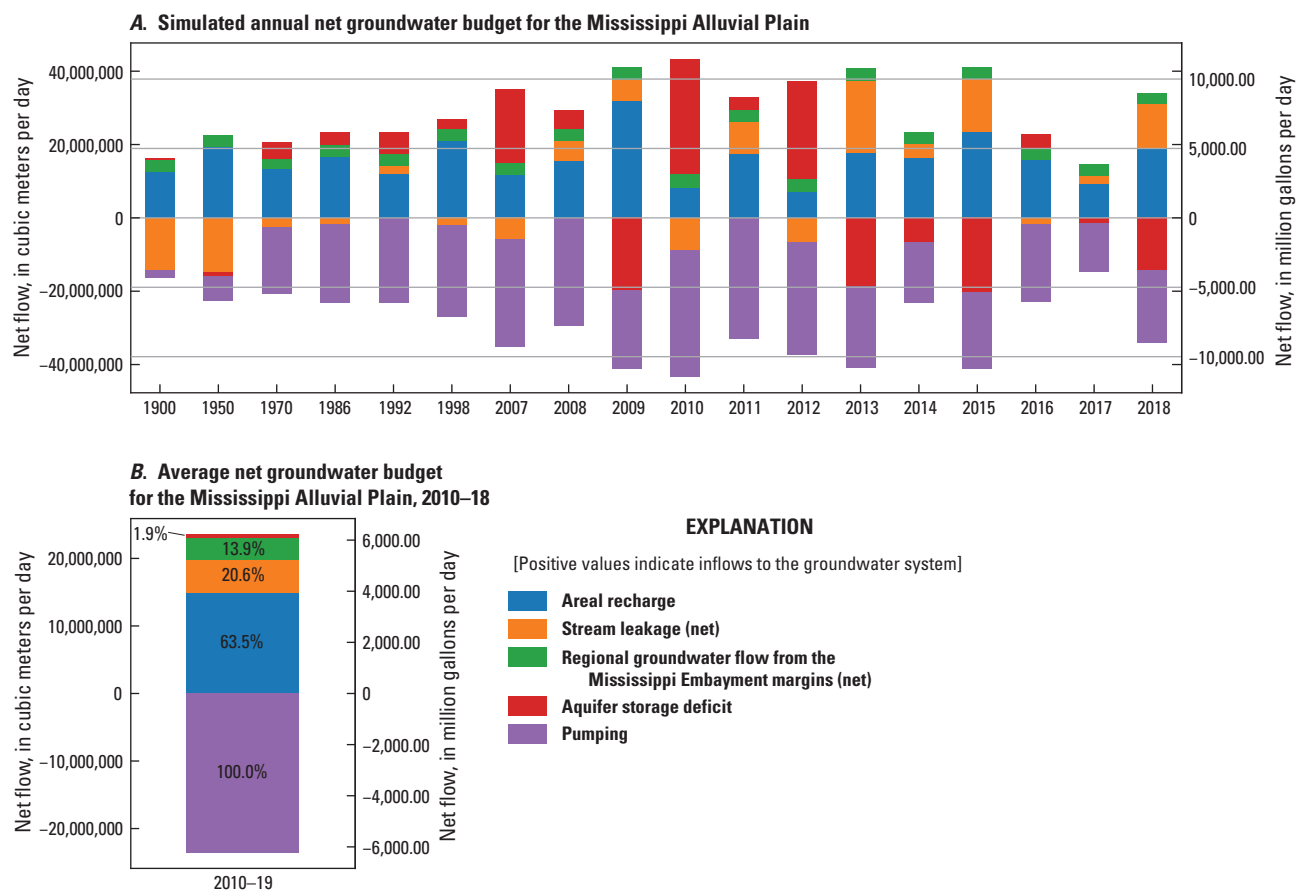


**Figure 3.2.** Water budget results for the Mississippi Alluvial Plain.

## Appendix 4. General Circulation Models Used in the Future Climate Scenarios

**Table 4.1** lists the General Circulation Models (GCMs) and greenhouse gas emissions scenarios used to drive the baseline forecasts of potential future groundwater levels. Downscaled gridded output from the GCM/scenario combinations listed was applied to the Soil-Water-Balance (SWB) model of Nielsen and Westenbroek (2023) to obtain estimates of net infiltration, surface water runoff and irrigation pumping for the period of 2020 to 2056 (Villers and Ladd, 2023). Five GCMs were selected for each of two future climate scenarios representing “middle” and “high” greenhouse gas emissions pathways (RCP 4.5 and 8.5; for example, Moss and others, 2010). The models were selected from the larger group of Coupled Model Intercomparison Project Phase 5 (CMIP5) models included in the National Climate Change Viewer

(Alder and Hostetler, 2013), based on the relative changes in mean precipitation and temperature simulated for the period of 2025-2049, compared to 1981-2000; for example, the IPSL-CM5A-MR model simulates the lowest amount of future precipitation among the GCMs included in the National Climate Change Viewer (Alder and Hostetler, 2013), and is therefore considered to be “dry.” “Cool” (least temperature increase), “warm,” “wet” and “dry” endmembers were selected from the RCP 4.5 and 8.5 scenarios, as well as the model that most closely matched the mean simulated temperature and precipitation changes across all models included by Alder and Hostetler (2013). Additional details are available in the “Future Climate Scenarios” section of this report.

**Table 4.1.** General Circulation Models (GCMs) used in the future climate scenarios (downscaled Coupled Model Intercomparison Project Phase 3 [CMIP3] and 5 [CMIP5] climate and hydrology projections [Bureau of Reclamation, 2022]).

[RCP, representative concentration pathway]

Model name	Institution	Future climate scenario	Relative model bias
HadGEM2-CC	Met Office Hadley Centre	RCP 4.5	Warm
IPSL-CM5A-LR	Institut Pierre-Simon Laplace	RCP 4.5	Mean
IPSL-CM5A-MR	Institut Pierre-Simon Laplace	RCP 4.5	Dry
MIROC-ESM	Japan Agency for Marine-Earth Science and Technology, Atmosphere and Ocean Research Institute (The University of Tokyo), and National Institute for Environmental Studies	RCP 4.5	Wet
MRI-CGCM3	Meteorological Research Institute	RCP 4.5	Cool
CCSM4	National Center for Atmospheric Research	RCP 8.5	Mean
CSIRO-Mk3-6-0	Commonwealth Scientific and Industrial Research Organization, Queensland Climate Change Centre of Excellence	RCP 8.5	Wet
IPSL-CM5A-MR	Institut Pierre-Simon Laplace	RCP 8.5	Dry
MIROC-ESM-CHEM	Japan Agency for Marine-Earth Science and Technology, Atmosphere and Ocean Research Institute (The University of Tokyo), and National Institute for Environmental Studies	RCP 8.5	Warm
INM-CM4	Institute for Numerical Mathematics	RCP 8.5	Cool

## References Cited

Alder, J.R., and Hostetler, S.W., 2013, USGS National Climate Change Viewer (ver. 2.0.2): U.S. Geological Survey digital data, accessed July 18, 2023 at <https://doi.org/10.5066/F7W9575T>.

Bureau of Reclamation, 2022, Downscaled CMIP3 and CMIP5 climate and hydrology projections: U.S. Department of Energy web page, accessed January 28, 2022, at [https://gdo-dcp.ucrlnl.org/downscaled\\_cmip\\_projections](https://gdo-dcp.ucrlnl.org/downscaled_cmip_projections).

Moss, R.H., Edmonds, J.A., Hibbard, K.A., Manning, M.R., Rose, S.K., van Vuuren, D.P., Carter, T.R., Emori, S., Kainuma, M., Kram, T., Meehl, G.A., Mitchell, J.F.B., Nakicenovic, N., Riahi, K., Smith, S.J., Stouffer, R.J., Thomson, A.M., Weyant, J.P., and Wilbanks, T.J., 2010, The next generation of scenarios for climate change research and assessment: *Nature*, v. 463, p. 747–756. [Also available at <https://doi.org/10.1038/nature08823>.]

Nielsen, M.G., and Westenbroek, S.M., 2023, Updated estimates of water budget components for the Mississippi embayment region using a Soil-Water-Balance model, 2000–2020: U.S. Geological Survey Scientific Investigations Report 2023–5080, 58 p., <https://doi.org/10.3133/sir20235080>.

Villers, J.J., and Ladd, D.E., 2023, Soil-Water-Balance forecasted climate model output for simulations of water budget components in the Mississippi Embayment Regional Aquifer System, 2020 to 2055: U.S. Geological Survey data release, <https://doi.org/10.5066/P9BC6UB8>.



**For more information about this publication, contact:**  
Director, USGS Upper Midwest Water Science Center  
1 Gifford Pinchot Drive  
Madison, WI 53726

For additional information, visit: <https://www.usgs.gov/centers/uppermidwest-water-science-center>

Publishing support provided by the Rolla Publishing Service Center

